Order Number 9406273

The determination/control of hydrogen behavior in low carbon steel as a function of surface treatment

Amey, Stephen Leonard, Ph.D.

Case Western Reserve University, 1993

U·M·I
300 N. Zeeb Rd.
Ann Arbor, MI 48106

THE DETERMINATION/CONTROL OF HYDROGEN BEHAVIOR IN LOW CARBON STEEL AS A FUNCTION OF SURFACE TREATMENT

by

STEPHEN LEONARD AMEY

Submitted in partial fulfillment of the requirements

for the Degree of Doctor of Philosophy

Faculty Advisors: Dr. Joe H. Payer and Dr. Gary M. Michal

Department of Materials Science and Engineering

CASE WESTERN RESERVE UNIVERSITY

May 1993

CASE WESTERN RESERVE UNIVERSITY

GRADUATE STUDIES

We hereby approve the thesis of

_____

candidate for the Ph.D.

degree.*

(signed) _____
(chair)

_____

_____

_____

_____

date 2/9/93

*We also certify that written approval has been obtained for any proprietary material contained therein.

THE DETERMINATION/CONTROL OF HYDROGEN BEHAVIOR
IN LOW CARBON STEEL AS A FUNCTION OF SURFACE TREATMENT

Abstract

by

STEPHEN LEONARD AMEY

Hydrogen behavior in low carbon (<0.05wt.%) steel was investigated by both experimental evaluations and by the development of a hydrogen transport model. A phenomenological model was developed to evaluate hydrogen entry and/or exit in metals exposed to an aqueous environment. The model may be used to analyze data obtained from hydrogen permeation experiments through metal membranes and allows study of both surface and bulk transport phenomena. The model can allow arbitrary chemical potentials of hydrogen on both sides of a sheet, in addition to an arbitrary initial hydrogen distribution within the metal. When compared to other popular models, the model presented fit the experimental data well and indicated that the entry, exit and metallurgy of a sheet is significant to hydrogen absorption. The model parameters may be used to characterize a given charging process. As such, multiple processes may be evaluated by using the model to calculate hydrogen distributions in a metal sheet. Permeation experiments on steel sheets showed that with decreasing pH, increasing i_c, electrolyte flow, surface roughness or temperature, hydrogen absorption will increase. In addition, titanium additions to ultra low carbon (0.005wt% C) steels were found to decrease the hydrogen diffusivity and to affect the permeation behavior. Furthermore, lead contaminanted steel surfaces were found to both increase or decrease the permeation current. This effect was found to be lead surface coverage and polarization control dependent. A zinc coating was found to be a barrier to hydrogen for thicknesses between 1 - 3.6μm. A typical acidic electropickling process was found to inject twice as much hydrogen as an alkaline electrocleaning process or an acidic Zn plating process.

Acknowledgements

Without the following people's aid and assistance, the completion of this project would have been much more difficult. I wish to thank first and foremost, both my faculty advisors, Dr. Joe Payer and Dr. Gary Michal; Dr. Payer, for his friendship, interest, principles, advice and Dr. Michal, for his sarcasm and wit, his willingness to weed through my equations and for his patient advice regarding the model. Next, I wish to thank my family, without whose encouragement I might never have set my goals this high.

I also wish to thank the LTV Steel Corporation and the Ohio Steel Futures Program for the expense account and all of the stress; George Eierman (LTV) for all of his input; Dr. George Themolous (LTV) for his profilometry work; Dr. Wayne Jennings for his discussions regarding surface science; Dr. Omer Dogan for his permeation work and his advice; Greg Shaw and Paul Janavicius for their input and advice regarding the entire blistering problem, hydrogen and steel; the entire corrosion group, who at a drop of a hat would help me with my golf game; the weather who ruined by golf game, but kept me working; the whole Department of Materials Science and Engineering for all of my years of fun and camaraderie at Case; Dr. Jim Cawley and Dr. Uziel Landau for their comments and advice during my defense.

Finally and perhaps most of all, I thank my wife, Kay, for putting up with the long work hours, my moods and for just making my life wonderful. Her patience and understanding is part of every page in this document.

Table of Contents

List of Figures and Tables

Chapter 1
Introduction

"...If [a condition exists] which would lead to the formation of H_2, it may leave atomic hydrogen in the metal, which then diffuses inwards, producing mischief..."

— U.R. Evans[1]

1.1 Hydrogen and the Problem

The interactions between hydrogen and steel have been investigated as far back[2] as 1864, yet there are still many unexplained or poorly understood phenomena. The interactions between hydrogen and steel are worthy of study due to the common usage of steel in industrial applications, the deleterious effect of hydrogen on many materials, and the presence of hydrogen in many industrial environments. Such interactions may be classified as either *environment-sensitive* or *bulk-interactive* effects. Environment sensitive effects (e.g., corrosion, bubble evolution) are phenomena that take place at external surfaces of the steel only when the steel is within a particular environment. Bulk-interactive effects (e.g., absorption, blistering, trapping) occur in the bulk of the steel as the result of absorbed hydrogen and may continue to influence the properties of the steel after removal from the environment which introduced the hydrogen. Both the environment sensitive and bulk-interactive phenomena have the steel surface in common; thus, anything which alters the steel surface is critical to hydrogen/steel interactions.

The steel industry produces an electrogalvanized, low carbon (LC) steel sheet for automotive applications. Zinc (Zn) is applied for corrosion protection. Prior to Zn plating, the steel is exposed to a variety of electrochemical processes designed to remove rolling oils, oxides and provide a uniform surface. Such processes are often termed the

electrocleaning and electropickling processes, depending on whether the pH of the solution is alkaline or acidic, respectively.

The electrocleaning, electropickling and the electrogalvanizing processes are very aggressive environments for the steel. The processes utilize high current densities (50 - 500 mA/cm^2), moderate temperatures (50-75°C), take advantage of vigorous solution agitation (continuous processing lines move the steel sheet through the processes at 300-500 feet/minute) and are all thought to inject hydrogen into the steel. After plating, the coiled steel sheet is sent to the automotive manufacturer where the steel is stamped into a part, painted and then, heated to 400°C to cure the paint. Sometimes blisters (< 100μm in diameter) that affect the aesthetic appearance of the electrogalvanized sheet are found at the Zn/steel interface. These blisters have been found both prior to and after the paint cure. The fact that the electroprocesses inject hydrogen and that analysis[3] of the blister gas exhibits predominantly H_2 and methane gas suggests that hydrogen plays a key role in the blistering of these steel products.

Although hydrogen does not move through the zinc coating, the absorbed hydrogen will attempt to become redistributed in the steel lattice. This is possible because the diffusivity in iron/steel is relatively high (~10^{-6} cm^2/s - see Table 2.D in Chapter 2), even at ambient temperatures. However, during redistribution in the steel sheet, a variety of defects, voids and dislocations may interfere with the diffusing hydrogen. When hydrogen encounters one of these structural anomalies, it may participate in a chemical reaction, depending on the temperature and the specific species, and discontinue its motion through the lattice. If the anomaly has a surface (e.g., a void, dislocation), hydrogen recombination to form hydrogen gas is possible. As long as

there is available hydrogen, this process will continue until an equilibrium between the gas and the hydrogen in the lattice exists.

Once the zinc coating is applied on the steel sheet, hydrogen absorbed from the electrocleaning and electropickling processes will redistribute in the steel to remove concentration gradients. This will include any anomalies in the bulk or at the Zn/steel interface. If the Zn is not fully adherent to the steel, these areas of poor adhesion become likely sites for recombination of hydrogen, since the absorbed hydrogen will probably be near the steel sheet external surface. If enough hydrogen is injected by the electroprocesses, then significant pressures can result locally at the zinc decohesion locations. If the pressures at these locations exceeds the flow stress of the zinc, then a blister grows.

1.2 Dissertation Intent

It is the intent of this thesis to examine and understand the hydrogen interactions with steels used for automotive applications as a function of the electrochemical processes present on the electrogalvanizing line. In particular, the knowledge gained will be used to understand the blistering of an electrogalvanized sheet. Although improving the adhesion of the zinc coating might minimize blistering, perfect adhesion on the atomic level is an unrealistic expectation. Therefore, to reduce or eliminate blistering, the goal is to understand the hydrogen kinetics due to many surface parameters and using this knowledge, recommend practices to minimize hydrogen absorption under industrial conditions. To accomplish this goal, the following is required:

- An experimental program to evaluate the effect of many process variables present on the electrogalvanizing line.
- A theoretical model which may be applied to experimental results to obtain material parameters.
- Surface analytical tools which may be used to characterize the material behavior.

Figure 1.1 illustrates the organization of the experimental investigations taken by this thesis. Chapter 2 presents a review of the pertinent literature for these areas. The experimental techniques used for this project are defined and illustrated in Chapter 3. The electrochemical permeation technique is particularly detailed. Chapters 4 proposes a model to study hydrogen behavior in metals under multiple charging conditions. In Chapters 5-9 the results obtained during this investigation are presented and are discussed relative to the hydrogen/steel interactions and the blistering phenomenon. Finally, in Chapter 10 the conclusions are breifly summarized and the recommendations for minimizing hydrogen absorption are presented.

Several distinct areas of research are presented in Chapters 4-9. It was necessary to develop a model to understand and predict hydrogen absorption behavior. This theoretical development is described in Chapter 4. Phenomonological results that pertain to the above described problem are presented in Chapters 5-8, but the application of the model is also highlighted. In Chapter 5, an evaluation of the effects of the controlling parameters (pH, current density, solution agitation, surface finish) upon the hydrogen behavior in low carbon steel is discussed. In Chapter 6, the effects of titanium additions to steel upon the hydrogen absorption processes is pursued. In Chapter 7, the

effect of different metallic contaminants on the steel surface, particularly lead, and their effect on the hydrogen behavior in low carbon steel is evaluated. The electrocleaning, the electropickling processes and the effect of a zinc coating and its ability to be a barrier to hydrogen entry and exit is evaluated in Chapter 8. Finally, Chapter 9 applies the model to several problems associated with the electrogalvanizing line and low carbon steel.

1.3 Conventions and Terminology

This dissertation traverses through several fields within materials science. In general, this thesis may be of interest to the fields of metallurgy and electrochemistry, but more specifically, the industries of steel production, electroplating, corrosion, coating and battery technology. Each of these fields utilizes different journal publications to address these issues and thus, utilize different units. This difference extends within a field or industry as well (e.g., compare the units used by a metallurgical journal and those used by the steel mill managers). Furthermore, there has been a growing trend to use SI units whenever possible by most scientific societies. However, much of this thesis utilizes electrochemical techniques, the literature of which consistently uses the cgs system. Thus, during the course of this dissertation, when discussing electrochemical phenomena, the cgs units system will be used. In all other cases, the SI system will be adopted.

In addition, the hydrogen literature uses many different sets of units to describe the amount of hydrogen dissolved in a metal. Table 1 presents several units encountered and the appropriate conversion formulas. This table was modified from one presented by McCright[4]. The units used for hydrogen concentration in this dissertation will be moles of hydrogen per cubic centimeter. Whenever possible the

ppm unit will also be given in parentheses. The former unit is that preferred by the electrochemical literature and the latter is that unit preferred by the metallurgical literature.

TABLE 1.A

Common Conversions for Hydrogen/Steel Systems

	Given units on left, desired units on top, multiply by factor below:					
	AC	**RV**	**wt%**	**GW**	**MC**	**ppm**
AC	---	1.58×10^{3}	1.805	20.08×10^{3}	0.14	18.05×10^{3}
RV	6.32×10^{-4}	---	1.14×10^{-3}	12.69	4.44×10^{-5}	11.4
wt%	0.554	887	---	11.1×10^{3}	7.8×10^{-2}	1×10^{4}
GW	4.98×10^{-5}	7.88×10^{-2}	8.99×10^{-5}	---	3.46×10^{-4}	0.899
MC	7.16	2.25×10^{4}	12.8	2.88×10^{3}	---	1.28×10^{5}
ppm	5.54×10^{-5}	8.77×10^{-2}	1×10^{-4}	1.11	7.8×10^{-6}	---

AC	: atoms H / atoms Fe	GW	:	cc H / 100g Fe	All calculations based upon:
RV	: cc H / cc Fe	MC	:	moles H / cc Fe	ρ=7.88g/cc
w/o	: g H / 100g Fe	ppm	:	0.0001 * w/o	m.w.(Fe) = 55.84g/mole

References for Chapter 1

1 U. R. Evans, The Corrosion and Oxidation of Metals: Scientific Principles and Practical Applications, Arnold, London, (1961), p. 397.

2 L. Cailletet, *Compt. Rend.*, 58, (1864) 327.

3 Private communication with Paul Janavicius, Case Western Reserve University.

4 R.D. McCright, Dissertation, Ohio State University, 1971.

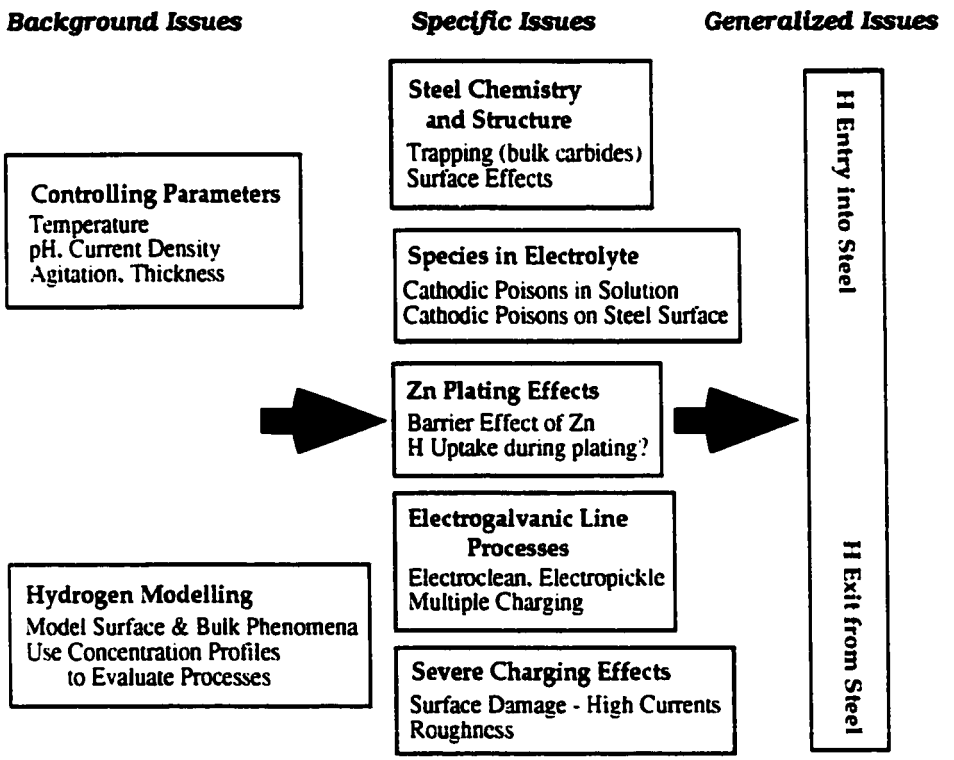

Figure 1.1: The above diagram illustrates the directions which were explored by this study.

Chapter 2
Background Review

Although the research problem and project were defined in Chapter 1, there is pertinent literature containing details obtained by previous studies that is of interest to later discussions. This review of pertinent literature is discussed in five main sections, each is relevant to a specific section that follows in later chapters.

2.1 Hydrogen Interaction with Metals

There is a considerable literature relating to hydrogen published every year, particularly since the 1950's. The goal of this literature review is not to be an all inclusive volume of the hydrogen literature. Such a goal would require a monumental effort. Rather, this review will be limited to identifying those effects pertaining to the research conducted by this thesis.

2.1.1 The Environmental Form of Hydrogen

Before the discussion of hydrogen interactions can begin, it is necessary to identify the form of hydrogen within a given environment. The natural state of hydrogen is not the same in different physical environments. In a gaseous environment, the natural state of hydrogen is a less reactive, molecular form, H_2. For example, at room temperature, hydrogen gas is not likely to dissociate spontaneously. For molecular hydrogen to dissociate to the more reactive atomic form, as shown in [2.1], much energy is required.

$$H_2 <=> 2H \qquad [2.1]$$

The dissociation energy, ΔH_{diss}, for this reaction is on the order of 440 kJ/mole. Conversely, in liquid environments, there is a tendency for water molecules to dissociate to hydrogen, H^+, and hydroxide, OH^-, ions to a small degree (e.g., $K_w = 10^{-14}$). Furthermore, if certain salts are added to water, hydrolysis occurs, resulting in the salt's dissociation into cations and anions. A good example of this type of dissociation is when hydrogen salts (acids) are added to aqueous solutions, resulting in an increase in protons.

When a metal is placed in either a liquid or gaseous environment, there is an interaction between the surroundings and the metal that occurs at the metal surface. The interaction may be described as a chemical or a physical interaction. Such classifications depend upon the nature of the metal and the environment. The metal surface atoms will have unsaturated bonds and will exist in a higher energy state than those in the metal bulk. The bulk atoms will have saturated bonds and be in a state of relative equilibrium. To reduce their surplus energy, the surface atoms will try to attach to various foreign particles from the metal's environment. If hydrogen is present, its small size relative to other species in solution and its high mobility (ionic conductivity ~350 $\Omega^{-1}cm^2/eq$) make it a likely species to attach to such a metal surface. These interactions and events can be described by surface reactions.

2.1.2 Hydrogen Surface Reactions

Figure 2.1 illustrates the three primary reactions which are discussed in the hydrogen literature when a metal surface is present in a hydrogen environment. They are the *hydrogen discharge* (HDR), the *hydrogen evolution* (HER) and the *hydrogen*

absorption (HAR) reactions. For the reactions to occur, the hydrogen must interact with the metal. The most likely mechanism would involve the ionic hydrogen becoming reduced on the metal surface. In acids, a protonated water molecule or the hydronium ion accepts an electron from the metal and results in a hydrogen atom adsorbing to the metal surface.

The Hydrogen Discharge Reactions

$H_3O^+ + e^- <=> H_{ads} + H_2O$ {in acid} [2.2]

$H_2O + e^- <=> H_{ads} + OH^-$ {in neutral/alkaline} [2.3]

In neutral or alkaline solutions, the primary source of hydrogen is the reduction of water. This results in the adsorption of hydrogen on the metal surface and the release of hydroxide into solution. Reactions [2.2] and [2.3] are the *hydrogen discharge reactions* for acidic and neutral/alkaline environments, respectively.

The discharge reaction (HDR) requires that a hydrogen ion moves to the metal surface and accepts an electron. Thus, the primary factor influencing the HDR is the metal surface, its ability to donate an electron and the hydrogen activity in the electrolyte. A good measure of the ability to remove an electron from a metal is the *work function*. The larger the work function of a metal, the more difficult it will be to donate an electron from the metal to a hydrogen ion. Conway[1] pointed out that few metals (e.g., Tl, Pb, Hg) have hydrogen surface behavior that is dominated by the HDR. Thus, with the exception of changing the hydrogen concentration in solution, few factors have been found to influence this reaction besides a chemical change of the metal surface.

Once hydrogen has adsorbed to the surface, two parallel reactions will compete with each other for this hydrogen supply. One of these competing reactions is the

hydrogen evolution reaction (HER). As previously discussed, it is not thermodynamically stable for two hydrogen atoms to spontaneously combine to the molecular form in solution because of the surplus energy the molecule would possess (i.e., the reaction is exothermic). However, the presence of a metal surface to absorb this energy may catalyze the reaction. Thus, two possible variations of the HER can occur and are listed in reactions [2.5] or [2.6a-b]. The HER may be *catalytic* as defined in [2.5] or it may be *electrodic* as defined in [2.6].

The Hydrogen Evolution Reactions

$H_{ads} + H_{ads} \Leftrightarrow H_2$ [2.5]

$H_{ads} + H_3O^+ + e^- \Leftrightarrow H_2 + H_2O$ {in acid} [2.6a]

$H_{ads} + H_2O + e^- \Leftrightarrow H_2 + OH^-$ {in neutral/alkaline} [2.6b]

If two adsorbed hydrogen atoms recombine on the metal surface due to the catalytic behavior of the metal, it is referred to as *catalytic desorption* (other names: chemical desorption, Tafel recombination, atom-atom step). This reaction is dependent upon hydrogen atoms colliding with each other on the metal surface. Reaction [2.5] may occur in either acidic or alkaline environments. Alternatively, if the catalytic character of the metal is low, a second discharge step may be involved to result in hydrogen desorption. The reactions for the appropriate (acidic or alkaline) environments are shown in reactions [2.6a-b] and are called the *electrochemical desorption* variation of the HER (other names: electrodic desorption, ion-atom combination). This reaction requires that the concentration of hydrogen be high to insure that discharging hydrogen would collide with an adsorbed hydrogen adatom.

Due to the fact that this reaction occurs because adsorbed hydrogen combines on the surface, the surface of the metal is key to the hydrogen evolution process. On the

atomic level, the number and distribution of hydrogen adsorption sites on the metal surface will influence the evolution reaction. On the practical level, a good indication of hydrogen evolution catalytic behavior is the *exchange current density*. For a given metal, the current density measured when the appropriate overpotential is applied to cause reaction [2.1] to initiate is the exchange current density. Table 2.A lists the exchange current density for a variety of metals. Note that metals such as platinum and palladium have very high, iron has a medium and lead and zinc have very low exchange current densities for the hydrogen reaction.

Table 2.A

Exchange Current Densities for Various Metals for the Reaction $H_2 = 2H^+ + e^-$

Metal	Log i_o (P)	Log i_o (KBR)	Metal	Log i_o (P)	Log i_o (KBR)
Re	-2.9	–	Ag	-7.2	-3.7 to -6.3
Pt(platinized)	-3.4	-3	Bi	–	-7
Pd	-3.6	-3	Sn	-7.3	–
Pt	-4.7	-2.8 to -3.1	Zn	-7.9	–
Ge	-4.7	–	Ti	–	-8.2
Rh	–	-3.6	Sb	-8.9	–
Ir	–	-3.7	Be	–	-9
Au	-5.0	-5.4 to -6	Ta	-9.1	–
Cd	-5.3	-10.8	Al	-9.5	–
W	-5.6	-5.9 to -6	Mn	–	-10.9
Fe	-5.8	–	Nb	–	-6.8 to -11
Co	-6.1	–	Hg	-12.6	-11.2 to -12.3
Mo	-6.2	–	Pb	–	-12 to -12.7
Ni	-6.3	-5.2 to -6.0	Tl	–	-11 to -16
Cu	-6.5	-8			

The units on i_o are A/cm^2. The values given are from two sources: (P) measured[2] in 1M H_2SO_4 and (KBR) measured[3] in various solutions from 0.1M to 1M H_2SO_4 and HCl; 5M for W.

The Hydrogen Absorption Reaction

$$H_{ads} <=> H_{abs} \qquad [2.7]$$

The other reaction which competes for the adsorbed hydrogen on a metal surface with the evolution reaction is the *hydrogen absorption reaction* (HAR) shown in equation [2.7]. the HAR is influenced by three primary factors. First, the amount of

adsorbed hydrogen directly influences the amount of hydrogen absorbed. This is clear from equation [2.7]. Thus, anything affecting the amount of adsorbed hydrogen (e.g., foreign surface atoms, surface inhomogeneities) could influence the absorption process. Secondly, since the HER competes for the same adsorbed hydrogen, the HAR could be affected indirectly by influencing the HER. Finally, the bonding between the metal atoms at the surface can affect the HAR. Because the accommodation of a hydrogen atom results in a slight distortion (9% in iron[4]) of the metal lattice, there is a resistance to hydrogen entry that may be described by an energy term: the activation energy, E_a. The activation energy for this process is strongly defined by the lattice bonding between different metal surface atoms and that between metal and foreign surface atoms. If an adsorbed hydrogen possesses more energy than E_a, then it can reduce its energy by becoming absorbed.

The reactions occurring on a metal surface are complex. The hydrogen discharge, hydrogen evolution and absorption reactions depend on both bulk metal and environmental factors.

2.1.3 Hydrogen Bulk Phenomena

Once hydrogen is absorbed by the metal, there are many metallurgical factors (e.g., lattice bonding, defects, foreign atoms) which will act to control the hydrogen behavior. The collective influence of such variables may be described by three terms: the *hydrogen solubility*, the *hydrogen diffusivity* and the *trapping of hydrogen*.

2.1.3.1 Hydrogen Solubility

The amount of hydrogen dissolved in a metal is dependent upon the ability of the metal to accommodate hydrogen atoms. The concentration of hydrogen dissolved in

a material under equilibrium with a hydrogen environment is called the *hydrogen solubility*. It measures a state of equilibrium, determined by the surrounding temperature and pressure, for a given metal-hydrogen system.

Ever since the early work[5] of Smith (1948), the literature recognizes three classes of metals with regards to their hydrogen behavior. Table 2.B illustrates the distinctions between some of the metals. Some metals form a compound with hydrogen that results in "salt-like" behavior (class A metal). Examples of a class A metals are many of the Group IA and IIA metals. Other metals form volatile gaseous compounds with hydrogen (class B metal). The metals on the right side of the periodic table, such as the hydrocarbons and the hydrides formed by arsenic, sulfur and lead typify class B metals. Finally, there are metals (class C metals) that participate in hydrogen occlusion or absorption. Of the class C metals, there are two types: those that absorb large amounts of hydrogen (e.g., Pd and Ti), and those that absorb, relative to the first class, low amounts of hydrogen (e.g., Fe, Cu).

Considering the class C metals, there are the endothermic and the exothermic occluders. When hydrogen is dissolved in a metal, the reaction from the atomic adsorbed hydrogen to the absorbed form results in an associated change in enthalpy which is positive or negative. This heat of solution, ΔH_{soln}, is on the order of 1-10 kcal/mole. If ΔH_{soln} is greater than zero, then the reaction is endothermic and the metal is called an *endothermic occluder*. Conversely, if ΔH_{soln} is less than zero, then the reaction is exothermic and the metal is called an *exothermic occluder*. Although subtle differences might be argued, the practical difference between the two classes is that the former allows minimal hydrogen absorption and the latter accommodates much hydrogen. Exothermic occluders are thought to absorb hydrogen into interstitial sites of

the metal lattice. Endothermic occluders are thought to be deformed severely by interstitial occlusion and thus, accommodate less hydrogen[6].

Table 2.B
Examples of Diverse Hydrogen Behavior by Element

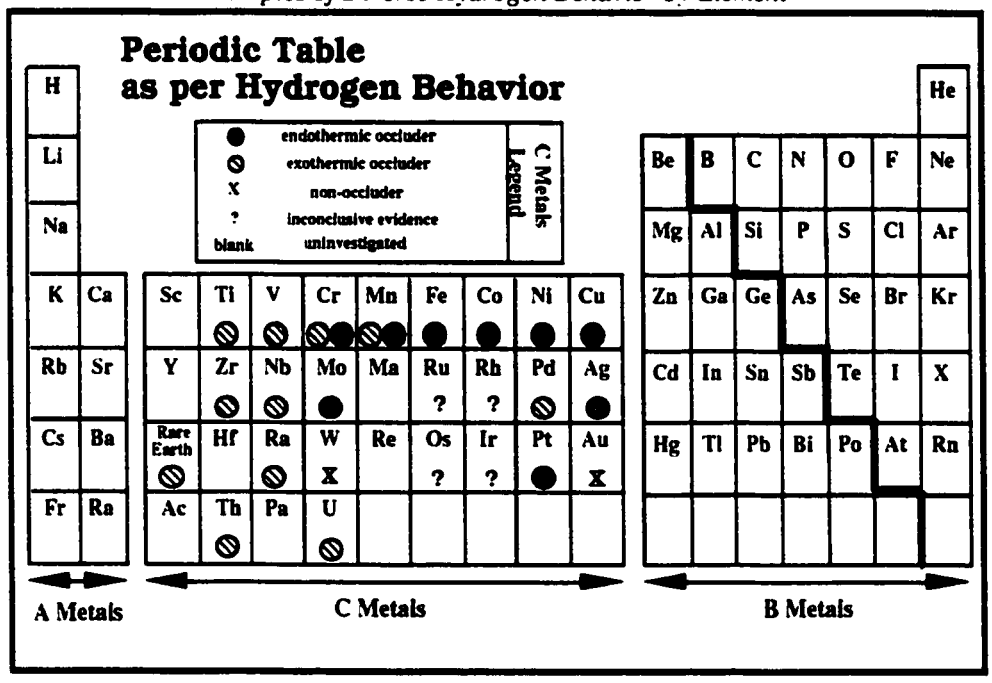

Figure 2.2 illustrates the effect of crystal structure on the solubility of hydrogen in an iron lattice. These structures have different size and different location interstices, resulting in different hydrogen behavior. Figure 2.3 displays the interstitial positions for the body-centered (α) iron lattice which is typical for steels used in electrogalvanizing operations. The largest interstitial site for α-iron occurs at (1/2, 1/4, 0). This tetrahedral site could accommodate an interstitial atom of 0.36Å radius. Dissolved hydrogen[7] has a radius of 0.46Å. Thus, when hydrogen is absorbed by a body-centered cubic structure (i.e., bcc-iron), distortion is likely. The ability of a metal to resist this distortion will define the solubility of hydrogen in the metal.

The solubility of hydrogen in iron and steel has been measured by many investigators, although most measurements and relations were performed at elevated temperatures. Figure 2.4 illustrates the effect of both temperature and pressure on the amount of hydrogen absorbed in low carbon steel. From such diagrams and from his own work, Sievert[8] derived the following relationship between the partial pressure, p, of hydrogen surrounding an iron piece and the solubility of hydrogen, C, within the metal under equilibrium:

$$C = A\, p^{-1/2} \exp(-B/T) \qquad \text{[Sievert's Law]} \qquad [2.8]$$

where A and B are constants and T is the temperature in degrees kelvin. Although A and B have been defined[6,9] by several workers, most of the definitions either only apply for elevated temperatures or were extrapolated to lower temperatures. Typical[10] solubility values for hydrogen in iron at one atmosphere and 25°C are predicted to be approximately one part in 10^8 by weight ($\sim 10^{-7}$ mol/cm^3). However, experimentally measured values are often higher.

Table 2.C shows several values for these constants as reported by various studies for use below 200°C. Several workers[6,11,12] have indicated that solubility versus temperature data below 390°C deviates from Sievert's Law. The two reasons proposed to explain this deviation are changes in the heat of solution[11] and hydrogen trapping[13]. It is enough to understand that the solubility of hydrogen in metals is hydrogen activity and temperature dependent and at lower temperatures ($T < 390$°C) the issue becomes complicated and may deviate from theory.

Table 2.C
Constants for Solubility Relations at Low Temperatures

A [mole $cm^3 atm^{-1/2}$]	B [°K]	T Range [°C]	Reference
1.48×10^{-2}	3280	< 400	Geller & Sun[6]
2.59×10^{-4}	3440	25	Quick & Johnson[9]

A and B are the temperature independent and dependent constants, respectively, which are used in equation [2.8] The "T Range" is the range of temperatures over which the constants were obtained from experimental results.

2.1.3.2 Hydrogen Diffusivity

Dissolved hydrogen in a metal is considered to be in one of three forms. The entry and diffusion of hydrogen occurs as neutral atoms[6], as protons[4], or as some form in between the two. In the latter two cases, the hydrogen donates its electron to the "sea of electrons" in the conduction band. The diatomic molecule, H_2, is not considered as a diffusing species because it would result in too much deformation of the iron lattice relative to an atomic species. In addition, the hydrogen flux through a metal sheet under steady-state conditions has been found[6] to be proportional to the square root of the hydrogen pressure up to pressures of 100 atmospheres. This experimental result follows the equilibrium described by reaction [2.1], thus strongly supporting the conclusion that hydrogen diffuses in the atomic form. Although studies[6,14] performed at higher pressures have given conflicting results, it has been suggested[15] that surface effects may be responsible for the anomalous behavior. Hence, in a specific sense, the form is unknown, however, more generally, the current view is that hydrogen enters, moves through and exits a metal in its atomic form.

Once hydrogen is absorbed into the metal, the hydrogen will redistribute in the metal to remove concentration gradients. There are five terms commonly used to describe motion of a solute species through or in a metal. They are the *effective*

diffusivity, the *apparent diffusivity*, the *true diffusivity*, the *lattice diffusivity* and the *permeability*. The effective and apparent terms are used synonymously, as are the true and lattice diffusivity terms. The diffusivities pertain only to the motion of hydrogen within the metal and is independent of environmental hydrogen concentration. On the other hand, the permeability is influenced by both the environment surrounding and the motion of hydrogen within the metal.

The difference between the true/lattice and the apparent/effective diffusivities is in the defects or inhomogeneities present in materials. The true diffusivity is the diffusivity of hydrogen in a fully annealed, ultra-pure, relatively defect free material. The term is generally reserved for elemental metals (e.g., Fe or Pd). The apparent diffusivity is that measured when impurity atoms, defects or any other surface or bulk effect is present that might influence the hydrogen motion (e.g., trap). The traditional method for measuring hydrogen diffusivities in metals has been the electrochemical or the gas-phase permeation techniques which will be discussed in detail in Chapter 3.

$$D = D_0 \exp(-Q/RT) \qquad [2.9]$$

The hydrogen diffusivity in steel, D, is a function of temperature, T and follows an Arrehnius relation, as in [2.9]. The parameters D_0, Q and R (the gas constant) are constants. Typical values of D_0 and Q, reported by various studies are listed in Table 2.D. Furthermore, Volkl and Alefeld[16] (1975) surveyed several studies from 1957 to 1971 which only measured room temperature, hydrogen diffusion values in iron. The values ranged from 1.4×10^{-8} to 8.3×10^{-5} cm^2/s and the mean was 3.3×10^{-5} cm^2/s.

Table 2.D
Arrehnius Constants for the Hydrogen Diffusivity in Iron at Low Temperatures

D_o [$cm^2 s^{-1}$]	Q [kJ mol^{-1}]	D(25°C) [$cm^2 s^{-1}$]	T Range [°C]	Reference
1.1×10^{-2}	36.41	4.56×10^{-9}	23-80	Barrer[16] (1940)
6×10^{-4}	5.57	6.33×10^{-5}	10-75	Beck[16] (1966)
2.2×10^{-3}	12.97	1.17×10^{-5}	10-100	Choi[17] (1971)
1.14	35.45	6.96×10^{-7}	23-84	Evans[16] (1969)
5.0×10^{-3}	14.23	1.60×10^{-5}	25-90	Frank/build-up[18] (1958)
1.9×10^{-2}	26.36	4.55×10^{-7}	25-90	Frank/decay[18] (1958)
1.2×10^{-1}	32.72	2.21×10^{-7}	25-200	Johnson[13] (1960)
6.5×10^{-2}	27.09	2.03×10^{-5}	15-60	Reiermann[16](1970)
6.1×10^{-2}	24.79	2.75×10^{-6}	15-60	Reiermann[16](1970)
3.65×10^{-3}	22.29	4.52×10^{-7}	25-650	Schwarz[16] (1965)
8.9×10^{-4}	12.76	5.13×10^{-6}	150-900	Stross[19] (1956)
7.6×10^{-4}	9.58	1.59×10^{-5}	100-800	Sykes[20] (1947)

All of these constants were obtained by testing high purity iron or annealed mild steel specimens. Several methods were used to obtain the data. The "T Range" is the temperature range over which the data was collected to calculate the constants.

2.1.3.3 Hydrogen Trapping

There were several anomalies in early diffusion studies which led to the description of new hydrogen behavior. Such anomalies may also be noted from Table 2.D. First, the values for D(25°C) vary by as much as a factor of 72. In addition, the activation energies for diffusion are either in the 10-12kJ or the 25-30kJ ranges. Furthermore, when an investigation, such as Frank[18] (1958) measured the D and Q values during hydrogen charging, why were the values different when the charging was stopped and the effusing hydrogen evaluated? Such behavior led researchers to believe that not all of the hydrogen entering a metal sheet was exiting even after long times.

Although many investigators have found an Arrehnius-type relation for diffusion of hydrogen at elevated temperatures, there is poor agreement[10] with theory below 400°C. Ham[6] (1938) and Darken[21] (1949) reported lower experimental

diffusivity values than the extrapolations from higher temperature theory would predict. Darken explained such deviations by suggesting the metal retains some of the diffusing hydrogen. Johnson and Hill[13] (1960) showed a change in activation energy, Q, from 12kJ/mole to 35kJ/mole for transitions from elevated temperatures to 200°C or lower. Johnson suggested that at higher temperatures (T> 200°C), hydrogen diffusion is dominated by an interstitial to interstitial hopping mechanism that gives rise to a lower E_a. However, at lower temperatures, some artifacts in the metal begin to dominate the hydrogen motion, thus increasing E_a. McNabb and Foster[22] assumed that hydrogen was delayed at fixed sites in the lattice called "traps." They classified such traps into three categories according to the difficulty in removing hydrogen from such traps. The three types are :

- *weak traps* artifacts having a negligible effect on delaying hydrogen motion.
- *strong traps* artifacts having a permanent effect on holding hydrogen.
- *active traps* artifacts whose attraction to hydrogen is between the strong and weak traps.

The trapping literature identifies these artifacts more specifically as voids, dislocations, or any other imperfection in the metal lattice, including precipitates or inclusions. It is true that this dissertation is primarily concerned with surface interactions, however, knowledge of the metal bulk and trapping behavior is critical to understanding the hydrogen permeation results to be discussed in Chapter 4.

2.2 Theoretical Analyses Used to Evaluate Hydrogen Permeation

Although Cailletet[23] (1864) first proposed hydrogen permeation through an alpha-iron sheet, mathematical analyses to help explain the hydrogen behavior did not

begin to appear until the late 1940's. Most of the analyses solve the second-order, parabolic equation for one-dimensional diffusion:

$$\frac{\partial C(x,t)}{\partial t} = D \frac{\partial^2 C(x,t)}{\partial x^2} \qquad [2.10]$$

where C represents the concentration of hydrogen in a sheet at a distance, x, from the surface and time, t. D is the hydrogen diffusivity. This is Fick's second law of diffusion.

Equation [2.10] can be conveniently applied to any system where one-dimensional diffusion takes place through a rectangular region ("the sheet") and where the hydrogen conditions outside this region can be defined. Typically, for such one-dimensional models, hydrogen is expected to enter one surface, move through the sheet and exit the other surface. To define such a situation, boundary conditions are chosen for the sheet's surfaces (denoted the 'entry' and 'exit' surfaces) and for the conditions inside the sheet. Typically, the surfaces are defined as having *constant hydrogen concentration* or *constant hydrogen flux*. It is common to define the sheet as being either devoid of hydrogen or as having some initial hydrogen distribution. The sheet may be further defined by the presence or absence of trapping sites and the addition of an additional term to [2.10].

The solutions to equation [2.10] are given in one of two forms. First, the solution may be given in terms of C(x,t). Such expressions are useful for defining hydrogen concentration profiles a sheet at any time, t. Alternatively, an expression may be obtained which defines the hydrogen flux at some time, t, relative to the steady-state

flux (i.e., $J(t)/J(\infty)$ or in terms of the current, $i(t)/i(\infty)$). This can be called the *relative rate of permeation*. To accomplish this action, Fick's first law of diffusion must be used,

$$J = \frac{i}{zF} = -D \frac{\partial C(x,t)}{\partial x} \qquad [2.11]$$

where J is the hydrogen flux through the sheet, i is the current density, D is the hydrogen diffusivity, z is the charge passed, and F is Faraday's constant. Utilizing equations [2.10]-[2.11] for time, t, and for time, $t=\infty$, will give $i(t)/i(\infty)$. Such an expression usually results in a simple equation that is in terms of variables which are all, but one, known from experimentation. Unfortunately, most of the analysis have complicated expressions for $C(x,t)$ that are in the form of a series or have distribution functions to integrate. Thus, to achieve the relative rate of permeation, requires the analysis to make several assumptions. Often higher order series terms are assumed to be negligible or that no hydrogen distribution exists at some initial time to allow such expressions to be obtained.

There are four types of analyses presented for the interaction of hydrogen with metals: *non-bulk/non-surface, non-bulk/surface, bulk/non-surface and bulk/surface* models. The code given here refers to the boundary conditions specified. Bulk and non-bulk are terms that indicate whether bulk phenomena (e.g., trapping, initial hydrogen distributions, etc.), beyond the diffusivity are taken into account. The surface and non-surface terms indicate whether or not hydrogen kinetics (e.g., hydrogen surface reactions or coverage) are considered for the surface of the sheet. Although the models will give approximately similar predictions for many cases, depending on the specific

system being studied, some models will be more appropriate than others. Two excellent sources for solving differential equations and the boundary conditions relevant to diffusion are by Crank[24] or by Carslaw and Jaeger[25].

2.2.1 Non-Bulk/Non-Surface Analyses

The first models applied to measure the permeation of hydrogen through a sheet were of the non-bulk/non-surface type. These models were primarily interested in obtaining expressions for the hydrogen diffusivity in pure metals such as palladium or alpha-iron. Equation [2.10] was solved using either Laplace[26,27] or Fourier[28,30] transformations. These solutions could be further distinguished by the use of error functions[26] or Taylor expansions[27] to approximate the functions present in the solutions. They may be presented as:

$$\frac{i(\tau)}{i(\infty)} \equiv \frac{2}{\sqrt{\pi\tau}} \exp\left(-\frac{1}{4\tau}\right) \quad \{\text{Laplace Solution: Error Function}\} \qquad [2.12]$$

$$\frac{i(\tau)}{i(\infty)} \equiv 1 - \exp(-6\tau) \quad \{\text{Laplace Solution: Taylor Expansion}\} \qquad [2.13]$$

$$\frac{i(\tau)}{i(\infty)} \equiv 1 - 2\exp\left(-\pi^2\tau\right) \quad \{\text{Fourier Solution}\} \qquad [2.14]$$

where $i(\tau)$ and $i(\infty)$ are the current densities at time, τ, and at long times, respectively. The time τ is equivalent to Dt/L^2, where t is the elapsed diffusion time and L is the sheet thickness.

Devanathan[28] defined several different "times" that could be distinguished during hydrogen permeation analyses. These times are useful for calculating the

hydrogen diffusivity and will also help illustrate the effects of different surface boundary conditions. The *break-through time*, t_b, is the time when hydrogen first leaves the metal through the exit surface. The *time-lag*, t_L, is that time when the relative current of permeation is equal to 0.6299. Plotting the natural logarithm of $(i(t)-i(\infty))/i(\infty)$ versus time allows the *rise time constant*, t_o, to be obtained. The slope of such a plot is equivalent to $1/t_o$. Finally, the *half-rise time*, $t_{1/2}$, is the time when the anodic current is one-half the steady-state value. These times have been used throughout the literature to obtain diffusivity values from electrochemical or gaseous permeation experiments. Since these times depend upon the relative current of permeation, boundary conditions chosen for a given analysis are significant. The expressions for the four time constants are given in Table 2.E. Chadhari[28] uses all of these times to determine diffusivity values from permeation data and gives a good review of their usage. The time-lag and the half-rise times are the two techniques most often encountered to measure the diffusivity.

Table 2.E
Comparing Boundary Conditions From Diffusivity Calculations

Condition	t_b	t_L	t_o	$t_{1/2}$
Constant Hydrogen Concentration[29]	$L^2/15.3D$	$L^2/6D$	L^2/π^2D	$0.14L^2/D$
Constant Hydrogen Concentration[26]	$L^2/15.3D$	$L^2/5.9D$	$L^2/4D$	$0.14L^2/D$
Constant Hydrogen Flux[30]	$L^2/13.0D$	$L^2/2D$	$L^2/2.49D$	$0.38L^2/D$
Constant Hydrogen Coverage[31]	$L^2/14.9D$	$L^2/3.6D$	$L^2/5.24D$	$0.224L^2/D$

This table was modified from one presented by Chadhari. The boundary conditions used to obtain the above expressions for the time constants are referenced. The solutions for C(x,t) obtained to calculate the time constants are all of the type Non-Bulk/Non-Surface. Although Pumphrey's[31] condition was decreasing flux in his paper, by assigning a constant S=2, Chadhari[28] argues this to be a constant coverage condition.

2.2.2 Bulk/Non-Surface Analyses

Similar solutions to equation [2.10] were obtained for the bulk/non-surface model types as in [2.12]-[2.14]. These solutions considered an initial hydrogen concentration in the sheet. Such concentrations were either defined as a position

function[17], f(x), or as a parameter[32] which represented the amount of absorbed hydrogen relative to the steady state amount. Both solutions as proposed by Choi[17] (1971) and Wu[32] (1987) were based upon techniques illustrated by Carslaw and Jaeger[25]. These techniques utilize Fourier transformations to solve [2.10], but have new complications in the boundary conditions within the sheet. Choi used the following initial and boundary conditions:

$$C(x,0) = 0 \qquad t=0;\ x < 0;\ x > L \qquad [2.15]$$

$$C(x,0) = f(x) \qquad t=0;\ 0 < x < L \qquad [2.16]$$

$$C(0,t) = C_o \qquad t>0;\ x = 0 \qquad [2.17]$$

$$C(L,t) = 0 \qquad t>0;\ L = 0 \qquad [2.18]$$

and found the hydrogen concentration of hydrogen to be expressed as:

$$C(x,t) = \frac{C_o x}{L} + \frac{2C_o}{\pi}\sum_{n=1}^{\infty}\left(\frac{\cos(n\pi)}{n}\right)\sin\left(\frac{n\pi x}{L}\right)\exp\left(-\left(\frac{n\pi}{L}\right)^2 Dt\right) + \frac{2}{L}\sin\left(\frac{n\pi x}{L}\right)\exp\left(\left(\frac{n\pi}{L}\right)^2 Dt\right)\int_0^L f(x')\sin\left(\frac{n\pi x'}{L}\right)dx' \qquad [2.19]$$

where C_0 is the concentration of hydrogen just inside the entry surface of the sheet at time t=0.

Wu[32] used Eqs. [2.15]-[2.18] as initial and boundary conditions, but assumed the entry surface hydrogen concentration would change from an initial value, C_0, to a final value, C_∞, during permeation. Hence, Wu subsitituted the following initial condition for Eq. [2.19]:

$$\frac{\partial C(0,t)}{\partial t} = B\,(C_\infty - C_o) \qquad t > 0;\ x = 0 \qquad [2.20a]$$

or

$$C(0,t) = C_\infty\,[(\lambda - 1)\exp(-Bt) + 1] \qquad t > 0;\ x = 0 \qquad [2.20b]$$

where B is a proportionality constant and λ is defined as C_o/C_∞. These assumptions provide an expression similar to that obtained by Choi[17], but with an added λ term that defines a non-steady state surface concentration in the sheet:

$$C(x,t) = C_\infty\left[(\lambda - 1)\,e^{-Bt} + 1\right]\left(\frac{L-x}{L}\right) + \sum_{n=1}^{\infty}\left[\frac{2C_\infty}{n\pi}\left(\frac{1-\lambda}{\frac{n^2}{\rho}-1}\left(e^{-Bn^2t/\rho} + e^{-Bt}\right) - \lambda\,e^{-Bn^2t/\rho}\right)\sin\left(\frac{n\pi x}{L}\right)\right] \qquad [2.21]$$

where

$$\rho = (B\,L^2/\,D\pi^2) \qquad [2.22]$$

The primary difference between the models proposed by these two investigators is that Wu is concerned with a changing surface concentration and the *amount* of hydrogen that could previously be present in the sheet, while Choi is interested in a constant surface concentration and both the *amount* and *position* of initial hydrogen.

As discussed in Section 2.1.3.3, a sufficient understanding of hydrogen traps has not yet been reached, however, two important concepts have been utilized in modelling the hydrogen permeation behavior. The first is that traps do exist and will significantly affect the diffusivity. Darken and Smith[21] (1949) first discussed trapping

and introduced the term "apparant diffusivity," which is distinct from the "true or lattice diffusivity." They related the diffusivity to the ratio of the total observed solubility and the lattice solubility.

Taking the idea one step further, McNabb and Foster[22] (1963) introduced the concept of "active trapping sites" to permeation modelling. Active traps did not simply trap hydrogen permanently, but could release the hydrogen if certain conditions were met. Thus, boundary conditions could now accommodate traps with different degrees of trapping strength. Unfortunately, the inclusion of such boundary conditions makes solving equation [2.10] difficult, if not impossible, with the exception of a few simple cases (e.g., no initial distribution, f(x), no detailed surface kinetics). The apparent diffusivity, D_{app}, was related to the lattice diffusivity, D, by:

$$D_{app} = \left(\frac{1}{1 + \left(\frac{Nk}{p}\right)}\right) D \qquad [2.23]$$

where N is the trap density, k is the trapping capture rate constant and p is the trapping release constant.

2.2.3 Non-Bulk/Surface Analyses

Iyer, Pickering and Zamanzadeh[33,34,35] introduced a new generation of hydrogen models with their "IPZ" model which could relate the hydrogen permeation to the rate constants of the hydrogen reactions occurring on the entry surface of the sheet. Instead of solving equation [2.10], Iyer, et al., considered the rates for the charging, recombination, absorption and permeation processes. Using equilibrium relationships,

they were able to relate permeation data to the rate constants, surface coverages and electrochemical constants (e.g., transfer coefficient) for the hydrogen surface reactions.

The IPZ model concentrates on the sheet surfaces to gain its information. Although the hydrogen diffusivity is necessary to complete the analysis, it is assumed rather than calculated from the model. Thus, bulk effects are neglected by this model. To utilize the IPZ model, it is necessary to obtain a polarization curve ($\log i_c$ vs η) for the entry surface of a metal foil and obtain the steady-state permeation current for each step in the polarization curve. Using this information and the equilibrium relationships that could be established[36] between the different hydrogen surface reactions, the IPZ model is able to gain information about each of the three hydrogen surface reactions, [2.1]-[2.6]. This model is the only analysis to gain information on the individual reaction rates on the entry surface from permeation data, however, the analysis requires rigorous experimental conditions.

2.2.4 Bulk/Surface Analyses

Finally, Makhlouf and Sisson[37] used heat transfer theory to include both surface and bulk effects in their permeation analysis. They simplified the entry hydrogen reactions to a single term, the *convective mass transfer coefficient*, h, while trying to include trapping effects. Makhlouf and Sisson were trying to solve modified equations from McNabb and Foster[22]:

$$\frac{\partial C(x,t)}{\partial t} + N\frac{\partial n}{\partial t} = D\frac{\partial^2 C(x,t)}{\partial x^2} \qquad [2.24]$$

$$\frac{\partial n}{\partial t} = KC(1 - n) - pn \qquad t > 0;\ 0 < x < L \qquad [2.25]$$

where C is the hydrogen concentration in the sheet at position, x, and time, t. N is the trap density in the sheet, n is the fraction of traps that are full, p is the release rate constant for a given trap and K is the rate constant for the trapping of hydrogen. They rewrote Eqs. [2.24]-[2.25] in terms of dimensionless variables:

$$\frac{\partial u}{\partial \tau} + \frac{\partial \omega}{\partial \tau} = \frac{\partial^2 u}{\partial X} \qquad [2.26]$$

$$\frac{\partial \omega}{\partial \tau} = \lambda u - \nu u \omega - \mu \omega \qquad [2.27]$$

where

$u = C(t)/C_\infty$ = relative concentration of diffusing hydrogen

$\omega = nN/C_\infty$ = relative concetration of trapped hydrogen

$\tau = Dt/L^2$ = reduced time

$X = x/L$ = relative distance

and

$$\lambda = \frac{NKL^2}{D}\ ;\quad \nu = \frac{C_\infty KL^2}{D}\ ;\quad \mu = \frac{pL^2}{D} \qquad [2.28]$$

They solved these equations using a finite difference method and assuming the following initial and boundary conditions:

$$u(x, 0) = \omega(x,0) = 0 \qquad t=0;\ \text{all } x \qquad [2.29]$$

$$-D\frac{\partial u(0, \tau)}{\partial x} = h\{u(0, \tau) - 1\} \qquad x=0 \qquad [2.30]$$

$$u(L, \tau) = 0 \qquad x=L \qquad [2.31]$$

Using the above equations, the authors perform several simulations which show the effects of the trapping parameters, λ, ν, and ω upon permeation behavior. In addition, they show that the parameter h is sensitive to the entry of hydrogen into the metal from a given environment. While this idea is good in concept, there were several problems with their analysis. Unfortunately, when trying to apply their analysis to experimental data, they were required to simplify their equations to the point where no trapping analysis could be performed. Their equations were simplified to:

$$J_\infty = -h(C_f - C_\infty) \qquad t=\infty;\ x=0 \qquad [2.32]$$

$$J_\infty = -D\frac{C_\infty - 0}{L} \qquad t=\infty;\ 0 < x < L \qquad [2.33]$$

$$J_\infty = 0 \qquad t=\infty;\ x=L \qquad [2.34]$$

where J_∞ is the steady-state hydrogen flux, C_∞ is the subsurface concentration of hydrogen at steady-state conditions and C_f is the equivalent of the fugacity of hydrogen in the electrolyte. This leaves three equations with six unknowns.

To reduce the number of unknowns, the authors chose to use a palladium coated surface as a standard and perform two permeation experiments: 1) with a Pd film on both surfaces and 2) with a Pd film only on the exit surface. They assumed that a palladium film elliminates all surface effects, thus, h would be large for a Pd coated surface and during such a permeation test, Eq. [2.33] could be neglected. Manipulating Eqs. [2.32]-[2.34] for the two experiments yields:

$$\frac{J_\infty^{Pd}}{J_\infty} = 1 + \frac{D}{hL} \qquad [2.35]$$

Although this approach is good in concept, there are several problems. First, while trying to simplify their equations, they claim that a palladium coating would make 'h' very large and thus, remove all surface effects. Yeager[38] has shown that despite the high hydrogen solubility in Pd, hydrogen absorption into Pd is significantly affected by metal surface morphology . Secondly, the analysis completely ignores the kinetics on the exit surface. Finally, a Pd coating will be removed by the substantial hydrogen evolution resulting from the application of a current density above 1-2 mA/cm^2. Hence, their analysis could only be utilized under very low current densities.

2.2.5 Limitations of the Analytical Models

A model which can adequately evaluate the hydrogen behavior in low carbon steel resulting from a wide variety of surface treatments must meet the following requirements:

1) The model must account for both surface and bulk phenomena as they affect hydrogen.
2) The fundamental parameters of the model must relate to real quantities or properties.
3) The fundamental parameters of the model must be obtained by simple algebra and experimental data.
4) The model must be able to handle multiple processes or environments on either side of a sheet and previously absorbed hydrogen in a sheet.
5) The model must be able to relate the fundamental parameters to actual hydrogen concentrations and distributions in a sheet.

Although the previous models are quite adequate for specific applications, , none of the previously described models can meet all of the above requirements. Although the models proposed by McNabb[22], Iyer[33-35] or Makhlouf[37] are satisfactory, they are either bulk-specific, surface specific or too simplified, respectively, to meet all of the requirements.

The set of criteria listed above has been suggested based upon the problems discussed with the above models. #1 is given so that all phenomena may be taken into account or studied. #2 and #3 are given so that the model is acquiring some quantity that is both useful and is easily obtained. To be complete, the model should be adaptable to any environmental condition on either side of the sheet, in addition to conditions within the sheet. Thus, #4 is suggested so that the model is independent of the experimental procedure. Finally, #5 is given to insure the hydrogen concentration as a function of position and time in the sheet is obtained. Such a distribution can predict the amount and location of hydrogen in a sheet exposed to a hydrogen environment for any time period desired.

2.3 Effect of the Controlling Parameters upon Hydrogen Behavior

Hydrogen may enter a steel sheet from a variety of sources on a plating line. After rolling, the steel undergoes several degreasing, cleaning and pickling steps before plating. These steps are designed to remove any rolling oils or surface oxides which remain from the production and thickness reduction of the steel sheet. These steps provide a uniform surface for plating. Once the zinc coating is applied, any hydrogen absorbed from previous processes is essentially trapped in the sheet.

The interaction between hydrogen and iron or steel has been well documented in several reviews[6,9,39]. Specific studies have emphasized the effects of pH[40,41], cathodic current[42,43,44,45], electrolyte agitation[46], or surface finish[37] or hydrogen diffusion[47,48]. However, most of these studies have been conducted under benign conditions (i.e., low current densities and minimal agitation). The electroprocesses (the electrocleaning, electropickling and electroplating steps) in steel plating lines operate under severe conditions of electrolyte pH, high current densities (-100 to 500mA/cm^2) and vigorous

agitation (line speeds of 90 to 150 m/min). Thus, there is a need to evaluate those parameters which may be controlled on an electrogalvanizing line at the more severe conditions. The following section will review the effects of these factors on hydrogen absorption or permeation in steel.

2.3.1 Effect of pH, Current and Overpotential on Hydrogen Absorption

Section 2.1.2 discussed several reactions that occur when steel is placed in a hydrogen environment. Although the reaction rates vary on different metals, it is evident that the modification of one of the reactions (e.g., the hydrogen discharge reaction) may affect the others (e.g., the hydrogen absorption reaction).

Often the hydrogen kinetics on various metals are characterized by the rate determining step for hydrogen evolution. It is known that the rate determining step on some metals changes with the supplied driving force. On iron, it has been established[45] that the rate determining step for hydrogen evolution is a coupled discharge-chemical desorption mechanism (equations [2.2] and [2.5]). This mechanism holds in both acidic and basic solutions, except when the applied overpotential exceeds 1V in alkaline solutions. In the latter case, the rate determining step is electrodic desorption (equation [2.6]).

Although equations [2.2]-[2.3] illustrate that the hydrogen discharge reaction is dependent on both the activity of hydrogen in solution and the supplied driving force, the application of external current is not required. Equation [2.36] shows that during the corrosion of iron, hydrogen ions can be reduced on the metal surface. This type of hydrogen reduction can result in hydrogen absorption. Studies[40,42] performed upon steel disagree as to which acids (HCl, H_2SO_4, H_3PO_4 and $HClO_4$) result in the most

hydrogen absorbed, however, all of the studies agree that metals exposed to acidic environments are susceptible to hydrogen absorption.

$$Fe + 2H^{+} \text{ ---> } Fe^{2+} + 2H_{ads} \qquad [2.36]$$

Experiments[21] under low cathodic current densities have shown that as the pH decreases, the amount of hydrogen uptake increases. In addition, Vagramyan[49] found the amount of hydrogen trapped in iron decreased drastically with increasing pH (from pH = 1 to pH = 3 at 25°C).

In addition to the studies of hydrogen activity, the effect of supplied current can be significant to hydrogen absorption. In 1922, Bodenstein[39] first proposed a relationship between the amount of hydrogen permeating a metal membrane and the applied cathodic current density (i_c) for constant pH. However, since that time several investigators[39] have found differing behavior. Raskov[6] described these differences by four regions on a permeability (P) versus $i_c^{1/2}$ plot (see figure 2.5). At very low current densities, there is a linear relationship between P and i_c (microAmps in and microAmps out). However, as i_c is increased, the relationship becomes more complicated and at very high i_c's, P becomes independent of current density. Finally, the minimum i_c necessary to reach this latter region is a function of both temperature and sheet thickness.

A permeability versus $i_c^{1/2}$ plot was suggested based upon the relationship between surface coverage of hydrogen and absorbed hydrogen. It was thought that at equilibrium, these two quantities would be proportional to one another. Rearranging and inserting into Fick's second law gives an expression where the steady-state flux, J.

is proportional to the surface coverage, θ, of hydrogen. For low coverages ($\theta < 0.1$), it has been shown[43] that :

$$\theta \propto \sqrt{i_c} \qquad [2.37]$$

and hence, for the same conditions,

$$J \propto \sqrt{i_c} \qquad [2.38]$$

The deviation from linearity shown in Figure 2.5 illustrates that the above condition of low coverages does not hold over all cathodic currents.

Equations [2.2]-[2.7] are indicative of the effects of adsorbed hydrogen on the hydrogen kinetics upon a metal surface. Controlling the cathodic current density influences the hydrogen flux at the cathode surface, however, by fixing the working electrode potential, the hydrogen surface coverage will be controlled. There have been many studies[43,45,46,50,51] of the effect of working electrode potential upon hydrogen absorption in iron or various steels. There were two significant conclusions: 1) the overpotential necessary to maintain a given i_c decreased with decreasing pH; and 2) the authors found the surface coverage of hydrogen to increase with increasing overpotential.

2.3.2 The Effect of Electrolyte Agitation upon Hydrogen Absorption

The effects of flow on transport processes can be significant. Typically in an electrochemical cell where two polarized electrodes are separated by an electrolyte, the ions may be transported towards (or away from) an electrode by three parallel

mechanisms: diffusion, migration and convection. The total flux of ions towards an electrode is the sum of each of the three contributing mechanisms.

Ions migrate from the bulk solution to the near region of the electrode. From this near region, the ions diffuse to the electrode surface. The size of the near region is defined by the dominance of the convection mechanism. Ions may be consumed (or produced) at an electrode faster than the migration or diffusion mechanisms can supply them. Hence, nearest to the electrode, a region may exist which will be depleted (or will contain an excess) of ions. If the convection mechanism is negligible, the diffusion layer, which forms across the near region shortly after current is applied to the cell will expand to form a concentration gradient extending the distance from the anode to the cathode. Such a situation could exist if the solution between the anode and cathode is stagnant.

Alternatively, if the electrolyte is agitated, the convection mechanism becomes more important in determining the ion concentration at the electrode surface. This results in a diffusion layer which extends only a short distance into the electrolyte from the electrodes. The thickness of the diffusion layer will depend on the electrolyte flow velocity and distribution and upon the fluid kinematic viscosity and diffusivity. Since the hydrogen discharge reaction is dependent upon hydrogen ions moving to the electrode surface, it is expected that by agitating the electrolyte the HDR will be enhanced and thus, will increase the amount of hydrogen absorbed.

2.3.3 The Effect of Surface Finish upon Hydrogen Absorption

Not much work has been reported on the effect of surface finish upon hydrogen behavior in steels. Makhlouf[37] found a 43% increase in permeation flux with a 180 grit

surface versus a 600 grit polished surface. Since Makhlouf was using the permeation results obtained from AISI 440 steel to illustrate his model, minimal or no information was reported as to his charging conditions.

Although steady-state permeation currents were not compared, Lee[52] reported the effects of mechanical polishing upon the hydrogen behavior in metals. Lee reported that polishing the surface with a one micron finish resulted in a deformation layer ~2.5μm thick. The authors showed that such deformation layers can affect the permeation of hydrogen via trapping phenomena.

2.4 Effect of Steel Surface Contaminants on Hydrogen Absorption

With regards to contaminants on steel, there were two studies which introduced a new phenomenon to the hydrogen-metal community. In 1936, a study[39] was published which reported the flux of hydrogen through a steel sheet increased in the presence of certain metal contaminants. In 1949, Bockris[53] reported that approximately one adsorbed arsenic atom per nickel surface atoms was sufficient for increased hydrogenation of the nickel electrode. These studies suggested not only that surface contaminants could affect the hydrogenation of a metal, but that only small concentrations were required.

The effect of various metal contaminants upon hydrogen uptake in iron or steel has been well studied, however sufficient understanding is still lacking. Many lists of the most damaging contaminants (i.e., those elements which result in the most hydrogen absorbed) have been proposed:

As > Se > Te > Sb > S > P > Bi > Hg > Pb	Baukloh[54]
P > S > As > Se > Sb > Te > Bi	Smialowski[39]
As > Se > Te	Kuznetsov[54]
Se > As > Te > Sb > S > P	Bardenheur[54]
As > Se > Te > S > Pb > Bi	Radhakrishnan[54]
S > P > Se > Te > As	Newman[55]

This list of conflicting results emphasizes the multiple methods used, the author's disregard for the concentration[51,56], pH[51,55] and/or polarization[57] dependence of these contaminants.

Since these contaminants increase the hydrogenation of the metal (i.e., promote the hydrogen absorption reaction), these species are called "promoters." The promoters may be found in several forms and may be classified as follows:

a)	*Group VA & VIA elements:*	P[55,58], As[53,54,55,57], Sb[54]; S, Se, Te[54,55]
b)	*Anionic Species:*	CNS^- (rhodanide)[51]; CN^- (cyanide), I^- (iodide)[46]
c)	*Carbon Species:*	CS_2 (carbon sulfide), CO (carbon monoxide), CON_2H_4 (urea)[55]; CSN_2H_4 (thiourea)[51,55]
d)	*Other Species:*	Pb[51,55]; Hg, Sn, F^-, Br^- [51]; napthalene[47,51]; Ce, Cu[56]

Most of the evidence reported in the literature is for the classes a)-c), while scanty and contradictory results have been reported for class d).

There are also several species known to decrease hydrogen absorption. These species may be broken into contaminants and coatings. Although the effect of a continuous coating is discussed in Section 2.4, the following contaminants have been reported in the literature to decrease the hydrogenation of metals:

e)	*Organic Species:*	nitriles[47]; C, S, O[59]
f)	*Metallic Species:*	Hg, Sn, Bi[54]; Cu, Ni, Ag[56]; square grid coatings[60] of Pt, Ni, Cu; implanted Pt[61]

Several ideas have been hypothesized to explain the increased hydrogenation by these contaminants. Shuler[54] (1949) proposed that the phenomenon is the result of the contaminant interacting with the adsorbed hydrogen in such a way to affect the iron-hydrogen bond energy. The contaminant would partially bond with the adsorbed hydrogen, resulting in a change in Fe-H bond strength. Parsons[62] (1951) found the adsorption of certain contaminants to saturate the adsorptive powers of noble metal surfaces. This would increase the energy levels of the remaining sites available for hydrogen adsorption and increase the surface coverage of hydrogen. Smialowski[39] (1955) postulated that formation of a volatile hydride was critical to increasing the hydrogen absorption reaction. This theory was based upon the fact that the Group VA and VIA elements all form volatile hydrides at large negative overpotentials. However, from the list given above, many of the species do not form hydrides (e.g., any of the anionic species), yet result in enhanced hydrogenation. Finally, Evans[63] (1961) suggested that the contaminants on a metal surface may interfere with or "poison" the recombination step and promote the hydrogen absorption reaction.

There are several problems with the results reported and the mechanisms proposed to explain promotion. First and foremost, there are conflicting results for many species. For example, lead and mercury have been included in both the list of promoters and those species which decrease hydrogenation. This primarily emphasizes the wide variety of conditions over which many of the studies were taken. As previously mentioned, many contaminants have concentration, pH and polarization dependencies. Thus, the lists that have been given should be taken with some caution. Furthermore, the metal hydride argument appears to have merit for the Group VA and VIA elements, however, the findings of McCright[57] clearly suggest that a volatile hydride is not

necessary. In addition, if the promoter-hydride bond strength has anything to do with the alteration of the iron-hydrogen bond, then anything adsorbing to iron except Hg, Cd and Zn would affect the iron-hydrogen bond energy (see table 2.F). Along similar lines, Bockris[64] proposed that since many promoters are electron rich, they don't interact with the hydrogen, but instead with the electronic shell of the iron atom. This would perhaps reduce the activation barrier for hydrogen entry.

Table 2.F
Metal-Hydride Bond Energies

H-Hg	9.5	**H-Pb**	42 ± 5	**H-Cr**	67 ±12	**H-S**	82 ± 3	**H-H**	104.21 ± 0.01
H-Cd	16.5	**H-Te**	64 ± 1	**H-Ni**	69 ± 3	**H-P**	82 ± 7	**H-OH**	119 ± 1
H-Zn	20.5	**H-As**	65 ± 3	**H-I**	71	**H-Pt**	84	**H-CN**	120
H-Fe	30 ± 3	**H-Bi**	66.7	**H-Se**	73 ± 1	**H-Br**	87.4		
H-Ti	~38	**H-Cu**	67 ± 2	**H-Au**	75	**H-Cl**	103.2		

The bond energies are given in kcal/mol. All values were obtained from the CRC Handbook of Chemistry and Physics[65] except for the value for iron which was obtained from Squires[66].

It is evident that the mechanism for hydrogen promotion via contaminants is still on the "phenomonological" level. It is clear that small amounts (less than a monolayer) of contaminants on a steel surface can increase the amount of hydrogen absorbed. Unfortunately, here is where the agreements end and the debates begin.

Although the hydrogen reactions on iron[47, 67, 68] and lead[69, 70, 71] have been investigated in depth, the effect of a partial lead coating on a metal and its influence upon the hydrogen kinetics has yet to be fully understood. Most of the literature pertinent to a lead-steel-hydrogen study may be grouped into the following classifications: (i) heavy metal impurity-induced embrittlement[72, 73, 74], (ii) lead-acid battery phenomena[75, 76, 77], (iii) protective coatings acting as barriers to hydrogen[60, 78, 79] and (iv) cathodic poisons catalytically affecting hydrogen kinetics[41,53,54,57,80]. The first category emphasizes

bulk effects between hydrogen and metallurgical variables, while the second category concentrates on non-ferrous impurities on lead substrates. Thus, it is of interest to evaluate the effect of lead impurities on a steel substrate. Much of the third category investigates continuous coatings on steel as effective barriers to hydrogen. Although the lead-steel system has been studied, there have been conflicting results reported. Hence, understanding the effect of a partial lead coating on steel is still lacking. The final group has exclusively investigated the Group IVA and VA metals. Although some cases[51,55] mention the effect of Pb impurities on hydrogen reactions, the effect, relative to arsenic or sulfur, is considered to be small, thus no data was shown and any effects were neglected in the discussion. Thus, it is of interest to perform a detailed study of lead impurities present both in an electrolyte and as a lead deposit upon steel.

2.5 Effect of a Coating on Steel upon Hydrogen Absorption

To physically affect the hydrogen absorption reaction, an electrodeposit or coating may be used as a barrier to hydrogen. Chatterjee[60] (1978) suggests that for a coating to be effective, it must be thick, continuous and impervious. Alternatively, a continuous coating that possesses a diffusivity that is much less than that in the base metal may be used as a good barrier candidate.

A coating on steel has generally been found to delay the hydrogen permeation through steel. There have been three different types of studies performed in the past:

- Hydrogen Absorption During the Plating of Iron or Steel
- Hydrogen Absorption Through Previously Coated Steel or Iron
- Ductility Experiments of Aged and Non-Aged Plated Steel

The most common study of the three types is that which evaluates the hydrogen absorbed during a plating operation. The difficulty inherent to this type of study is the problem of obtaining a continuous electrodeposit. Most of these studies were conducted by permeation testing. Although in all cases, the coating resulted in a decrease in hydrogen flux versus a non-plated steel, the anodic current never decreases to zero. Such behavior is indicative of two possible phenomena. First, the deposit is not a barrier to hydrogen, or secondly, holes or small perforations are present in the deposit. The following electrodeposited coatings have been examined in this fashion: Cr, Ni[42,60,78,79], Cd[50,61], Fe[50], Sn[60,61], Pb[60,78,79], Co[79].

The second category above is a true test of the barrier effectiveness of a coating to hydrogen permeation. Chatterjee[60] performed permeation tests upon continuous and discontinuous coatings. He looked at electrodeposited Pt, Cu and Ni coatings on iron. He found all to decrease the amount and flux of hydrogen through the membranes. He also deposited these coatings in a square grid pattern. Although the coatings were not continuous, the partial coatings decreased the amount of hydrogen absorbed. Thus, there are two effects a coating can play with respect to hydrogen permeation. There is the "barrier" effect and the "catalytic" effect. The former blocks hydrogen from entering the steel, while the latter affects the hydrogen kinetics on the steel surface. Although there have been other studies[60,61], these were upon continuous, thermally evaporated coatings (Cd, Al, Mg, Zn, Zn-Pb) and exhibited similar behavior.

During typical electrogalvanizing processes, the low carbon steel sheet will be sent through a number of plating cells (sometimes up to 20). In each cell, zinc is deposited upon the steel substrate until a full thickness (3-15 micron) is reached. Although efficiencies are often high (~92%) during the zinc plating operations due to

the high overvoltage of hydrogen on zinc, some hydrogen is reduced upon the steel during zinc deposition. Zeilmaker[42] suggests the maximum influx of hydrogen takes place during the initial stages of plating and then, decreases sharply over time. Kudryautsev[81] suggests that the zinc coating satisfies Chatterjee's criterion[60] after the deposit reaches thicknesses of between two and seven microns. This is consistent with studies that examined partial Zn coatings and their effect upon hydrogen permeation[82]. Although these groups were studying the hydrogen permeation during metal deposition and porous coatings were probably formed due to the geometry of the permeation cell, the substantial reduction of hydrogen flux in these studies supports the current thinking of zinc as a barrier to hydrogen egress from steel.

2.6 The Effect of Metallurgical Variables upon Hydrogen Absorption

Hydrogen movement in steel has been found to be affected by two metallurgical factors: impurity elements and microstructural considerations. Furthermore, such factors should be grouped further into surface and bulk effects. Surface effects change the coverage of hydrogen on the metal surface or alter the hydrogen fugacity outside the metal. Bulk effects influence the hydrogen behavior in steel by acting as hydrogen sinks or sources.

Table 2.G
Effect of Alloying Elements on Hydrogen Absorption

Element	Effect on HAR	Element	Effect on HAR
Al [83]	-	P [84,85]	+
C [84]	+	S [84,85]	+
Cr [6,84,85]	+	Si [84,85]	-
Cu [84]	-	Ta [6]	+
Mn [84,85]	+	Ti [6,83,84,85, 86,87,88]	+/-
Mo [87,88,89]	?	V [6,84]	?
Nb [6]	+	Zr [6]	+
Ni [85]	?		

References are given in brackets. The code is + for increased, - for decreased hydrogenation, +/- indicates that the hydrogenation effect is dependent upon processing, and ? indicates conflicting results have been reported.

Alloying elements are often added to iron during the steel making process to increase corrosion resistance, promote second phase formation and increase formability of the steel: Al, C, Cr, Cu, Mn, Mo, Nb, Ni, P, S, Si, Ta, Ti, V and Zr. Since the steel of interest here is that which is electrogalvanized for automotive applications, the amount of such elements added to iron is of limited quantities (<0.5wt.% C and <0.2wt.% others). Although many of the studies performed to study the effect of such alloying additions did not perform metallurgical investigations to back up their conclusions, the trends which were observed and are listed in Table 2.G. Virtually all of the studies were conducted by mechanically testing steels of different compositions and evaluating the susceptibility to hydrogen embrittlement. Furthermore, almost all the studies emphasized that the behavior noted from a particular element appeared to have synergistic effects with other elements (particularly C, N and S contents).

Microstructural effects are keyed to the mechanical stress state in the lattice. The amount of hydrogen absorbed is affected by inclusion density, size, shape[84], steel phase[6], crystal structure[90] and the amount of mechanical working performed[91]. The results from such studies indicate that the denser the atomic packing, the more dislocations in the surface region, and the higher the stress state in the lattice, the less hydrogen will be absorbed. In fact, the current indication[9] is that the stress state in the lattice is much more important to determining the hydrogen solubility than the elastic or chemical properties of the inclusions present.

The two steels of particular interest to this work are the low (< 0.05 wt% C) and the ultra-low (<0.005 wt% C) carbon steels. Two elements that are present in such steels and provide both a chemical and a microstructural influence on the steel are

carbon and titanium. The more carbon present, the higher the strength of the steel, the more brittle the steel may become and the more hydrogen may become trapped. Titanium is added to steels to insure all supersaturated carbon precipitates from the solid solution as titanium carbide particles. As a result, the ultra low carbon steels with titanium additions are called "stabilized" steels.

If the solidification of the steel from high temperatures into the ferrite region of the iron-carbon phase diagram is rapid, then carbon can be retained in the solid solution. The carbon will precipitate out of solution over time, even at room temperatures. The precipitation results in a finely dispersed set of iron carbide particles, Fe_3C, in the steel. This precipitation process is called "aging" or more formally, "quench aging." It results in increased hardness, yield strength and tensile strengths, a decrease in elongation and reduction of area in a tension test, an increase in transition temperature of ductile to brittle fracture in a notch impact test and a decrease in magnetic permeability[92].

Table 2.H
Standard Formation Free Energies for Carbide Formers

Reaction	-A [kJ/mol]	B [J/mol°K]	$\Delta G°_{298}$ [kJ/mol]	T Range [°C]
$3Fe(s) + C(s) = Fe_3C(s)$	-25.94	-23.14	19.04	25-190
$3Fe(s) + C(s) = Fe_3C(s)$	-26.69	-24.77	19.31	190-840
$Ti(s)\alpha + C(s) = "TiC"(s)$	183.05	10.08	-180.05	25-882
$V(s) + C(s) = VC(s)$	24.10	6.28	-98.96	900-1100
$Zr(s) + C(s) = "ZrC"(s)$	184.51	9.20	-181.77	25-1900

A and B are constants[92] that allow the linear equation $\Delta G = A + BT$. The quotes on the compound indicate a non-stoichiometric compound.

To avoid "quench aging" in steels one of two procedures are performed. The steel can be cooled relatively slowly to avoid rapid supersaturation of the carbon. Steel held in the temperature range of 540° to 315°C for a few minutes[92] typically is not susceptible to aging. An alternative to such heat treatments and the procedure currently

in use today is to decarburize the steel. This can be done with the addition of certain alloying elements which are aggressive carbide formers. Table 2.H gives a list of several elements that form carbides and their standard formation free energies[92]. Although the free energy of formation would depend on several factors (e.g., temperature, activity of element added and carbon in ferrite), the table allows useful comparisons to be made regarding the thermodynamic driving force for carbide formation relative to cementite (Fe_3C). It is evident that the elements Ti, V and Zr have significantly larger driving forces than iron to form carbides.

During the solidification of ferrite, the solubility of carbon decreases significantly with temperature. However, due to the slow diffusional transformation to form Fe_3C, a period of aging is expected. Such aging processes result in variable mechanical properties over a period of time. If it is not necessary to maintain a minimal amount of carbon in the steel, a post-solidification heat treatment may reduce the aging period to a negligible time. However, to remove the carbon from solution and minimize aging effects, aggressive carbide formers (e.g., Ti, Nb, V) are often added to the steel. The solubility of TiC in ferrite is almost negligible, hence, precipitation is quick and efficient.

The interaction between hydrogen and titanium carbide precipitates has been well documented[39,93,94,95,96,97,98], however, such studies were performed upon high strength steels with significantly more carbon present. When stabilization is desired, extra titanium is added to insure all the carbon precipitates out of the iron solution. Previous studies have focussed exclusively upon the influence of TiC upon the hydrogen transport processes in the steel bulk and have neglected the effect of the "excess titanium" present. Although there have been studies[99] of titanium additions to

ultra low carbon, iron alloys, these have also centered upon bulk interactions with hydrogen. Thus, there is a need to study the hydrogen behavior in ultra low carbon steel. Since hydrogen absorption results directly from surface reactions, there is a need to understand the effect of titanium and titanium carbide on such reactions.

References for Chapter 2

1 B.E. Conway and J.O'M. Bockris, J. Chem. Phys., 26, (1957) pp. 532-541.

2 M. Pourbaix, Atlas of Electrochemical Equilibria in Aqueous Solutions, NACE, Houston, TX, 1974.

3 G. Kortum and J.O'M. Bockris, Textbook of Electrochemistry, vol. II, Elsevier, Amsterdam, 1951. Also, J.O'M. Bocris and A.K.N. Reddy, Modern Electrochemistry, vol. 2, Plenum Press, New York, 1970.

4 C.E. Sims, Gas in Metals,ASM, Cleveland, Ohio, 1953, pp149-150.

5 D.P. Smith, Hydrogen in Metals, University of Chicago Press, Chicago, IL, (1948).

6 E.E. Fletcher and A.R. Elsea, *DMIC Report 219*, (1965) pp. 1-80.

7 R.D. McCright, Dissertation, Ohio State University, 1971.

8 D.R. Gaskell, Introduction to Metallurgical Thermodynamics, 2nd edition, Hemisphere Publishing Corporation, New York, 1981, pp. 473.

9 J. P. Hirth, *Met. Trans. A*, **11A** (1980) pp. 861-890.

10 P. Shewman, Diffusion in Solids, 2nd edition, Minerals, Metals and Materials Society, Warrandale, PA, 1989, p. 122.

11 M.L. Hill and E.W. Johnson, *Trans. Met. Soc. AIME*, **221** (1961) pp. 622-629.

12 P.L. Chang and W.D.G. Bennett, *J. Iron Steel Inst.*, **170** (1952) pp. 205-213.

13 E.W. Johnson, M.L. Hill, *Trans. Met. Soc. AIME*, **218** (1960) pp. 1104-1112.

14 C.J. Smithells and C.E. Ransley, *Proc. Roy. Soc. Lond.* , **A150**, (1935) pp. 172-197.

15 W.L. Bryan and B.F. Dodge, *A.I.Ch.E.J.*, 9[2] (1963) pp. 223-228.

16 J. Volkl; G. Alefeld; in Diffusion in Solids; Recent Developments, eds. A.S. Nowick, J.J. Burton, Academic Press, New York, 1975, pp. 281-283.

17 J.Y. Choi, *Met. Trans.*, 1 (1970) pp. 911-919.

18 R.C. Frank, D.E. Swets, D.L. Fry, *J. Appl. Phys.*, **29** (1958) pp. 892-898.

19 T.M. Stross, F.C. Tompkins, *J. Chem. Soc. (Lond)*, (1956) pp. 230-234.

20 C. Sykes, H.H. Burton, C.C. Gegg, *J. Iron Steel Inst.*, **156** (1947) pp. 155-180.

21 L.S. Darken and R.P. Smith, *Corrosion*, **5**, (1949) 1-15.

22 A. McNabb and P.K. Foster, *Trans. of TMS AIME*, **227** (1963) pp. 618-627.

23 L. Cailletet, *Compt. Rend.*, **58**, (1864) 327.

24 J. Crank, The Mathematics of Diffusion, Oxford University Press, New York, NY (1956).

25 H.S. Carslaw and J.C. Jaeger, Conduction of Heat in Solids, Clarendon Press, Oxford, U.K., (1959).

26 J. McBreen, L. Nanis, W. Beck, *J. Electrochem. Soc.*, **113**, (1966) pp. 1218-1222.

27 S.K. Yen and H.C. Shih, *J. Electrochem. Soc.*, **135**[5] (1988) pp. 1169-1170.

28 B.S. Chaudhari and T.P. Radhakrishnan, *Corr. Sci.*, **30**[12] (1990) pp. 1219-1234.

29 M.A.V. Devanathan and Z. Stachurski, *Proc. Roy. Soc. Lond.*, **270A** (1962) pp. 90-102.

30 Zuchner reference in B.S. Chaudhari and T.P. Radhakrishnan, *Corr. Sci.*, **30**[12] (1990) pp. 1219-1234.

31 P.H. Pumphrey, *Scripta Met.*, **14** (1980) pp. 695-701.

32 E. Wu, *J. Electrochem. Soc.*, **134**[9] (1987) pp. 2126-2133.

33 R.N. Iyer, H.W. Pickering, I. Takeuchi, M. Zamanzadeh, *Scripta Met.*, **22** (1988) 911-916.

34 R.N. Iyer, H.W. Pickering, M. Zamanzadeh, *J. Electrochem. Soc.*, **136**[9] (1989) 2463-2470.

35 R.N. Iyer, H.W. Pickering, *J. Electrochem. Soc.*, **137**[11] (1990) 3512-3514.

36 B. E. Wilde, C.D. Kim, *Corrosion*, **42**[4] (1986) pp. 243-245.

37 M.M. Makhlouf and R.D. Sisson, Jr., *Met. Trans.*, **22A**, (1991) 1001-1006.

38 R.R. Adzic, D. Gervasio, I. Bae, B. Cahan, and E. Yeager, *NSF/EPRI Workshop on Anomalous Effects in Deuterated Materials*, Washington, D.C., October 16-18, 1989, pp. 1-17.

39 M. Smialowski, Hydrogen in Steel, Pergamon Press, Oxford & Addison-Wesley Publishing, Reading Massachussetts, (1962): pp.88-90.

40 R.M. Hudson, *Corrosion*, **20** (1969) p.24t.

41 J.O'M. Bockris, *Chem. Rev.*, **43** (1948):525-577.

42 H. Zeilmaker, *Electrodepos. & Surf. Treat.*, **1** (1972/73): p. 109.

43 J.O'M.Bockris, Proceedings of Stress Corrosion Cracking and Hydrogen Embrittlement of Iron Base Alloys, NACE, 1973: p. 286.

44 J.O.'M. Bockris, J. McBreen, L. Nanis, *J. Electrochem. Soc.* **112**, [10](1965): p. 1028.

45 K. Bolton, L.L. Shreir. *Corrosion Sci.*, **3** (1963): pp. 17-33.

46 M. Shirkhanzadeh. *Corrosion Sci.*, **2** (1988): 201-206.

47 W. Beck, J. O'M. Bockris, J. McBreen, L. Nanis. *Proc. Roy. Soc. Lond.*, **290A** (1965) 191-206.

48 A. S. Nowick, J.J. Burton. Diffusion in Solids, Academic Press, New York, (1975) pp. 281-284.

49 A.T. Vagramayan, Y.S. Petrova. The Mechanical Properties of Electrolytic Deposits, Consultants Bureau, New York, (1962).

50 M.A.V. Devanathan, Z. Stachurski, W. Beck, *J. of Electrochem. Soc.* **110**, [8](1963): pp. 886-890.

51 T. Zakroczynski Hydrogen Degradation of Ferrous Alloys, R. A. Oriani, J. P. Hirth, M. Smialowski, eds., Noyes Pubs., Park Ridge, NJ, 1985, pp. 215-250.

52 J.-L. Lee, J.T. Waber, Y.-K. Park. *Scripta Met.*, **20** (1986) pp. 823-828.

53 J. O'M. Bockris and B. E. Conway. *Trans. of the Faraday Soc.*, **45** (1949) 989-999.

54 T. P. Radhakrishnan and L. L. Shreir. *Electrochimica Acta*, **11** (1966) 1007-1021.

55 J. F. Newman and L.L. Shreir, *Corrosion Sci.*, **9** (1969) 631-641.

56 I. Singh and M. Singh, *Corrosion*, **43**[7] (1987) 425-429.

57 R.D. McCright and R.W. Staehle. *J. Electrochem. Soc.*, **121**[5] (1974) 609-618.

58 E.M. Riecke, B. Johnen and R. Moeller. *Corrosion Sci.*, ?

59 P.L. Andrew and A.A. Haasz. *J. Vac. Sci. Tech. A*, **8**[3] (1990) 1807-1813.

60 S.S. Chatterjee, B. G. Ateya and H.W. Pickering, *Metall. Trans.*, **9A** (1978) 389-395.

61 M. Zamanzadeh, A. Allam, H.W. Pickering and G.K. Hubler. *J. Electrochem. Soc.*, **127**[8] (1980) 1688-1693.

62 R. Parsons and J. O'M. Bockris. *Trans. of Far. Soc.*, **47** (1951) p. 914.

63 U. R. Evans, The Corrosion and Oxidation of Metals: Scientific Principles and Practical Applications, Arnold, London, (1961), p. 397.

64 J. O'M. Bockris, A. Damjanovic and R.J. Mannan. *Electroanal. Chem. & Interfac. Electrochem.*, **18** (1968) 349-361.

65 Handbook of Chemistry and Physics, 63rd edition, R.C. Weast ed., CRC Press, Boca Raton, FL, (1982), pp. F-185-189.

66 R. R. Squires, *J. of Amer. Chem. Soc.*, **107** (1985) pp. 4385-4390.

67 A. Saraby-Reintjes, *Electrochimica Acta*, **31**[2] (1986) pp. 251-254.

68 C.D. Kim, B.E. Wilde, *J. Electrochem. Soc.*, **118**[2] (1971) pp. 202-206.

69 M.N.C. Ijomah, *J. Electrochem. Soc.*, **134**[12] (1987) pp. 2960-2966.

70 D.J.G. Ives, F.R. Smith, *Trans. Far. Soc.*, **63** (1967) 217-233.

71 H.W. Salzberg, *J. Electrochem. Soc.*, **100**[4] (1953) pp. 146-151. Continued in L.W. Gastnirt, H.W. Salzberg, *J. Electrochem. Soc.*, **104**[12] (1957) pp. 701-703.

72 A. Druschitz and P. Gordon, Embrittlement by Liquid and Solid Metals, M.H. Kamdar ed., Metallurgical Soc. of AIME, Warrendale, PA, (1984) pp. 285-315.

73 S. Mostovoy and N.N. Breyer, *Trans. ASM*, **61**, (1968) pp. 219-232

74 J.J. Lewandowski, Y.S. Kim and N.J.H. Holroyd, *Metall. Trans. A*, **23A** (1992) pp. 1679-1689.

75 K. Vijayaamohanan, S. Sathyanarayana, *J. Power Sources*, **30**[1-4] (1990) pp. 169-175.

76 H. Sanchez, Y. Meas, I. Gonzalez, M.A. Quiroz, *J. Power Sources*, **32** (1990) pp. 43-53.

77 C.Y. Chan, A.T. Kuhn, *Oberflache-Surface*, **20**[1] (1979) pp. 7-14.

78 H. P. Tardif and H. Marquis, *Can. Metall. Quart.*, **1** (1962) pp. 153-171.

79 I. Matsushima, H.H. Uhlig, *J. Electrochem. Soc.*, **113**[6] (1966) pp. 555-559.

80 H. Ferber, H. Kasten, G.K. Wolf, W.J. Lorenz, H. Schneickert, H. Folger, *Corr. Sci.*, **20** (1980) pp. 117-128.

81 V.N. Kudryautsev, et.al., Metal-Hydrogen Systems, ed. T.N. Veziroglu, Pergamon Press, New York, (1981) pp. 251-258.

82 S. Rashkov, C. Bozhkov, V. Kudryavtsev, K. Pedam, S. Bagaev, *J. Electroanal. Chem.* **248**, (1988): p. 421.

83 B.D. Kal'ner and V.I. Malkin, *Prot. of Metals*, **15**[2] (1979) 169-170.

84 E. Lunarska, *Hydrogen Degrad. of Ferr. Alloys*, R.A. Oriani, J. Hirth, M. Smialowski, eds., Noyes Publications, Park Ridge, New Jersey, (1985): pp. 712-736.

85 A. W. Thompson, I. M. Bernstein, Advances in Corrosion Science and Technology, vol. 7, eds. M.G. Fontana, R.W. Staehle, Plenum Press, New York, 1980, pp. 53-175.

86 L. W. Vollmer, *Corrosion*, **8** (1952) 326-332.

87 E. Snape, *Corrosion*, **24** (1968) 261-282.

88 J.A. Marquez, I. Matsushima, H.H. Uhlig, *Corrosion*, **26** (1970) 215-222.

89 G. Sandoz, *Met. Trans.*, **2**, (1971) 1055-1063.

90 R.D. McCright, *Proc. of SCC & HE of Iron Base Alloys*, NACE, France (1973).

91 B. E. Wilde, T. Shimada, *Scripta Met.*, **22** (1988) p.553.

92 The Making, Shaping and Treating of Steel, 10th ed., eds. W.T. Lankford, Jr., N.L. Samways, R.F. Craven, H.E. McGannon, AISE, Herbick & Held, Pittsburg, PA. (1985), pp. 1283-1287.

93 S. Linderoth and A.V. Shiskin, *Phil. Mag. A*, **55**[3] (1987) 291-300.

94 P.H. Pumphrey, Hydrogen in Metals, Bernstein & Thompson, eds., AIME, New York, (1981) 105-111.

95 B.G. Pound, *Acta Metallurg.*, **38**[12] (1990) 2373-2381.

96 B.G. Pound, *Acta Metallurg.*, **39**[9] (1991) 2099-2105.

97 V.P. Pancheshnaya, V.M. Knyazheva, Zh.V. Klimenko and M.M. Anotova, *Prot. of Metals*, **16**[6] (1980) 550-556.

98 G.M. Pressouyre and I.M. Bernstein, *Metallurg. Trans. A*, **9A** (1978) 1571-1580.

99 K. Yang, M.Z. Cao, X.J. Wan and C.X. Shi, *Scripta Met.*, **22** (1988) 1373-1378.

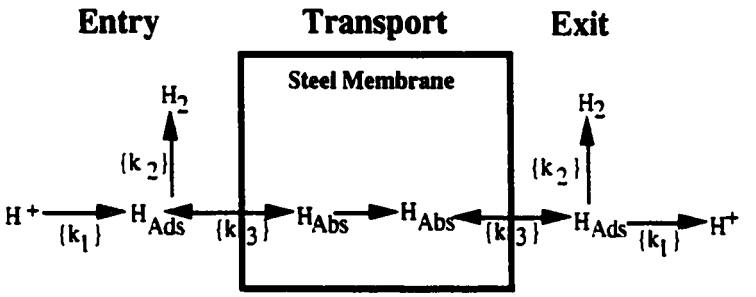

Entry Processes:

$H^+ + e^- + Fe \leftrightarrow FeH_{ads}$	(Hydrogen Discharge Reaction)
$2FeH_{ads} \leftrightarrow H_2 + 2Fe$	(Hydrogen Recombination Reaction)
$FeH_{ads} \leftrightarrow FeH_{abs}$	(Hydrogen Absorption Reaction)

Transport Processes:

- Diffusion of Hydrogen
- Trapping of Hydrogen
- Hydride Formation

Exit Processes:

$FeH_{abs} \leftrightarrow FeH_{ads}$	(Hydrogen Absorption Reaction)
$2FeH_{ads} \leftrightarrow H_2 + 2Fe$	(Hydrogen Recombination Reaction)
$FeH_{ads} \leftrightarrow H^+ + e^- + Fe$	(Hydrogen Discharge Reaction)

Figure 2.1: The above diagram illustrates the primary reactions between hydrogen and a metal immersed in a hydrogen environment.

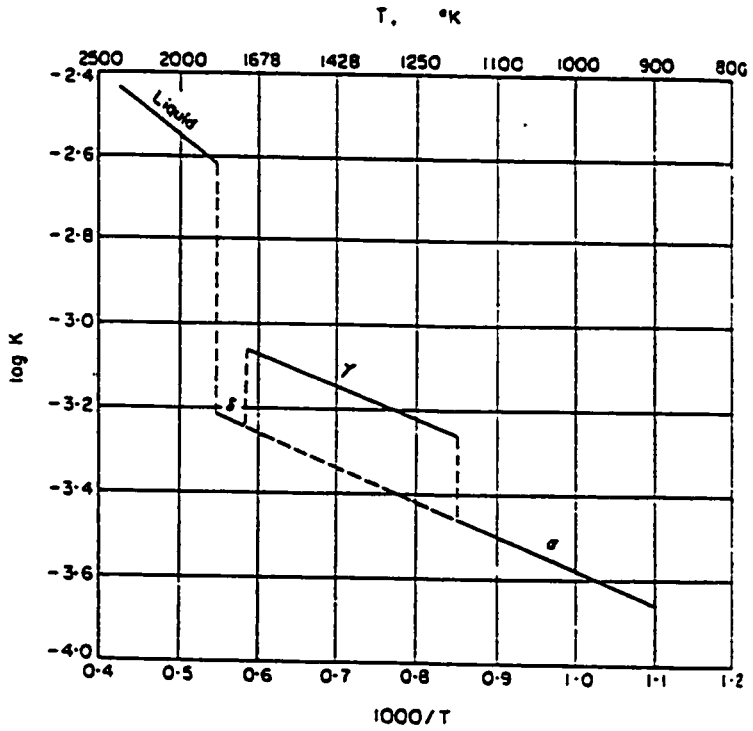

Figure 2.2: The effect of crystal structure on the solubility of hydrogen is shown for iron. This figure was adapted from Smialowski[39].

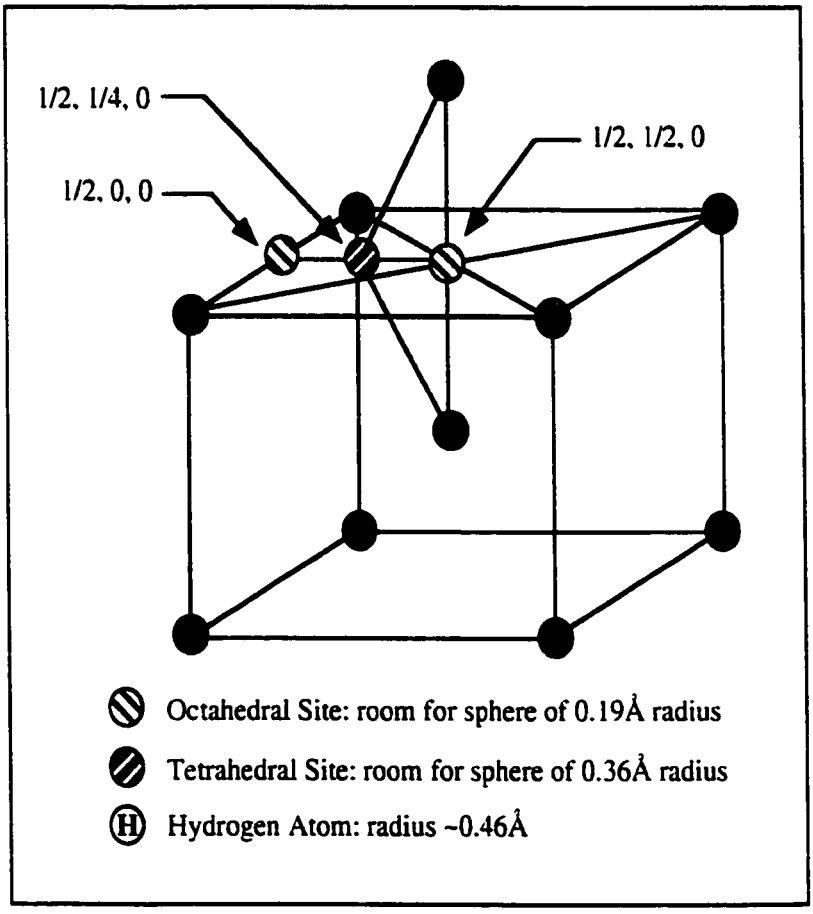

Figure 2.3: The most likely positions for hydrogen to occupy once absorbed in a base-centered cubic lattice are the interstitial locations noted above. This figure was adapted from Fletcher[6].

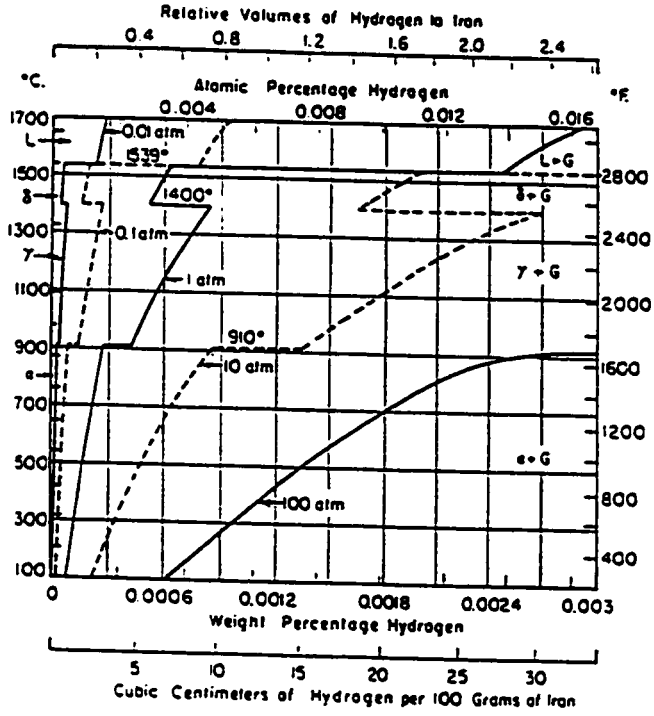

Figure 2.4: The effect of temperature and pressure on the amount of hydrogen absorbed from gaseous environments in a low carbon steel is shown above. This figure was adapted from Sims[4].

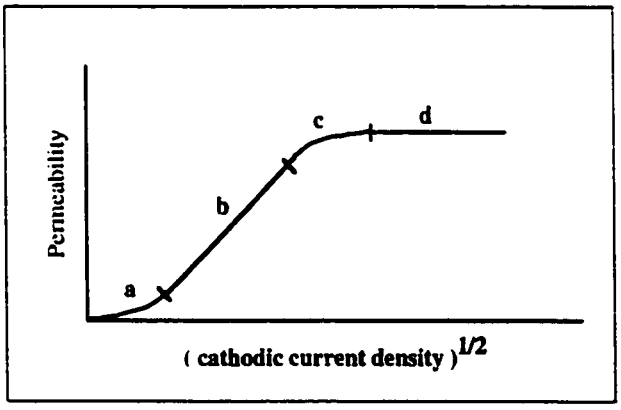

a: $P \alpha i_c$

b: $P \alpha i_c^{1/2}$

c: P = complex $f(i_c)$

d: $P \neq f(i_c)$

Figure 2.5: The proposed relationship between the steady-state hydrogen flux, J, and the cathodic current is shown above. This figure was adapted from Fletcher[6].

Chapter 3
Materials and Methods

This chapter emphasizes the materials used, the experimental techniques and procedures used during this investigation. Due to the diversity of conditions used for the different sets of experiments, the emphasis here will be on the techniques. For the specific conditions of a particular experiment, refer to the appropriate results section in Chapters 4-8. Since the materials preparation and solutions used depend upon the techniques utilized during this study, it will be useful to describe the *methods* before the *materials*.

3.1 Methods - Techniques to Identify Hydrogen in a Material

There are several available techniques (see Table 3.A) to measure the amount of hydrogen in materials. However, the electrochemical methods have some distinct advantages. To simulate and study the electrogalvanizing environment, these advantages become necessities.

The electrogalvanized plating of steel is an electrochemical process. The most satisfying approach to study such a process is utilizing a technique that mimics the plating process. Although the electrochemical methods to be described below are not used in all cases to plate zinc on steel, they are usually used to reduce the hydrogen on the steel or one of the other electrodes present. Thus, the methods to be described are techniques which will allow the study of hydrogen reduction and its interaction with steel.

In addition to simulating the plating process, electrochemical tests have the ability to provide a large range of driving forces for a particular process to take place.

Very large hydrogen activities may be provided on the steel surface. This flexibility provides a very convenient tool to study the reactions occurring on the steel surface.

Table 3.A
Techniques to Measure Hydrogen in Materials

Technique		Pros versus Cons
Permeation	(Gas)	Pros: consistent; yields kinetic and C_0 information. Allows atomically clean surfaces to be characterized. Cons: very surface sensitive. Requires thin specimens.
	(Electrochemical)	Pros: consistent; yields kinetic and C_0 information. Allows very high fugacities to be maintained. Cons: information is function of electrolyte. Best results require thin specimens.
Barnacle		Pros: Similar to electrochemical permeation test; Only requires the anodic cell; good for previously H exposed specimens; portable! Cons: information is a *f*(electrolyte); adhering to specimen may be a problem. Good for comparative purposes only.
Potentiostat Double Pulse		Pros: From a single cell, charge hydrogen in, then draw out. Controllable charging and retrieving hydrogen environment. No delay between charging and withdrawing. Information about trapping and HAR. Cons: When polarization is switched, the situation is not immediately defined. Alkaline electrolytes must be used when testing steel specimens to prevent anodic dissolution.
Auger Electron Spectroscopy		Pros: Compare AES line shapes to gain bonding & charge transfer information; Cons: Subjective, indirect; surface sensitive; vacuum may promote outgassing.
Reflection Electron Energy Loss Microscopy		Pros: Allows phases of dissolved H or hydrides to be distinguished; not a function of the surface topography. Cons: vacuum promotes outgassing.
Secondary Ion Mass Spectroscopy		Pros: Shows specifically the location of H on the surface and as a depth profile of the specimen. May show segregation of traps. Mass spectroscopy analysis detects hydrogen directly. Cons: The vacuum promotes outgassing; isotope tagging method analyzes D, not H; for comparative purposes only.
Nuclear Reaction Analysis		Pros: Quantifiable to 1mm depth. Gives consistent C_0 information. Cons: Sensitive to 100ppm+; specimens must be sent to SUNY; Bombardment may change surface structure.
Volumetric-Vacuum Extraction		Pros: Consistent estimates of hydrogen solubility. Cons: not as sensitive as other techniques, no kinetic information.

Finally, most other techniques (see Table 3.A) used to measure hydrogen in a system, do so indirectly, while the electrochemical methods measure direct changes in the hydrogen processes occurring on the steel.

3.1.1 Methods - The Permeation Test

The electrochemical permeation technique allows the accurate measurement of the instantaneous rate of permeation of electrolytic hydrogen through a metal membrane. The technique may be described by two separate three-electrode cells, sharing a common working electrode. On one side of the working electrode is the cathodic cell. Cathodic polarization of the working electrode surface produces a high hydrogen activity at that surface via water reduction. Such reduction processes are measured by the cathodic current. This procedure allows a wide range of hydrogen fugacities to be achieved and maintained on the metal surface. The working electrode is a metal membrane that is made from the material of interest. On the other side of the working electrode is the anodic cell. Anodic polarization of this surface provides a low hydrogen activity. Due to the concentration gradient, hydrogen moves from the cathodic surface, through the membrane to exit into the anodic cell. Once the hydrogen has reached the membrane surface exposed to the anodic cell, it is oxidized and the resulting current is measured. Since the amount of hydrogen entering and leaving the specimen is directly proportional to the current measured, by measuring the anodic and cathodic currents, very accurate determinations of the permeating hydrogen may be obtained. Typical information extracted from a permeation current versus time curve are identified in figure 3.1.

Electrochemical permeation tests[1] were conducted on low carbon steels. These tests were performed to fulfill two primary objectives. First, it was of interest to distinguish bulk differences in hydrogen permeability. Secondly, it was necessary to understand the effect the different surface treatments had upon the hydrogen surface reactions.

The experiments were carried out in two cylindrical glass cells of either 70ml or 500ml size. The cells had separate chambers for an auxiliary and a reference electrode. The auxiliary and the reference electrode were separated from the main cell by a glass frit and a Luggin capillary tube, respectively.

The auxiliary electrodes in the anodic and cathodic cells were a platinum sheet (2.54 x 2.54 cm^2) and a dimensionally stable anode (2.54 x 2.54 cm^2 mesh), respectively. Saturated calomel electrodes were used as reference electrodes in both cells. The test area of the working electrode exposed in both cells was 1.767 cm^2 (for the 70ml cells) or 2.480 cm^2 (for the 500ml cells). Both chambers of the permeation cell were deaerated with N_2, bubbled through distilled water before entering the main cell. The anodic cell was potentiostatically polarized to +0.450 V-SCE. The anodic current was monitored prior to testing until the current was less than 1 $\mu A/cm^2$. The cathodic cell was filled with solution and the permeation test was conducted galvanostatically. To obtain accurate working electrode potentials a current interrupt technique was adopted. For the non-room temperature tests, a separatory funnel, wrapped with heating tape was used to continually add fresh solution to the cathodic cell. The solution would exit from the cell via a stop cock and be recycled into the separatory funnel. This procedure allowed satisfactory ($\pm 2°C$) temperature control. The data were collected by an 80286 type computer utilizing a Metrobyte DASH8 board and

Labtech Notebook. The equipment used and the arrangement are illustrated in figure 3.2.

3.1.2 Permeation Cell Designs

The two cell designs illustrated in Figures 3.3 and 3.4 utilize several advantages over previous designs. Both cells use wide silicone rubber gaskets to interface between the cells and the specimen. Although several types of gaskets were experimented with, this type was found to be superior to hard rubber gaskets (e.g., O-ring seals) because of their flexibility, ability to resist leaks and lack of crevice corrosion susceptibility (i.e., more surface area). The cell in Figure 3.3 utilizes multiple ports to allow insertion of electrodes or bubblers and to add solution. The glassware for this cell fits in a Teflon sleeve which has fittings for the gaskets. The entire apparatus is supported by a single C clamp. This system allows the cells to be assembled and manipulated conveniently. The fact that the diameter of the cell is larger than the test area allows the hydrogen which evolves to move off the specimen and collect in the cell and not on the specimen. The cell in Figure 3.4 has built in ports for the reference and auxiliary electrodes. The cells are sealed together with an O-ring clamp. For this design, each cell must be supported by a single clamp. The glass tube closest to the specimen surface is sloped to prevent bubbles from collecting on the specimen surface. Both cells take advantage of stopcocks to quickly remove solution from the cells.

There are several experimental difficulties that may be avoided by proper cell design. A good cell design will have the following features:

- the cell must allow simple and reproducible assembly.
- the cell must be easily cleaned.

- the cell must allow evolving hydrogen to leave the specimen surface.
- the cell must allow solution to be flushed and added
- the seals between the cells must be flexible and reliable.

Although many designs could be used, there are several concerns. First, if many tests are to be performed, then maintaining a simple design will insure consistency and convenience. Secondly, the high sensitivity of the permeation test to ppm levels of chemical impurities requires that the cell be thoroughly cleaned before each test. Furthermore, since most designs include rigid cells, it is necessary to find a flexible material to interface between the cell and the specimen. This will provide a water-tight seal which will prevent crevice corrosion from occurring. Additionally, during a permeation test, there are several features which are convenient. Having several ports on the cell for adding and removing solution make the cells more flexible in terms of the kind of tests that may be run. Finally, at higher currents, there can be significant hydrogen evolution. If the cell is not designed to help remove these bubbles, they may rest on the specimen surface and promote corrosion (more specifically, a lack of cathodic protection) and will change the charging conditions.

3.1.3 Recognizing Anomalous Permeation Curves

One of the advantages of the permeation experiment, is that the anodic current versus time curve is an excellent tool to determine whether a test is being performed properly. There are at least four different types of curves that may be acquired from a given test.

Figure 3.5 shows a permeation curve from an ideal test. There are several points of interest from such a curve. First, the initial part of the curve is the noise level in the

system prior to the start of a test and is considered to be a zero level until hydrogen begins permeating the foil. When hydrogen begins to exit the foil, there is a gradual rise to a steady-state plateau. The remaining curves (figures 3.6 - 3.8) show anomalous behavior either in the rise of the curve or in the plateau and are considered to be non-ideal curves.

Figure 3.6 is an example of "noisy behavior." Such a curve has jumps in current of $0.4\mu A/cm^2$ or more and a wavy appearance. Such behavior is typical of crevice corrosion during the permeation test. It is caused by gaskets which are either too tight and are buckling or are too loose and are leaking.

In addition, if a spike occurs in the anodic curve, immediately after initiation of the test, as in Figure 3.7, then problems may arise in interpreting the results. These spikes appear to shift the noise level to higher currents and thus, make diffusivity calculations impossible. Such a situation is indicative of applying too large a voltage drop across the double layer. In practical terms, the system has been shocked. To minimize such "shocks," two procedures should be followed. Never apply a large cathodic potential/current when the system is not under some previous potential/current control. A good guideline is to never "step" the potential/current by more than a factor of ten. Whenever, possible, "ramp" the potential/current quickly to the desired condition. Only step the potential/current when necessary and only at low magnitudes.

Figure 3.8 is an example of non-steady state permeation behavior. Notice the rise in the curve to a maximum and then a decrease to a relatively steady-state plateau. This is indicative of a change in the surface or subsurface of the foil. Such behavior is usually the result of environmental conditions (e.g., current density, hydrogen activity)

that are high or severe. Conditions of this type are thought to be changing the surface over the course of the test, thus the change in hydrogen behavior. When this behavior was obtained, two permeation currents were used to obtain the κ discussed in Chapter 4. A value was taken at the maximum in the curve and at the steady-state point. This method was performed to get upper and lower bounds for the value of κ. Hence, when this procedure was used in Chapters 5-9, a "max" and a "stdy-st" label will be attatched in tables and a shaded range will be given in figures.

The four curves discussed here illustrate several possible curves which may arise during a permeation test and how to recognize them. Usually unusual behavior can be explained by some effect on the entry surface of the foil. Although these are not the only examples of anomalous behavior, these were the most commonly encountered during the research leading to this dissertation.

3.1.4 The Current Interrupt Technique

To measure the potential of the working electrode during a galvanostatic experiment, there are two options:

a) Using a reference electrode, a voltmeter and a Luggin capillary tube measure the voltage on the voltmeter between the reference and the working electrode.

b) Use a reference electrode, a Luggin capillary tube, a potentiostat/galvanostat with IR correction capability, a voltage programmer (e.g., PAR 175 programmer) and an oscilloscope.

The first option will measure the potential at the working electrode, however, this value will also include unwanted voltages due to the IR drop from solution effects (e.g., bubbling) and the geometry of the cell. Such measurements under high charging

conditions can present problems because the IR drop (i.e., ohmic resistances) may be larger than the value of interest.

The second option is designed to identify the amount of IR drop due to a particular charging condition and allow a more accurate value of the working potential to be obtained. It is called the *current interrupt* technique[1-2]. There are several modern potentiostat/galvanostats that can handle this technique: in this study the BC1200 was used. Figure 3.2 illustrates the equipment and the connections made for this method.

To perform current interuption, the BC1200 is run in galvanostat mode, but the programmer (e.g., a PAR175), which is fed into the galvanostat, controls the voltage. The programmer is set to switch the current on and off quickly. This is done so that the BC1200 can also measure the potential of the working electrode. The potentiostat can only measure the potential if the galvanostat is shut off. Hence, this technique is a method of tricking the potentiostat! If this current on and current off is done quickly, the galvanostatic condition is effectively unchanged. For the PAR 175, the largest ratio to current on and off is 11:1 (the current is on 11/12 and off 1/12 a time period). By setting the pulse frequency of the programmer to 1kHz, the current is on 11/12 of a millisecond and off for 1/12 of a millisecond. To this point, only the overall potential (i.e., the working electrode potential + the overpotential due to IR effects) has been measured.

To remove the IR influences from the measured potential requires the use of an oscilloscope. Feeding the output voltage from the potentiostat to the oscilloscope (use the DC input) allows the signal from the programmer-BC1200-cell to be studied. Using the on/off pulsing from the programmer produces a strange square wave signal

on the oscilloscope (see figure 3.9a). The straight lines indicate when the current is on and the curved lines are the decay of the potential when the current is shut off. It is this decay curve that will allow the IR drop to be identified and allow a more accurate working electrode potential to be obtained.

On several modern potentiostats is a feed-back circuit called either "IR bridge" (BC1200) or "IR correction" (PAR 173). Using these feed-back circuits, the voltage going to the oscilloscope (the actual cell conditions remain as before) may be adjusted to bring the bottom of the decay curve up to a point where it almost connects with the original "on" signal (see figure 3.9b). Moving the curve up too high (figure 3.10a) is the "over corrected" situation and the working electrode potential noted will be too low. Not moving the curve up high enough (figure 3.10b) results in the "under corrected" situation with some IR voltages still affecting the measurement and the working electrode potential will be too high. The dial on the feed-back circuit allows the IR drop for this condition to be calculated and the voltage now read from the potentiostat is a "corrected" value for the working electrode potential. Such procedures were performed on every galvanostatic permeation experiment.

3.2 Methods - The Barnacle Test

The barnacle technique[3,4] is an electrochemical method utilizing the anodic cell of a permeation test to evaluate relative amounts of hydrogen in metals previously exposed to hydrogen environments. The technique and analysis are described elsewhere[5]. If a non-uniform hydrogen distribution is present in a metal sheet, then the following equation[7] may be used to obtain the solubility, C_S, of hydrogen just inside the metal surface. This situation would hold if the part were cathodically polarized in a

hydrogen environment for a short time and barnacle tested before the hydrogen could redistribute:

$$\frac{i(t)}{zF} = C_s \sqrt{D\pi} \left(\frac{1}{t} - \frac{1}{\sqrt{t + t_o}} \right) \qquad [3.1]$$

i_t is the anodic current density at some time, t, during the anodic discharge of hydrogen. The diffusivity, D, measured from a permeation test, and t_o, the time spent in cathodic polarization of the specimen are also noted.

The barnacle technique may be used to obtain the *hydrogen injection potential.* The hydrogen injection potential is defined as the value of C_s after thirty minutes of barnacle testing has elapsed. It is used to characterize an environment's ability to inject hydrogen into a substrate.

Steel specimens were charged in the solution of interest for thirty minutes. Thirty minutes was chosen as a charge time so that significant differences between the solutions might be observed more easily. After 30 minutes of charging, the solution was dumped. The cell was flushed with deionized water and methanol. The anodic connections were then made and 0.1M NaOH solution was added. The anodic current and potential versus time were monitored. After 40 minutes the experiment was stopped.

	Process Information	Information Depth	Detection Limits	Typical Advantages
SEM EDS	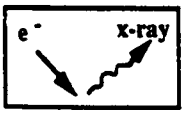	1 micron Na - U	Bulk only 50-100ppm	Photos to 40000x
AES		20 Angstroms Li - U	10^{-1} 1000ppm	Surface Feature ID Good Spatial Resolution Surface Chemical Info
SIMS	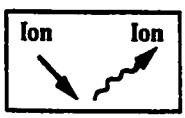	10 Angstroms H - U	10^{-5} 1ppm	General Surface Chemistry Species ID Ultra surface sensitive
XPS	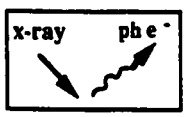	30 Angstroms Li - U	10^{-1} 1000ppm	General Surface Chemistry Bonding Information

Detection Limit gives both a "monolayer sensitivity" based upon 10^{15} atoms/cm^2 and typical bulk concentration sensitivities.

3.3 Methods - Surface Analytical Techniques

In order to characterize the steel specimens exposed to a variety of conditions, it was necessary to utilize several surface analytical techniques. The different methods used were auger electron spectroscopy (AES), scanning electron microscopy (SEM) with energy dispersive spectroscopy attachment (EDS), secondary ion mass spectroscopy (SIMS) and x-ray photoelectron spectroscopy (XPS). Several techniques were used because each method has distinct advantages over the others.

All of the techniques listed above take advantage of the processes that result from a particle beam interacting with a material. The bombarding particles (electrons or x-rays) used in AES, EDS or XPS interact with the outer shell electrons and cause electron transitions to different energy levels. These transitions result in the release of

secondary electrons, photoelectrons or x-rays. SIMS utilizes an ion beam (Argon ions) to sputter surface atoms into a detector (mass spectrometer). Due to the scattering in a material, the escape depth for such released or sputtered particles is shallow, thus making such techniques particularly surface sensitive.

Specimens to be analyzed by either AES, SIMS or XPS were degreased prior to being placed in the vacuum chamber. The degreasing procedure used an ultrasonic cleaner and different solvents. The specimens were rinsed in methanol and then degreased for five minutes each in isopropyl alcohol and then Freon. The specimens were air blown dry and mounted in the specimen holder.

3.3.1 Auger Electron Spectroscopy

When it was necessary to identify and characterize a specific topographical species on the steel surfaces, auger electron spectroscopy was used. The Perkin Elmer PHI model 660 Scanning Auger Microprobe (SAM) system was used to accomplish this task. Specimens were usually rinsed in methanol and Freon prior to introduction to the vacuum chamber. The attached scanning electron microscope (SEM) was used to select and survey scans were taken to characterize a specific surface feature. The survey scans were obtained over the range 0-1000eV.

To measure the air formed oxide thickness on the steels, an auger depth profile was performed. The carbon, iron and oxygen peaks were monitored. The sputtering system was calibrated using a 1000Å Ta_2O_5 oxide film.

3.3.2 Scanning Electron Microscopy with Energy Dispersive Spectroscopy

Often it was necessary during this study to view the morphology of the steel surfaces to verify or explain behavior. The JEOL 35-CF scanning electron microscope (SEM) was used to accomplish this task. In addition, the Cambridge S4-10 energy dispersion (EDS) attachment to this microscope was also used to gain surface chemistry information. Copper tape was used to electrically ground the metallic specimens to the holder. Thus, no coating techniques were used.

3.3.3 Secondary Ion Mass Spectroscopy

When an impurity was present on the steel surface in very small quantities (ppm), the Perkin-Elmer PHI 3600 Dynamic secondary ion mass spectrometer (SIMS) subsystem attached to the Perkin Elmer PHI model 660 Scanning Auger Microprobe (SAM) system was used. Secondary ion mass spectroscopy (SIMS) was performed to characterize the steel surface chemistry at low levels. Specimens were usually rinsed in methanol and Freon prior to introduction to the vacuum chamber. Survey scans were taken to characterize the surface, while depth profiles were taken to detect segregation effects. Positive SIMS surveys and depth profiles were conducted upon the stabilized steel specimens over the range of 40 to 100 mass/charge ratios. During the depth profiles the primary mass/charge ratio for iron, titanium and titanium oxide (TiO) were examined to a depth of 200Å.

3.3.4 X-Ray Photoelectron Spectroscopy

When it was necessary to gain information about the relative amounts of an elemental species on the steel surface, x-ray photoelectron spectroscopy (XPS) was used. Although AES could also accomplish this task, XPS can gain information from a larger area (thus, more of an average would be obtained) and XPS is more sensitive than

AES to the heavier elements (e.g., Pb). The PHI 5400 x-ray photoelectron spectrometer was used to accomplish this task. Specimens were usually rinsed in methanol and Freon prior to introduction to the vacuum chamber. Magnesium K_α (15keV) radiation was used during the scans. Survey scans were taken to identify specific species and multiplex scans were conducted to quantify the specific amounts of those species present on the surface. Survey scans were obtained over the range 0-1000 eV.

3.4 Methods - Linear Polarization

Linear polarization scans were performed to characterize the steel surfaces by electrochemical means. A Princeton Applied Research PAR 173 potentiostat with a PAR 175 Universal programmer controlled the experiment. The data were fed into a DASH8-PGA A/D card in a 80386SX-type computer. The data were monitored using Labtech Notebook.

The experiments were carried out in a 1000ml glass cell using a 1.4 cm^2 ultra low carbon steel (see Table 3.B) sheet working electrode. The steels were polished to a 1200 grit (15.2 micron) finish, rinsed with distilled water and coated with "stop-off" lacquer (Micropeel) prior to being introduced to the cell. The measurements were made under deaerated conditions by flowing nitrogen gas into the cell.

The cell had a separate compartment for the reference electrode (saturated calomel) and the auxiliary electrode (graphite rod). A Luggin capillary at a distance of approximately 2mm distant from the working electrode was used to minimize the IR drop. All potentials are referred to the normal hydrogen electrode.

The cathodic polarization (V-Log i) curves were obtained by means of a potential step technique following a holding of the working electrode at -1V-NHE for five minutes in N_2 saturated solution where the air formed oxide was reduced. The scan rate used for the potential steps was -1mV/s. The scan was initiated at a potential 25 mV anodic to the open circuit potential. Tafel constants were obtained by sampling a decade of data above 1 mA/cm^2.

3.5 Methods - Cleaning Procedures

Due to the high sensitivity of the permeation and polarization tests, all glassware that was used for this study underwent stringent cleaning procedures prior to being used. All glassware was cleaned of all deposits by an Alconox™ scrubbing. The glassware was soaked in a concentrated sulfuric acid bath for a minimum of 12 hours. The glass was removed, rinsed with tap water, distilled water, acetone, methanol and then, baked in an oven at 110°C. For the experiments of particular sensitivity (e.g., polarization tests, lead tests, etc.), the glassware, bubbler tubes and gaskets were additionally boiled in distilled water for 30 minutes, removed and baked dry.

3.6 Materials

3.6.1 Materials Used in this Study

Permeation foils were prepared from low carbon steel sheets. The specific composition of the steel sheets are listed in Table 3.B in weight percent (balance is Fe). The entry surface of the foils was polished to a 1200 grit (15.2 micron) finish. The exit surface was polished to a 2400 grit (9 micron) finish and then Pd plated. The Pd plating procedure is discussed elsewhere[6]. A narrow (3mm x 1mm x 8mm) steel strip was spot welded to each specimen for electrical contact.

Table 3.B

Specific Compositions of Steels used in Investigation

Steel	04LC	005BH	004Ti1	004Ti2	Fe	005D
C	0.040	0.005	0.004	0.004	0.0001†	0.005
Mn	0.22	0.170	0.070	0.120	0.0001†	0.30
P	0.012	0.008	0.008	0.009	0.0005†	0.015
S	0.012	0.007	0.007	0.006	0.0005†	0.008
Si	0.012	0.006	0.009	0.010	0.0001	0.03
Al	0.057	0.062	0.025	0.059	0.0001	0.05
Cr	0.18	0.019	0.018	0.015	0.0001†	?
Ti	0.003	0.003	0.051	0.080	0.0002†	0.05
Mo	0.003	0.003	0.005	0.005	0.0002†	?
Ni	0.024	0.019	0.022	0.024	0.0001	?
Cu	0.026	0.021	0.025	0.038	0.0001	?
N_2	0.003	0.006	0.003	0.003	0.0005†	?
O_2	0.005	0.002	0.004	0.004	0.0005†	?
Pb	0.0005†	0.0005†	0.0005†	0.0005†	0.0005†	?
Sn	0.003	0.003	0.002†	0.002†	0.0003†	?
Nb	0.002†	0.002†	0.002†	0.002†	0.0005†	0.035
V	0.002†	0.002†	0.002†	0.002†	0.0001†	?
Sb	0.002†	0.002†	0.002†	0.002†	0.0005†	?
Ca	0.0005†	0.0005†	0.0005†	0.0005†	0.0001	?
B	0.0005†	0.0005†	0.0005†	0.0005†	0.0005†	?

The † symbol indicates the detection limits for the equipment used in the analysis.
The ? symbol indicates that the analysis did not look for this element.

Table 3.C

Solutions used in Investigation

Test/Procedure Solution	Solution Used
Permeation test anodic chamber solution	0.1M NaOH
Permeation test cathodic chamber solution	test dependent
"Electrocleaning" solution	(Parker Amchem EC-76 based; pH ~11)
"Electropickling" solution	(H_2SO_4 based; pH ~0.5)
"No-Metals solution"	(H_2SO_4 based with Na_2SO_4; pH ~0.5)
pH test cathodic solution	H_2SO_4 based
Current Density test cathodic solution	(H_2SO_4; pH=1)
Agitation test cathodic solution	Electropickling solution
Zinc Barrier test cathodic solution	No-Metals solution (pH~2.7)
Zinc Plating test cathodic solution	(No Metals solution; 1.4M Zn ions)
Stabilization test cathodic solution	(H_2SO_4; pH=1)
Lead test cathodic solution	(H_2SO_4; pH=1 with Lead Acetate)
Contaminants test plating solution	(H_2SO_4; pH=1 with either Au,Ni, Pb or Pt ions)

"cathodic solution" refers to the solution used in the cathodic chamber of the permeation cell. For the catalysis tests, the Au, Ni, Pb, and Pt ions were added with Atomic Absorption Standard Solutions to the acid.

3.6.2 Solutions

All solutions were prepared from reagent grade chemicals and distilled water. With the exception of the three process solutions below, all solutions used in cathodic experiments were pre-electrolyzed (i_C = -4 mA/cm^2) with a ~16 cm^2 steel cathode and a dimensionally stable anode for a minimum of 24 hours before testing . The solutions used in this investigation are listed in table 3.C. The No-Metals solution is typical of acidic, plating buffer solutions used in electrogalvanizing operations.

3.6.3 Palladium Plating Procedure

It was shown by Bockris[7] (1948) that to insure high discharge efficiency during polarization of steel, a thin (<1000Å) coating of palladium should be applied. Devanathan[1] (1962) affirms this fact and states that such a coating is necessary to achieve low noise levels (by minimizing corrosion) and to assure a high oxidation efficiency for any hydrogen exiting a permeation foil during a permeation experiment. Thus, all permeation foils used in this investigation were coated with Pd on the surface that would be exposed to the anodic chamber of the permeation test.

A "Palladium Plating Concentrate" was made ahead of time to make life easier during testing. The concentrate was made as follows. One gram of palladium chloride ($PdCl_2$) was added to 100 ml of distilled water at 80°C. The solution appeared brown and murky. Small quantities (~1-2g) of sodium nitrite were added to the solution. After each addition, the mixture was swirled. With subsequent additions of sodium nitrite, the mixture became more of a clear, yellowish-urine color. It was useful to add as little sodium nitrite as possible to attain this state or upon cooling, a gelatinous film formed on the mixture. Occasionally, it was also necessary to use the end of a glass rod to break up the $PdCl_2$ crystals. The concentrate was allowed to cool before using.

The plating procedure follows from Fullenwider[6] and is as follows. To plate the permeation foils, one milliliter of concentrate was used for every square centimeter to plated. The desired amount of concentrate was added to 500ml of 0.2M NaOH. A 2.54 x 2.54 cm^2, an inert titanium coated, rare earth oxide anode was used, while the steel to be plated was the cathode. The plating was done galvanostatically at -0.5mA/cm^2 until a shiny yellow coating was obtained. A typical plating time is 20 minutes. To insure a good coating, the solution was occasionally agitated for the first 5 minutes. After which, the solution was stirred at a low rate. The permeation foil was removed from solution, rinsed with distilled water, acetone, methanol and hot air blown dried. For best results, this procedure should be done 2-3 days prior to permeation testing.

To gain good signal to noise ratios during a permeation test, it is important to obtain a continuous Pd coating. Care must be taken not to "smudge" the coating with fingerprints. If it is desired that only one side of the permeation foil should be coated with palladium, then masking tape may be used to effectively shield the surface not to be plated. After plating, a quick wiping of this surface with 2400grit (9 micron) silicon carbide paper insures against any unwanted Pd remaining on the surface for testing.

References for Chapter 3

1 M.A.V. Devanathan and Z. Stachurski, *Proc. of Roy. Soc. of Lond.* **A270**, (1962) 90-102.

2 BC1200 manual.

3 J.J. DeLuccia and D.A. Berman, Electrochemical Corrosion Testing, ASTM STP 727, ASTM, (1981): 256-273.

4 D.A. Berman, W. Beck and J.J. DeLuccia, Hydrogen in Metals, I.M. Bernstein & A.W. Thompson, eds., ASTM, Metals Park, Ohio, (1974): p. 595.

5 ASTM F 1113-87.

6 M.A. Fullenwider. Hydrogen Entry and Action in Metals, Pergamon Press, Inc., Elmsford, New York, (1983).

7 J.O'M. Bockris, *Chem. Rev.*, 43 (1948):525-577.

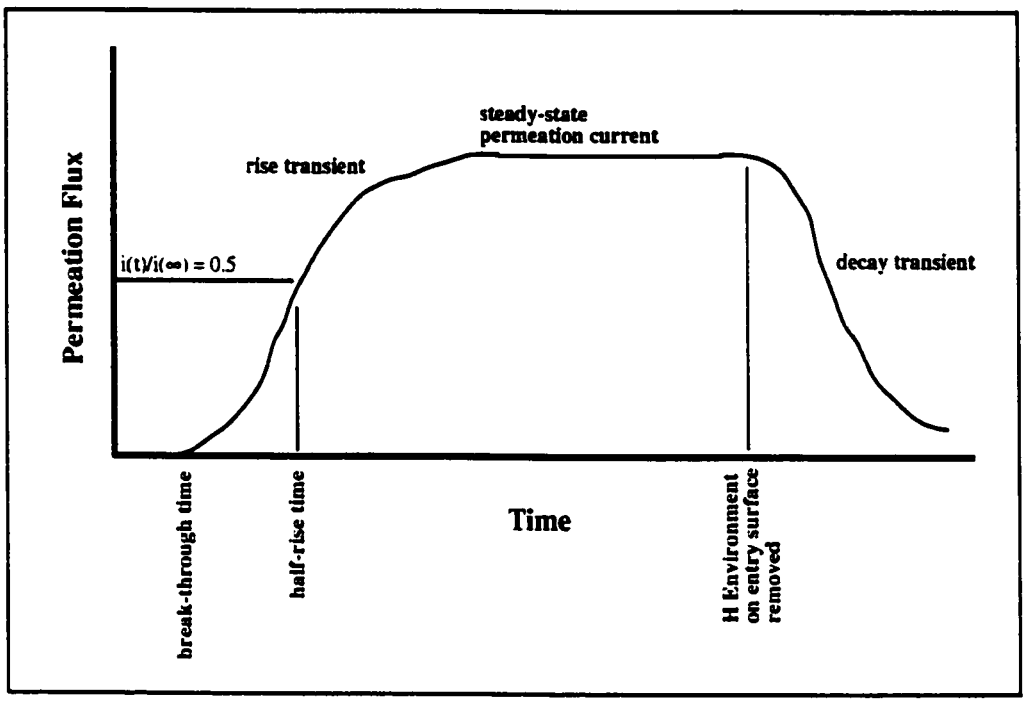

Figure 3.1: Typical information obtained from a permeation curve.

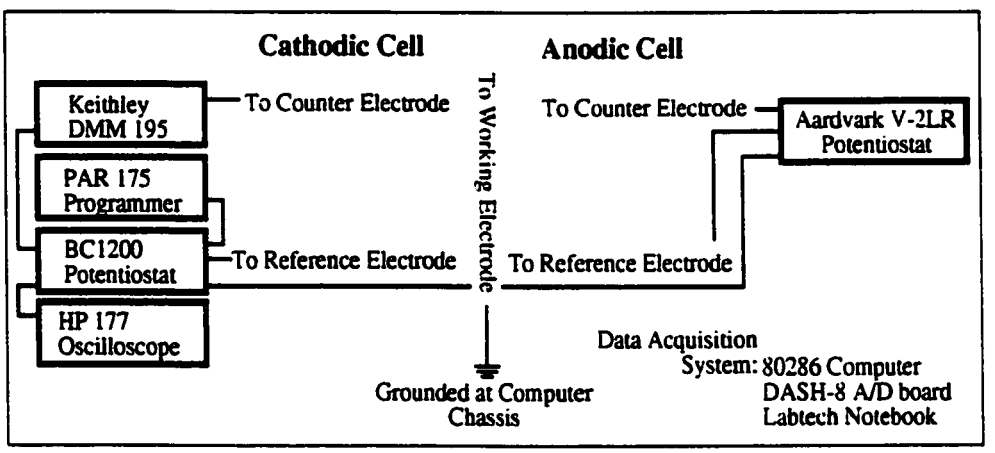

Figure 3.2: The above diagram illustrates the primary equipment used during permeation tests for this study. Note that this full setup was used during galvanostatic experiments. During potentiostatic experiments, the programmer and oscilloscope were not needed.

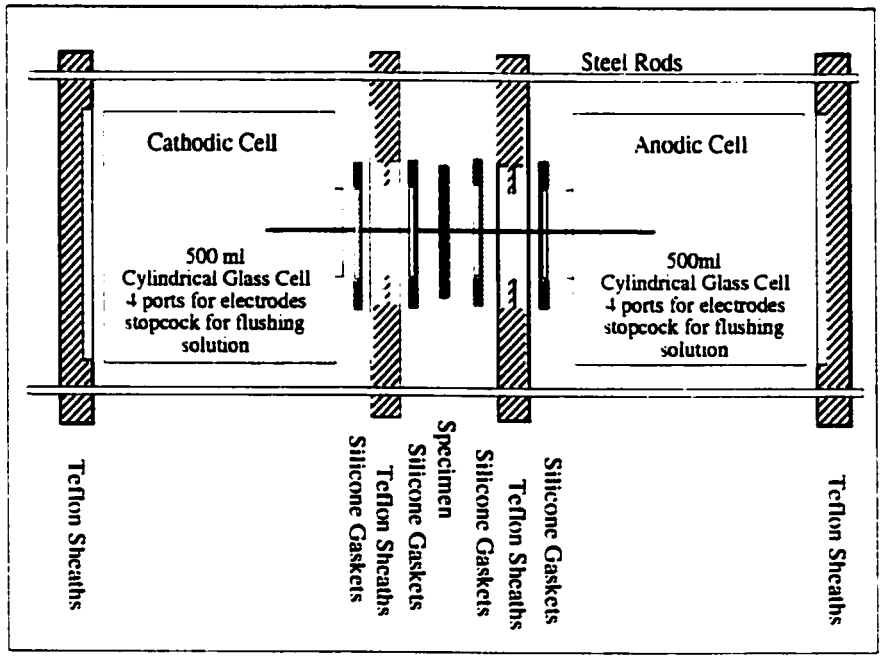

Figure 3.3: A diagram of the 500ml permeation cell design with clamping system.

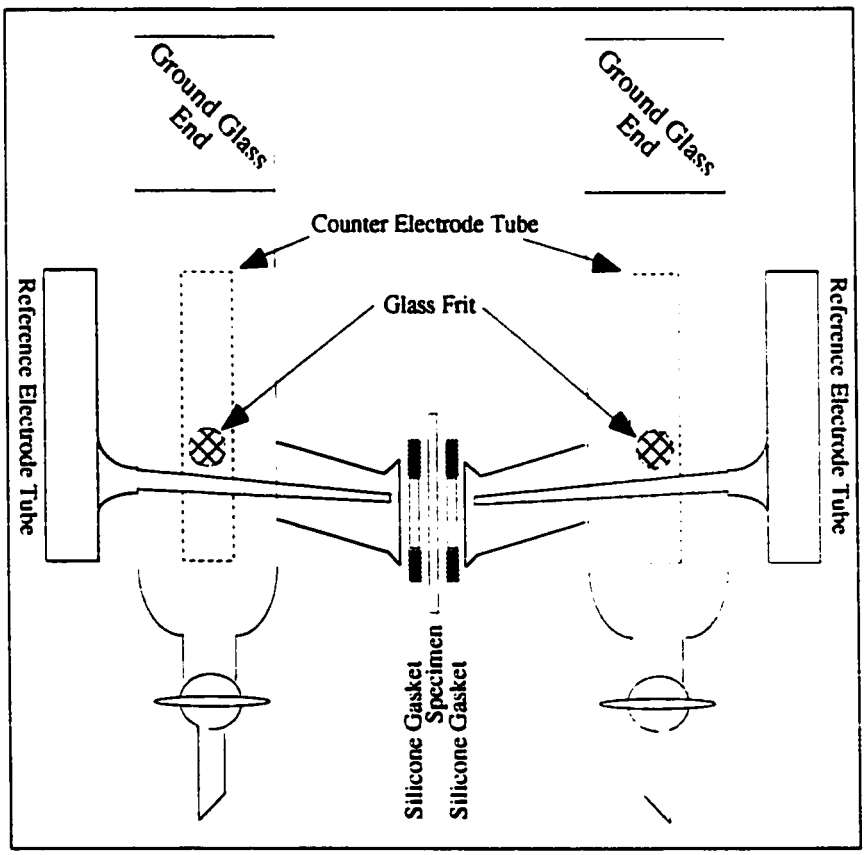

Figure 3.4: A diagram of the 70ml permeation cell design.

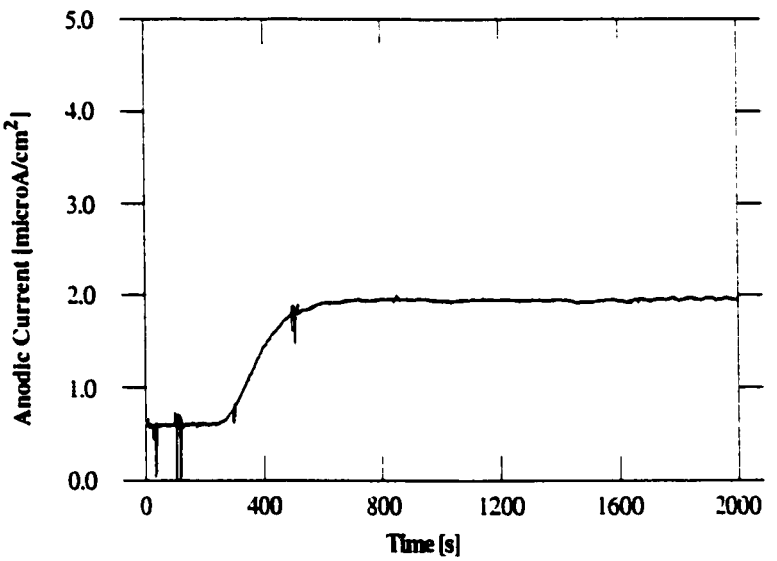

Figure 3.5: An example of an ideal permeation curve.

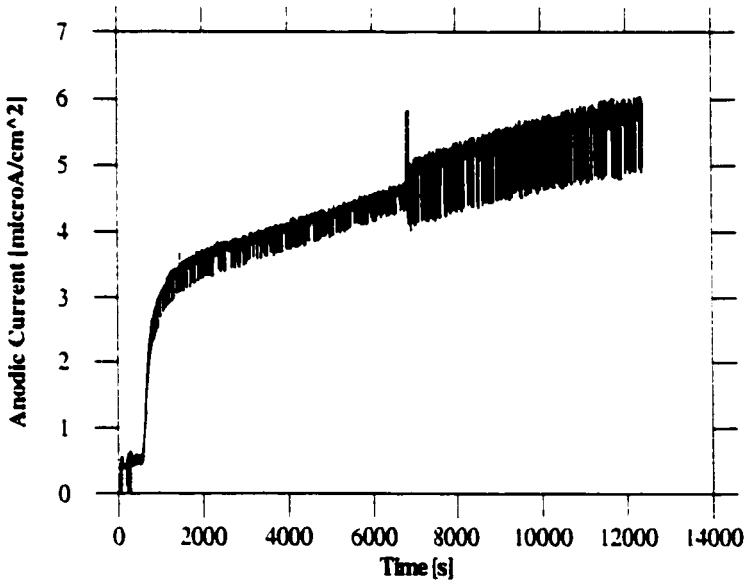

Figure 3.6: An example of a "noisy" permeation transient. Probably the cells are clamped too tight or there is leaking occuring which results in crevice corrosion of the specimen.

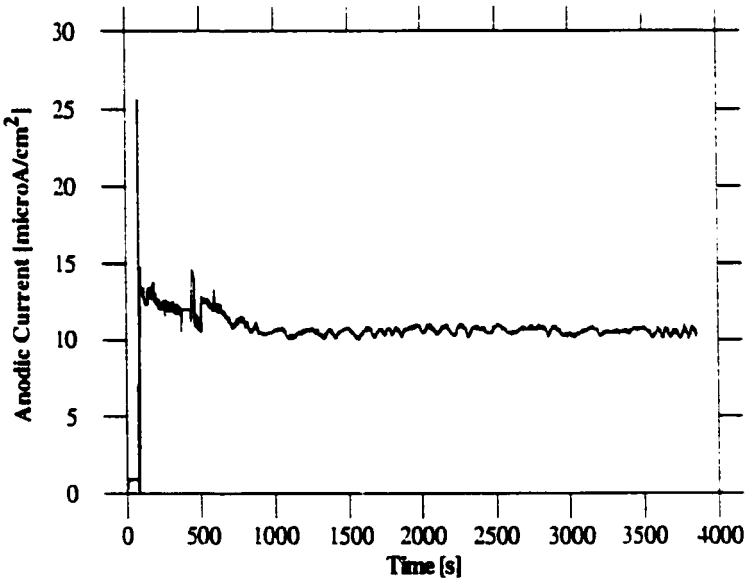

Figure 3.7: An example of a "shocked" permeation transient. Too great a step in voltage was applied. For example, the entry surface potential was not under potential control before stepping to a large negative potential.

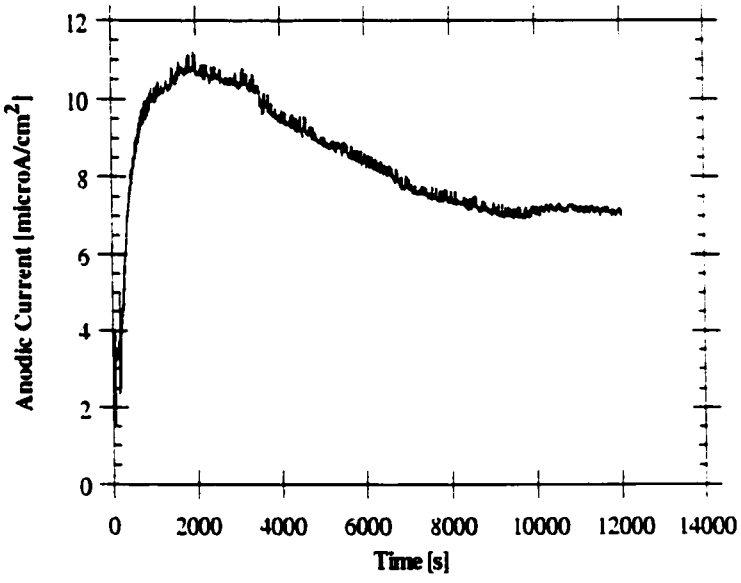

Figure 3.8: An example of a "non-steady state" permeation transient. Such a situation generally occurs when large negative overpotentials are applied in acidic solutions.

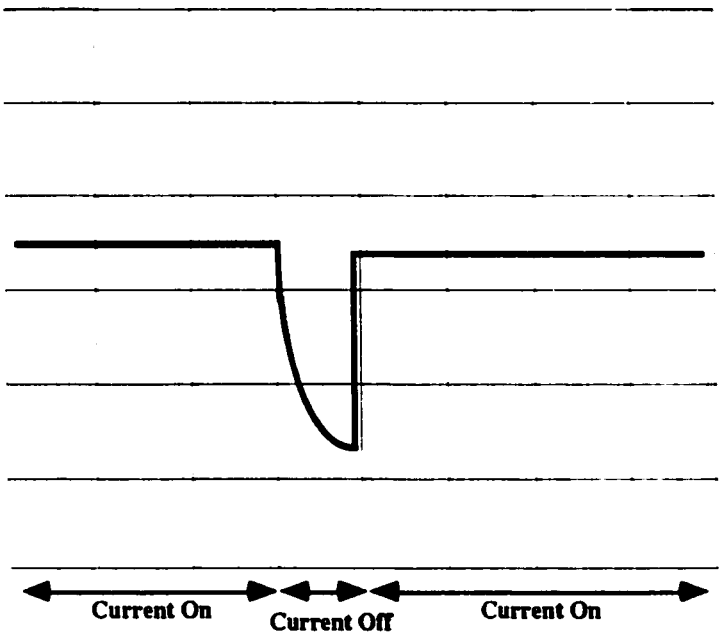

Figure 3.9a: *Current Interupt Technique - Frame #1 :* An example of the square wave signal applied during a permeation test. No correction has been applied.

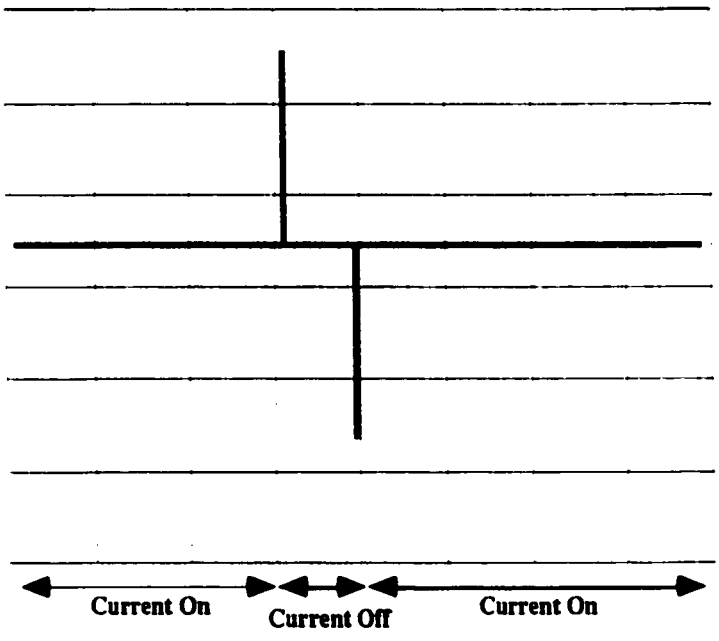

Figure 3.9b: *Current Interupt Technique - Frame #2 :* An example of the square wave signal applied during a permeation test. Proper correction has been applied.

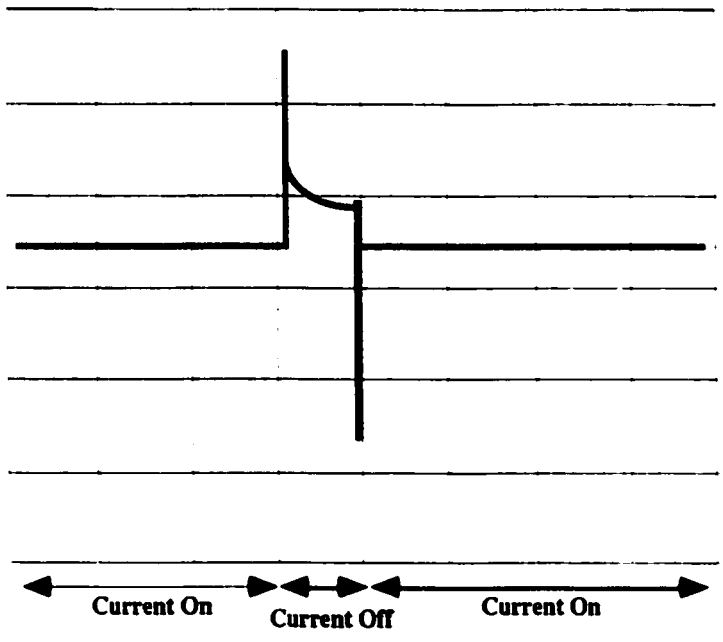

Figure 3.10a: *Current Interupt Technique - Frame #3 :* An example of the square wave signal applied during a permeation test. Too much correction has been applied.

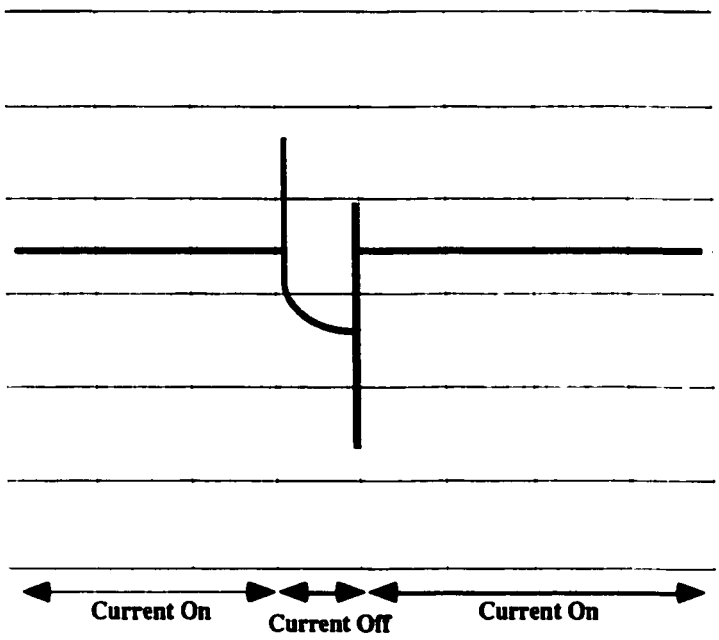

Figure 3.10b: *Current Interupt Technique - Frame #4 :* An example of the square wave signal applied during a permeation test. Not enough correction has been applied.

Chapter 4

Modelling Hydrogen Entry and Exit in Metals Exposed to Multiple Charging Processes

4.1 Introduction

4.1.1 Background

There has been recent interest[1,2] in hydrogen absorbed from industrial processes, such as electrocleaning, electropickling, and plating. These processes operate at high current densities (0.5 to 12kA/m^2) and significant electrolyte flow rates (line speeds of 90 to 150 m/min) upon metal sheets.

Since Devanathan and Stachurski[3] first applied the permeation technique to metallic foils, there have been many models proposed to understand the hydrogen interaction with a metal electrode. Such models have been applied to permeation data to obtain hydrogen diffusivities, surface solubilities[4,5,6,7,8,9], trapping constants[10,11] and surface reaction rate constants[12] for various metals. More recently, a model[13] has been proposed which evaluates the hydrogen behavior during permeation by consolidating all surface effects into a single term.

To effectively evaluate the hydrogen behavior for various industrial processes, a flexible model is required. Such a model must be applicable to results obtained from a hydrogen permeation experiment. The model must be able to evaluate both surface and metallurgical (e.g., diffusivity) phenomena. In addition, the model must be able to handle both arbitrary charging conditions on either side and an arbitrary hydrogen distribution within a metal sheet. Finally, the model must be able to evaluate hydrogen behavior resulting from multiple charging processes.

Although previous models allowed a wide variety of situations to be studied, none of the models met the needs outlined above. Hence, the objective of this work was to develop a model for hydrogen entry and exit behavior in metals that meets the above needs.

4.1.2 A Phenomenological Hydrogen Transport Model

If hydrogen is generated at a metal surface, there are several reactions that may take place to varying degrees. Primarily, there is the discharge (II), the recombination (III) and the absorption (IV) reactions:

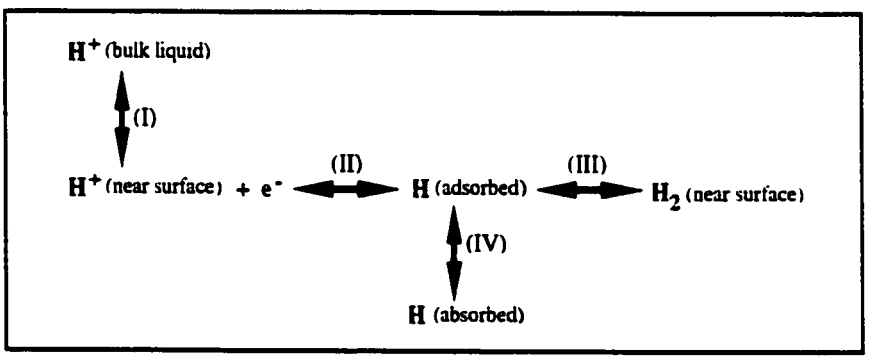

From (II) it is evident that the amount of adsorbed hydrogen is a function of hydrogen activity in solution (the pH) and the electrochemical driving force (supplied voltage). If reactions (I) - (III) are in equilibrium, then the Nernst Equation may be written as:

$$E_w = E^o - \frac{RT}{nF} \ln\left(\frac{(f_{H_2})^{n/2}}{(a_{H^+})^n}\right) \qquad [4.1]$$

E_w is the potential of the metal during polarization, E^o is the standard potential necessary for hydrogen evolution, a_{H^+} is the activity of hydrogen in solution, R is the

gas constant, T, the temperature, n, the number of electrons passed in the reaction, F is Faraday's constant and f_{H_2} is the activity of hydrogen on the metal surface.

Furthermore, if reactions (III) - (IV) are in equilibrium, a Sievert's relationship may be experimentally derived. This represents the relationship between the amount of hydrogen soluble in a metal and the fugacity of hydrogen external to the metal. Hirth[14] presented the following equation for amount of hydrogen absorbed in iron:

$$C_H = (2.59)(10^{-4}) \sqrt{f_{H_2}}\, e^{(-3440/T)} \qquad [4.2]$$

where C_H is the concentration of hydrogen in mol/cm^3, f_{H_2} is in atmospheres and T is in degrees Kelvin. Thus, by measuring the pH of solution, E_w during a given charging condition and using Eqs. [4.1]-[4.2], the concentration of hydrogen beneath a metal surface during a given charging condition might be obtained. However, during some charging processes, for example, in the presence of cathodic poisons or other such phenomena, reactions (I) - (IV) are not necessarily in equilibrium. It was in this light that Bockris[15] and Archer[16] cautioned the usage of Eqs. [4.1] and [4.2] to predict hydrogen solubility in metals. Although such caution is justified, the model presented here utilizes this fact to its advantage.

Figure 4.1 illustrates several parameters this paper utilizes to describe the geometry of a permeation experiment. The parameters c_1 and c_2 are the hydrogen concentrations as predicted by Eqs. [4.1]-[4.2]. The actual concentrations of hydrogen beneath the metal surfaces at positions x=0 and x=L are c(0,t) and c(L,t), respectively. J is the hydrogen flux through the sheet. Inside the sheet, the hydrogen motion is controlled by Fick's second law with D as an effective diffusivity as described by

McNabb[9] (see Chapter 2, equation [2.23]). The parameters, κ_1 and κ_2, are constants called *mass transfer coefficients*.

For this model the deviation between the predicted (c_1 and c_2) and actual ($c(0,\infty)$ and $c(L,\infty)$) hydrogen concentrations is described by a flux gradient[17]. The following relationship for the steady-state flux, J^{∞}, at the surfaces of the metal may be written as:

$$J^{\infty}/\kappa_1 = (c1 - c(0,\infty)) \qquad x=0 \qquad [4.3a]$$

$$J^{\infty}/\kappa_2 = (c(L,\infty) - c_2) \qquad x=L \qquad [4.3b]$$

The κ terms are constants that define the deviation from Sievert/Nernstian behavior. When κ is large (e.g., approaching ∞), then the deviations from Sievert/Nernstian behavior are small ($c_1 \sim c(0,\infty)$). Conversely, when κ is small (e.g., approaching 0), then the deviations from Sievert/Nernstian behavior are significant ($c_1 >> c(0,\infty) \sim 0$).

Notice that the definitions of c_1 and $c(0,\infty)$ or c_2 and $c(L,\infty)$ do not define chemical or electrochemical reactions. They express a relationship between ideal and realistic quantities with any deviation defined by the parameter κ. Thus, any phenomena that would invalidate the application of Eqs. [4.1]-[4.2] can be quantified for a given charging condition by κ. It has been suggested[13], that such coefficients can account for roughness, texture, grain size, heat treatment, and catalytic effects, as well as chemical interactions between the surface and the surrounding environment.

This paper presents a phenomenological model with the following assumptions: (i) Hydrogen ions in the electrolyte will interact with a metal surface to result in both hydrogen absorption and hydrogen evolution; (ii) It is also assumed that the hydrogen evolution step occurs as:

$$nH^+ + ne^- \Leftrightarrow (n/2)H_2$$

(iii) For a metal that allows water reduction to occur on its surface, it will be assumed that c_l, the hydrogen concentration beneath the metal surface, as determined by Eqs. [4.1]-[4.2], is always greater than or equal to the actual hydrogen concentration, $c(0,\infty)$, beneath the metal surface; (iv) For a metal that allows hydrogen oxidation to occur on its surface, it will be assumed that c_l is always less than or equal to the actual hydrogen concentration, $c(0,\infty)$; (vi) The boundary conditions assume that first order kinetics are followed for both metal sheet surfaces; (vii) Finally, both the diffusivity and the κ terms are assumed to be independent of the hydrogen concentration in the metal sheet.

The model will be presented in portions. First, a development of the equations and boundary conditions will be given. This section will be followed by the application of the model to theoretical and experimental data. From such applications, the utility of this model will be discussed.

4.2 Theoretical Development

To evaluate the transport effects of hydrogen through a metal sheet, it is necessary to solve a second-order parabolic equation :

$$\frac{\partial C}{\partial t} = -D\frac{\partial^2 C}{\partial x^2} \qquad 0 \le x \le L \qquad [4.4]$$

Surface effects are defined using the following boundary conditions:

$$-D\frac{\partial C}{\partial x} + \kappa_1 (C - c_l) = 0 \qquad x=0 \qquad [4.5]$$

$$-D\frac{\partial C}{\partial x} + \kappa_2 (C - c_2) = 0 \qquad x=L \qquad [4.6]$$

$$C(x,0) = f(x) \qquad t=0 \qquad [4.7]$$

The parameter, C, is the hydrogen concentration at position, x, and time, t, into a sheet of thickness, L. In addition, c_1 and c_2 are the hydrogen concentrations on either side of the metal sheet as predicted by Eqs. [4.1]-[4.2]. D is the hydrogen diffusivity in the metal. There may also be a non-uniform initial distribution of hydrogen, f(x), in the sheet. The mass transfer coefficient on surface (x=0) is κ_1 and on surface (x=L) is κ_2.

Although a finite difference approach similar to that used by Makhlouf[13] could have been used to solve [4.4]-[4.7], such solutions were more complicated (i.e., contained more unkown independent variables) and were more difficult to utilize with experimental data.

Alternatively, Carslaw and Jaeger[17] suggest the following strategy to solve a differential equation of this type. Assume the solution of Eq. [4.4] and the above boundary conditions may be divided into a time dependent and a steady state function.

$$C(x,t) = w(x,t) + u(x) \qquad [4.8]$$

where u(x) is the steady-state function satisfying:

$$D\frac{\partial^2 u}{\partial x^2} = 0 \qquad 0 < x < L \qquad [4.9]$$

$$-D\frac{\partial u}{\partial x} + \kappa_1(u - c_1) = 0 \qquad x=0 \qquad [4.10]$$

$$D\frac{\partial u}{\partial x} + \kappa_2(u - c_2) = 0 \qquad x=L \qquad [4.11]$$

and w(x,t) is the non-steady state function satisfying:

$$\frac{\partial w}{\partial t} = -D\frac{\partial^2 w}{\partial x^2} \qquad 0 < x < L \qquad [4.12]$$

$$-D\frac{\partial w}{\partial x} + \kappa_1 w = 0 \qquad x=0 \qquad [4.13]$$

$$D\frac{\partial w}{\partial x} + \kappa_2 w = 0 \qquad x=L \qquad [4.14]$$

$$w(x,0) = f(x) - u(x) \qquad t=0 \qquad [4.15]$$

Solution of Eq. [4.9], suggests u(x) is of the form.

$$u(x) = k_1 x + k_2$$

where k_1 and k_2 are constants. Consideration of the boundary conditions illustrated by Eqs. [4.9]-[4.11], yields a solution of :

$$u(x) = \frac{(c_2 - c_1)\, h_1 h_2}{h_1 + h_2 + h_1 h_2 L} x + \frac{h_1 c_1 + h_2 c_2 + c_1 L h_1 h_2}{h_1 + h_2 + h_1 h_2 L} \qquad [4.16]$$

where h_1 and h_2 may be defined by:

$$h_n = \frac{\kappa_n}{D} \qquad [4.17]$$

Solution of Eq. [4.12], suggests[17] w(x,t) is of the form.

$$w(x,t) = \sum_{n=1}^{\infty} Z_n(x)\, e^{-D\beta_n^2 t} \int_0^L Z_n(x')\,(f(x') - u(x'))\,dx' \qquad [4.18]$$

where

$$Z_n(x) = A(\beta_n, \kappa_1, \kappa_2, D, L)\, T(\beta_n, x) \qquad [4.19]$$

$$A(\beta_n, \kappa_1, \kappa_2, D, L) = \sqrt{\frac{2(\beta_n^2 + h_2^2)}{(\beta_n^2 + h_1^2)\left[L(\beta_n^2 + h_2^2) + h_2\right] + h_1(\beta_n^2 + h_2^2)}} \qquad [4.20]$$

$$T(\beta_n, x) = \beta_n \cos(\beta_n x) + h_1 \sin(\beta_n x) \qquad [4.21]$$

and β_n is a parameter that satisfies the transcendental equation:

$$\tan \beta_n L = \frac{\beta_n (h_1 + h_2)}{\beta_n^2 + h_1 h_2} \qquad [4.22]$$

Combining Eqs. [4.18]-[4.22] provides the following solution:

$$w(x,t) = \sum_{n=1}^{\infty} AT\, e^{-D \beta_n^2 t} \left(AE + \int_0^L Z_n(x')\, f(x')\, dx' \right) \qquad [4.23]$$

where

$$E(\beta_n, \kappa_1, \kappa_2, D, L) = \frac{e_1}{\beta_n} + e_2 + \frac{e_3}{\beta_n} \qquad [4.24]$$

$$e_1 = \cos(L\beta_n)\left[k_1 L h_1 - k_1 + h_1 k_2\right] \qquad [4.25]$$

$$e_2 = -\sin(L\beta_n)\left[k_2 + \frac{k_1 h_1}{\beta_n^2} + L k_1\right] \qquad [4.26]$$

$$e_3 = k_1 - k_2 h_1 \qquad [4.27]$$

Combining Eqs. [4.8], [4.16] and [4.22], allows the concentration of hydrogen at any point, x, and any time, t, in a metal sheet to be expressed as:

$$C(x,t) = k_1 x + k_2 + \sum_{n=1}^{\infty} AT\, e^{-D \beta_n^2 t} \left(AE + \int_0^L Z_n(x')\, f(x')\, dx' \right) \qquad [4.28]$$

It should be also noted that a special situation[17] arises when κ_1 and κ_2 are both zero. In such an event, Eq. [4.22] produces only complex roots, thus resulting in a complex C(x,t). Since hydrogen neither enters nor leaves the sheet, the following term is added to Eq. [4.28] to yield a real numbered C(x,t):

$$\frac{1}{L} \int_0^L f(x)\, dx$$

The flux of hydrogen, J, through a sheet is related to the concentration gradient that exists across a membrane through Fick's first law. The current density at a point x_o is related to the flux by:

$$J(x=x_o) = \frac{I(x=x_o)}{zF} = -D\left(\frac{\partial C}{\partial x}\right)_{x_o} \qquad [4.29]$$

where z is the number of electrons required to complete the reaction (+1 eq/mol) and F is Faraday's constant (96,500 C/eq).

Using the above information and Eqs. [4.28] and [4.29], the current measured on the exit face (x=L) of the sheet during a permeation test may be given by :

$$I(x=L,t) = -zFD\left(k_1 + \sum_{n=1}^{\infty} A^2 E T\, e^{-D\beta_n^2 t}\right) \qquad [4.30]$$

where

$$T'(x=L) = h_1\beta_n \cos(\beta_n L) - \beta_n^2 \sin(\beta_n L) \qquad [4.31]$$

To drive the model and utilize Eq.[28] and [4.30], several pieces of information are needed. The effective diffusivity of hydrogen in the metal, D, the values of κ_1 and κ_2 for the surface conditions, the Sievert/Nernstian hydrogen concentrations, c_1 and c_2, on either side of the sheet and the initial distribution of hydrogen in the metal, f(x) are all required. The permeation test creates a simplified situation to obtain several of the parameters necessary to drive the model.

During a permeation experiment, several things are known. The hydrogen concentrations (c_1, c_2) on either side of the foil are known from potential and pH measurements, the Nernst Equation and the use of Eqs. [4.1]-[4.2]. The diffusivity may

be obtained from a curve fitting of Eq. [4.30] to experimental data. This will be an effective diffusivity. Furthermore, the initial distribution, f(x), may be assumed to be zero by either baking the specimen to be tested or by holding the sheet surfaces at anodic potentials prior to testing.

Once steady state hydrogen transport conditions are established across the entry surface, the metal sheet and the exit surface, the following three equations define the same constant flux, J_∞.

$$\frac{J_\infty}{\kappa_1} = c_1 - c(0,\infty) \qquad [4.32]$$

$$\frac{J_\infty L}{D} = c(0,\infty) - c(L,\infty) \qquad [4.33]$$

$$\frac{J_\infty}{\kappa_2} = c(L,\infty) - c_2 \qquad [4.34]$$

These three equations contain the two unknowns κ_1 and κ_2, in addition to the unknown surface hydrogen concentrations, $c(0,\infty)$ and $c(L,\infty)$. During a permeation test, the exit side of the metal foil is palladium coated and anodically polarized to immediately oxidize any exiting hydrogen. Since $c_2 \sim c(L,\infty)$ during such conditions, the test allows the assumption that κ_2 is large. Once this assumption is made, it follows that $c(L,\infty)$ is approximately equal to the known quantity c_2. This in turn reduces the system of equations to two equations in two unknowns, and the values for κ_1 and $c(0,\infty)$ are uniquely defined.

4.3 Applications of the Model

4.3.1 Impact of Model Parameters upon Permeation

To have a better understanding of how κ_1, κ_2 and D affect the permeation current, i^{∞}, three *flux-control* curves were calculated. Using Eqs. [4.32]-[4.34] the following expression is valid at steady-state :

$$J^{\infty} = \frac{c_1 - c_2}{\left(\frac{L}{D} + \frac{1}{\kappa_1} + \frac{1}{\kappa_2}\right)} \qquad [4.35]$$

Varying either κ_1, κ_2 or D, while maintaining the other parameters constant allows a set of flux values to be obtained. Plotting this set of fluxes versus a given variable yields an effective tool for permeation studies. Eq. [4.35] may help determine whether the permeation behavior is under "Nernst/Sievertian" or "deviant" control for a given set of c_1, c_2 and L.

The charging conditions chosen for calculating the flux curves assume c_1 and c_2 are 10^3 mol/m^3 and 10^{-10} mol/m^3, respectively, and when not varied, the diffusivity is 10^{-10} m^2/s, κ_1 is 10^{-9} m/s and κ_2 is 1 m/s. These parameters are based upon cathodic and anodic charging conditions of pH=1 H_2SO_4, i_c=-500A/m^2 and pH=12 NaOH, E_a=0.206V-NHE, respectively, for a 10^{-3} m thick steel sheet.

Based upon the flux curves in Figure 4.2, the parameters listed in Table 4.A were selected to evaluate the effect of κ_1, κ_2 and D upon permeation behavior. Three sets of simulations were performed, each of which illustrates the effect of either κ_1, κ_2, or D on the anodic current versus time plots. In each simulation, D, κ_1 and κ_2 were

supplied, thus allowing calculation of the current density versus time curve. The results of the simulations are illustrated in Figures 4.3-4.5.

Figure 4.3 shows the results of simulations #1 through #4 where κ_1 and κ_2 were held constant and D was varied, thus, emphasizing *bulk transport* effects. Although all plots reach the same i^{∞}, there is variation in the break-through time and in the inflection of the curves. The break-through time is that time when the anodic current reaches a measurable value. The fact that the i^{∞} is the same for all of the simulations, suggests κ is controlling the height of the permeation curve under these charging conditions. This is supported by the flux curve in Figure 4.2.

TABLE 4.A
Flux Simulation Results

Simulation	D[m^2/s]	κ_1[m/s]	κ_2 [m/s]	i^{∞} [A/m^2]
1	3×10^{-9}	1×10^{-9}	1.00	0.100
2	5×10^{-10}	1×10^{-9}	1.00	0.100
3	1×10^{-10}	1×10^{-9}	1.00	0.100
4	5×10^{-10}	1×10^{-9}	1.00	0.100
5	5×10^{-10}	3×10^{-8}	1.00	2.733
6	5×10^{-10}	1×10^{-8}	1.00	0.946
7	5×10^{-10}	5×10^{-9}	1.00	0.478
8	5×10^{-10}	1×10^{-9}	1.00	0.100
9	5×10^{-10}	1.04×10^{-9}	1.00	0.100
10	5×10^{-10}	1.04×10^{-9}	1×10^{-5}	0.100
11	5×10^{-10}	1.04×10^{-9}	1×10^{-6}	0.100
12	5×10^{-10}	1.04×10^{-9}	1×10^{-8}	<0.100‡

‡ Note from figure 4.5 that i never reaches $0.1 A/m^2$. [$L = 10^{-3}$ m]

Figure 4.4 shows the results of the *hydrogen entry* simulations (#5-8). This simulation set was characterized by a constant diffusivity and κ_2, but having a variable κ_1. The break-through times were all the same, however, the value of i^{∞} increased with increasing κ_1. Figure 4.2 suggests that the values of κ_1 chosen for the simulations

emphasize "Nernst/Sievertian deviant" and "mixed" behavior. Figure 4.4 illustrates that as κ_1 increases, so does the permeation current. This illustrates that the height of the anodic current versus time curve is considerably dependent on the foil surface condition. It is also evident that for this charging condition, "Nernst/Sievertian" controlled permeation is indicative of non-realistic permeation currents (several A/m^2, instead of the typical 0.2 A/m^2 or less).

Figure 4.5 shows the results of the *hydrogen exit* simulations (#9-12). This simulation set held κ_1 and D constant, while varying κ_2. i^∞ was calculated and is shown in Table 4.B. Figure 4.5 illustrates clearly that if $\kappa_2 > 10^{-5}$, then i^∞ does not vary significantly. However, if κ_2 is chosen to be less than 10^{-5}, then the concentration of hydrogen will begin to build up under the exit surface and will begin to influence the height of the permeation curve. The permeation literature[8,18] has maintained that foils be treated prior to testing to prevent anodic dissolution on the exit face of the metal. Figure 4.5 illustrates the need for maintaining consistency of the permeation foil exit surfaces and that a permeation test is a potential tool for evaluating the exit behavior of hydrogen from a variety of surfaces.

4.3.2 Application of the Model to Permeation Data

To illustrate the use of and to validate the model, a "surface related" phenomena was produced in the cathodic chamber of a permeation cell. The phenomenon chosen was catholyte agitation by a flow pump. By increasing the electrolyte agitation, the mass transfer resistances in solution would be decreased. Hence, it was expected that under such conditions, the permeation current would increase, thus, increasing the value of κ_1 and $c(0,\infty)$.

Permeation curves were produced for conditions of A) agitation, but no polarization, B) stagnant solution and cathodic polarization. C) agitation and cathodic polarization and are illustrated in Figure 4.6. A low carbon (~0.05%C) steel was chosen for the studies. The steady-state permeation current, i^{∞}, the working electrode potential, E_w, and the half-rise time ($i(t)/i(\infty) = 1/2$), $t_{1/2}$, obtained from the tests are listed in Table 4.B.

TABLE 4.B
Results Obtained from Permeation Tests

Process	E_w [V-NHE]	i^{∞}[A/m^2]	$t_{1/2}$[s]
A) Agitation-Charging	-0.362	12.5×10^{-2}	354
B) Charging only	-0.362	8.6×10^{-2}	307
C) Agitation only	-0.243	2.2×10^{-2}	370

N_2/ Process A.B or C / low carbon Steel / Pd / 0.1M NaOH / N_2.
$L = 10^{-3}$m; T = 22°C; charging solution is 1.1M H_2SO_4; i_c = -500A/m^2

To apply the model proposed by this paper to the data set requires that the effective diffusivity be determined. Using Eq. [4.30], the data in Table 4.B and varying D allowed the model to be fit to the experimental data. The best fit was obtained with a hydrogen diffusivity of 6×10^{-10} m^2/s for all of the experimental curves.

Figures 4.7-4.9 illustrate the fitting of various models to the experimental data. The figures include several simulated curves based upon other models from the literature (see Table 4.C) and a curve obtained with $D=6 \times 10^{-10}$ m^2/s and Eq. [4.30]. The simulations from these other models were calculated from the half-rise times listed in Table 4.B and the expressions listed in Table 4.C. Although this may at first appear to be an unfair comparison because our model uses the entire curve to obtain D, while these other models use a single data point ($t_{1/2}$), the latter procedure is that proposed by

these models. Furthermore, there are other models[9,12] that would probably give a satisfactory fit to the curve, but require previous knowledge of various constants (e.g.,surface reaction rate constants) before fitting and so were not considered.

Table 4.C lists the diffusivities that were determined from each model for the processes #A, #B and #C. All three analyses using the constant concentration boundary condition (CC) yield very similar values for D (e.g., 2 - 2.8 x 10^{-10} m^2/s) for all processes #A-C. The constant flux boundary condition yields a higher value for D (e.g., 6.4 - 7.7 x 10^{-10} m^2/s). This range of values was close to that predicted by the proposed model (e.g., 6.0 x 10^{-10} m^2/s). Although none of the curves fits the experimental data exactly, the models listed in Table 4.C only fit the experimental data well over specific regions of the curves in Figures 4.7-4.9 (e.g., short times or long times). The model proposed by this paper fit the curves best of all for both short, intermediate and long times. Thus, the effective diffusivity for the steel tested by processes #A, #B and #C is assessed to be 6 x 10^{-10} m^2/s. This value of D is within the range of accepted values for low carbon steel[19].

TABLE 4.C
A Comparison of Diffusivity Analyses

Analyses	Expression for D	Expression for $i(t)/i(\infty)$	D [$10^{-10}m^2/s$] #A	#B	#C
CC - Yen[6]	$(0.116\ L^2)/t_{1/2}$	$1 - \exp(-6\tau)$	2.0	2.4	2.0
CC- Fourier[5]	$(0.140\ L^2)/t_{1/2}$	$1 - 2\exp(-\pi^2\tau)$	2.8	2.5	2.4
CC- Laplace[5, 8]	$(0.140\ L^2)/t_{1/2}$	$2(\pi\tau)^{-1/2}\exp(-1/4\tau)$	2.8	2.5	2.4
CF - Laplace[8]	$(0.379L^2)/t_{1/2}$	$1 - (4/\pi)\exp(-\pi^2\tau/4)$	6.7	7.7	6.4
Proposed Model	Curve Fit Procedure	Eq [30]	6.0	6.0	6.0

CC: constant coverage; CF: constant flux; Laplace or Fourier refers to solution type of Eq. [4.4]. $\tau = Dt/L^2$

Using the data in Table 4.B, the effective diffusivity, the Eqs. [4.32]-[4.34] and assuming κ_2 was large, the parameters found in Table 4.D were calculated. As shown in Table 4.D, κ_1 and $c(0,\infty)$ increase with agitation.

Although processes #A and #B use higher charging currents and have higher permeation currents than process #C, it is interesting that the κ_1's obtained for processes #A and #B in Table 4.D are an order of magnitude smaller than the κ_1 obtained for process #C. However, by comparing the respective values of c_1 and κ_1 for the three processes, it is evident that κ_1 is a measure of the efficiency with which the hydrogen provided by a given process (c_1) is absorbed into the metal (c(0,L)). Process #C transfers to the metal a larger percentage of the hydrogen provided than either process #A or #B. However, for the latter two processes there is considerably more hydrogen available than for the former. Thus, more hydrogen is absorbed from processes #A and #B than from #C. Such a conclusion is further supported by the considerable hydrogen evolution witnessed during processes #A and #B which was lacking in process #C. Thus, both the mass transfer coefficient, κ_1, and the effective hydrogen concentration, c_1, provided by a given process are important to hydrogen absorption.

TABLE 4.D
Parameters Calculated from Permeation Data

Process	c_1 [mol/m^3]	κ_1 [m/s]	c(0,t) [mol/m^3]	c(L,0) [mol/m^3]	κ_2 [m/s]	c_2 [mol/m^3]
A) Agitation-Charging	3.43×10^{3}	3.78×10^{-8}	1.62	1.30×10^{-10}	1.0	10^{-16}
B) Charging only	3.43×10^{3}	2.60×10^{-8}	1.11	8.91×10^{-11}	1.0	10^{-16}
C) Agitation only	3.17×10^{1}	7.25×10^{-7}	0.285	2.28×10^{-11}	1.0	10^{-16}

4.3.3 Modelling Hydrogen Absorption from Single and Multiple Processes

To utilize the full power of this model, more than calculating the κ_1 parameter for a given charging condition should be attempted. The permeation test yields information that takes an hour or several hours to obtain. Most industrial processes that reduce hydrogen on a metal surface occur in fractions of that time (i.e., seconds). To apply the experimentally obtained information to industrial processes, it is useful to evaluate the amount of absorbed hydrogen in very short time frames.

The following procedure is recommended to accomplish this task. Permeation tests should be performed under the process, or processes, of interest. From these experiments, values of κ_1, c(0, L) and c_1 may be obtained using Eqs. [4.1], [4.2] and [4.32]-[4.34]. Using these values that were measured for each process and for a given process time, Eq. [4.28] may be used to calculate the hydrogen concentration profile in a sheet undergoing a process or processes for a specified time.

The power of the technique is threefold: 1) Parameters measured under laboratory conditions may be used to simulate realistic processes; 2) Non-uniform distributions of hydrogen may be present in the sheet for each simulation, thus, allowing consecutive processes to be evaluated; 3) Evaluation of hydrogen absorption and desorption is illustrated by concentration profiles in a metal for any time.

This procedure is illustrated by using the permeation results obtained from charging three identical steel sheet specimens under different cathodic processes. It was assumed that the permeation tests (see Table 4.B) were performed to simulate three "electroprocesses of interest" on a low carbon steel sheet. Using the "agitation with charging," "charging only," and the "agitation only" results (Tables 4.B & 4.D), the

three simulations were performed for t = 10 seconds each. It was assumed that the sheets are cathodically polarized on both sheet surfaces (i.e., $\kappa_1=\kappa_2$ for the profile simulation).

The concentration profiles generated from these simulations are illustrated in Figure 4.10. By integrating the curves contained in Figure 4.10, the total amount of hydrogen absorbed from the individual process steps, C_{ind}, was determined and is listed in Table 4.E. The agitation-charging condition produced the highest amount of absorbed hydrogen.

TABLE 4.E
Results of Hydrogen Profile Simulations

Process	C_{ind}[moles]	C_{mult}[moles]
A) Agitation-Charging	2.59×10^{-9}	1.61×10^{-9}
B) Charging only	1.78×10^{-9}	1.11×10^{-9}
C) Agitation only	4.59×10^{-10}	2.86×10^{-10}

Eq. [4.28] suggests that the effects of multiple processes may also be treated. Using a similar procedure as above, permeation tests may be performed and the respective parameters should be obtained for each process of interest. For the first process, process time and f(x) = 0 (no initial distribution), Eq. [4.28] may be used to calculate the concentration profile. Using a looping scheme, this profile is fed back into Eq. [4.28] as f(x), along with the new parameters for the next process. This looping scheme may be repeated for any number of processes. This procedure will allow multiple processes of different electrochemical conditions to be evaluated as a whole.

As an example of such a procedure, the three processes simulated above will be used in a multiple process simulation. Each process used above will be immediately followed by an anodic process of equal length (10 seconds). For illustration purposes, several assumptions will be made for the anodic cycle. The anodic cycle will be assumed to occur over a short enough interval so as to make corrosion processes negligible. In addition, the anodic cycle will provide hydrogen concentrations, c_1=c_2, that are zero. Although no experiments have been performed to evaluate the hydrogen exit kinetics, for illustration purposes, it will be assumed that the hydrogen may exit with less resistance than entry. Thus, all processes used $\kappa_1 = 10^{-5}$ m/s for the anodic simulation. Using Eq. [4.28] for each of the three process sets, the curves in Figure 4.11 were obtained. The amount of hydrogen from each process set is listed in Table 4.E.

4.3.4 Advantages and Limitations of the Model

The model presented by this paper has several distinct advantages over other models. (i) The model allows a given charging situation to be uniquely quantified by a single data set of c_1, κ_1, $c(0,\infty)$, $c(L,\infty)$, κ_2, c_2 and D values. (ii) The hydrogen permeation is defined not only on the entry, but also on the exit surface of the metal sheet. (iii) An arbitrary hydrogen distribution may also be defined within the sheet. (iv) The κ parameters allow quantification of phenomena which result in deviations from Nernst/Sievert behavior. Thus, for the first time, a model is presented to extend the thermodynamic treatment of Nernst to higher fugacities. (v) The model allows multiple sets of charging parameters to be used to simulate the effects of multiple charging processes lasting an arbitrary process time.

The model presented by this paper, however, has several limitations. (i) Although the model can clearly state that deviation from Nernst/Sievert behavior is occurring, as stated, it can't differentiate between the various surface reactions to determine the responsible mechanism. (ii) The model can't quantify non-steady state permeation effects (e.g., a decrease in permeation due to subsurface damage[13]) with a single set of c_1, $c(0,\infty)$, $c(L,\infty)$, c_2, D. For example, if D became more increasingly dependent upon concentration, then it is reasonable that the actual situation would deviate from that predicted by Eqs. [4.1] and [4.2]. Hence, if such behavior is assumed to be accounted for by κ_1, then a range of κ_1 values could be specified. Such a suggestion should be theoretically and experimentally investigated. (iii) The flux curves as illustrated in Figure 4.2 clearly show when Nernst/Sievertian behavior is dominant, however, to relate this to "surface dominant" or "diffusion dominant" behavior still needs to be investigated. (iv) The equations presented in this paper provide a strong methodology for analyzing hydrogen effects in iron and iron alloys, but to be used with metal sheets other than iron alloys requires that a relationship similar to Eq. [4.2] be experimentally derived for the metal-hydrogen system of interest. Notwithstanding the above limitations, the model does extend the utility of such expressions as Eqs. [4.1]-[4.2] and provides some insight to the surface and subsurface phenomena that can affect permeation.

4.4 Conclusions

A model was presented to evaluate hydrogen entry and/or exit in metals exposed to an aqueous environment. The model can be applied to permeation data and can be used to evaluate both surface and metallurgical hydrogen interactions. The model geometry is sufficiently general enough to handle arbitrary charging conditions on

either side of and an arbitrary hydrogen distribution within a metal sheet. The model can also evaluate hydrogen behavior resulting from multiple charging processes.

Simulated permeation curves were presented to show the influence of the model parameters upon permeation behavior. The parameters κ_1, κ_2 and D were all found to affect the shape of a permeation curve.

The model was validated by the application to solution agitation during permeation of a low carbon steel sheet. By curve fitting the model to experimental data, the diffusivity, surface solubilities and κ on both sides of a metal sheet were obtained. When compared to other popular models, the model presented by this paper fit the experimental data well for short, intermediate and long times. The diffusivity of 6×10^{-10} m^2/s is within the range of accepted values for low carbon steel. In addition, both κ_1 and $c(0,\infty)$ were found to increase with increasing agitation.

The model provides several useful tools for analyzing hydrogen permeation data. First, by applying the model to permeation data, the charging process used for the experiment may be characterized by several parameters obtained by the model. Second, using one or more of these parameter sets, the effect of one or more charging processes may be evaluated by using the model to calculate hydrogen distributions in a metal sheet. This allows the amount and distribution of hydrogen in a sheet to be determined for an arbitrary amount of time. Finally, for a given charging condition, a flux curve may be calculated which may help determine the effect of influencing κ_1, κ_2 or D upon the steady-state flux.

DEFINITIONS OF SYMBOLS

A	reduced parameter from Eq. [4.12]
β_n	transcendental parameter from Eq. [4.15]
C(x,t)	concentration of hydrogen at position, x and time, t
c_n	the effective hydrogen concentrations (fugacity) in the environment on either side of the sheet
c(0,∞)	the steady state hydrogen concentration just underneath the entry surface
c(L,∞)	the steady state hydrogen concentration just underneath the exit surface
D	the diffusion coefficient of hydrogen in the metal
E	reduced parameter from Eq. [4.17]
E_w	the working electrode potential
e_n	reduced parameters from Eq. [4.18]
f(x,t)	an initial distribution of hydrogen in a sheet
f_{H_2}	the activity of hydrogen on a metal surface that is in equilibrium with an equivalent absorbed hydrogen concentration within the metal
F	Faraday's Constant (96,500 C/eq)
h_n	a *normalized mass transfer coefficient*
i^∞	the steady state permeation current density
I	the current density at a particular time t and position $x=x_o$
J	the hydrogen flux through the sheet surface
J^∞	the hydrogen flux through the exit surface of the sheet
κ_n	the *mass transfer coefficient*
k_n	a reduced variable for Eq. [4.10]
L	sheet thickness
T	reduced parameter from Eq. [4.12]
u(x,t)	the steady state solution of Eq. [4.1]
w(x,t)	the non-steady state solution of Eq. [4.1]
Z	reduced parameters from Eq. [4.12]
z	the number of electrons passed for the reduction or oxidation of hydrogen (eq/mole)

References for Chapter 4

1 J.H. Payer, G.M. Michal and C. Rogers: *Corrosion/91*, paper no. 405, NACE, 1991.

2 J.H. Payer and G.M. Michal: submitted to *SAE Transactions*, Detroit, MI. 1991.

3 M.A.V. Devanathan and Z. Stachurski: *Proc. Roy. Soc. Lond. A*, 1962, vol 270, pp. 90-102.

4 M.A.V. Devanathan, Z. Stachurski and W. Beck: *J. Electrochem. Soc.*, 1963, vol. 110, pp. 886-90.

5 J.McBreen, L. Nanis, and W. Beck: *J. Electrochem. Soc.*, 1966, vol. 113, 1218-1222.

6 S.K. Yen and H.C. Shih, *J. Electrochem. Soc.*, 1988, vol. 135, no. 5, 1169-1170.

7 J.Y. Choi: *Met. Trans.*, 1970, vol. 1, pp. 911-919.

8 M.A. Fullenwider: Hydrogen Entry and Action in Metals, Pergamon Press, Inc., Elmsford, N.Y., 1983, pp. 4-17.

9 P.H. Pumphrey; *Scripta Met.*, 1980, vol. 14, pp. 695-701.

10 A. McNabb and P. Foster: *Trans. TMS-AIME*, 1963, vol. 227, pp. 618-627.

11 L. Coudreuse and J. Charles: *Corros. Sci.*, 1987, vol. 27, nos. 10/11, pp. 1169-1181.

12 R.N. Iyer, H.W. Pickering and M. Zamanzedeh: *J. Electrochem. Soc.*, 1989, vol. 136, no. 9, pp. 2463-2470.

13 M.M. Makhlouf and R.D. Sisson, Jr.: *Met. Trans. A*, 1991, vol. 22, pp. 1001-1006.

14 J.P. Hirth: *Metall. Trans. A*, 1980, vol. 11, pp. 861-890.

15 J.O'M. Bockris and A.K.N. Reddy: Modern Electrochemistry, Plenum Press, New York, NY, 1970, pp. 906-908.

16 M.D. Archer and N.C. Grant: *Proc. Roy. Soc. Lon. A*, 1984, vol. 395, pp. 165-183.

17 H.S. Carslaw and J.C. Jaeger: Conduction of Heat in Solids, 2nd ed., Clarendon Press, Oxford, Great Britain, 1959.

18 M.A.V. Devanathan and Z. Stachurski: *J. Electrochem. Soc.*, 1964, vol 111, pp. 619-623.

19 J. Volkl and G. Alefeld: in Diffusion in Solids: Recent Developments, eds. A.S. Nowick, J.J. Burton, Academic Press, New York, 1975, pp. 281-283.

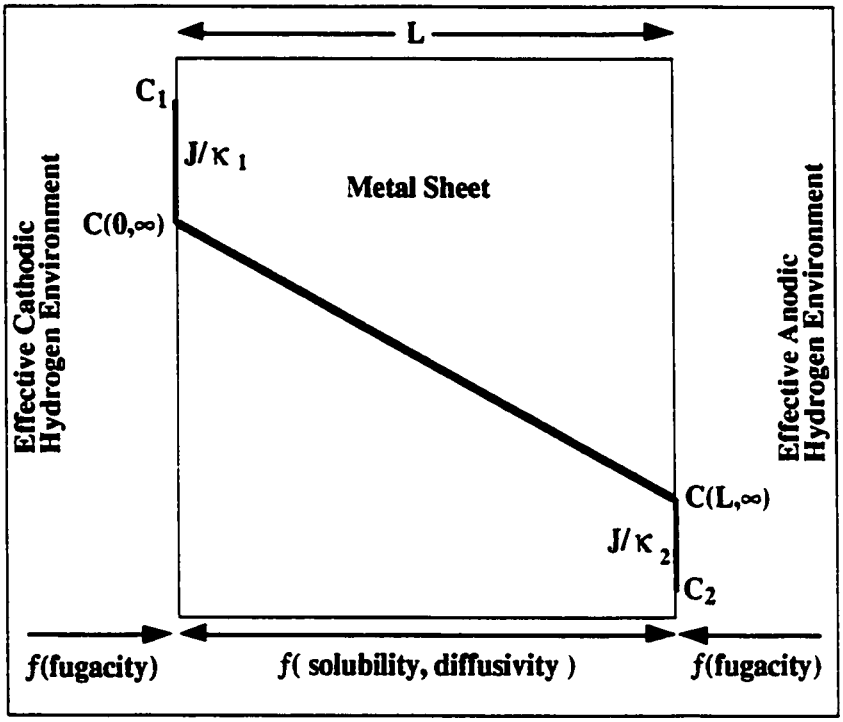

Figure 4.1: The effective geometry of a permeation test as viewed by our model.

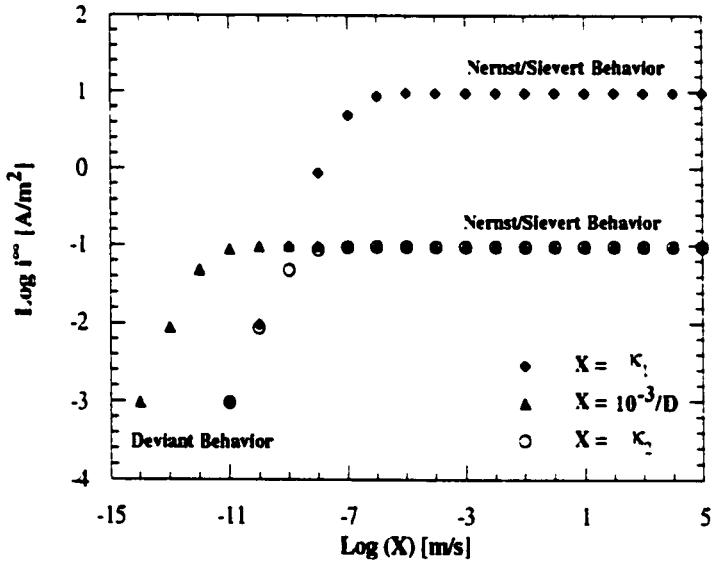

Figure 4.2: Three flux curves are illustrated. The curves are based upon Eq. [4.35] and show the variance of the flux when one parameter varies while maintaining the other parameters constant. The three parameters investigated are κ_1, κ_2 and D.

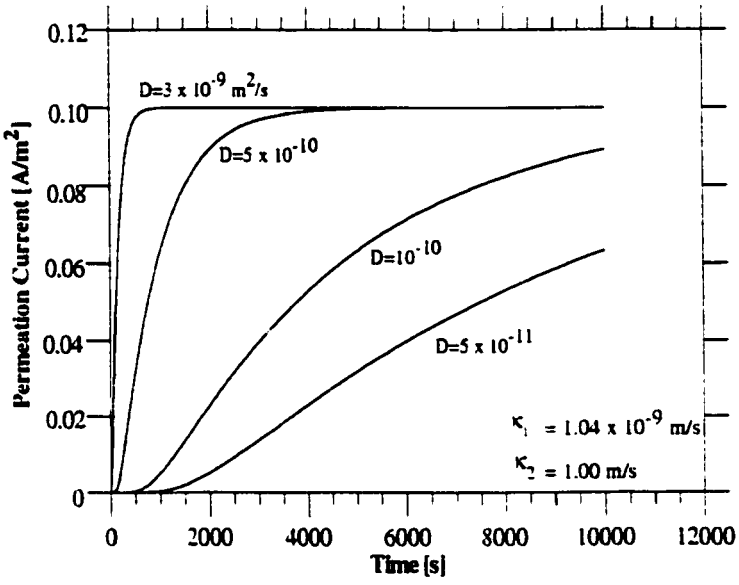

Figure 4.3: *Bulk Transport Effects* : The effect of hydrogen diffusivity on the hydrogen permeation current (simulations 1-4). κ_1 and κ_2 are held constant for this simulation. L = 10^{-3} m.

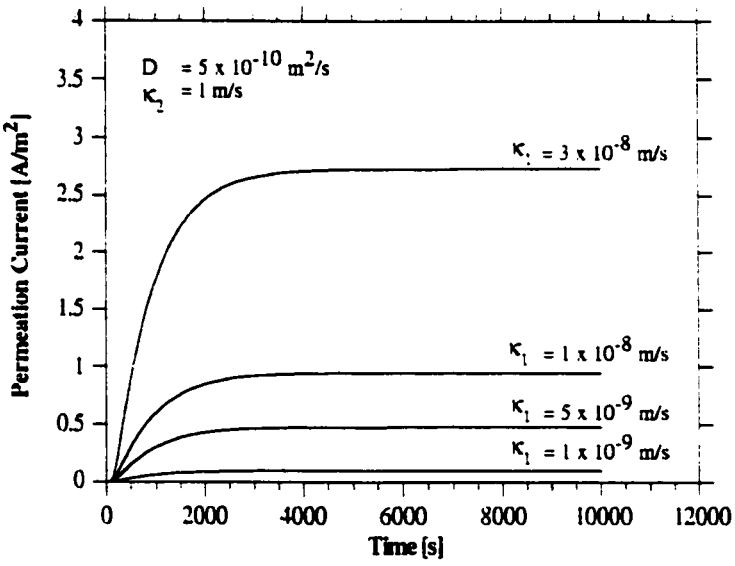

Figure 4.4: *Entry Effects* : The effect of κ_1 on the hydrogen permeation current (simulations 5-8). D and κ_2 are held constant for this simulation. L = 10^{-3} m.

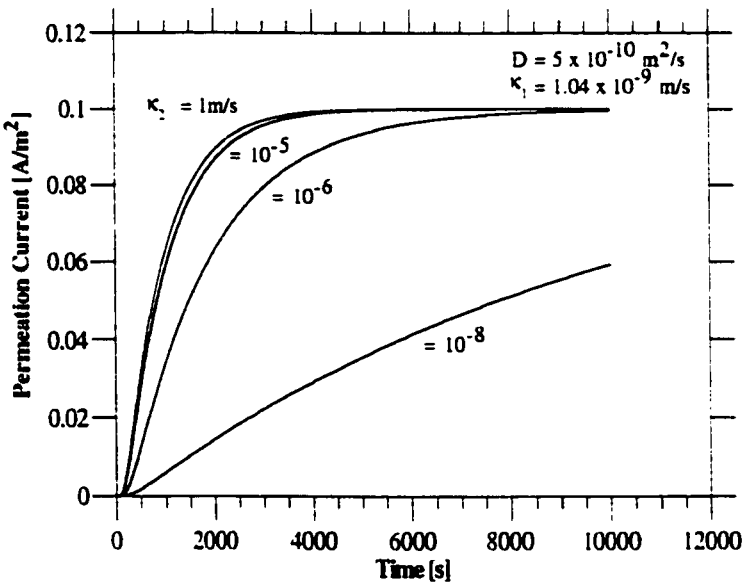

Figure 4.5: *Exit Effects* : The effect of κ_2 on the hydrogen permeation current (simulations 9-12). D and κ_1 are held constant for this simulation. L = 10^{-3} m.

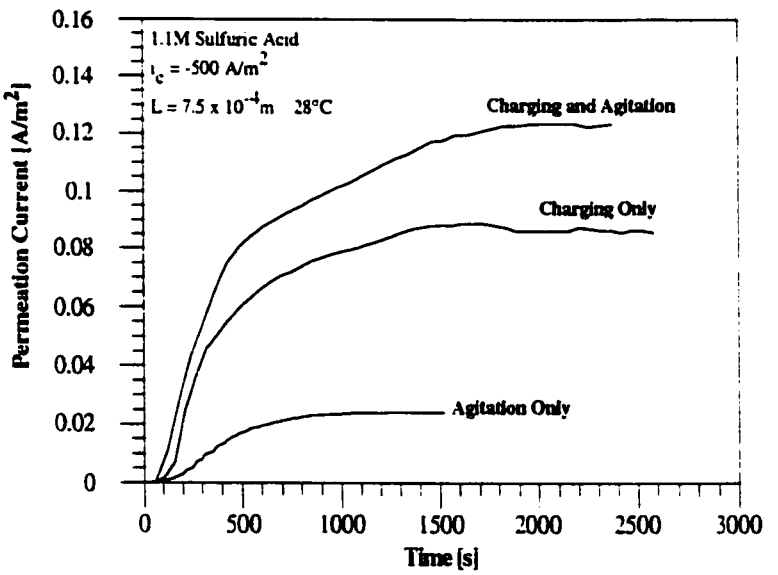

Figure 4.6: *The Effect of Catholyte Agitation.* Experimental permeation curves for A) Agitation and Charging/Cathodic Polarization (i_c = -500A/m^2). B) Charging only (i_c = -500A/m^2). C) Agitation only. The permeation tests were performed as: N_2/ process A.B or C/ steel / Pd / 0.1M NaOH / N_2.

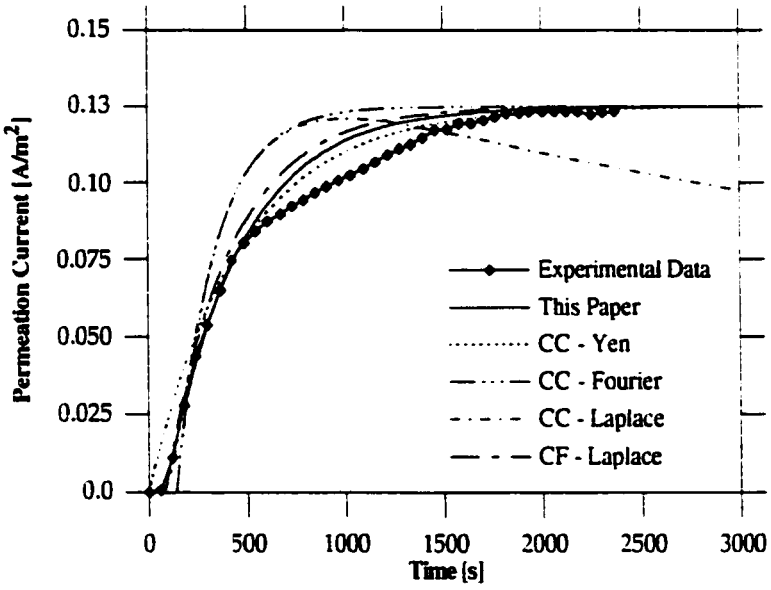

Figure 4.7: Curve Fit of Process #A) Agitation - Charging. Simulated curves as defined in Table 4.C are overlayed on the data.

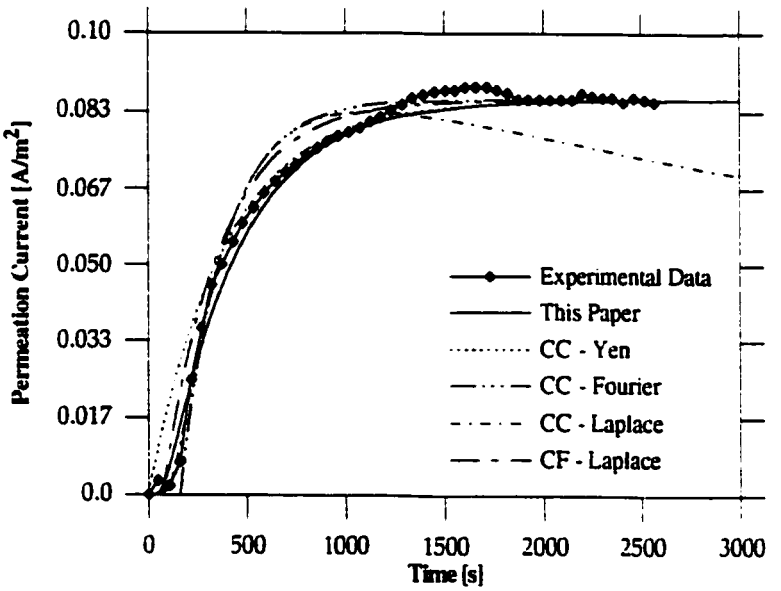

Figure 4.8: Curve Fit of Process #B) Charging Only. Simulated curves as defined in Table 4.C are overlayed on the data.

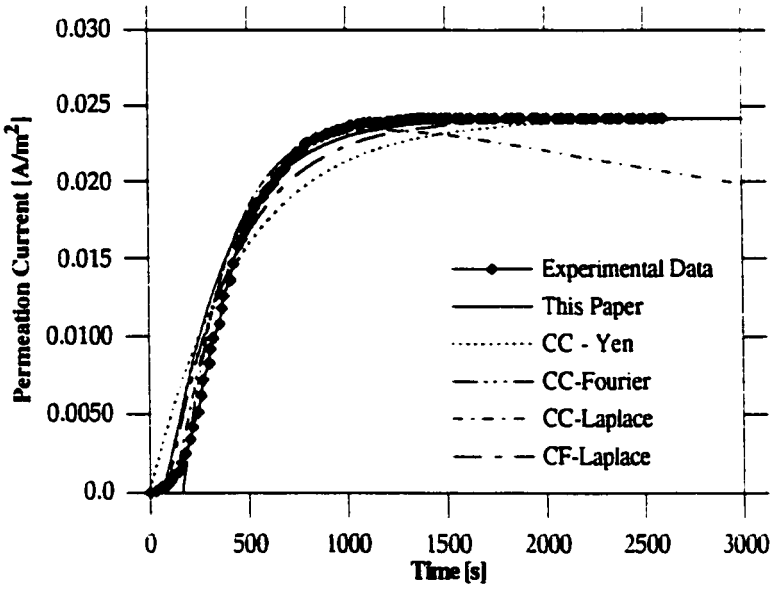

Figure 4.9: Curve Fit of Process #C) Agitation Only. Simulated curves as defined in Table 4.C are overlayed on the data.

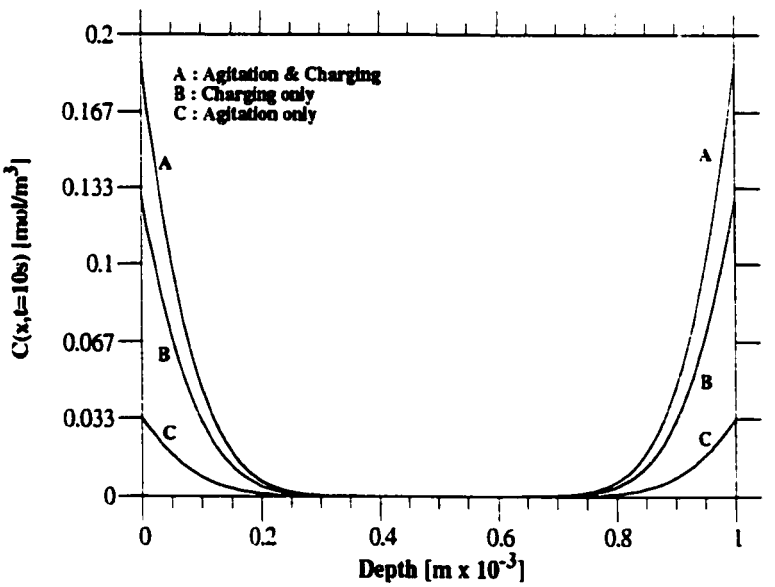

Figure 4.10: *Hydrogen Concentration Profiles from Single Processes.* Three hydrogen concentration profiles in a low carbon steel sheet of thickness = 10^{-3} m are shown. Each represents a different cathodic charging condition that lasts 10 seconds: A) Agitation and Charging (i_c = -500A/m^2), B) Charging only (i_c = -500A/m^2), C) Agitation only.

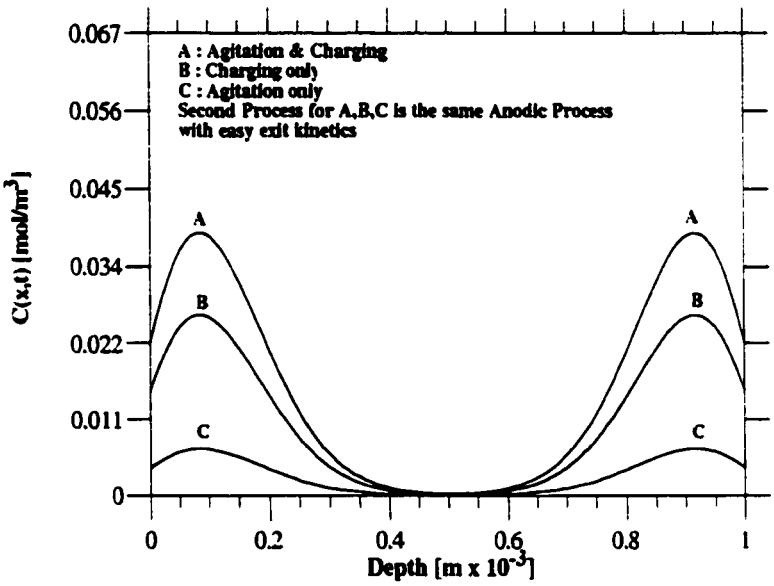

Figure 4.11: *Hydrogen Concentration Profiles from Multiple Processes.* Three hydrogen concentration profiles in a low carbon steel sheet of thickness = 10^{-3} m are shown. Each represents the result of two charging conditions that lasts 10 seconds each: A) Agitation and Charging (i_c = -500A/m^2), followed by Anodic Polarization; B) Charging only (i_c = -500A/m^2), followed by Anodic Polarization; C) Agitation only, followed by Anodic Polarization.

Chapter 5

Electroprocess Parameters that Control Hydrogen Absorption in Low Carbon Steel

5.1 Introduction

There has been recent interest[1,2] in hydrogen that is absorbed from various electrochemical pre-treatment processes on an electrogalvanizing line. Such absorbed hydrogen may diffuse to areas of poor adhesion along the Zn/Steel interface and form blisters in the coating. A typical substrate material for electrogalvanizing is cold rolled, low carbon (0.05 wt.%C) steel.

The interaction between hydrogen and iron or steel has been well documented in several reviews[3,4,5]. Specific studies have emphasized the effects of pH[6,7], cathodic current[8,9,10,11], electrolyte agitation[12], surface finish[13] or hydrogen diffusion[14,15]. However, most of these studies have been conducted under benign conditions (i.e., low current densities and minimal agitation). The electroprocesses (the electrocleaning, electropickling and electroplating steps) in steel plating lines operate under severe conditions of electrolyte pH, high current densities (-100 to 500mA/cm^2) and vigorous agitation (line speeds of 90 to 150 m/min). Thus, there is a need to evaluate those parameters which may be controlled on an electrogalvanizing line at the more severe conditions.

This study provides a base data set for this steel/charging system which may be used in future investigations. The effect of the controlling parameters was evaluated as to their influence on the hydrogen absorption in low carbon steel. In particular, the effect of low electrolyte pH, cathodic current density, electrolyte agitation and surface

finish were investigated. An analytical model[16] was employed to understand the hydrogen entry kinetics.

5.2 Results

5.2.1 The Effect of Electrolyte pH upon H Permeation

Both the hydrogen permeation rate and the applied overpotential were found to vary with pH during the galvanostatic permeation tests. The test was performed by adjusting the charging solution to a specific pH level with sulfuric acid. Beginning with the 2.6 pH condition, a permeation test was performed until steady-state conditions were achieved. The charging solution was flushed from the cathodic cell and fresh solution at a lower pH was added. The solutions tested were of pH 2.6, 1.0 and 0.

Figure 5.1 shows the effect of pH on the hydrogen permeation behavior under galvanostatic conditions (-0.5 mA/cm^2). Notice that with decreasing pH, the steady-state permeation current increases. In addition, the pH= 0 solution showed non-steady state behavior. Looking at figure 5.1, the anodic current density decreased to a steady value (11$\mu A/cm^2$) after attaining a maximum (55$\mu A/cm^2$). This suggests a change in the surface or subsurface was occurring over the course of the test[9].

TABLE 5.A
The Effect of pH on Hydrogen Permeation

pH	i_c [mA/cm^2]	i_a^∞[$\mu A/cm^2$]	E_w [V-SCE]
0.0 (10M)	-0.5	55.0(11.0)*	-0.470
1.0	-0.5	8.7	-0.585
2.6	-0.5	0.8	-0.785

T= 25°C. L= 0.075cm.

The overvoltages for each solution, necessary to maintain the constant current condition, are shown in figure 5.2 and listed in table 5.A (the values reported were obtained at the end of the permeation test). The overvoltage was found to decrease with

decreasing pH. Although these overvoltages are higher than the overpotentials for hydrogen evolution, the hydrogen overpotential on iron decreases with decreasing pH[7]. The results reported here are consistent with this idea.

5.2.2 The Effect of Cathodic Current upon H Permeation

The influence of cathodic current density upon hydrogen permeation was studied over the range of -0.25 mA/cm^2 to -100mA/cm^2 in pH = 1 sulfuric acid. The tests were performed by two methods. The first method ("the step test") was performed by setting i_c and allowing steady-state conditions to occur. Once steady-state conditions had been reached, the i_c was adjusted to a higher i_c value. A single specimen was used for all i_c steps. The second method ("the single test") was performed by setting i_c and allowing steady-state conditions to occur, but a different specimen was used for each i_c.

TABLE 5.B
The Effect of Cathodic Current on Hydrogen Permeation

i_c	i_a^∞ [$\mu A/cm^2$]		E_w [V-SCE]		i_a^∞/i_c [%]	
[mA/cm^2]	Step	Single	Step	Single	Step	Single
0.25	2.35	2.6	-0.533	-0.517	0.94	1.04
0.5	2.70	3.0±0.3	-0.550	-0.537	0.54	0.60
1	3.30	3.9	-0.594	-0.587	0.33	0.39
10	5.7(6.1)	–	-0.681		0.06	–
40	–	5.8	–	-0.689	–	0.02
50	18(22)	8.6	-0.697	-0.692	0.02	0.02
100	22(33)	13±2(16±1)	-0.722	-0.696	0.02	0.01

Catholyte: pH=1,H_2SO_4; Anolyte: 0.1M NaOH; T=25°C; L= 0.075cm. The value in parentheses is the maximum in the permeation current. Standard deviation values are given for values obtained from three or more tests.

For i_c's which were greater than 10mA/cm^2 for the step method or greater than 50mA/cm^2 for the single tests, there are two features on a permeation curve that are of interest to these results. For low i_c's, the anodic current rises to a steady-state value (i^∞) for long times. However, for higher i_c's, the current increases to a maximum and then

decreases to some relatively steady-state value. Where this principle applies, Table 5.B lists both values and Figure 5.3 shows a range for the steady-state permeation current.

Figure 5.3 illustrates the results of both methods in the traditional[5] form of i^{∞} vs $i_c^{1/2}$. From the figure, the steady-state permeation current increases with increasing cathodic current. For i_c's < 10 mA/cm^2, the results follow similar trends to those reported by Racszinski[5]. However, at higher i_c's the anomalous maximum behavior not reported in Racszinski's work makes comparisons difficult. Both the step and single methods produced similar trends, however, the magnitude of the steady-state current for the step method was found to be 2-3 times larger than the single method results. This increased anodic currents can only be attributed to a change in the surface condition of the steel due to prolonged charging conditions, particularly at the higher cathodic current levels.

Figure 5.4 illustrates the effect of the cathodic current density upon the permeation efficiency. The permeation efficiency ($P_e = 100i^{\infty}/i_c$ %) is a measure of the amount of hydrogen exiting the steel sheet, normalized to the amount provided on the entry surface. From the figure, it is evident that only a minimal percentage (<1%) of hydrogen on the entry surface transports through and exits the sheet. As the cathodic current density increases, the P_e decreases. This result indicates that as the current density increases, a larger percentage of available hydrogen on the entry surface participates in hydrogen gas evolution.

Figure 5.5 illustrates the effect of i_c upon E_w over long charging times. The steel working potential was found to shift to more negative potentials with increasing the

cathodic current. In addition, for cathodic current densities greater than 10mA/cm^2, the potential does not change significantly. This may be explained by the enhanced hydrogen evolution on the steel surface. Each potential was measured after steady-state permeation conditions were reached (a minimum of 3.5 hours of charging). If the data set is assumed to be linear, the $d\eta/d\log i_c$ value was -53 and -57mV for the step and single test methods, respectively. The value reported[10] for iron at 20°C in 0.1M H_2SO_4 is -115 mV. This deviation may be explained by a lack of significant agitation, by the significant charge time prior to overvoltage measurement and the severe cathodic currents used.

TABLE 5.C
The Effect of Electrolyte Agitation on Hydrogen Permeation

Process	i_∞ [μA/cm^2]	E_w [V-SCE]
Agitation only	2.2	-0.487
Charge only	8.6	-0.606
Agitation + Charge	12.5	-0.606

Agitation was performed by a flow pump. The permeation tests were performed by Dr. Omer Dogan at the LTV Steel Technical Center, Brecksville, OH. i_c = -50mA/cm^2 in the electropickling solution. L= 0.070 cm.

5.2.3 The Effect of Electrolyte Agitation upon H Permeation

Agitation was found to significantly affect the amount of hydrogen permeating the steel sheets. Figure 5.6 illustrates the results from the agitation permeation tests. The parameters obtained from the tests are listed in table 5.C. The three catholyte conditions were a) electrolyte agitation via a flow pump, no charging, b) i_c = 50mA/cm^2 and no agitation, c) i_c = 50mA/cm^2 and agitation as in a). It is evident from the figure that electrolyte agitation increases the steady-state anodic current by 30%. A similar dramatic effect was found by Shirkhanzadeh[12] when he rotated carbon steel electrodes and measured the resulting permeation behavior. He found the permeation current to

increase 25% when the rotation speed was tripled. He attributed the enhanced permeation to the increase in the rate of the discharge reaction. Although the flow conditions used in this paper are different from those used by Shirkhanzadeh, the trend is consistent; increasing the electrolyte flow rate, increases the permeation rate.

5.2.4 Effect of Surface Finish upon H Permeation

Figure 5.7 illustrates the increase in the permeation current as the surface finish was varied from 1200 grit (15.2μm) to 320 grit (46μm). The entry surfaces of permeation foils were polished to the specific finishes and then tested. Similar specimens were characterized by profilometry. The profilometry showed that the average surface roughness number, R_a, increases with decreasing grit number. The results are listed in table 5.D. Thus, the steady-state permeation current increases with increasing average roughness number. Makhlouf[13]. measured a 30% increase in permeation current with a change in surface finish (600 to 180) in an AISI 4340 steel foil. Although the specific charging condition was not given in the Makhlouf paper, the results presented here are consistent with that author's reported trend.

TABLE 5.D

The Effect of Steel Surface Finish on Hydrogen Permeation

Grit [#]	Grit Size [μm]	R_a [μm x 10]	i_a^∞ [μA/cm^2]	E_w [V-SCE]
320	46.2	30.5 ± 0.2	5.22 ± 0.2	-0.585
500	30.2	1.310 ± 0.003	4.77 ± 0.2	-0.584
1200	15.2	0.70 ± 0.02	2.56 ± 0.2	-0.584

i_c = -0.5mA/cm^2; T=25°C; L= 0.070 cm. Profilometry was performed by Dr. George Themolous at the LTV Steel Technical Center, Brecksville, OH.

5.3 Discussion of the Results

5.3.1 The Hydrogen Diffusivity for the Low Carbon Steel

The diffusivity, D, for hydrogen in the low carbon steel used in this investigation was found to have a 25°C value of 6.0×10^{-6} cm^2/s. Using the electrochemical permeation technique, data was obtained that allowed satisfactory fit[16] by the model's simulations. This value for D is consistent with values reported for similar steels[5] and should be considered to be an "apparent diffusivities" as discussed by McNabb[17].

5.3.2 Influence of the Controlling Parameters upon Hydrogen Behavior

The controlling parameters have been discussed in terms of permeation current, however, to gain more insight, it would be useful to relate these results to what is occurring on the steel's entry surface. Recall from Chapter 4 that Eq. [5.1] describes the steady-state hydrogen flux in terms of both surface (κ_1, κ_2) and bulk (D) parameters:

$$J^{\infty} = \frac{\Delta C}{\left(\frac{L}{D} + \frac{1}{\kappa_1} + \frac{1}{\kappa_2}\right)} \approx \frac{\Delta C}{\left(\frac{L}{D} + \frac{1}{\kappa_1}\right)} \qquad [5.1]$$

Since κ_2 is very large due to the experimental design[16], the flux reverts to a simplified expression that is a function of the entry-surface kinetics and the diffusivity. Since the controlling parameters are expected to have only a minimal effect on D, κ_1 is a useful parameter to evaluate. Once steady state hydrogen transport conditions are established across the entry surface, the metal sheet and the exit surface, the following three equations[16] define the same flux, J_∞.

$$J_{\infty} = \kappa_1 (c_1 - c(0, \infty)) \quad [5.2]$$

$$J_{\infty} = D \frac{c(0,\infty) - c(L,\infty)}{L} \quad [5.3]$$

$$J_{\infty} = \kappa_2(c(L, \infty) - c_2) \quad [5.4]$$

From Eqs. [5.2]-[5.4] the solubility of hydrogen just inside the entry surface, $c(0, \infty)$, and the value of κ_1 may be calculated. These values are listed in table 5.E.

TABLE 5.E
Model Parameters as a Function of Controlling Parameters

Condition	κ_1 [cm/s]	$c(0,\infty)$ [mol/cm^3]	C(10s) [mol]
pH=0 (10M) max	5.21×10^{-5}	7.12×10^{-6}	1.79×10^{-8}
pH=0 (10M) min	6.85×10^{-6}	1.42×10^{-6}	2.40×10^{-9}
pH=1	1.57×10^{-6}	1.13×10^{-6}	1.84×10^{-9}
pH=2.6	1.16×10^{-8}	1.04×10^{-7}	1.70×10^{-10}
As pH decreases	**increase**	**increase**	**increase**
i_C=0.25	7.08×10^{-6}	3.37×10^{-7}	5.83×10^{-10}
i_C=0.5	3.60×10^{-6}	3.89×10^{-7}	6.48×10^{-10}
i_C=1	6.43×10^{-7}	5.05×10^{-7}	8.14×10^{-10}
i_C=40	1.79×10^{-8}	7.51×10^{-7}	1.21×10^{-9}
i_C=50	2.36×10^{-8}	1.11×10^{-6}	1.79×10^{-9}
i_C=100 max	3.05×10^{-8}	1.68×10^{-6}	2.69×10^{-9}
i_C=100 min	3.75×10^{-8}	2.07×10^{-6}	3.30×10^{-9}
As i_c increases	**decrease**	**increase**	**increase**
Agitation	7.25×10^{-5}	2.85×10^{-7}	4.59×10^{-10}
Charge only	2.60×10^{-6}	1.11×10^{-6}	1.78×10^{-9}
Agitation/charge	3.78×10^{-6}	1.62×10^{-6}	2.59×10^{-9}
With Agitation	**increase**	**increase**	**increase**
1200 grit finish	5.12×10^{-7}	3.32×10^{-7}	5.38×10^{-10}
500 grit finish	9.60×10^{-7}	6.18×10^{-7}	1.02×10^{-9}
320 grit finish	1.05×10^{-6}	6.76×10^{-6}	1.11×10^{-9}
As grit # decreases	**increase**	**increase**	**increase**

Both κ_1 and $c(0,\infty)$ were found to be affected by the changes in hydrogen charging conditions. The value of κ_1 is shown in Table 5.E to increase with decreasing pH, decreasing i_C, increasing agitation and decreasing grit number. Figures 5.8-5.9 illustrate the effects of the controlling parameters upon $c(0,\infty)$. The hydrogen concentration just beneath the surface, $c(0,\infty)$, is shown to increase with increasing

current density, agitation or decreasing grit finish or pH. The lowest value for which a range of $c(0,\infty)$ values were obtained (i.e., when non-steady state behavior was found) was $\sim 10^{-5.7}$ mol/cm^3. This was similar for both the pH and the cathodic current tests (see Figure 5.8). Such values are consistent with those obtained by Bockris for similar behavior on iron.

The hydrogen discharge reaction, Eq [5.5], predicts that the amount of hydrogen on the metal surface is dependent upon the amount of available hydrogen and the applied driving force (I or η). The hydrogen absorption reaction, Eq. [5.6] suggests that by substantially increasing the amount of available hydrogen, the hydrogen absorption reaction is enhanced. Both lowering the pH and increasing the agitation in the electrolyte increases the supply of available hydrogen for use by the discharge reaction. The pH changes the hydrogen concentration in solution, while the agitation lowers mass transfer resistances. Thus, the enhancement of κ_1 by lowering the pH of increasing the agitation in solution is due to increasing the discharge reaction rate.

$$H^+ + e^- = H_{ads} \qquad [5.5]$$

$$H_{ads} = H_{abs} \qquad [5.6]$$

Equation [5.5] also predicts that the amount of hydrogen adsorbed to the steel surface should increase with increasing applied current. However, the permeation results show that by increasing the cathodic current density, the amount of hydrogen absorbed, $c(0,\infty)$ and i_a^∞, increases, but κ_1, decreases (Table 5.E). The fact that $c(0,\infty)$ and i^∞ increased with i_c is consistent with [5.5] and [5.6]. However, the decrease in κ_1 is an increase in the amount of deviation from Nernst/Sievertian behavior. Hence, such a decrease in κ_1 predicts that another reaction is significantly affecting the concentration of adsorbed hydrogen on the metal surface (e.g., hydrogen evolution). If

a decrease in κ_1 were due to increasing mass transfer resistances alone, κ_1 and $c(0,\infty)$ would both decrease. While increasing the hydrogen flux, the hydrogen adsorption sites become increasingly more saturated, resulting in an enhancement of the hydrogen evolution reaction.

5.3.3 The Effect of Surface Morphology upon H Permeation

The surface finish permeation results can be explained by a) a change in surface area or, b) a rate change in the hydrogen surface reactions. To effectively evaluate the effect of surface finish upon hydrogen permeation it is useful to develop the influence of surface finish upon surface area. The surface finish is dependent upon the number and size of polishing scratches.

Assume for discussion purposes that a sheet of charging area L x L contains N scratches of depth h. Although this analysis holds for more complex arrangements, for simplicity, assume that each scratch is parallel to all others on the steel surface. In addition, assume that the scratch morphology is defined as in figure 5.10. To determine the maximum influence of scratches upon area, the maximum number of scratches is also assumed.

The scratches made during polishing are due to the size of the SiC particles, g (the average diameter of the particle), on the polishing paper. Scratches could be placed no closer than half the particle size from the center of each scratch. Thus, the maximum number of scratches is $N=2L/g$. Furthermore, the scratch depth, h, is related to the particle size, g, by $h=g/G$, where G is a constant (>1).

The surface area of a steel sheet uniformly covered with polishing scratches may be defined by equation [5.7]:

$$\text{Surface Area} = L^2 - N(2h\sin(Q/2))L + 2N(2h\sin(Q/2))L$$

$$= L^2 + 4(L/G)\sin(Q/2) \qquad [5.7]$$

Notice that the surface area does not change with the surface finish if the surface is covered uniformly with scratches. Thus, when comparing different surface finishes, there is no difference in surface area, however, there are significant differences in the number and distribution of scratches.

Thus, the enhanced permeation is not due to changes in surface area, but is, in fact, due to the enhancement of the surface reaction kinetics. The increased permeation of the 320 grit finish over the 1200 grit finish may be due to the former's surface having fewer scratches or larger scratches.

The surface finish most likely affects the adsorbed hydrogen on the metal surface. The number and distribution of scratches on the metal surface will affect both the distribution of adsorption sites and the ability of hydrogen bubbles to evolve. Furthermore, since the tests were performed galvanostatically, then the current density was constant for a given area. However, at sharp ledges, the area is infinitely small, thus, the current density is extremely high. Hence, many sharp peaks on the surface could cause the current to increase locally. Such an effect if widespread enough could increase the hydrogen fugacity locally at the metal surface and more hydrogen would be absorbed. Table 5.E shows κ_1 and $c(0,\infty)$ to both increase with fewer/larger scratches. Although this investigation does not identify a specific mechanism for the influence of the surface finish upon hydrogen absorption, this work emphasizes the significance of the surface morphology upon hydrogen permeation.

5.3.4 Affecting the Hydrogen Absorption Reaction

From Eqs. [4.5]-[4.7], an expression for the hydrogen concentration in the metal sheet (Eq. [4.28]) as a function of position and time in a metal sheet may be obtained. This expression is dependent upon κ_1, κ_2, D, c_1, c_2, and L which are defined in figure 4.1. In addition, the expression is a function of processing time and the hydrogen distribution already present in the metal sheet. The complete expression is defined explicitly elsewhere[16]. Using such an expression, allows hydrogen concentration profiles to be calculated for different treatments acting on the steel sheet. Such profiles provide useful tools to compare different hydrogen environments by examining both the total amount (Table 5.E) of hydrogen absorbed and the penetration depth into the steel sheet (Figures 5.11-6.12) under non-equilibrium conditions.

Concentration profiles have been calculated for the following conditions. Each parameter studied and listed in table 5.E was considered to be a surface treatment acting on either side of a low carbon steel sheet for 10 seconds.

The effect of short (e.g., 10 seconds) chargings on a metal sheet have several ramifications when predicting the amount of hydrogen absorbed by a given condition. The amount of hydrogen absorbed was integrated from the hydrogen distributions and is listed in table 5.E for all of the controlling parameters. In addition, the hydrogen distribution curves shown in the cross section of a 0.01cm steel sheet are shown as examples in figures 5.11-6.12. There are two particular features of these curves that require further discussion: the surface solubility, c(0,10s)=c(0.01cm,10s), and the penetration depth.

After a 10 second process, the surface solubility does not equal that at equilibrium, $c(0,\infty)$. This fact is very important when attempting to predict the amount of hydrogen absorbed due to a short charging process. If $c(0,\infty)$ is used to predict behavior, the prediction will overestimate the amount of hydrogen absorbed.

The penetration depth of the hydrogen distribution in a sheet for short charging times is a function of both the rate of hydrogen entry and the severity of the charging condition. The two parameters that characterize these factors are κ_1 and $c(0,\infty)$. If a process has a high κ_1 and a high $c(0,\infty)$ (easy hydrogen entry, high hydrogen supply for absorption), the hydrogen distribution will penetrate deep in short charge times. Conversely, if a process has a low κ_1 and a low $c(0,\infty)$ (difficult hydrogen entry, low hydrogen supply for absorption), then the hydrogen distribution will not penetrate far from the surface. These two examples are illustrated by the distributions resulting from the pH tests (see figure 5.11). In this case, as pH is lowered, both the value of κ_1 and $c(0,\infty)$ increase.

Alternatively, if κ_1 is low and $c(0,\infty)$ is high (difficult hydrogen entry, high hydrogen supply for absorption) or if κ_1 is high and $c(0,\infty)$ is low (easy hydrogen entry, low hydrogen supply for absorption), then a more complicated situation has occurred and intermediate penetration depths will result. Either there is a large supply of hydrogen, but it can't be absorbed quickly, or there is quick absorption, but not much of a hydrogen supply. In both cases, intermediate penetration depths will be reached with the specific permeability being determined by the particular combination of κ_1 and $c(0,\infty)$. A good example of this behavior is in the cathodic current simulations (see figure 5.12). As the cathodic current is increased, κ_1 decreases, but $c(0,\infty)$ increases.

Notice that the amount of hydrogen absorbed and the c(0, 10s) both vary significantly with cathodic current, but the penetration depth is approximately the same. To further illustrate this point, the penetration depth may be significantly changed by decreasing the pH by 1 (increases hydrogen activity by factor of 10) or the current must be increased by a factor of 100.

5.4 Conclusions

This study provided a database of parameters which are present in the surface treatment of steel prior to the application of an electrogalvanized coating and their effect upon hydrogen permeation behavior. The analytical model[16] applied to the data proved to be useful in both analyzing and interpreting the results.

With a decrease in pH or cathodic current density or an increase in electrolyte agitation or surface roughness (R_a), the deviation from Nernst/Sievertian behavior was shown to decrease. More specifically, the rate of hydrogen absorption was found to increase. Furthermore, with increases in either cathodic current density, solution agitation or or surface roughness (R_a) or with a decrease in pH, the surface solubility, $c(0,\infty)$, increases.

As the current density was increased, a greater proportion of the current was found to participate in hydrogen evolution. In addition, by increasing the current density above 10 mA/cm^2 or decreasing the pH to very low levels (<1), anomalous permeation curves were obtained suggesting surface or subsurface damage.

Several model[16] parameters were useful in interpreting the results. κ_l was found to be sensitive to surface phenomena which might influence hydrogen absorption. In addition, for short charge times, the penetration depth of absorbed hydrogen was found to be a function of κ_l, $c(0,\infty)$, and D. At longer charge times, the penetration depth is determined by D and $c(0,\infty)$ alone.

References for Chapter 5

1 J.H. Payer and G.M. Michal, *Proc. of 5th Auto.Prev.of Corr.*, P-250, Dearborn, MI. (1991), 53-63.

2 J.H. Payer, G.M. Michal and C. Rogers: *Corrosion/91*, (1991): paper no. 405.

3 M. Smialowski, Hydrogen in Steel, Pergamon Press, Oxford & Addison-Wesley Publishing, Reading Massachussetts, (1962): pp.88-90.

4 J.P. Hirth, *Metallurg. Trans.*, **11A**, (1980): pp. 861-890.

5 E.E. Fletcher and A.R. Elsea, "Hydrogen Movement in Steel--Entry, Diffusion and Elimination," *DMIC Report*, **219** Battelle Memorial Institute, (1965).

6 R.M. Hudson, *Corrosion*, **20** (1969) p.24t.

7 J.O'M. Bockris, *Chem. Rev.*, **43** (1948):525-577.

8 H. Zeilmaker, *Electrodepos. & Surf. Treat.*, **1** (1972/73): p. 109.

9 J.O'M.Bockris, Proceedings of Stress Corrosion Cracking and Hydrogen Embrittlement of Iron Base Alloys, NACE, 1973: p. 286.

10 J.O'M. Bockris, J. McBreen and L. Nanis, *J. Electrochem. Soc.*, **112**[10], (1965): p. 1028.

11 K. Bolton and L.L. Shreir, *Corrosion Sci.*, **3** (1963): pp. 17-33.

12 M. Shirkhanzadeh, *Corrosion Sci.*, **2** (1988): 201-206.

13 M.M Makhlouf and R.D. Sisson, Jr., *Metallurg. Trans. A*, **22A** (1991) 1001-1006.

14 W. Beck, J. O'M. Bockris, J. McBreen and L. Nanis, *Proc. Roy. Soc. Lond.*, **290A** (1965) 191-206.

15 A. S. Nowick and J.J. Burton, Diffusion in Solids, Academic Press, New York, (1975) pp. 281-284.

16 S.L. Amey, G.M. Michal and J.H. Payer: submitted to *Metallurgical Transactions A*, spring 1992.

17 A. McNabb and P.K. Foster: *Trans.of TMS-AIME*, vol. 227, (1963): pp. 618-627.

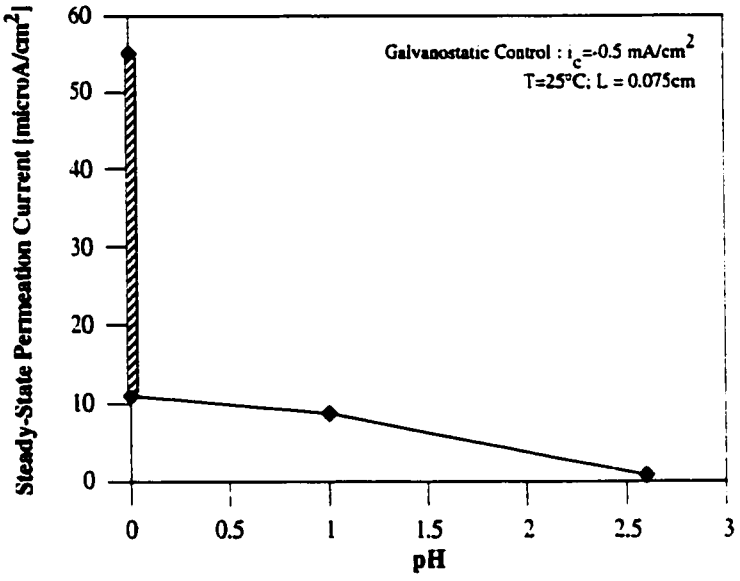

Figure 5.1 The effect of pH on hydrogen permeation through low carbon steel. A range is given for those permeation experiments yielding a maximum and a steady-state value.

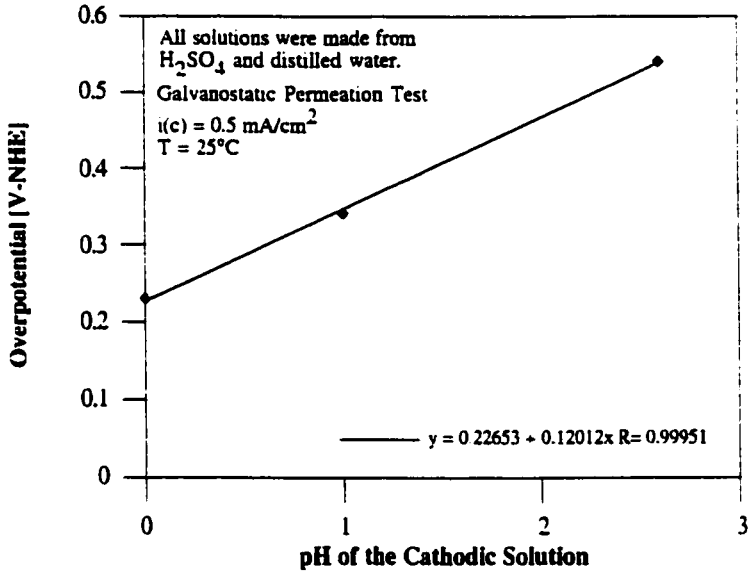

Figure 5.2 The effect of pH on the steel electrode potential during galvanostatic polarization at i_c = -0.5mA/cm^2.

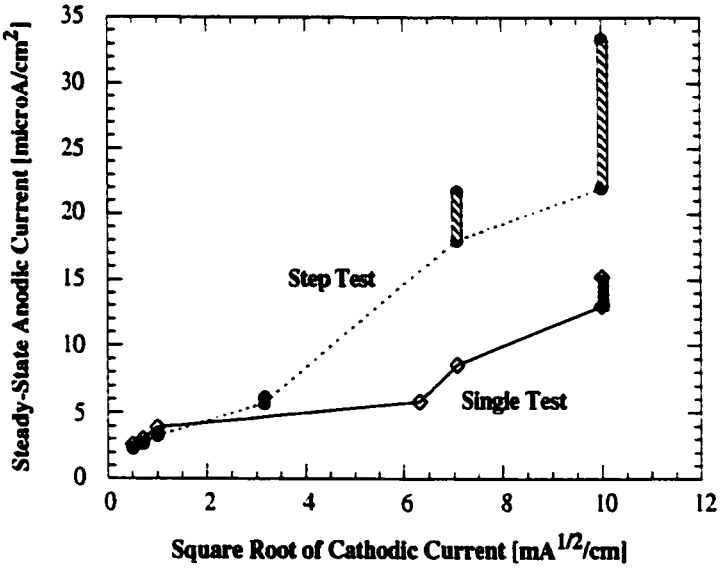

Figure 5.3 The effect of the cathodic current density on the steady-state hydrogen permeation current. Two data sets are listed: the step test and the single test. Ranges are given for those permeation experiments yielding a maximum and a steady-state value.

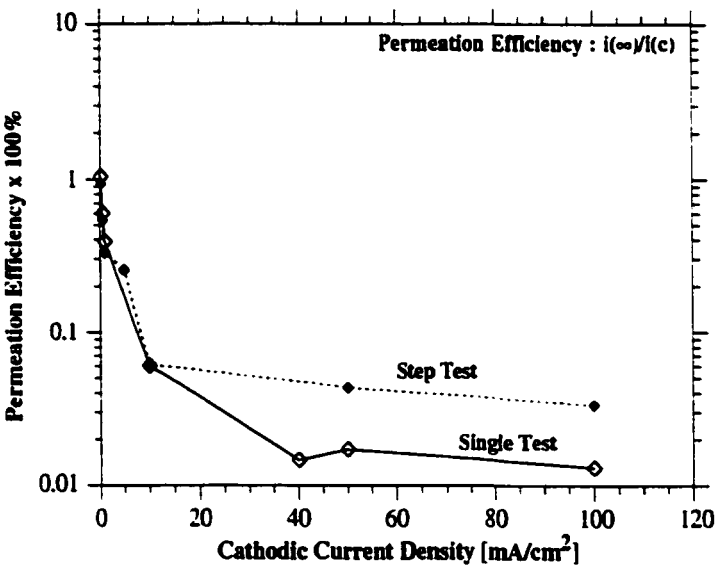

Figure 5.4 The effect of the cathodic current density on the permeation efficiency. Two data sets are listed: the step test and the single test. The steady-state values were used from those tests yielding a maximum and a steady-state value.

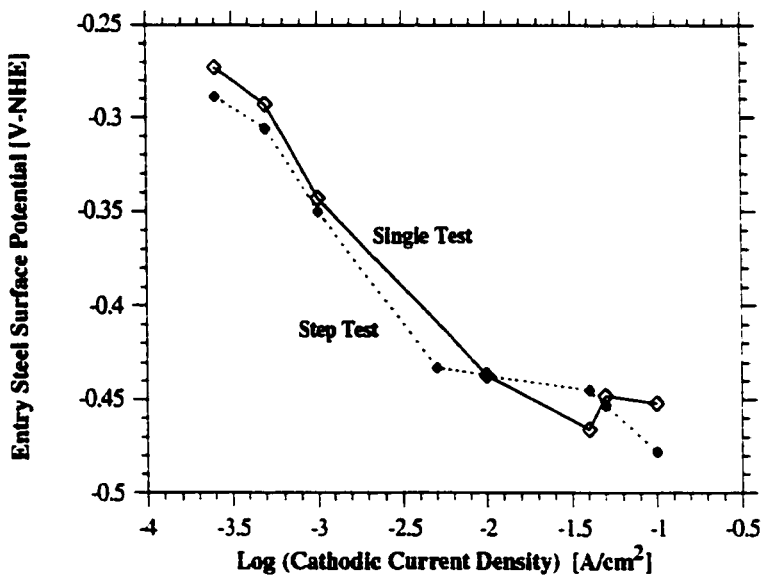

Figure 5.5 The effect of the cathodic current density on the steel electrode potential. Two data sets are listed: the step test and the single test.

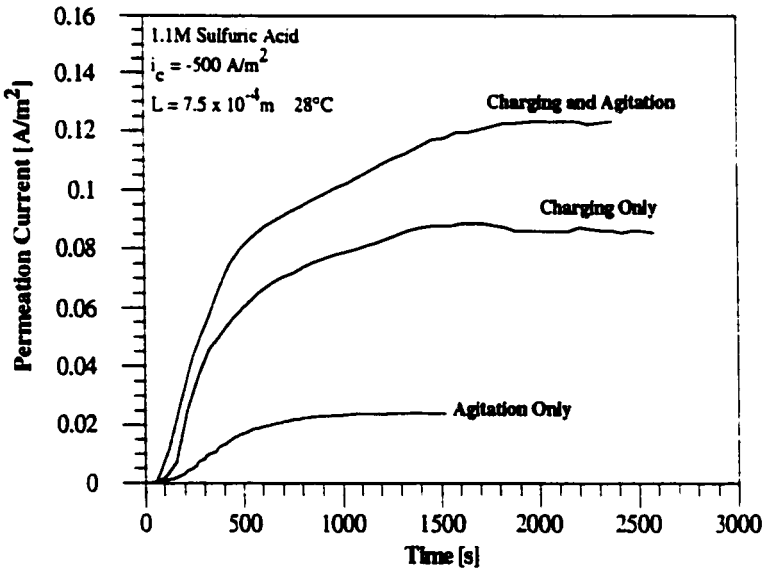

Figure 5.6 Experimental permeation curves for a) Agitation and Charging/Cathodic Polarization (i_C = -50mA/cm^2), b) Charging only (i_C = -50mA/cm^2), c) Agitation only. Agitation is performed by a flow pump. L = 0.075 cm.

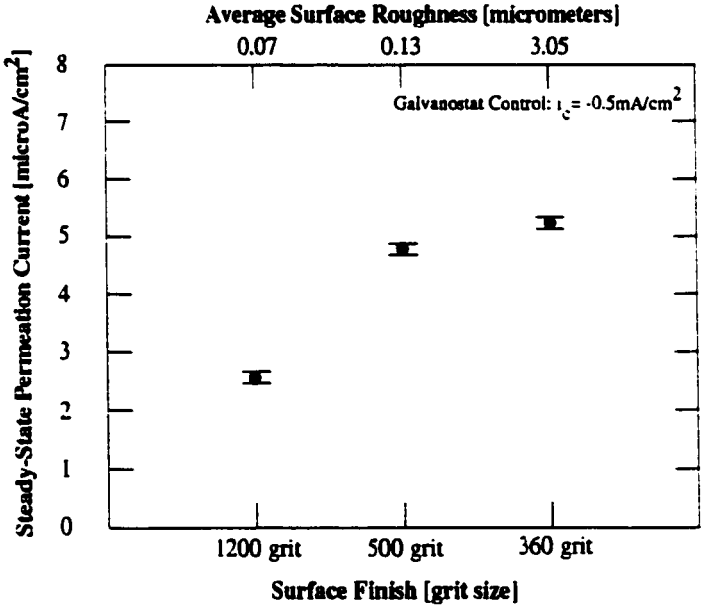

Figure 5.7 The effect of surface finish upon the steady-state hydrogen permeation current.

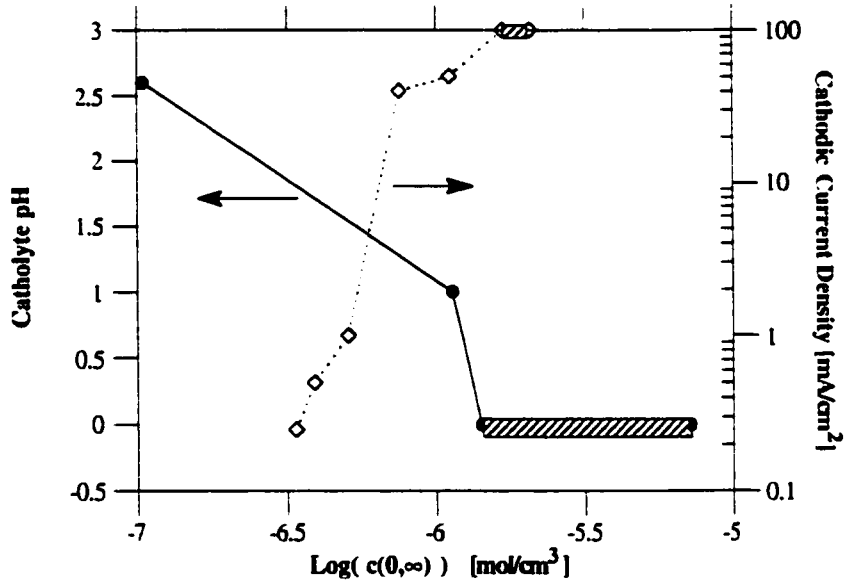

Figure 5.8 The effect of Cathodic Current and pH upon surface solubility. Note that ranges have been given for those permeation curves with maxima and steady-state behavior.

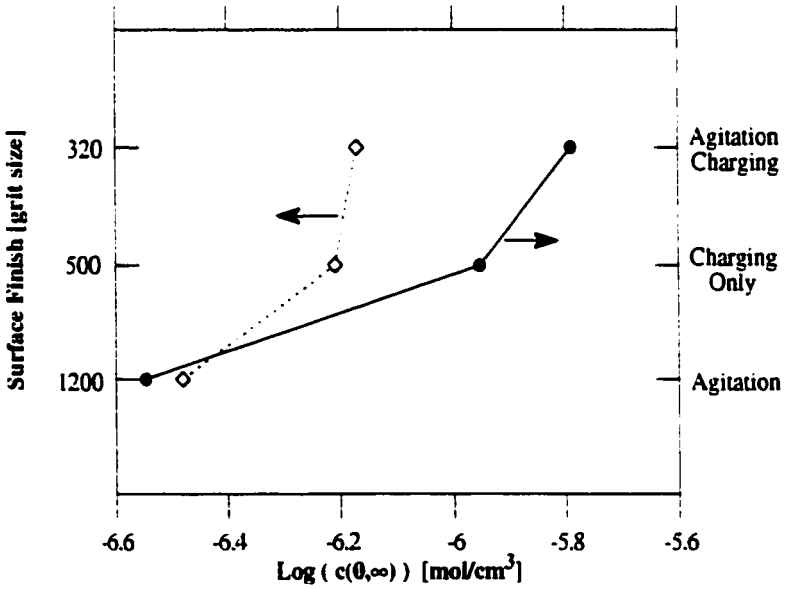

Figure 5.9 The effect of Agitation and Surface Finish upon the surface solubility.

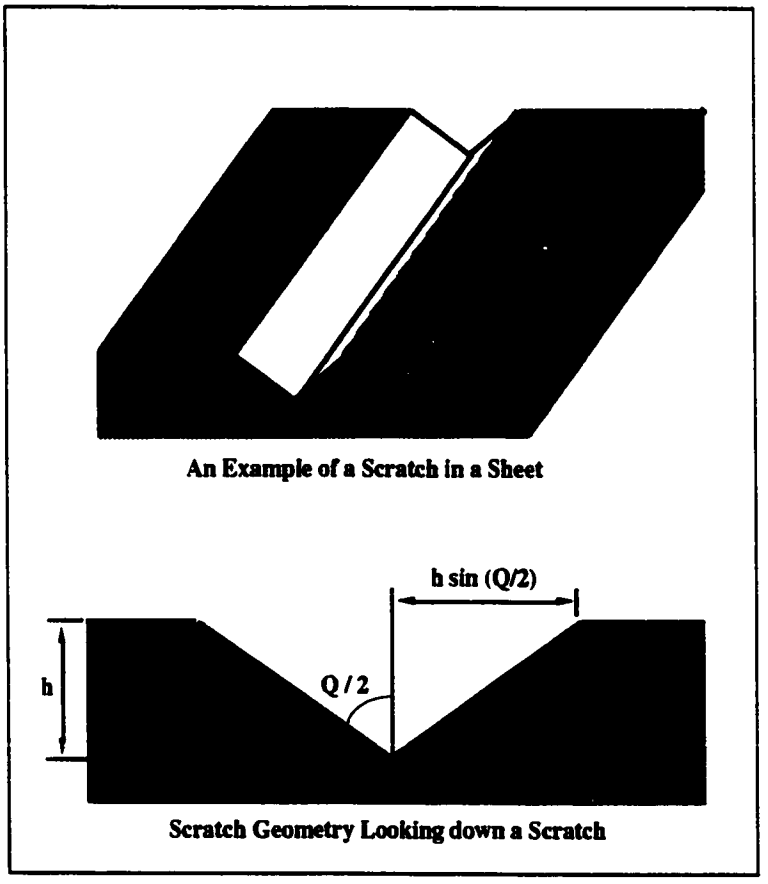

Figure 5.10 The Geometry of a scratch in a metal sheet.

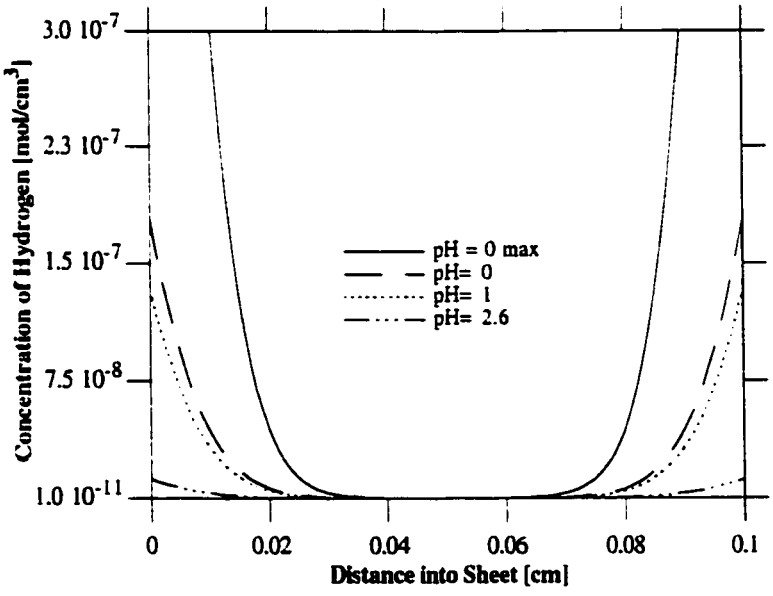

Figure 5.11 The hydrogen concentration profile in a one millimeter sheet that has both surfaces exposed to different pH processes for 10 seconds. Note that the steel has been charged on both surfaces. A range is given for those permeation experiments yielding a maximum and a steady-state value.

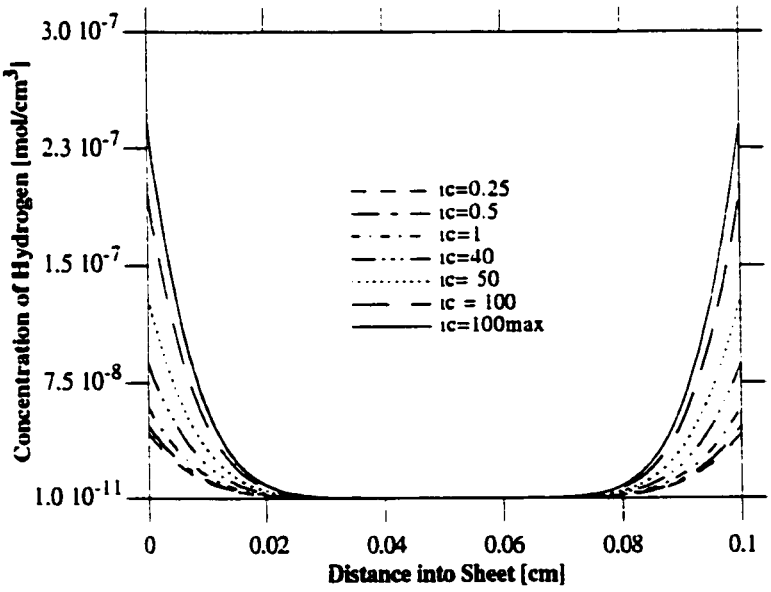

Figure 5.12 Several hydrogen concentration profiles in a one millimeter sheet that has both surfaces exposed to different cathodic current processes for 10 seconds. Note that the steel has been charged on both surfaces. A range is given for those permeation experiments yielding a maximum and a steady-state value.

Chapter 6

The Effect of Titanium Additions to Ultra Low Carbon Steel upon Hydrogen Permeation

6.1 Introduction

There has been recent interest[1] in hydrogen that is absorbed from various electrochemical pre-treatment processes on an electrogalvanizing line. Such absorbed hydrogen may diffuse to areas of poor adhesion along the Zn/Steel interface and form blisters in the coating. A candidate material for automotive applications is ultra low carbon (<0.005 wt.% C) steel that is stabilized by titanium additions of typically less than 0.08wt.%.

The interaction between hydrogen and titanium carbide (TiC) precipitates has been well documented[2, 3, 4, 5, 6, 7, 8], however, such studies were performed upon high strength steels with significantly more carbon present. When stabilization is desired, extra titanium is added to insure all the carbon precipitates out of the iron solution. Previous studies have focussed exclusively upon the influence of TiC upon the hydrogen transport processes in the steel bulk and have neglected the effect of the "excess titanium" present. Although there have been studies[9] of titanium additions to ultra low carbon, iron alloys, these have also centered upon bulk interactions with hydrogen. Recall from Chapter 4 that the permeation of hydrogen is dependent upon both surface and bulk interactions (see Eq. [4.35])Thus, there is a need to study the hydrogen behavior in ultra low carbon steel. Since hydrogen absorption results directly from surface reactions, there is a need to understand the effect of titanium and titanium carbide on such reactions.

In this chapter, the effect of titanium additions to stabilize ultra low carbon steel will be examined relative to two considerations: catalytic surface interactions and microstructural trapping effects. The hydrogen behavior will be studied experimentally by the electrochemical permeation technique. The surfaces of the steels will be characterized by linear polarization, Auger electron and secondary ion mass spectroscopy. An analytical model[10] will be employed to understand the hydrogen entry kinetics.

6.2 Materials Used in Study

Permeation foils were prepared from Fe, 04LC, 005D, 005BH, 004Ti1 and 004Ti2 steel sheets. The particular compositions are described in detail in Chapter 3.

TABLE 6.A
Excess Titanium Information for Different Steels at 22°C

Steel	Ti:C	$[Ti]_{free}$
005BH	0.15	0
004Ti1	2.94	0.017
004Ti2	4.76	0.047

The excess titanium can be estimated as: $[Ti]_{free}$ = (wt% Ti) - [(4)(wt%C) + (3.4)(wt%N) + (1.5)(wt%O)] from Pressoure[10]

The primary difference between the 005BH, 004Ti1 and the 004Ti2 ultra low carbon steels is in the amount of titanium added for stabilization of the carbides. The 005BH steel was not stabilized with titanium and thus, has almost exclusively iron carbides, while the 004Ti steels have titanium carbides. To insure titanium stabilization occurs to completion, more titanium was added to the 004Ti steels than the stoichiometric amount. This is noted in Table 6.A by the Ti:C ratio in the steels. This excess titanium will be present in the steels as free titanium and the amounts are listed in

Table 6.A. While the 004Ti steels have similar TiC concentrations, they do have different excess titanium concentrations.

6.3 Results

6.3.1 The Hydrogen Behavior of Three Different Steels

Figure 6.1 illustrates the results from permeation testing three steels (Fe, 04LC and 005D) differing in carbon content. It is admitted that there are other factors which also vary in these steels, however, the primary difference is in the kind of carbides (e.g., iron carbides versus titanium or niobium carbides) and the total amount of carbon present. The experiment was conducted under potentiostatic control (E_c = -1V-SCE) in 0.1M NaOH at 25°C.

Notice in Figure 6.1 that the break-through times for the steels were found to vary (~100 vs ~650 vs ~1000 seconds). This suggests that the diffusivities for the three steels is different. The results show that hydrogen diffused more readily through the pure iron (Fe) than either carbon steel. The mobility of the hydrogen was slowed greatest (based upon break-through times) by the ultra low carbon steel (005D). This suggests that the titanium and niobium carbide inclusions are more effective in delaying hydrogen than the iron carbides. This result is similar to others reported for higher titanium steels[5,6,8].

Although the steels were coated on both surfaces with a thin palladium coating, there were noticeable differences in steady-state permeation behavior between the 005D and either the Fe or 04LC steel. The iron (Fe) and low carbon steel (04LC) both showed similar steady-state behavior, but the ultra low carbon steel (005D) had a permeation current which was only half that of the other two steels. Since the test was

only run for 3000s (a relatively short time), it is possible that the test was not run long enough and the current for that sample has yet to reach steady-state. Despite this apparent anomaly, it is clear that changing the steel metallurgy can have a significant effect upon the hydrogen behavior.

6.3.2 The Hydrogen Behavior of the Ultra Low Carbon Steels

Figure 6.2 displays the different hydrogen permeation behavior for three ultra low carbon steels (005BH, 004Ti1, 004Ti2). The steel surfaces were charged at -0.5mA/cm^2 in pH=1 sulfuric acid during the permeation tests. For these tests, only the exit surfaces of the steel sheets were coated with Pd.

The ultra low carbon steels were different in steady-state permeation current, i^{∞}, anodic curve shape and break-through times. The pertinent data from the permeation tests are listed in Table 6.B.

Two primary conclusions may be derived from the permeation current data. The ultra low carbon steels showed increasing i^{∞} as:

	004Ti1	<	005BH	<	004Ti2
i^{∞} [μA/cm^2] :	0.5		1.1		1.5

Secondly, it is evident from Figure 6.2 that the 004Ti2 steel exhibits non-steady state permeation behavior. Consequently, two values for the hydrogen permeation current are listed in Table 6.B: the permeation current value at the maximum and at the steady-state condition. These can be considered upper and lower bounds for the hydrogen permeation. Such hydrogen behavior is described by Bockris[11] to indicate high hydrogen absorption and possible subsurface void formation.

In addition to the steady-state permeation behavior, the data in Figure 6.2 show a difference in the break through times for the three steels. The break through time is that time when the anodic current increases above the noise level. The diffusivities, obtained by curve fitting Eq. [4.30] to the data and listed in Table 6.B, emphasize this difference. Both of the 004Ti steels have lower diffusivity values than the 005BH steel.

TABLE 6.B
Permeation Data for Different Steels at 22°C

Steel	$D_{25°C}$ [$cm^2/s \times 10^{-6}$]	i^{∞} [$\mu A/cm^2$]	E_w [mV-NHE]
005BH	2	1.1 ± 0.3	-323 ± 18
004Ti1	0.5	0.5 ± 0.1	-305 ± 18
004Ti2 [stdy-st]	n/a	1.52 ± 0.03	-282 ± 9
004Ti2 [maximum]	0.5	2.05 ± 0.03	-282 ± 9

Due to the non-steady state behavior, two values are listed for the 004Ti2 steel: one is the value at the permeation maximum and the other is the long term steady-state value . These can be considered upper and lower bounds for the permeation behavior. The limits of uncertainty are the standard deviations in the data collected from a minimum of 3 tests.

6.3.3 Permeation Tests as a Function of Thickness

From equation [6.1], the permeability (J^{∞}) of hydrogen through a metal membrane is a function of both the surface condition (κ) and the hydrogen diffusivity (D) in the metal. Other variables in the equation are the sheet thickness, L, and the concentration gradient, $c_1 - c_2$, across the metal sheet. To more clearly define the ultra low carbon steel permeation behavior, permeation tests were conducted upon different sheet thicknesses for the three steels.

$$J^{\infty} = \frac{\Delta C}{\left(\frac{L}{D} + \frac{1}{\kappa_1} + \frac{1}{\kappa_2}\right)} \approx \frac{\Delta C}{\left(\frac{L}{D} + \frac{1}{\kappa_1}\right)} \qquad [6.1]$$

Figure 6.2 illustrates the hydrogen permeation behavior for the three steels as a function of sheet thickness (0.08 - 0.04 cm). For each ultra low carbon steel and over the thicknesses studied, similar steady-state permeation currents were obtained.

6.3.4 Characterization of Electrochemical Behavior

To better understand the permeation behavior for the three steels, the electrochemical behavior of the steel surfaces was characterized. Potential and polarization measurements were performed to distinguish differences in the hydrogen discharge and hydrogen evolution reactions. Although the permeation tests were conducted galvanostatically at -0.5mA/cm^2, the working potential, E_w, of the steels was found to vary (see Table 6.B) as: 005 < 004Ti1 < 004Ti2. In particular, the 004Ti2 steel required significantly less applied voltage to achieve the galvanostatic condition than the other steels. This suggests that the surfaces of the steels were electrochemically different during the charging. Since the steels were polished and prepared similarly, this difference must be the result of a chemical difference on the steel surface.

TABLE 6.C
Tafel Constants for the Ultra Low Carbon Steels

Steel	Log i_o [A/cm^2]	a [mV]	b [mV/decade]	E_c [V-NHE]
005BH	-4.9 ± 0.3	790 ± 40	162 ± 19	-0.270
004Ti1	-5.0 ± 0.1	790 ± 20	159 ± 1	-0.267
004Ti2	-4.9 ± 0.2	810 ± 20	165 ± 3	-0.267

Figure 6.4 shows the polarization results of the ultra low carbon steels. The polarization tests were conducted to determine the dependence of the hydrogen evolution reaction on the permeation results. Tafel constants were calculated and are listed in Table 6.C. It is clear from this data that the Tafel behavior is not significantly different between the steels and is similar to that of iron[12].

6.3.5 Characterization of the Steel Surface

To verify that titanium is present on the surface and to characterize the ultra low carbon steels, surface analysis techniques were employed. The thickness of the oxide formed after polishing, but prior to testing was characterized by auger electron spectroscopy (AES). Since the principal bulk compositional differences among the steels were in titanium content and due to the low concentrations of titanium present in the steels, secondary ion mass spectroscopy (SIMS) was also used to characterize the steel surfaces.

An AES depth profile on the 004Ti2 steel contained in Figure 6.5 suggests that although the surfaces were polished to a 1200 grit finish, from the standpoint of surface analytical techniques, this is a non-flat surface. Such surfaces make interpretations difficult. It is clear from the oxygen trace in the depth profile that an oxide is present. The oxygen trace levels out to a baseline that continues to 200 Å. This result indicates that although the oxide has been penetrated in some areas (e.g., on top of a grain), other areas being analyzed (e.g., the sides of a grain) still possess some of the oxide. Taking the baseline as "zero oxide", allows an estimate of the oxide thickness to be approximated at 40 - 65Å.

The SIMS depth profiles for the 005BH, the 004Ti1 and the 004Ti2 steels are displayed in Figure 6.6. The increased signal at low sputter depths (<60Å) is at least in part due to enhanced ionization from sputtering within the oxide. It is worth noting that to make quantitative conclusions in traditional SIMS studies, special standards are often used. Although no standards of titanium, titanium oxide, iron or of iron oxide were

used in this investigation, the analysis applied here is only used to indicate whether a steel possesses more titanium or titanium oxide than that of the others.

The profiles shown in Figure 6.6 are for the primary iron (64 mass/charge), titanium (48 mass/charge) and TiO (64 mass/charge) ratios. The 004Ti2 steel was found to have 3.2 standard deviations more titanium on the surface than the 004Ti1 steel. No titanium was detected for the 005BH steel. These results are consistent with the bulk compositional analysis listed in Table 3.B. Similar statistical analyses on the titanium oxide peak detected no measurable difference between the two 004Ti steels, although more TiO was found on these than for the 005BH steel.

6.4 Discussion

6.4.1 The Effect of Titanium Additions on H Behavior in ULC Steel

It is evident from the permeation data that the steels have different permeation characteristics. Applying the Eqs. [6.2]-[6.4] to the permeation data allows the surface solubility, $c(0,\infty)$, and convective mass transfer coefficients, κ_l, to be calculated. These calculated parameters are listed in Table 6.D. From the $c(0,\infty)$ and the κ_l values, the 005BH and the 004Ti1 steels exhibit similar entry surface kinetic behavior. Furthermore, the values calculated for the 004Ti2 steel suggests hydrogen entry is much easier than on the other two steels. However, the permeation current of the steels increases as:

	004Ti1	<	005BH	<	004Ti2
i^{∞} [$\mu A/cm^2$] :	0.5		1.1		1.5

$$J_{\infty} = \kappa_l \left(c_l - c(0, \infty) \right) \qquad [6.2]$$

$$J_\infty = D\,\frac{c(0,\infty) - c(L,\infty)}{L} \qquad [6.3]$$

$$J_\infty = \kappa_2(\, c(L,\infty) - c_2) \qquad [6.4]$$

To explain this behavior, recall equation [6.1] which shows the hydrogen flux to be dependent upon both κ_1 and D/L. Since κ_1 is similar for the 004Ti1 and 005BH steels, the only way for the hydrogen flux to be less than that for 005BH, is that $D_{004Ti1} < D_{005BH}$. The data in Table 6.C supports this conclusion. In addition, the D_{004Ti2} is similar to D_{004Ti1}, however, the value for κ_1 for the 004Ti2 steel is much higher than those for the other steels, thus supporting its higher permeation current. The reasons for the higher κ_1 value will be discussed later in section 6.4.2 and 6.4.4.

It is of note that the reduced diffusivity, relative to the 005BH steel, measured for these steels is consistent with other TiC trapping studies[2-9] of various higher strength steels. These studies were analyzing steels with much higher titanium additions than evaluated here, but the trend is similar. It is clear that the diffusivity does vary with titanium additions, but the mechanism is an unsettled issue.

TABLE 6.D
Calculated Permeation Parameters

Steel	$c(0,\infty)$ [mole/cm^3]	κ_1 [cm/s]
005BH	3.4×10^{-7}	2.2×10^{-7}
004Ti1	7.8×10^{-7}	1.1×10^{-7}
004Ti2 [stdy st]	2.4×10^{-6}	5.1×10^{-6}
004Ti2 [maximum]	3.1×10^{-6}	9.1×10^{-6}

The permeation data was shown to be independent of thickness for 0.08-0.04cm. At first glance, the hydrogen flux, J, should vary with the reciprocal of the foil thickness, L, under steady-state conditions:

$$J = \frac{i^{\infty}}{zF} = \frac{D}{L}\Delta C \qquad [6.5]$$

where i^{∞} is the steady-state permeation current, z is the charge number, F is Faraday's constant, D is the hydrogen diffusivity and ΔC is the concentration difference on either side of the foil. However, this suggests a linear dependence of flux upon thickness. The data is not consistent with this relation. Examining equation [6.1] shows a relation dependent upon both surface and bulk effects. The data listed in Tables 6.C and 6.D show that the value of κ_l is approximately two orders of magnitude smaller than the D/L term. Thus, the hydrogen flux should be independent of thickness until the thickness is ~ two orders of magnitude thicker than the thicknesses tested. Thus, the data are consistent with equation [6.1]. This fact emphasizes how the surface of the steel can influence and dominate the permeation behavior.

The following explanation is proposed for the permeation behavior in these steels. There are two key constituents in these steels affecting the permeation behavior. First, the titanium carbide particles act as hydrogen traps and reduce the hydrogen diffusivity. Secondly, the amount of excess titanium added enhances hydrogen entry.

The addition of TiC particles to the ultra low carbon steel structure (004Ti1) reduces the apparent D, thus decreasing the hydrogen flux compared to the non-stabilized steel (005BH). Although there is excess titanium in the 004Ti1 steel, there is not enough to result in any significant effect. This is supported by the similar values of κ_l and dissimilar D values for the two steels (004Ti1 and 005BH). For the 004Ti2 steel, there is a similar amount of TiC present as in the 004Ti1 steel, but significantly

more "excess" titanium exists in the 004Ti2 steel. Although the diffusivity is reduced relative to that of the 005BH steel, the much larger κ_l value dominates the permeation and yields a higher flux.

6.4.2 The Influence of Excess Titanium upon κ_l

The increased hydrogen entry efficiency, as exemplified by κ_l, is due to the enhancement of the hydrogen absorption kinetics. The overpotentials utilized to galvanostatically charge the steels vary by at most 15%. The κ_l values for the steels vary by considerably greater amounts (up to an order of magnitude). The variance in the overpotentials suggests some difference in the discharge kinetics, however, this difference does not explain the large difference in κ_l. In addition, since the polarization behavior is not substantially different on the three steels (i.e., the Tafel slopes shown in Table 6.C were similar) and the SIMS results confirm that more titanium is present on the 004Ti2 than on the 004Ti1 or on the 005BH, it is plausible that the excess titanium added to stabilize the steel enhances the hydrogen absorption kinetics, but does little to affect recombination kinetics. Possible mechanisms for the enhanced absorption process will be discussed in section 6.4.5.

6.4.3 The Influence of Excess Titanium upon Hydrogen Diffusivity

The amount of excess titanium present may either diminish the trapping effects of the titanium particles or enhance the hydrogen motion through the steels. Although the 004Ti steels have similar TiC concentrations and $D_{004Ti2} \sim D_{004Ti1}$, the values for κ_l are significantly different. The primary difference between the 004Ti steels is the significantly higher amount of excess titanium present in the 004Ti2 steel. Examining values for $c(0,\infty)$ in Table 6.D and i^{∞} in Table 6.B shows differences in entry surface solubility of 12%, while that of the hydrogen flux is 52%. The enhanced flux must

come from a) reduced hydrogen trapping, or b) enhanced hydrogen motion with either effect resulting from the excess titanium present. Although further studies are necessary to determine this effect unequivocally, it is clear that the excess titanium does influence the motion of the hydrogen in the bulk.

6.4.4 The State of the Steel Surface During Hydrogen Permeation

Prior to the permeation tests, the ultra low carbon steels possess air-formed oxides. Such oxides are predominantly iron oxides (FeOOH, Fe_3O_4) that are either doped with whatever metal species are on the steel surface or are mixed with separate metal oxides (e.g., MnO_2, Al_2O_3, TiO_2). During the permeation tests, the working potential (see Table 6.B) of the steels was noted to be cathodic to the corrosion potentials of the steels (see Table 6.C). However, even if, globally, the steel is under cathodic protection, for low overpotentials, local corrosion can still occur. The Pourbaix[13] diagrams for the Fe-H_2O, Mn-H_2O, and Al-H_2O systems indicate metal dissolution or at least, unstable oxide decomposition for a pH=1 solution at -0.3 V-NHE. The corresponding diagram for titanium indicates TiO_2 is the stable species. Experimentally, more cathodic potentials could be used, but such a solution increases the possibility of surface hydrogen damage[17]. The effect shown in Figure 6.2 for the 004Ti2 steel emphasizes this fact.

Two possibilities are proposed for the steel surfaces tested. First, the oxide could decompose readily, leaving a metal surface. Secondly, the oxide on the steel surface could partially decompose during charging, leaving islands of oxide on a metal surface. For both possibilities, it is probable that some metal dissolution occurs, however, atomic absorption experiments before and after a permeation test indicate that

only a few monolayers of iron are removed during the course of the experiment. Although Pourbaix diagrams are based upon thermodynamics and don't necessarily predict what *does* exist in a system, they are appropriate for predicting what is *not* present. It is highly probable that option one does not hold. Thus, it is reasonable to assume that much of the iron oxide decomposes early in the permeation process, leaving a steel surface involved in slow dissolution with some titanium and/or titanium oxide (for the 004Ti steels).

6.4.5 The Effect of Stabilization on H Absorption

Although titanium stabilization has been shown to affect the hydrogen permeation behavior, the mechanism for the enhanced permeation current in the 004Ti2 steel is not clear from this study. Hence, the following mechanisms are proposed to explain the behavior with the hope that future investigations will hone in on the dominant mechanism for hydrogen absorption in these steels.

The following mechanisms are based upon the knowledge that titanium additions to steel result in: 1) a steel surface with Ti species dispersed in islands across its surface as carbides or oxides; 2) enhanced oxidation in the form of titanium oxide or titanium doped, iron oxide occurs on the surface during charging; and 3) the enhanced permeation resulted only in the steel with significant excess titanium.

- The Ti species, particularly the oxide, could act as a less effective conductor than the steel surface. This could create an increase in the current density, locally, at the non-oxide areas. This would increase the fugacity at such locations and would result in more hydrogen becoming absorbed. However, for such a

situation to exist, the excess titanium would need to insulate at least 2/3 of the available area to increase the cathodic current density and thus, the permeation current of the 004Ti2 steel to 3 times that for the 004Ti1 steel. Such a coverage of the steel surface by titanium oxide is not possible with the amount of excess titanium present.

- The titanium species on the surface could provide more efficient adsorption sites for hydrogen, thus increasing the surface coverage of hydrogen on the metal surface.

- The titanium species on the surface could "discourage" hydrogen recombination by preventing adsorbed hydrogen atoms from becoming nearest neighbors.

To gain a better understanding of the effect of hydrogen absorbed by ultra low carbon steel during cathodic processes (e.g., electropickling or plating operations), it is necessary to consider both hydrogen entry and hydrogen trapping factors. It is evident from this study and others that hydrogen is both absorbed and trapped by the steel during processes that expose the steel to hydrogen.

Recently, however, absorbed hydrogen has been found to collect at coating/steel interfaces resulting in coating and other problems (e.g., blisters)[1]. To minimize such problems two approaches may be attempted: 1) reduce the amount of hydrogen that is absorbed, or 2) reduce the mobility of hydrogen in the steel. The ideal solution would be the addition of a species that could serve both approaches. If ultra low carbon steel is to be used in situations where such problems could arise, the titanium stabilized steels

should be considered as an alternative. The addition of titanium can affect both the hydrogen diffusivity and the hydrogen absorption kinetics.

This procedure should be used with caution because the addition of too much titanium (e.g., 0.080wt.%), could result in enhanced hydrogen absorption kinetics. Too much of an enhancement increases the permeation to such a level as to make the beneficial effect of the traps questionable. The excess titanium added to insure complete stabilization, affects the hydrogen absorption process substantially, but does not necessarily increase the hydrogen mobility. Since similar hydrogen absorption kinetics to the non-stabilized steel are achieved with lower titanium additions (e.g., 0.051wt.%) and the degree of stabilization does not change with increased titanium additions (i.e., the diffusivity is similar for the ULC steels), it makes sense for hydrogen sensitive applications to maintain the titanium additions below 0.051wt.%.

6.5 Conclusions

This investigation considered the effect of titanium additions to ultra low carbon steel upon the hydrogen permeation through steel sheets. This study considered both bulk and surface kinetic factors in evaluating the steels.

For a given ultra low carbon steel and over several sheet thicknesses, the steady-state permeation currents measured are found to be independent of thickness. An expression was proposed to explain this behavior. It was verified that for the steels tested, the permeability of hydrogen was surface dominated. For a given thickness, the hydrogen permeation behavior for the ultra low carbon steels is found to be different in both exiting hydrogen flux and apparent hydrogen diffusivity. The differences in

permeation behavior are due to the amount of excess titanium added to the steels for stabilization. These differences are present in both the bulk and on the steel surface.

The amount of hydrogen absorbed by the steels increases with increasing titanium additions. Although the Tafel behavior of the ultra low carbon steels was not significantly different, the 004Ti steels have surfaces that are more amiable to hydrogen entry than the non-stabilized steel. This is probably due to the increased amount of titanium oxide on the metal surface.

The hydrogen diffusivity was found to have an unusual relationship to the amount of titanium added for stabilization. Although both stabilized steels had lower diffusivities than that measured for the non-stabilized steel, the lowest diffusivity was not measured for the stabilized steel with the most excess titanium. Such behavior suggests a synergistic relationship between the titanium and titanium carbide trapping.

References for Chapter 6

1 J.H. Payer and G.M. Michal, *Proc. of 5th Auto.Prev.of Corr.*, P-250, Dearborn, MI, (1991), 53-63.

2 M. Smialowski, Hydrogen in Steel, Pergamon Press, New York, (1962).

3 S. Linderoth and A.V. Shiskin, *Phil. Mag. A*, 55[3] (1987) 291-300.

4 P.H. Pumphrey, Hydrogen in Metals, Bernstein & Thompson, eds., AIME, New York, (1981) 105-111.

5 B.G. Pound, *Acta Metallurg.*, 38[12] (1990) 2373-2381.

6 B.G. Pound, *Acta Metallurg.*, 39[9] (1991) 2099-2105.

7 V.P. Pancheshnaya, V.M. Knyazheva, Zh.V. Klimenko and M.M. Anotova, *Prot. of Metals*, 16[6] (1980) 550-556.

8 G.M. Pressouyre and I.M. Bernstein, *Metallurg. Trans. A*, 9A (1978) 1571-1580.

9 K. Yang, M.Z. Cao, X.J. Wan and C.X. Shi, *Scripta Met.*, 22 (1988) 1373-1378.

10 S.L. Amey, G.M. Michal and J.H. Payer, submitted to *Metallurgical Transactions A*, spring 1992.

11 J.O'M. Bockris and P.K. Subramanyan, *J. Electrochem. Soc.*, **118**[7] (1971) 1114-1119.

12 T. Okada, *Electrochim. Acta*, **27**[9] (1982) 1273-1280.

13 M. Pourbaix, Atlas of Electrochemical Equilibria in Aqueous Solutions, NACE, Houston,TX, 1974.

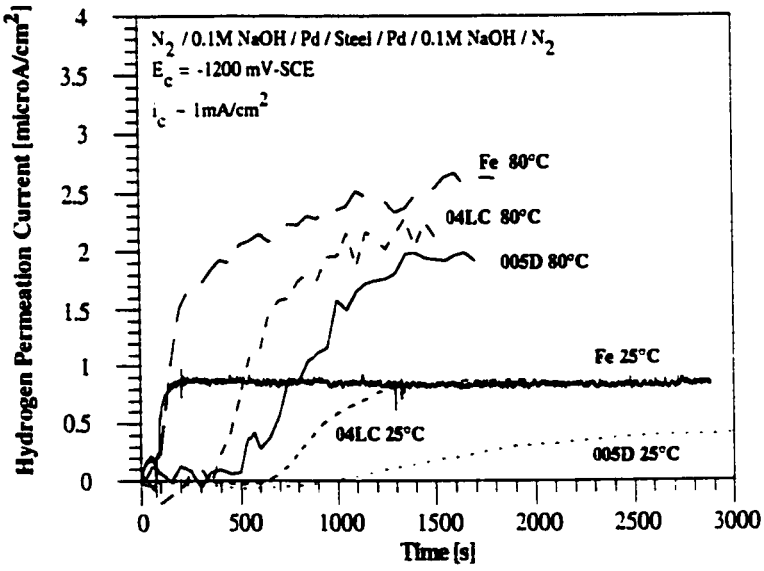

Figure 6.1: Permeation Behavior of three steels differing in carbon content: Fe, 04LC, 005D. The surfaces of the foils were coated with Pd.

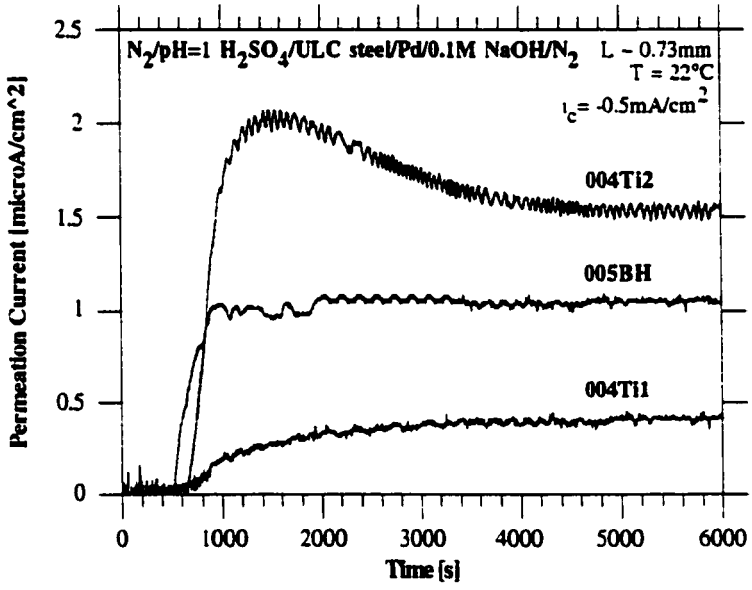

Figure 6.2: The permeation behavior of three different ultra low carbon steels differing primarily in titanium content: 005BH, 004Ti1, 004Ti2.

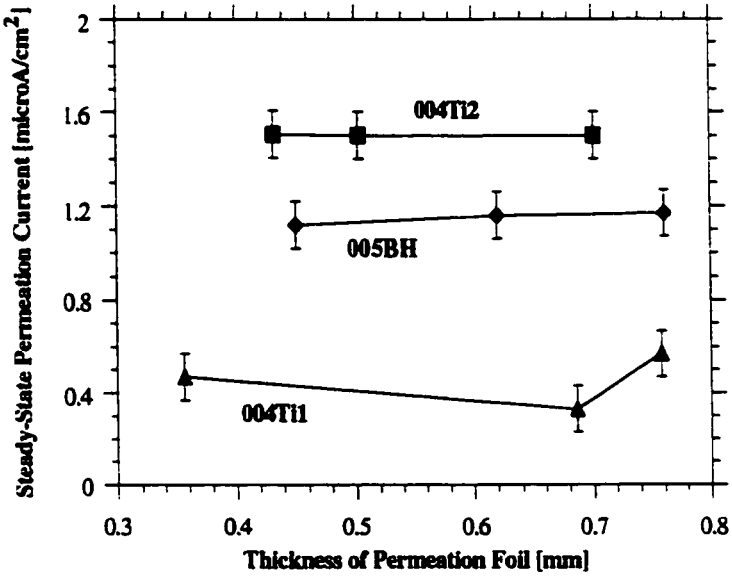

Figure 6.3: The steady-state hydrogen permeation behavior for the three ultra low carbon steels as a function of thickness. The error bars are the standard deviation of the data obtained from a minimum of three tests.

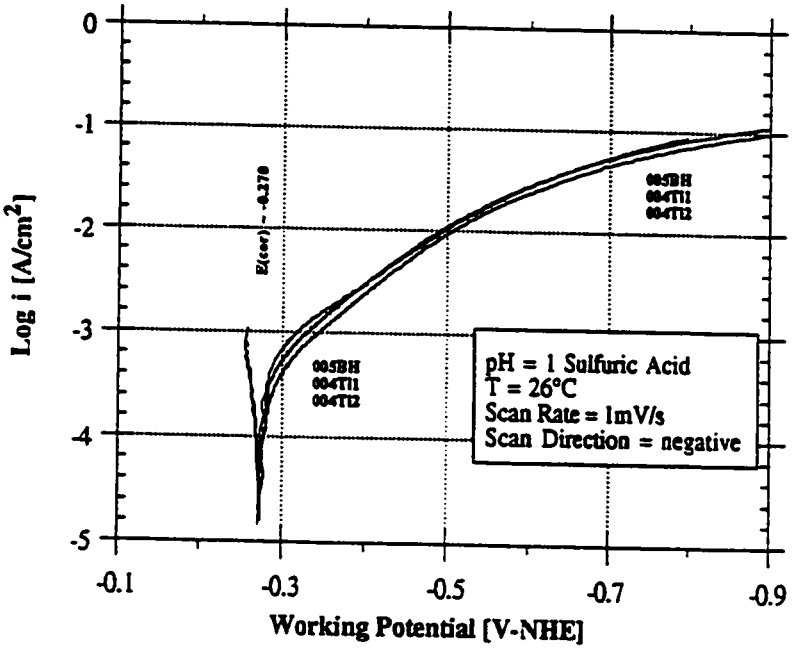

Figure 6.4: The linear polarization results of the ultra low carbon steels is illustrated. The working electrode test area was 1.4 cm^2, polished to a 1200 grit finish. The scan rate was -1mV/s. The solution was deaerated pH = 1 H_2SO_4.

a)

b)

c)

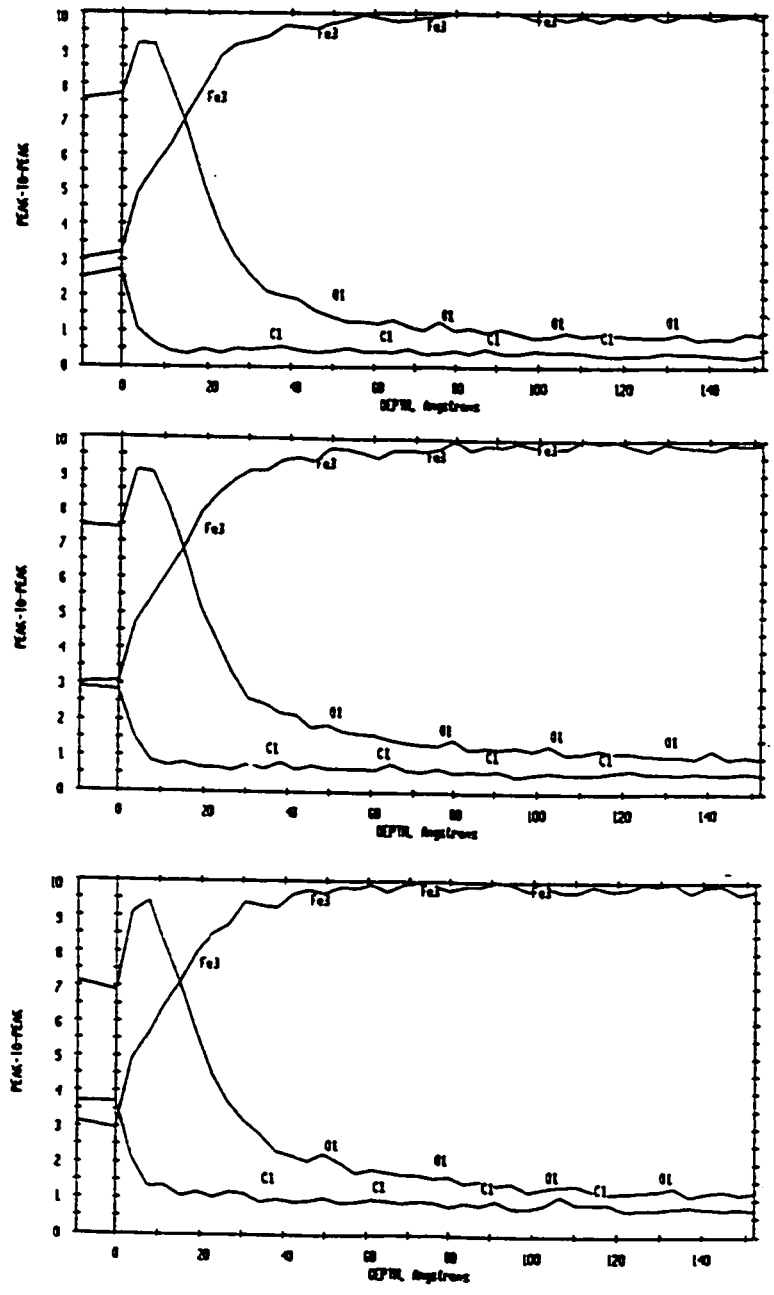

Figure 6.5: The AES depth profiles for the ultra low carbon steels is illustrated. The primary carbon, oxygen and iron peaks were monitored. The sputter rate was ~40Å/minute and the raster size was 3 x 3 mm^2.

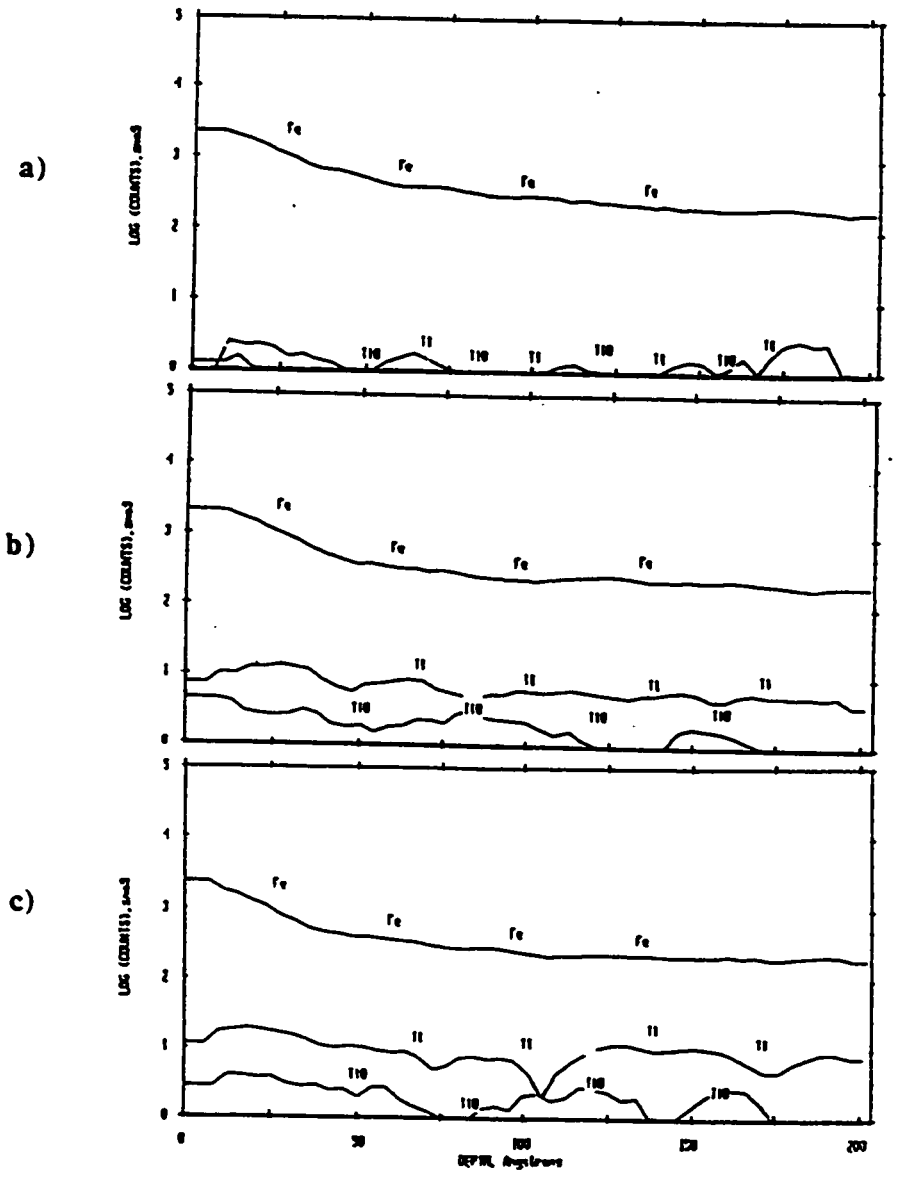

Figure 6.6: The positive SIMS depth profiles for the ultra low carbon steels: a) 005BH, b) 004Ti1, c) 004Ti2. Note the differences in the primary Ti (48), Fe(56) and TiO (64) mass/charge ratios. The sputter rate was ~20Å/minute and the raster size was 6 x 6 mm^2.

Chapter 7

Hydrogen Absorption on a Lead Contaminated Steel Surface from a Sulfuric Acid Environment

7.1 Introduction

There has been recent interest[1] in hydrogen that is absorbed in low carbon (0.05wt.% C) steel sheet from various electrochemical pre-treatment processes on an electrogalvanizing line. Such absorbed hydrogen may diffuse to areas of poor adhesion along the Zn/Steel interface and form blisters in the coating. Lead anodes are typically used to electropickle steel sheet prior to plating with zinc. As such, lead undergoes dissolution over time and may reach levels of 15 ppm in solution. Since the steel is polarized cathodically, the lead may deposit on the steel surface and thus, affect the hydrogen absorption process.

Although the hydrogen reactions on iron[2, 3, 4] and lead[5, 6, 7, 8] have been investigated in depth, the effect of a partial coating on a metal upon the hydrogen kinetics has not been studied to any great extent. Most of the literature pertinent to a lead-steel-hydrogen study may be grouped into the following classifications: (i) heavy metal impurity-induced embrittlement[9, 10, 11], (ii) lead-acid battery phenomena[12, 13, 14], (iii) protective coatings acting as barriers to hydrogen[15, 16, 17] and (iv) cathodic poisons catalytically affecting hydrogen kinetics[18, 19, 20, 21, 22]. The first category emphasizes bulk effects between hydrogen and metallurgical variables, while the second category concentrates on non-ferrous impurities on lead substrates. Thus, it is of interest to evaluate the effect of lead impurities on a steel substrate. Much of the third category investigates continuous coatings on steel as effective barriers to hydrogen. Although the lead-steel system has been studied, there have been conflicting results reported. Hence,

understanding the effect of a partial lead coating on steel is still lacking. The final group has exclusively investigated the Group IVA and VA metals. Although some cases mention the effect of Pb impurities on hydrogen reactions, the effect, relative to arsenic or sulfur, is considered to be small, thus no data was shown and any effects were neglected in the discussion. Thus, it is of interest to perform a detailed study of lead impurities present both in an electrolyte and as a lead deposit upon steel.

In this chapter, the effect of lead in sulfuric acid upon hydrogen absorption in low carbon (0.05 wt.% C) steel will be examined relative to three considerations: the kinetic effect of lead in solution, the kinetic effect of a partial coverage of lead and the barrier effectiveness of a partial lead coating. The hydrogen behavior will be studied experimentally by the electrochemical permeation technique. The surface of the steels will be characterized both by linear polarization, scanning electron microscopy and x-ray photoelectron spectroscopy. An analytical model[23] will be employed to understand the hydrogen entry kinetics.

7.2 Results

7.2.1 The Effect of Lead in Solution upon Hydrogen Permeation

Figure 7.1 illustrates the effect of lead (Pb) ions in solution (~1.1M H_2SO_4) during a galvanostatic permeation test (i_c = -50mA/cm^2) on 04LC steel at 25°C. The amount of hydrogen permeating the steel sheet was found to increase with increasing lead in solution from 4.4 to 8.7ppm. Due to the small volume of solution (<40ml) used during such experiments, it is likely that the solution became depleted of lead ions due to the deposition onto the steel surface. Thus, at steady-state conditions the situation being tested was not a steel surface that was exposed to a solution containing lead ions,

but rather a lead contaminated steel surface that was exposed to a relatively lead free solution.

The effect of a lead contaminated electrolyte during a potentiostatic permeation test (E_c = -0.456 V-NHE) of a steel electrode in the presence of an acidic solution (pH=1 H_2SO_4) is shown in Figure 7.2. The steel used for these tests was 04LC steel that was cold rolled to 50% of its standard thickness (final thickness = 0.037 cm). The permeation cell used during these tests contained at least twice the volume of solution compared to the galvanostatic tests previously performed. Solutions containing 5, 10 or 15 ppm Pb ions decreased the permeation current over that obtained from a non-Pb containing solution. Solutions containing 150ppm lead ions (not shown in figure), resulted in substantially reduced permeation currents (e.g., 0.1 $\mu A/cm^2$) relative to those obtained from non-Pb containing solutions.

Figure 7.2 shows a decrease in steady-state permeation current from tests run with 5ppm to 150ppm lead in the charging solution. This suggests that the increased lead concentration results in increased coverage of lead deposited on the steel surface. The increased coverage results in increased blockage of the steel absorption sites. This fact is particularly emphasized by the negligible permeation current obtained by the 150ppm test. Since the amount of solution used during these tests was 70ml, it is probable that the solution becomes depleted of lead during the early portion of the test. Thus, for all of the solutions but the 150ppm contaminated electrolyte, a continuous coating is not maintained on the steel. This also explains why steady-state permeation currents were obtained and not permeation currents that slowly decreased over time. The latter suggestion is typical of permeation test results obtained during the electrodeposition of continuous cadmium or tin coatings on iron[24, 25, 26]. In such

cases, the permeation current would rise to a maximum and then decrease sharply to a finite value, where it would remain for the remainder of the test.

7.2.2 The Effect of a Lead Deposit upon Hydrogen Permeation

Since the solution tests produced results which suggested that the lead plated out of solution to deposit on the steel surface, it was of interest to evaluate the hydrogen permeation behavior of previously lead deposited steel specimens.

To evaluate such specimens, a procedure was adopted which allowed deposition of the lead in one solution and the permeation testing in another. The deposition solution was lead contaminated to a specific concentration (5,10 or 15ppm). The potential of the steel surface in the cathodic cell of the permeation test was fixed cathodic to the deposition potential of lead. After two minutes, the cell was flushed twice under potential control with non-contaminated solution and then permeation tested in the non-contaminated electrolyte.

The results from such a test are given in Figure 7.2. Notice that the steady-state permeation current, i^{∞}, was found to increase with increasing lead concentration in the deposition solution with concentrations up to 10ppm Pb ions. This trend reversed with the i^{∞} decreasing with lead concentration in the deposition solution from 10 to 15ppm Pb ions.

The morphology of the steel surfaces exposed to the lead containing solutions were investigated by scanning electron microscopy. The results from the investigation are shown in Figures 7.3 - 7.5. The morphology of the metal surfaces immediately after lead deposition were similar to a non-deposited steel surface. This was true regardless

of whether the lead deposit was made from a 5, 10 or 15ppm solution (7.3a, 7.4a, 7.5a). This suggests that the lead was deposited uniformly. However, if such surfaces were charged in pH=1 H_2SO_4 for 3 hours after deposition, significant changes occurred to the surface morphology (7.3b, 7.4b, 7.5b). Although the specimen treated with the 5ppm solution did not change much from 7.3a to 7.3b, the specimens with lead deposits from the 10 and 15ppm solutions developed white crystalline nodules. The nodules were identified by Auger electron spectroscopy to be lead.

7.2.3 The Effect of Other Metals than Pb on Hydrogen Permeation

Since the lead deposits were found to affect the permeation behavior through the steel, it was of interest to compare the lead deposited steel to that of steel contaminated with other metals. The contaminants were chosen based upon the relative values for hydrogen overpotential. Figure 7.6 illustrates the effect of several contaminants on steel upon hydrogen permeation. The contaminants were electrodeposited from pH=1 sulfuric acid solutions polarized at -600 mV-SCE for one minute. The concentration of contaminants in the deposition solution was 10 ppm of the metal ions. The permeation current obtained from potentiostatic tests was found to increase as:

Contaminant:	Pb	<	Ni	~	Fe	<	Pt
i^{∞} [$\mu A/cm^2$]:	~2		~13		~13		~39

Linear polarization tests were performed upon the contaminant surfaces to determine the effect of the exchange current density. The hydrogen exchange current density is shown for each surface in Figure 7.6. Notice that i_0 increases as:

Contaminant:	Pb	<	Fe	~	Ni	<	Pt
Log i_o: [A/cm^2]:	-5.1		-4.7		-4.8		-4.1

Galvanostatic permeation experiments upon lead or platinum contaminated steel surfaces was also investigated. The steel surface was exposed to solutions containing either no contaminant, 10ppm Pb ions or 10ppm Pt ions in 0.1M sulfuric acid. The steel was charged for one minute under 50 mA/cm^2 cathodic current. This charging condition resulted in a 2% coverage of Pb relative to Fe on the surface as measured by XPS. The solutions were flushed and non-contaminated solution was added. The permeation tests were then performed under a cathodic current density of -0.5 mA/cm^2. The permeation behavior relative to a bare steel surface is shown in Figure 7.7. In this case, both contaminant surfaces were found to increase the permeation current, relative to bare steel. In addition, the working electrode potential was measured after steady-state permeation was reached by a current interrupt technique. The E_w was found to vary as:

Contaminant:	Pb	<	Bare Steel	<	Pt
E_w [V-NHE]:	-0.546		-0.306		-0.266

7.2.4 Characterization of Contaminated Steel Surfaces

The contaminated surfaces were characterized by X-ray photoelectron spectroscopy (XPS) to verify independently from permeation results that the metallic contaminants truly deposited on the steel. The specimens were stored in analytical grade methanol prior to testing. After the standard preparatory treatment described in Chapter 3, the specimens were introduced to the vacuum chamber. Survey scans from 0 to 1000eV and multiplex scans for the primary iron, oxygen, carbon and contaminant were taken. The characterization consisted of identifying the contaminant's existence on

the steel surface and in a semi-quantitative fashion determine the relative coverage of the contaminant on the surface.

Figures 7.8 - 7.11 illustrate the survey scans taken from the different contaminated specimens immediately after deposition. Although the XPS scans clearly identify lead and platinum, they do not identify any nickel peaks. This suggests that either nickel did not deposit on the steel or that after potential control was removed, the Ni corroded off the steel surface.

TABLE 7.A
Relative Coverages on Pb/Steel Samples by XPS

Deposition Solution	%PbvsFe	Monolayer Coverage
5ppm	2.7 ± 0.4	~0.32
10ppm	1.7 ± 0.8	~0.20
15ppm	1.0 ± 0.5	~0.12
150ppm	18.0 ± 0.5	~2.16

The coverage is relative to the primary iron peak. The coverage was first determined relative to O, C and Fe. After determining the Pb signal was real, the O and C signals were deleted from the relative coverage. The Monolayer Coverage is based upon the XPS depth sensitivity (30Å) in steel being approximately 12 monolayers.

Table 7.A lists the relative coverages of the specimens exposed to lead deposition solutions and for the specimen permeation tested in the 150ppm lead solution. The results show that the deposition procedure deposits approximately 12 to 30% of a lead monolayer on the steel. In addition, for prolonged charging in more concentrated solutions (e.g., 150ppm), more than a monolayer of lead could be deposited. The scatter in the data emphasizes the problems encountered when transfering a specimen from a potential controlled environment to a non-controlled environment. Despite the scatter, the data for the specimens exposed to the 5-15ppm

solutions show that the more concentrated deposition solution gives less signal than the less concentrated deposition solution. This suggests the possibility that the lead is not depositing uniformly, but may be depositing as nodules or dendrites that are not observed by the SEM photos. Such behavior for lead deposition has been noted by others from both acetate and chloride baths[177].

7.3 Discussion

7.3.1 Application of the Model to the Pb/Steel Surface

Using Eq. [4.30] the model described in Chapter 4 was used to curve fit the experimental data for the Pb contaminated steel results. As shown in Figure 7.12 the lead contaminants did not significantly hinder the hydrogen diffusing through the steel. Using the diffusivity for the reduced 04LC steel of 2×10^{-7} cm^2/s and Eqs. [4.32]-[4.34], the following model parameters were obtained.

TABLE 7.B
Calculated Permeation Parameters

Surface	c_l [mol/cm^3]	κ_l [cm/s]	$c(0,\infty)$ [mol/cm^3]
Blank	5.2×10^{-3}	2.6×10^{-8}	2.5×10^{-6}
5ppm D	5.2×10^{-3}	3.0×10^{-8}	2.9×10^{-5}
10ppm D [maximum]	5.2×10^{-3}	3.8×10^{-8}	3.7×10^{-5}
10ppm D [steady-st]	5.2×10^{-3}	2.7×10^{-8}	2.6×10^{-5}
15ppm D	5.2×10^{-3}	1.3×10^{-8}	1.3×10^{-5}
5ppm S	5.2×10^{-3}	1.8×10^{-8}	3.6×10^{-5}
10ppm S	5.2×10^{-3}	1.6×10^{-8}	1.5×10^{-5}
15ppm S	5.2×10^{-3}	7.0×10^{-9}	6.7×10^{-6}

D and S indicate the data used was from the deposit or solution tests respectively.

Since the diffusivity was found not to change for the different specimens, the change in the permeation current must be due to a surface related phenomenon. This fact is supported by the changes in κ_1 as seen in Table 7.B. Notice that as κ_1 increases, the steady-state permeation current was found to increase (see figure 7.2).

7.3.2 The Effect of Hydrogen Evolution upon the Pb/Steel Surface

It is evident from both the SEM evaluations and the XPS results that the lead-steel surface morphology changes with the deposition solution and with charging time. The SEM photos in Figures 7.3 - 7.5 illustrate that initially the lead deposits on the steel in a uniform manner. However, after prolonged charging in a non-lead charging solution, lead crystals or nodules are found on the surface. The XPS results in Table 7.A suggest that low coverages of lead (<0.3) are present after deposition, but the higher concentrated lead deposition solutions yield lower coverages.

To explain these results, the following mechanism is proposed. Initially, the lead is deposited in a uniform manner on the steel surface. The fact that the higher concentrated deposition solutions gave lower coverages suggests that further deposition may occur uniformly upon lead sites already deposited on the steel surface. This would be consistent with Figures 7.3-5a. As the surface is exposed to hydrogen evolution over a period of time, the lead nodules form and grow to reduce the surface energy. This would be consistent with Figures 7.3-5b.

Although not shown by this work, these conclusions suggest that it is possible for an initial monolayer deposit of lead to form in a uniform manner and completely block the hydrogen permeation. The permeation test using the 150ppm lead solution

and Table 7.A support the blocking mechanism. However, over time, the formation of lead nodules would occur, exposing the steel surface and thus, permitting the hydrogen to penetrate the steel sheet.

7.3.3 Contamination on Steel and Mechanisms for Hydrogen Absorption

Lead-contaminated steel surfaces exposed to a sulfuric acid environment can affect the amount of hydrogen absorbed as evidenced by either increasing or decreasing the permeation current. This statement is supported by the conflicting reports of lead as a hydrogen promoter.

The surface reactions of interest to hydrogen absorption are the hydrogen discharge reaction (HDR -- Eq. [7.1] and the hydrogen evolution reaction (HER -- Eqs. [7.2] or [7.3]). The HER is in competition with the absorption reaction for the concentration of adsorbed hydrogen on the metal surface. Hence, to affect the hydrogen absorption reaction, three things may be done: 1) change the catalytic character of the surface so that less or more current is necessary to reduce water to hydrogen, 2) change the surface coverage of hydrogen, or 3) affect the ability of hydrogen bubbles to form or evolve. The difficulty lies in determining more specifically how these mechanisms occur.

The Hydrogen Discharge Reactions

$H_3O^+ + e^- \Leftrightarrow H_{ads} + H_2O$ {in acid} [7.1]

The Hydrogen Evolution Reactions

$H_{ads} + H_{ads} \Leftrightarrow H_2$ [7.2]

$H_{ads} + H_3O^+ + e^- \Leftrightarrow H_2 + H_2O$ {in acid} [7.3]

The behavior of the Pb/Steel surface is dependent upon the amount of lead that is deposited on the steel surface. For small coverages of lead on the steel surfaces (from this study, 1 minute deposition), the permeation current is decreased ($i^{\infty}_{pb} \sim (1/6)i^{\infty}_{blank}$). By doubling the deposition time, the permeation current is increased over a non-contaminated surface when the lead concentration is less than 10ppm in the deposition solution (for 5ppm, a 15% and for the 10ppm a 46% increase in i^{∞}). However, for longer deposition times and more concentrated solutions, the permeation current decreases and in some cases (e.g., 15 or 150ppm specimens), this decrease is to a value significantly less than that for the bare steel (for 15ppm, a 62% and for the 150ppm, a 98% decrease in i^{∞}).

Under potential control the hydrogen absorption behavior can be described by the amount of lead on the surface. For very small coverages, the lead probably blocks either adsorption or absorption sites on the steel. Although the exchange current density is reduced, there is not enough lead to increase the amount of H_{ads} appreciably. This is emphasized by the comparison of the surfaces exposed to Pb and to Pt (see Figure 7.3). For higher amounts of lead on the surface, the hydrogen exchange current density becomes more appreciably reduced, thus providing a larger surface coverage of hydrogen and an increase in permeation current. This is supported by the Deposit tests for 5 and 10ppm in Figure 7.2. As the amount of lead on the surface increases, the lead begins to block absorption sites, thus, decreasing the permeation current. This is supported by the results in Figure 7.2.

For lead contaminated surfaces under galvanostatic control, the line drawn between blocking hydrogen entry and enhanced surface coverage becomes less clear. If lead is on the steel surface, the controlling device will supply enough potential to

maintain the set current. As noted in Figures 7.1 and 7.8, such situations result in the lead/steel specimen being exposed to higher potentials than a bare steel specimen. This will result in higher fugacities at the surface and will increase hydrogen absorption.

7.4 Conclusions

The effect of different amounts of lead, both in solution and on a low carbon steel surface, were shown to affect the hydrogen permeation behavior. The tests run with lead in solution resulted in the lead plating out of the electrolyte over the course of the permeation test. The lead contaminated steel surfaces tested in non-lead solutions resulted in surface morphology changes during hydrogen evolution.

Lead was shown to act as both a promoter and a blocker to hydrogen entry in low carbon steel. The lead acts to reduce the exchange current density of the surface, thus, increasing the amount of hydrogen remaining on the steel surface. In addition, it was proposed that the lead occupies favorable hydrogen absorption/adsorption sites. The dominating mechanism is a function of the amount of lead on the surface of the steel under potentiostatic conditions. Under galvanostatic conditions of both low and high current densities, the increased overpotential of the lead contaminated steel surface was responsible for the increase in permeation current.

References for Chapter 7

1 J.H. Payer and G.M. Michal. *Proc. of 5th Auto.Prev.of Corr.*, P-250, Dearborn, MI, (1991), 53-63.

2 J.O'M. Bockris, J. McBreen and L. Nanis, *J. Electrochem. Soc.*, **112**[10] (1965) pp. 1025-1031.

3 A. Saraby-Reintjes, *Electrochimica Acta*, **31**[2] (1986) pp. 251-254.

4 C.D. Kim and B.E. Wilde. *J. Electrochem. Soc.*, **118**[2] (1971) pp. 202-206.

5 M.N.C. Ijomah. *J. Electrochem. Soc.*, **134**[12] (1987) pp. 2960-2966.

6 D.J.G. Ives and F.R. Smith. *Trans. Far. Soc.*, **63** (1967) 217-233.

7 H.W. Salzberg, *J. Electrochem. Soc.*, **100**[4] (1953) pp. 146-151. Continued in L.W. Gastnirt and H.W. Salzberg, *J. Electrochem. Soc.*, **104**[12] (1957) pp. 701-703.

8 Kure/Yeager Thesis (1956).

9 A. Druschitz and P. Gordon, Embrittlement by Liquid and Solid Metals, M.H. Kamdar ed., Metallurgical Soc. of AIME, Warrendale, PA, (1984) pp. 285-315.

10 S. Mostovoy and N.N. Breyer, *Trans. ASM*, **61**, (1968) pp. 219-232

11 J.J. Lewandowski, Y.S. Kim and N.J.H. Holroyd, *Metall. Trans. A*, **23A** (1992) pp. 1679-1689.

12 K. Vijayaamohanan and S. Sathyanarayana, *J. Power Sources*, **30**[1-4] (1990) pp. 169-175.

13 H. Sanchez, Y. Meas, I. Gonzalez and M.A. Quiroz, *J. Power Sources*, **32** (1990) pp. 43-53.

14 C.Y. Chan and A.T. Kuhn, *Oberflache-Surface*, **20**[1] (1979) pp. 7-14.

15 S.S. Chatterjee, B.G. Ateya and H. W. W. Pickering, *Metall. Trans. A.*, **9A** (1978) pp. 389-395.

16 H. P. Tardif and H. Marquis, *Can. Metall. Quart.*, **1** (1962) pp. 153-171.

17 I. Matsushima and H.H. Uhlig, *J. Electrochem. Soc.*, **113**[6] (1966) pp. 555-559.

18 J.O'M. Bockris and B.E. Conway,. *Trans. Far.Soc.*, **45** (1949) 989-999.

19 J.O'M. Bockris, *Chem. Rev.*, **43** (1948) pp. 525-577.

20 T.P. Radhakrishnan and L.L. Shreir, *Electrochimica Acta*, **11** (1966) pp. 1007-1021.

21 H. Ferber, H. Kasten, G.K. Wolf, W.J. Lorenz, H. Schneickert and H. Folger, *Corr. Sci.*, **20** (1980) pp. 117-128.

22 R.D. McCright and R.W. Staehle, *J. Electrochem. Soc.*, **121**[5] (1974) pp. 609-618.

23 S.L. Amey, G.M. Michal and J.H. Payer, submitted to *Metallurgical Transactions A*, spring 1992.

24 H. Zeilmaker, *Electrodepos. & Surf. Treat.*, **1** (1972/73): p. 109.

25 M. Zamanzadeh, A. Allam, H.W. Pickering and G.K. Hubler, *J. Electrochem. Soc.*, **127**[8] (1980) 1688-1693.

26 M.A.V. Devanathan, Z. Stachurski and W. Beck, *J. of Electrochem. Soc.* **110**, [8](1963): pp. 886-890.

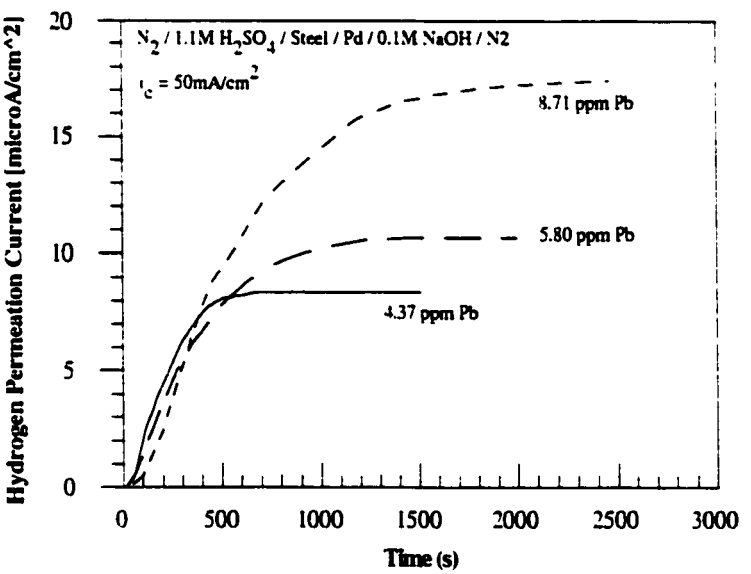

Figure 7.1: Permeation behavior of low carbon steel exposed to a sulfuric acid electrolyte with different concentrations of lead present under galvanostatic control at 25°C.

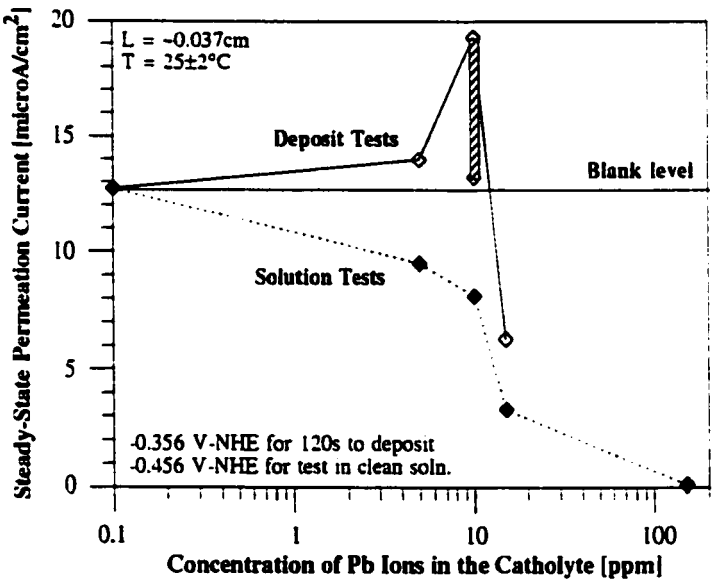

Figure 7.2: The influence of lead upon the steady-state permeation current. Permeation tests were conducted with lead ions in a pH=1 sulfuric acid electrolyte (solution tests) or were conducted in purified pH=1 sulfuric acid after lead deposition (deposit tests) from a Pb contaminated solution.

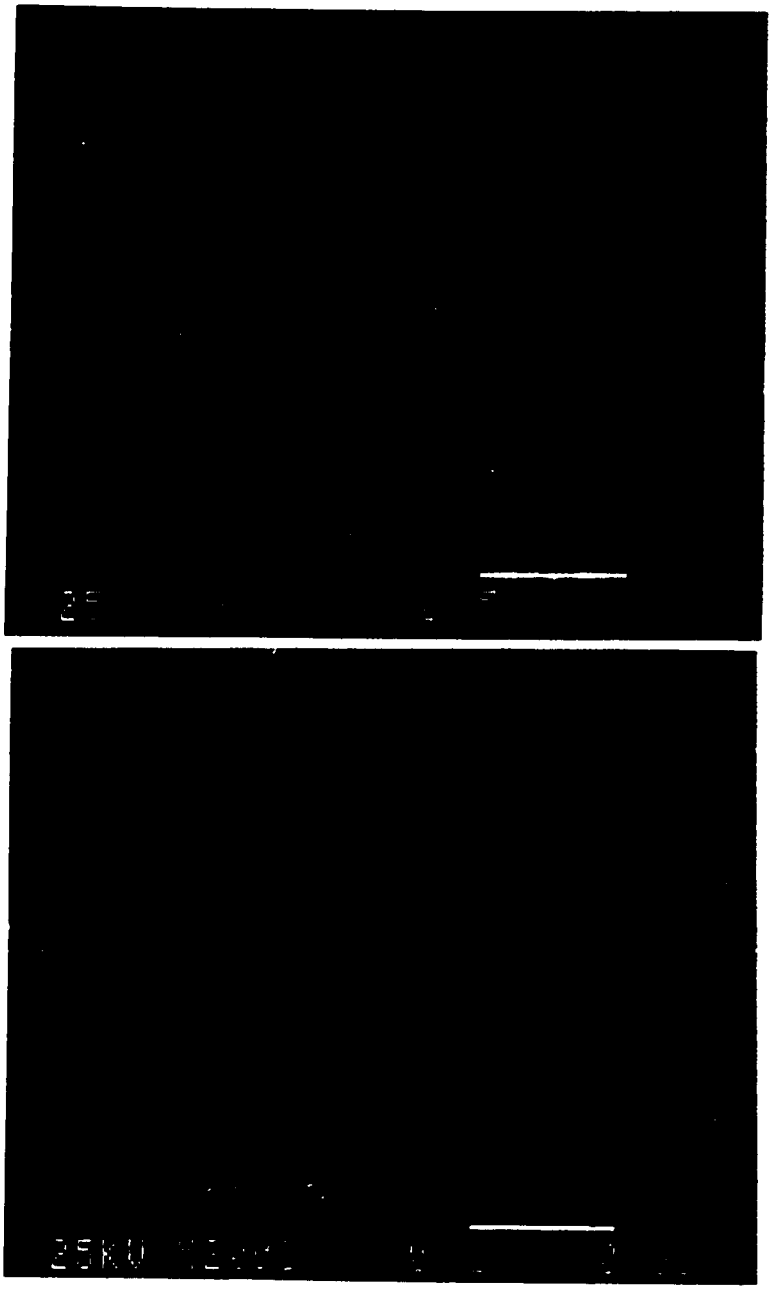

Figure 7.3: The surface morphology of the Pb/steel a) immediately after Pb deposition from a 5ppm Pb solution, and b) after 3 hours of cathodic charging (E_C = -456 mV-NHE) in purified pH=1 sulfuric acid.

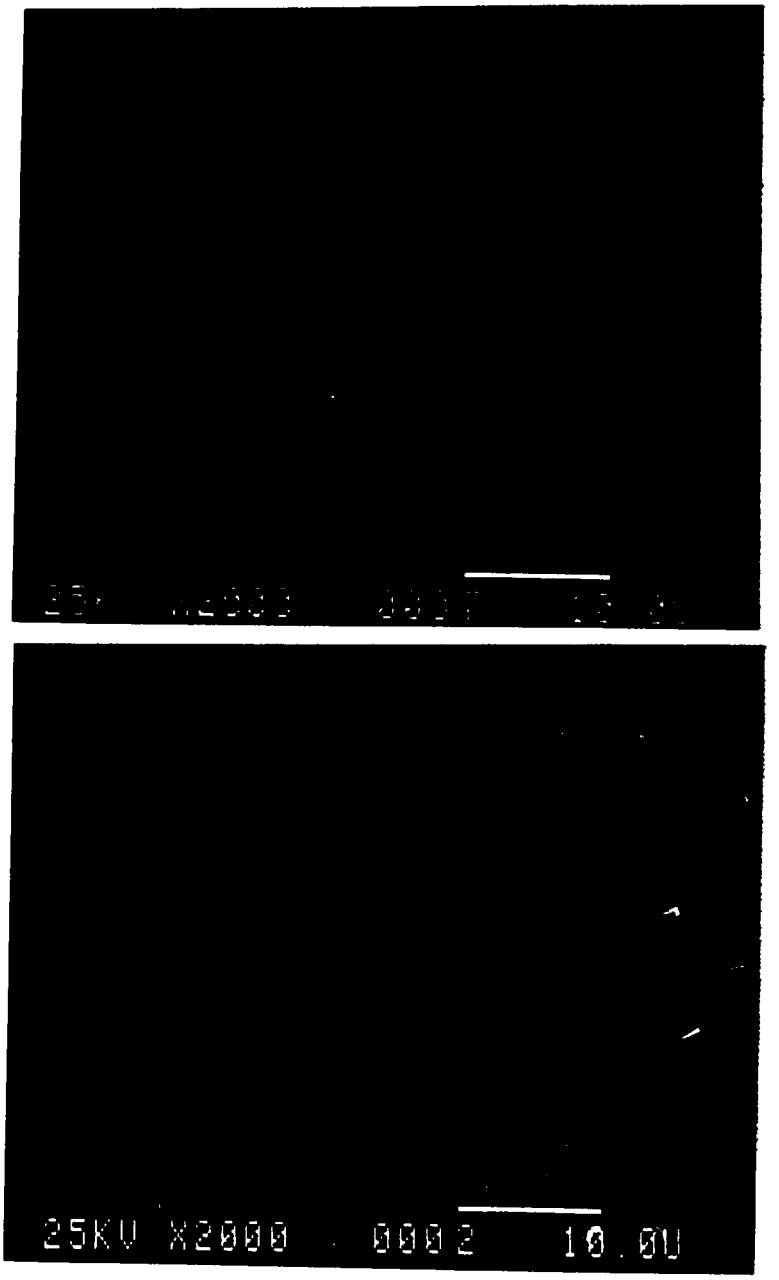

Figure 7.4: The surface morphology of the Pb/steel a) immediately after Pb deposition from a 10ppm Pb solution, and b) after 3 hours of cathodic charging (E_C = -456 mV-NHE) in purified pH=1 sulfuric acid.

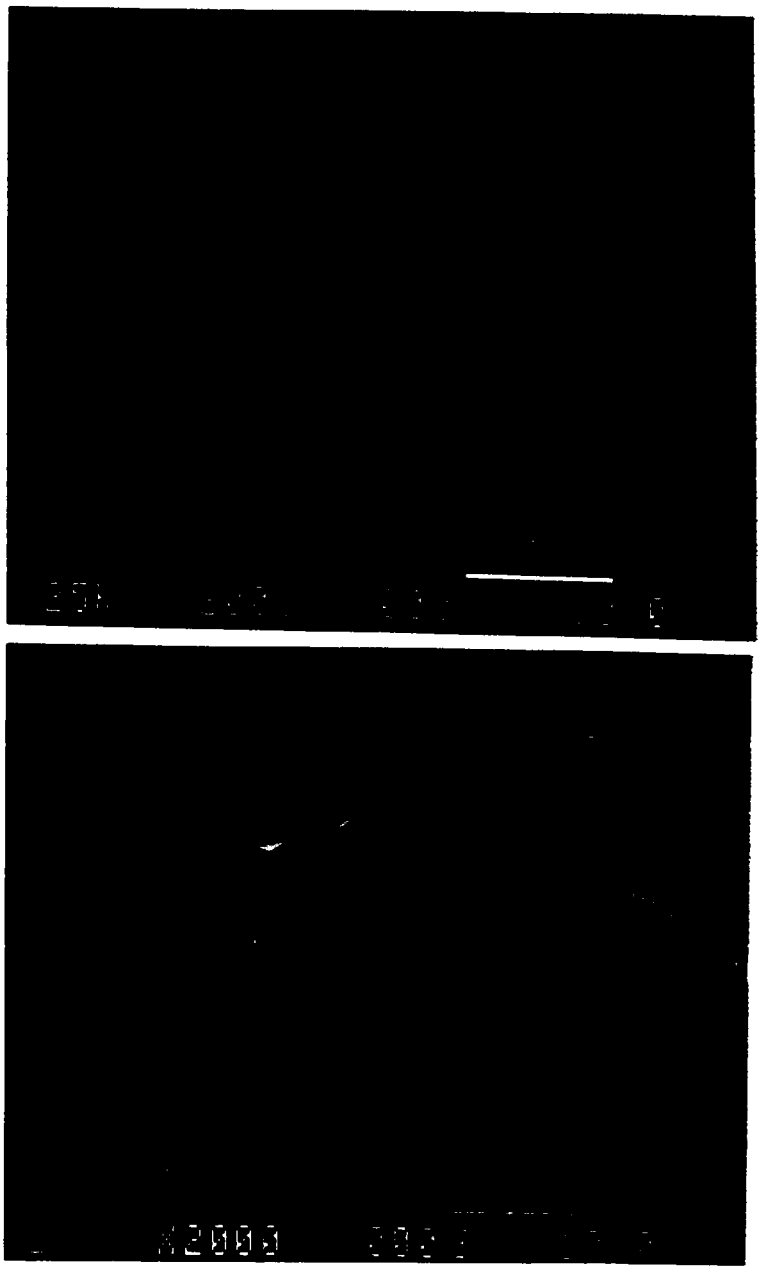

Figure 7.5: The surface morphology of the Pb/steel a) immediately after Pb deposition from a 15ppm Pb solution, and b) after 3 hours of cathodic charging (E_C = -456 mV-NHE) in purified pH=1 sulfuric acid.

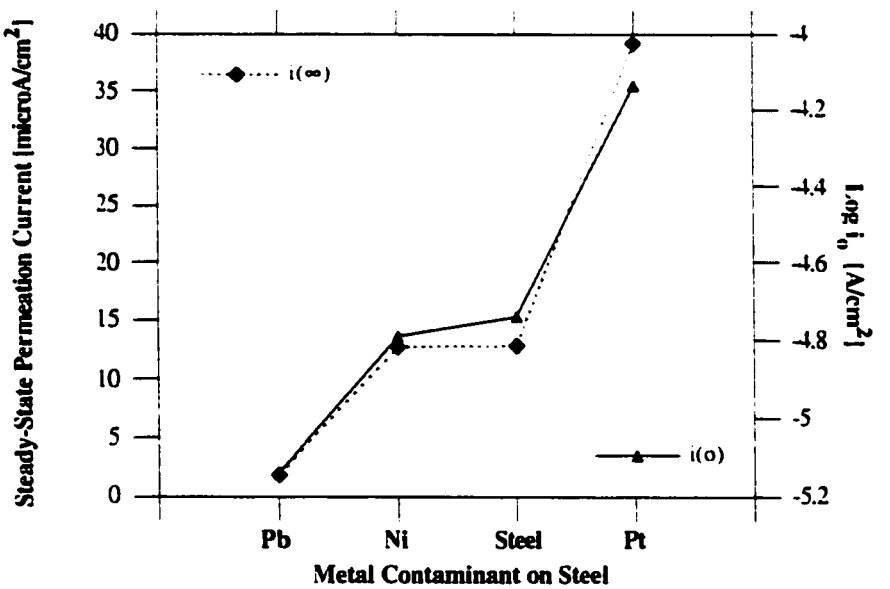

Figure 7.6: The effect of Pb, Pt and Ni contaminants on steady-state permeation current and exchange current density. Contaminants were deposited for 1 minute at -0.356 V-NHE and then, permeation tested (E_c = -0.456 V-NHE) in purified pH=1 sulfuric acid. Exchange current densities were obtained via linear polarization tests.

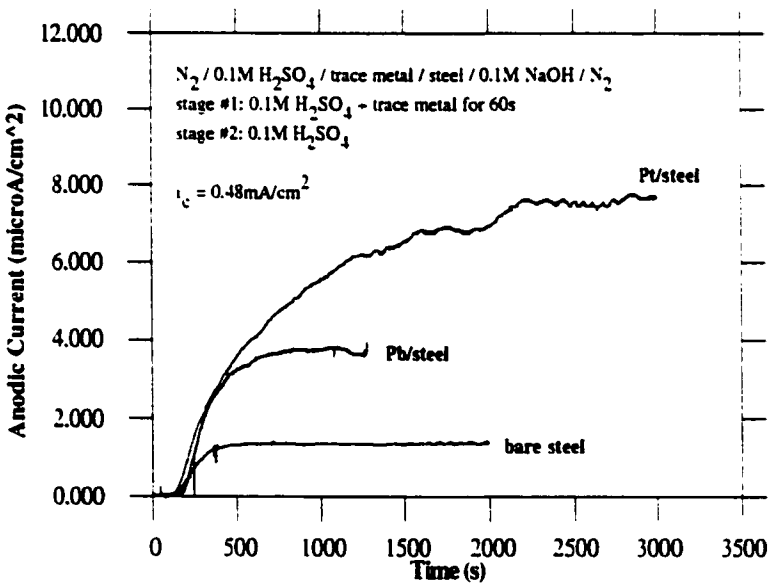

Figure 7.7: Effect of Galvanostatic control upon a Pb or Pt contaminated steel surface. The permeation test was conducted in non-contaminated sulfuric acid solution. The deposition occured at -50mA/cm^2 for 1 minute. Permeation test was conducted at -0.5mA/cm^2.

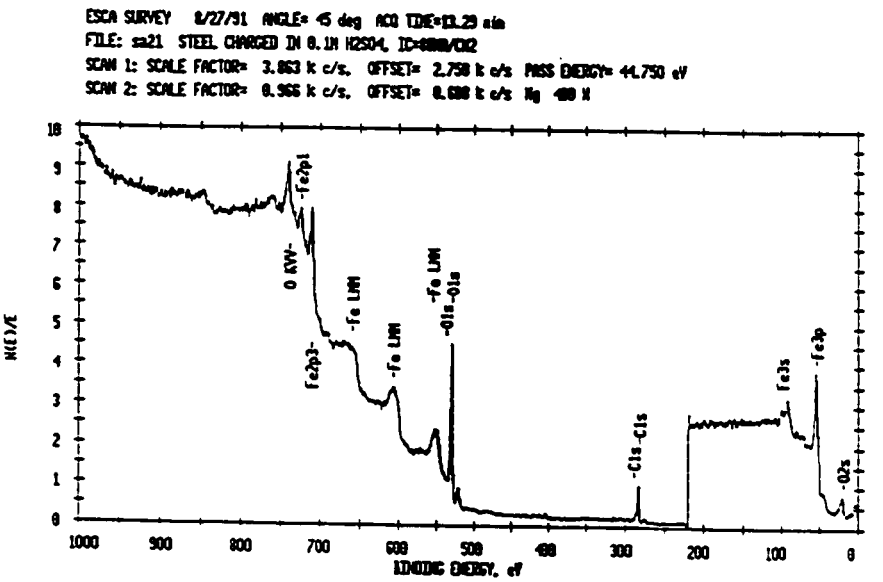

Figure 7.8: An X-ray photoelectron survey scan of a non-contaminated steel surface.

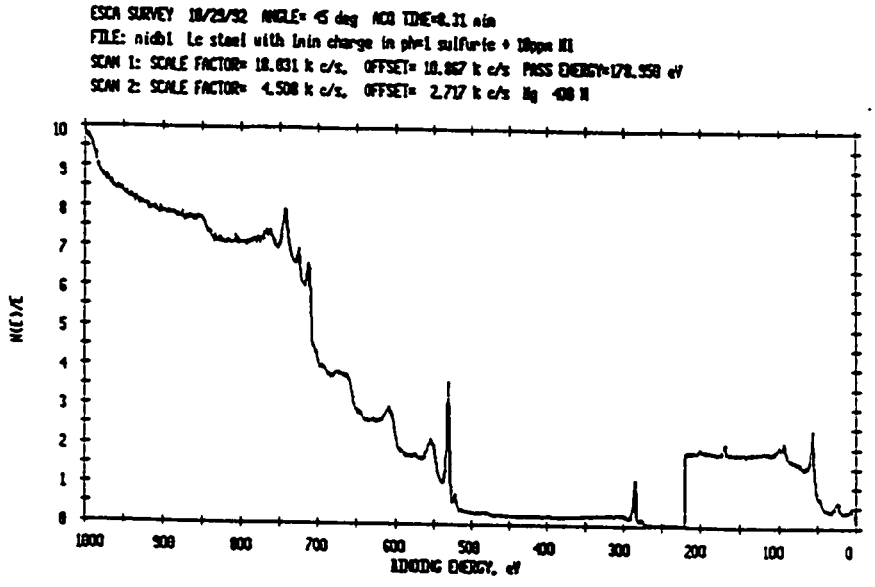

Figure 7.9 An X-ray photoelectron survey scan of the Ni-contaminated steel surface after a 60s charging in a 10ppm Ni contaminated, pH=1 sulfuric acid solution at -0.356 V-NHE.

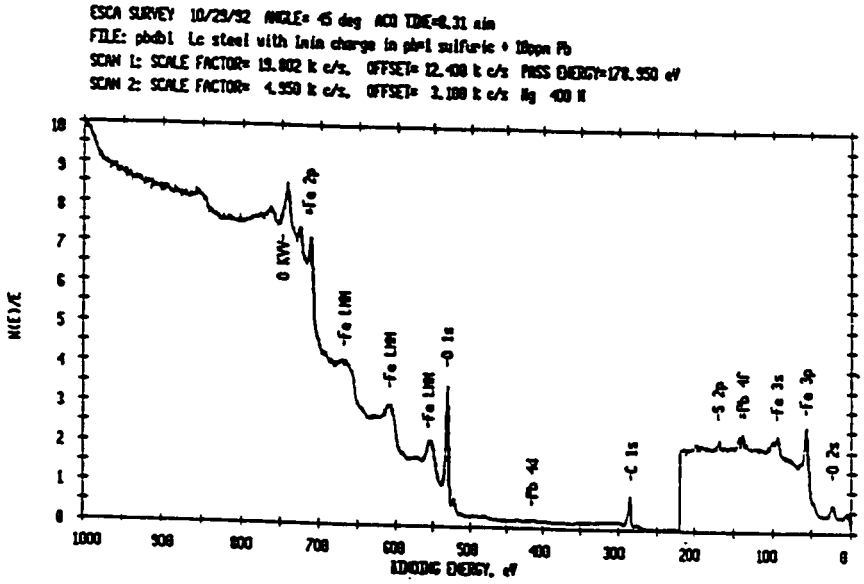

Figure 7.10 An X-ray photoelectron survey scan of the Pb-contaminated steel surface after a 60s charging in a 10ppm Pb contaminated, pH=1 sulfuric acid solution at -0.356 V-NHE.

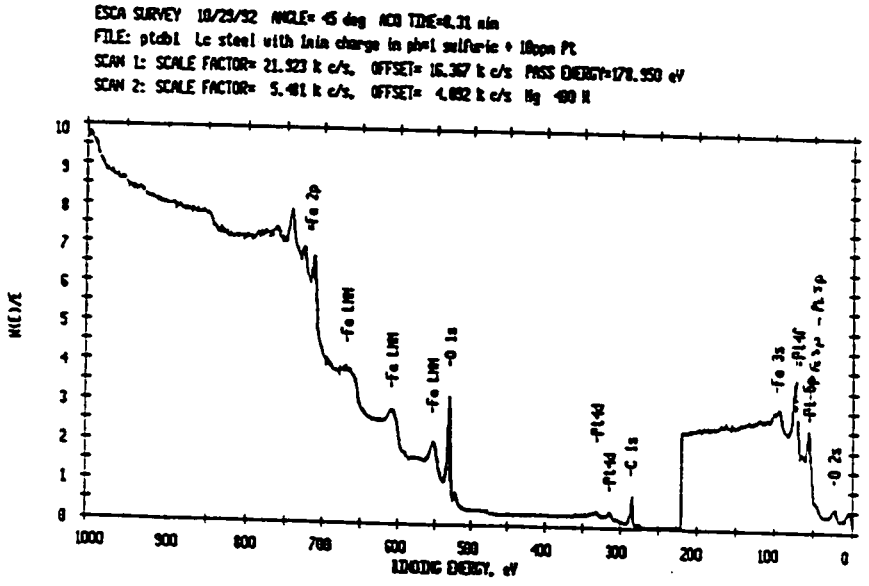

Figure 7.11 An X-ray photoelectron survey scan of the Pt-contaminated steel surface after a 60s charging in a 10ppm Pt contaminated, pH=1 sulfuric acid solution at -0.356 V-NHE.

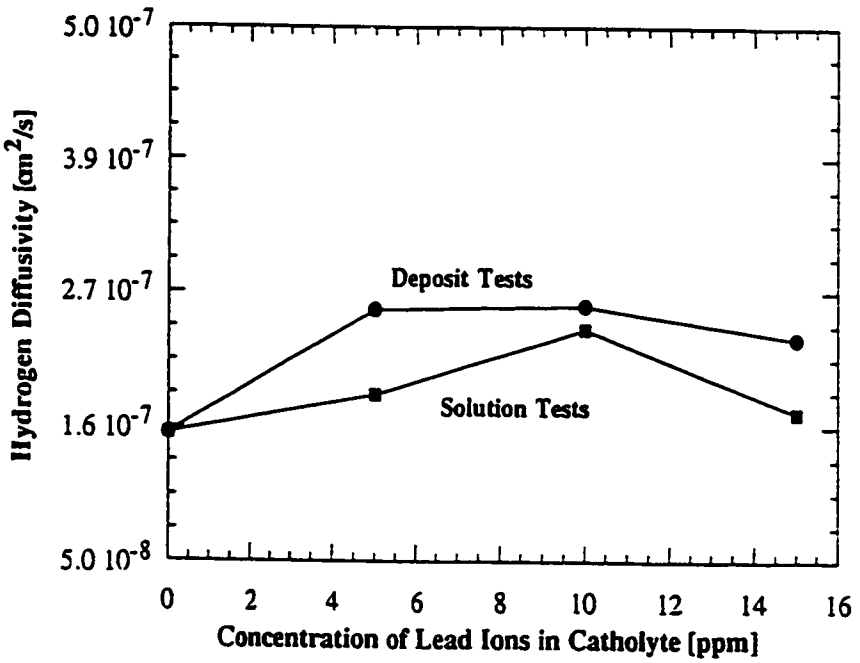

Figure 7.12 The effect of the Pb on the hydrogen diffusivity through the steel sheet as a function of the lead concentration in the deposition solution.

Chapter 8

The Role of the Electroprocess Steps in the Hydrogen Absorption of Electrogalvanized Steel

8.1 Introduction

There has been recent interest[1,2] in hydrogen that is absorbed from various electrochemical pre-treatment processes on an electrogalvanizing line. Such absorbed hydrogen may diffuse to areas of poor adhesion along the Zn/Steel interface and form blisters in the coating. A typical substrate material for electrogalvanizing is cold rolled, low carbon (0.05 wt.%C) steel.

Hydrogen may enter a steel sheet from a variety of sources on a plating line. After rolling, the steel undergoes several degreasing, cleaning and pickling steps before plating. Once the zinc coat is applied, any hydrogen absorbed from previous processes is essentially trapped in the sheet. The cleaning, pickling, and plating steps are termed the "electroprocesses" of the electrogalvanizing line because an applied current is present.

The interaction between hydrogen and iron or steel has been well documented in several reviews[3,4,5]. Specific studies have emphasized the effects of pH[6,7], cathodic current[8,9,10,11], electrolyte agitation[12], surface finish[13] or hydrogen diffusion[14,15]. However, most of these studies have been conducted under benign conditions (i.e., low current densities and minimal agitation). The electroprocesses (the electrocleaning, electropickling and electroplating steps) operate under severe conditions of electrolyte pH, high current densities (-100 to 500mA/cm^2), vigorous agitation (line speeds of 90 to 150 m/min) and moderate temperatures (55 - 71°C). Chapter 5 has evaluated those

parameters which may be controlled on an electrogalvanizing line at the more severe conditions. However, there is a need to evaluate the three electroprocesses as to their ability to contribute to the amount of absorbed hydrogen.

In addition, the effectiveness of various metal coatings as barriers to hydrogen have been previously studied[16,17,18,19,20,21], however, there have been few[22,23,24] that have investigated zinc coatings. Furthermore, such studies have concentrated their efforts on coatings that were applied by non-industrial techniques (e.g. vapor deposition or low current density deposition). Therefore, it is necessary to evaluate the barrier effectiveness of an electrogalvanized coating that was applied under the severe conditions of the plating line.

In this chapter, the effect of three typical process step conditions (an alkaline, an acidic and a zinc plating step) were evaluated as to their influence on the hydrogen absorption in low carbon steel. In addition, the barrier effectiveness of zinc coatings of different thicknesses on steel to hydrogen penetration were evaluated. An analytical model[25] was employed to understand the hydrogen entry kinetics and evaluate the amount of hydrogen absorbed from the different process steps.

8.2 Results

8.2.1 Testing the Electroprocess Conditions

The barnacle test results shown in Figure 8.1 were obtained by charging steel sheets under the various process charging conditions. In addition to using the EC, EP and No-metals plating (NMP) solutions, the tests were performed at 25°C and elevated temperatures. If the more severe charging conditions can be characterized as those with

lower pH and higher cathodic current densities. Figure 8.1 illustrates that with increasing charging severity and temperature, the steel absorbs more hydrogen.

The permeation results obtained by using the electroprocesses conditions (electrocleaning (EC), electropickling(EP) at -100mA/cm^2) in the cathodic cell are listed in Table 8.A. Figure 8.2 illustrates that both the electrocleaning and the electropickling solutions show an increase in i^{∞} with temperature. This result is consistent with trends found by other studies of hydrogen permeation through iron[10,26], nickel[8,20] or palladium[9].

The EP process (59°C) has almost a three-fold higher permeation current over the EC process (71°C). Furthermore, when the solutions are compared at the same temperature, the EP solution has a 3.7 (at 59°C) and a 3 (at 25°C) fold higher permeation current than that of the EC solution.

TABLE 8.A

Permeation Results for the Electroprocesses Conditions.

Process	T (°C)	i^{∞} [μA/cm^2]	E_w [V-SCE]
Electrocleaning	25 ± 2	4.5 ± 0.2	-1.550 ± 0.005
Electrocleaning	59 ± 2	8.4 ± 0.2	-1.510 ± 0.005
Electrocleaning	71 ± 2	11.2 ± 0.2	-1.480 ± 0.005
Electropickling	25 ± 2	13.5 ± 0.2	-0.695 ± 0.005
Electropickling	59 ± 2	31.1 ± 0.2	-0.570 ± 0.005
Plating Buffer	25 ± 2	6.2 ± 0.2	-0.689 ± 0.005

The uncertainty values listed are the experimental error in making the measurement. The steel sheet thickness for the tests was 0.073 ± 0.02 cm.

8.2.2 The Hydrogen Diffusivity for the Low Carbon Steel

The apparent diffusivities (D) for hydrogen in our low carbon steel are shown in Figure 8.3 as a function of temperature. The diffusivities were obtained by curve fitting

our model to the permeation data obtained for the processes at the respective temperatures. Although the values for D were not measured in the traditional fashion[27], they are consistent with the values reported for iron and other low carbon steels[5]. These values for D should be considered to be "apparent diffusivities" as discussed by McNabb[28].

Figure 8.3 illustrates the effect of temperature upon the hydrogen diffusivity. As the temperature increases, the diffusivity increases. This trend is consistent with studies performed on Ni, Pd and other metals[22]. If an Arrehnius relation is assumed, the slope of the natural logarithm of D versus reciprocal temperature plot (see figure 8.3) yields a value for the activation energy, Q, for diffusion of 30.4 and 40.7 kJ/mol from acidic and alkaline data sets, respectively. Similarly, values for the temperature independent diffusion coefficient, D_0, of 1.506 and 50.7 cm^2/s from acidic and alkaline data sets, respectively. The small number of data points used to obtain the ln D vs 1/T plot explains the deviation in Q values between the two data sets. Regardless, the values found for Q and D_0 are in reasonable agreement with values reported by Evans[29], Barrer[29] and Johnson[30] for steel with some trapping character.

8.2.3 The Barrier Effect of a Zinc Coating

If zinc is present in solution when a cathodic current is applied, the zinc will deposit upon the steel sheet. Figure 8.4 illustrates that under such conditions, the permeation current behaves similarly to a non-zinc solution, however, it quickly reaches a current which is much lower than the non-zinc solution. This current may decrease over time, but the reduction does not reach zero even after several hours of polarization. This result is typical of other studies[17,18] evaluating plating baths by the hydrogen

permeation technique. The anodic current does not drop to zero because the permeation cell used does not provide sufficient convection for a uniform coating to be deposited. In fact, zinc dendrites would form over time in our cells which extended 2-3 cm perpendicular from the steel surface. The non-uniform or porous coating allows a small amount of hydrogen to continue to permeate the sheet. The porosity in the zinc coating was verified by scanning electron microscopy.

Permeation specimens, prepared from 10μm thick zinc coated steel sheets that were electrogalvanized under production line conditions, were found to significantly affect the hydrogen permeation behavior. The zinc coating thickness was varied by metallographic techniques and verified by X-ray fluorescence spectroscopy. Since typical zinc plating lines (~500mA/cm^2) have high current efficiencies (~92%), a charging current of -40mA/cm^2 was used for the permeation tests.

Figure 8.5 shows that all specimens with at least a 3.6μm Zn coating on the steel surface exposed to the cathodic chamber of the permeation cell were barriers to hydrogen entry over a 4 hour charging period. In fact, the anodic current decreased over the course of the test. Kudryavtsev[22] reported that zinc coatings prepared from non-industrial conditions acted as hydrogen barriers when the coating thickness was between 2 and 7 microns.

Specimens with coating thicknesses of less than 3μm, but greater than 1μm, were found to decrease the permeation current relative to a non-coated steel surface (see Figure 8.5). This is consistent with other studies[22-24] upon Zn and with studies[17-21] which investigated other transition metal coatings (Cd,Co,Cr,Cu,Ni,Pb,Sn) on nickel or iron alloys. In addition, when 1 micron thick Zn coatings on steel specimens were back

charged with hydrogen, blisters in the Zn/steel coating resulted. This suggests that very thin coatings (~1μm) can act as barriers to hydrogen. Secondly, it is possible that the measurable permeation behavior noticed was from small punctures in the coating from the metallographic polishing of the zinc coating. Finally, it can be concluded that the Zn coating stops hydrogen absorption early on (e.g., first plating cell) in the plating process.

8.3 Discussion

8.3.1 Application of Model to Electroprocess Results

The electroprocess steps have been discussed in terms of permeation variables, however, to gain more insight, it would be useful to relate these results to what is occurring on the steel's entry surface.

$$J_{\infty} = \kappa_1 \left(c_1 - c(0, \infty) \right) \qquad [8.1]$$

$$J_{\infty} = D \frac{c(0,\infty) - c(L,\infty)}{L} \qquad [8.2]$$

$$J_{\infty} = \kappa_2 \left(c(L, \infty) - c_2 \right) \qquad [8.3]$$

Recall from Chapter 4 that from Eqs. [8.1]-[8.3], the solubility of hydrogen just inside the entry surface, $c(0, \infty)$, and the value of κ_1 may be calculated. Furthermore, utilizing Eqs. [8.1]-[8.3], a relation for the steady-state hydrogen flux may be obtained in terms of both surface (κ_1, κ_2) and bulk (D) parameters:

$$J^{\infty} = \frac{\Delta C}{\left(\frac{L}{D} + \frac{1}{\kappa_1} + \frac{1}{\kappa_2}\right)} = \frac{\Delta C}{\left(\frac{L}{D} + \frac{1}{\kappa_1}\right)} \qquad [8.4]$$

Since κ_2 is very large due to the experimental design[25], the flux reverts to a simplified expression that is a function of the entry-surface kinetics and the diffusivity. Equations [8.1]-[8.4] will prove useful in the discussions below.

The electroprocess values for κ_1 and $c(0,\infty)$ provide a unique opportunity to study the model parameters and their dependence upon both solution chemistry and temperature. The values for the electroprocesses are listed in Table 8.B. The convective mass transfer coefficient, κ_1, was shown to vary in cm/s as:

EC(25°C)	< EP(25°C)	< EP(59°C)	< EC(59°C)	< EC(71°C)
8.33×10^{-9}	1.22×10^{-7}	2.20×10^{-6}	3.69×10^{-6}	6.17×10^{-5}

The value in parentheses for each process is the temperature for the process and the temperature at which the permeation tests were performed.

TABLE 8.B
Model Parameters as a Function of Controlling Parameters

Process	c_1 [mol/cm^3]	κ_1 [cm/s]	$c(0,\infty)$ [mol/cm^3]
EC (25°C)	5.60×10^{-3}	8.33×10^{-9}	1.40×10^{-6}
EC (59°C)	2.45×10^{-5}	3.69×10^{-6}	8.82×10^{-7}
EC (71°C)	2.72×10^{-6}	6.17×10^{-5}	8.42×10^{-7}
EP (25°C)	1.15×10^{-3}	1.22×10^{-7}	4.20×10^{-6}
EP (59°C)	1.50×10^{-4}	2.20×10^{-6}	3.27×10^{-6}
As T increases	**decreases**	**increases**	**decreases**
PB (25°C)	3.36×10^{-3}	1.79×10^{-8}	7.51×10^{-7}

Furthermore, the surface solubility, $c(0,\infty)$ of hydrogen in the metal was shown to vary in mol/cm^3 as:

EC(71°C)	< EC(59°C)	< EC(25°C)	< EP(59°C)	< EP(25°C)
8.42×10^{-7}	8.82×10^{-7}	1.40×10^{-6}	3.27×10^{-6}	4.20×10^{-6}

Figure 8.6 shows that κ_1 increases and $c(0,\infty)$ decreases with temperature for a given solution and, in this case, this effect is independent of the two solutions used. In addition, with the pH of the EC and EP solutions being ~11 and ~1, respectively, the surface solubility was found to decrease with increasing pH.

As the temperature is increased, the hydrogen flux permeating the steel sheet is enhanced. Such enhancement in flux may be explained by both an increase in the hydrogen diffusivity and by an increase in κ_1. Since the overpotential necessary to maintain a given current condition decreases with increases in temperature, a lower hydrogen fugacity is required to maintain the same flux on the entry surface. As a result, κ_1 must increase to account for the increased efficiency of hydrogen absorption. This example illustrates how κ_1 may be used to evaluate surface phenomena. By increasing the temperature, the entry kinetics are enhanced, resulting in more hydrogen absorbing, as evidenced from the permeation current values.

Although the flux increases with temperature, the $c(0,\infty)$ decreases. This is because the diffusivity increases significantly from 25°C to 71°C. Thus, more hydrogen is entering the steel (from κ_1 and i^∞ values), but the increased diffusivity of the hydrogen moves any absorbed hydrogen deeper into the metal, resulting in a lower *surface concentration* just under the surface of the metal. This example illustrates the importance of not using the surface solubility alone to determine the amount of hydrogen absorbed from a particular cathodic process.

8.3.2 Determination of Dominant Mechanism for Hydrogen Permeation

Equation [8.4] indicates that the hydrogen flux is dependent upon both surface effects (κ_1) and bulk effects (D/L). For a given permeation test, the temperature, the diffusivity and the thickness are constant. Hence, by varying the convective mass transfer coefficient, a range of steady-state permeation currents or hydrogen fluxes may be obtained. Plotting the steady-state permeation current versus κ_1 yields a curve which will determine the controlling mechanism for hydrogen permeation at a given charging condition. Such controlling flux curves may be divided into three regions. When κ_1 is large, relative to D/L, the permeation is surface controlled. When κ_1 is small, relative to D/L, the permeation is diffusion controlled. When κ_1 is similar to D/L, the permeation behavior is under a mixed control mechanism.

Figure 8.7 illustrates five curves for the five different charging conditions of the electroprocess preplating steps. The curves were calculated from inserting the data listed in table 8.B, the appropriate diffusivity and a sheet thickness of 0.070cm into Eq. [8.4]. The box on the figure identifies the range of κ and i^{∞} found for the electroprocess step conditions. From Figure 8.7 it is evident that under the electroprocess step conditions, the permeation behavior is under a surface controlling (i.e., κ_1) mechanism. Since κ_1 is most likely affected by a surface/subsurface phenomenon, it should be possible to control the amount of hydrogen absorbed by engineering the surface of the metal.

8.3.3 The Pre-Plating Electroprocesses

From Eqs. [4.5]-[4.7], an expression for the hydrogen concentration (Eq. [4.28]) as a function of position and time in a metal sheet may be obtained. This expression is dependent upon κ_1, κ_2, D, c_1, c_2, and L which are defined in figure 4.1. In

addition, the expression is a function of processing time and the hydrogen distribution already present in the metal sheet. The complete expression is defined explicitly elsewhere[25]. Using such an expression, allows hydrogen concentration profiles to be calculated for different treatments acting on the steel sheet. Such profiles provide useful tools to compare different hydrogen environments by examining both the total amount (Table 8.C) of hydrogen absorbed and the penetration depth into the steel sheet (Figures 8.8-8.9) under non-equilibrium conditions.

Concentration profiles have been calculated for two different situations. First, each process listed in Table 8.C was considered to be acting on either side of a low carbon steel sheet. The processes were each to act for ten seconds. Thus, the profiles shown in Figure 8.8 are a cross-section of the steel immediately after ten seconds of exposure to a given process. The second situation considers the effect of multiple charging processes on the hydrogen distribution in the steel. Figure 8.9 represents the result of two, ten second processes acting subsequently to each other. The first process is identical to that shown in Figure 8.8. The second process applies an anodic potential to the steel, resulting in zero hydrogen coverage. For this process, the exit kinetics were assumed to be "easy" ($\kappa_1 = 10^{-3}$ cm/s). This second process was used to understand the effect of additional processes applied identically to the profiles generated in 10 seconds by the electroprocesses.

Figure 8.8 shows the electropickling processes (25°C and 59°C) having the highest concentration of hydrogen near the surfaces of the sheet. The higher the temperature, the higher the concentration at the surface and the deeper the penetration. Figure 8.9 is consistent with Figure 8.8 only in the fact that the 59°C EP process and the 25°C EC process have the highest and lowest, respectively, surface concentrations.

The higher temperature EC processes surpassed the 25°C EP process during the multiple charging. Furthermore, for all of the processes, the multiple charging cycle left the maximum hydrogen concentration approximately 0.01cm from the surfaces. It is evident that high hydrogen activity is important for the amount of hydrogen entering the steel, however, under anodic cycles, the diffusivity or more specifically the temperature plays a dramatic role in the hydrogen distribution in a steel sheet.

In addition to the concentrations predicted by the model, it is important to consider the solubility limit of the metal. Although there is much disagreement in the literature as to what is this limit in iron at temperatues below 200°C, an estimate can be made. Separately, Geller[5] and Quick[4] experimentally proposed different relationships for the solubility of hydrogen in iron. Using the average of the two values predicted by these two studies, the solubility of hydrogen in iron may be estimated to be 1.24×10^{-7} mol/cm^3, 3.95×10^{-7} mol/cm^3 and 5.41×10^{-7} mol/cm^3 at 25°, 59° and 71°C, respectively. Using these values as limits and the model's predictions, the concentration profiles were made for this steel. When the model predicts higher concentrations than the solubility limits, it is reasonable to assume that the steel becomes strained due to the excess hydrogen. The EP (25°C) and EP (59°C) profiles both exemplify such behavior. In such situations, the steel may become "damaged" as described by Bockris[9].

Integrating the curves in Figures 8.8-8.9 yield the total amount of hydrogen absorbed for the given processing. The amounts for each of the curves is shown in Table 8.C. The values support the previously discussed behavior. It is clear that the EP process injects more hydrogen than the EC process and temperature is significant to the hydrogen distribution.

TABLE 8.C
Results of Hydrogen Profile Simulations

Process Condition	$C_{individual}$ [moles/cm^3]	$C_{multiple}$ [moles/cm^3]
EC (25°C)	9.34×10^{-10}	5.19×10^{-10}
EP (25°C)	2.81×10^{-9}	1.55×10^{-9}
PB (25°C)	1.20×10^{-9}	
EC (59°C)	1.80×10^{-9}	1.15×10^{-9}
EP (59°C)	6.59×10^{-9}	4.21×10^{-9}
EC (71°C)	3.21×10^{-9}	2.15×10^{-9}

All of the above processes were considered to act on both surfaces of a 1mm low carbon steel sheet. The first column is for the given process lasting 10 seconds. The second column is for the given process lasting 10 seconds, followed by an anodic cycle (easy exit kinetics - $\kappa_1 = 10^{-3}$ cm/s) for 10 seconds.

8.3.4 Estimating the Amount of Hydrogen Absorbed from Plating

To estimate the amount of hydrogen absorbed from the plating process step requires that the amount of time that the steel is exposed to the hydrogen environment is known. To approximate this time, Faraday's Law can be used. The weight, W, of a metal deposited from a cathodic process is related to the current, I, used in that process. If 100% efficiency is assumed:

$$W = (M\ I\ t) / (z\ F) \qquad [8.5]$$

M is the molecular weight of the metal deposit (for Zn: 65.37g/mole), t is the time for deposition, z is the charge passed (for Zn: +2) and F is Faraday's constant. To convert the weight to an average thickness, y, the density of the metal (for Zn: 7.133g/cm^3), ρ, and the area of the cathode can be used:

$$y = W / (\rho\ A) \qquad [8.6]$$

Manipulating Eqs. [8.5] and [8.6] yields and equation to obtain the deposition time, t:

$$t = (y \rho z F A) / (M I) \qquad [8.7]$$

If it is assumed that a plating current density of -500 mA/cm^2 and from the zinc barrier results, a y of 1 to 3 μm (Zn: 6 to 24 g/m^2), then the deposition time can be calculated as 1.97 to 7.09 seconds. A typical charge time for the either electroprocess step is 4 seconds. Therefore, relative to the EC or EP process steps, the plating process exposes the steel sheet to a hydrogen environment for approximately 50% to 200% as much time.

Using such information as a guideline and the charging parameters in Table 8.B, a plating process (PB) lasting 5 to 20 seconds will inject between 6 x 10^{-10} and 2.4 x 10^{-9} mol/cm^3. Since this charging condition will change over time, it may be more realistic to assume that half of these amounts are absorbed by the sheet. Hence, the three process steps may be compared as follows at 25°C:

PB^{lb}	<	EC(25°C)	<	PB^{ub}	<	EP(25°C)	
3.0 x 10^{-10}		9.3 x 10^{-10}		1.2 x 10^{-9}		2.8 x 10^{-9}	in mol/cm^3

The *lb* and *ub* are the lower and upper bounds, respectively, as described above for the plating step.

At elevated temperatures (55 to 59°C), similar assumptions can be made which suggest that the plating process will probably inject a similar amount of hydrogen to the EC step. This conclusion may be deduced by comparing the ratio of absorbed hydrogen of the EC to the EP step at different temperatures, noting the ratio is maintained and assuming a similar ratio is followed for the PB step to the EP step.

Having made such deductions, there are two important facts concerning the electroprocess steps. First, all of the electroprocesses inject hydrogen. Secondly, the electropickling step injects at least twice as much hydrogen as either the electrocleaning or the plating step.

8.4 Conclusions

From this study, it is evident that there are several variables on the electrogalvanizing line that affect the amount of hydrogen absorbed. The permeation test and the transport model provided very useful information for evaluating the different parameters and electroprocesses.

The temperature was found to significantly affect the hydrogen permeation behavior. Although the amount of hydrogen absorbed did not change much from 25°C to 71°C, the diffusivity over the same range increased an order of magnitude. By increasing the temperature for a given electroprocess, the efficiency of the hydrogen absorption reaction increased significantly (an order of magnitude or more) and the surface solubility increased.

The electropickling process injects 3.7 times the hydrogen as the electrocleaning process when acting at the same temperature for 10 seconds (6.6×10^{-9} vs 1.8×10^{-9} mol/cm^3 at 59°C). If the electrocleaning step is run at 71°C, the electropickling process (59°C) injects 2.8 times the amount of hydrogen if both processes are performed for 10 seconds (6.6×10^{-9} vs 3.2×10^{-9} mol/cm^3). It is clear that the electropickling process step injects more hydrogen than the electrocleaning process step and temperature is significant to the hydrogen distribution.

A 10μm (65 g/m^2) Zn coating acts as a barrier to hydrogen entry and exit. A 3.6μm (24 g/m^2) coating shows similar behavior. The high efficiency of the deposition process and the barrier effect of the Zn result in the plating process injecting much less hydrogen (~1/2 as much) than the electropickling process. The plating step probably injects a similar amount to that of the electrocleaning process step.

References from Chapter 8

1 J.H. Payer and G.M. Michal, *Proc. of 5th Auto.Prev.of Corr.*, **P-250**, Dearborn, MI, (1991), 53-63.

2 J.H. Payer, G.M. Michal and C. Rogers: *Corrosion/91*, (1991): paper no. 405.

3 M. Smialowski, Hydrogen in Steel, Pergamon Press, Oxford & Addison-Wesley Publishing, Reading Massachussetts, (1962): pp.88-90.

4 J.P. Hirth, *Metallurg. Trans.*, **11A**, (1980): pp. 861-890

5 E.E. Fletcher and A.R. Elsea, "Hydrogen Movement in Steel--Entry, Diffusion and Elimination," *DMIC Report*, **219** Battelle Memorial Institute, (1965).

6 R.M. Hudson, *Corrosion*, **20**, (1969): p. 24t.

7 J.O'M. Bockris, *Chem. Rev.*, **43** (1948):525-577.

8 H. Zeilmaker, *Electrodepos. & Surf. Treat.*, **1**, (1972/73): p. 109.

9 J.O'M.Bockris, Proceedings of Stress Corrosion Cracking and Hydrogen Embrittlement of Iron Base Alloys, NACE, 1973: p. 286.

10 J.O'M. Bockris, J. McBreen and L. Nanis, *J. Electrochem. Soc.*, **112**, [10](1965): p. 1028.

11 K. Bolton and L.L. Shreir, *Corrosion Sci.*, **3** (1963):17-33.

12 M. Shirkhanzadeh, *Corrosion Sci.*, **28** (1988):201-206.

13 M. M. Makhlouf and R.D. Sisson, Jr., *Meallurg. Trans. A*, **22A** (1991) 1001-1006.

14 W. Beck, J.O'M. Bockris, M.S. Genshaw and P.K. Subramanyan, *Metallurg. Trans.*, **2A**, (1971): p. 883.

15 A.S. Nowick and J.J. Burton, Diffusion in Solids, Academic Press, New York, (1975) pp. 281-284.

16 S.S. Chatterjee, B.G. Ateya and H.W. Pickering, *Metallurg. Trans.*, **9A**, (1978): p. 389.

17 M. Zamanzadeh, A. Allan, C. Kato, B. Ateya and H.W. Pickering, *J. Electrochem. Soc.*, **129** (1982) 284-289.

18 M.A.V. Devanathan, Z. Stachurski and W. Beck, *J. Electrochem. Soc.*, **110**[8] (1963) 886-890.

19 S. Rashkov, C. Bozhkov, V. Kudryavtsev, K. Pedam and S. Bagaev, *J. Electroanal. Chem.*, **248**, (1988): p. 421.

20 W. Beck, J.O'M. Bockris, M.S. Genshaw and P.K. Subramanyan, *Met.allurg. Trans.*, **2A**, (1971): p. 883.

21 I. Matsushima and H.H. Uhlig, *J. Electrochem. Soc.*, **113**, (1966): p. 555.

22 V.N. Kudryautsev, S.P. Bagaev, B.F. Ljachove and K.S. Pedan, Metal-Hydrogen Systems, ed. T.N. Veziroglu, Pergamon Press, New York, (1981) pp. 251-258.

23 H. P. Tardif and H. Marquis, *Can. Metall. Quart.*, **1** (1962) pp. 153-171.

24 K.S. Pedan, S.P. Bagaev, V.N. Kudryavtsev and Yu. D. Gamburg, *Zashchita Metallov*, **19**[6] (1983) 889-894.

25 S.L. Amey, G.M. Michal, J.H. Payer: submitted to *Metallurgical Transactions A*, spring 1992.

26 W. Beck, J. O'M. Bockris, J. McBreen and L. Nanis, *Proc. Roy. Soc. Lond.*, **290A** (1965) 191-206.

27 B.S. Chaudhari and T.P. Radhakrishnan, *Corr. Sci.*, **30**[12] (1990) pp. 1219-1234.

28 A. McNabb and P.K. Foster: *Trans.of TMS-AIME*, **227**, (1963): pp. 618-627.

29 J. Volkl; G. Alefeld: in Diffusion in Solids: Recent Developments, eds. A.S. Nowick, J.J. Burton, Academic Press, New York, 1975, pp. 281-283.

30 E.W. Johnson, M.L. Hill, *Trans. Met. Soc. AIME*, **218** (1960) pp. 1104-1112.

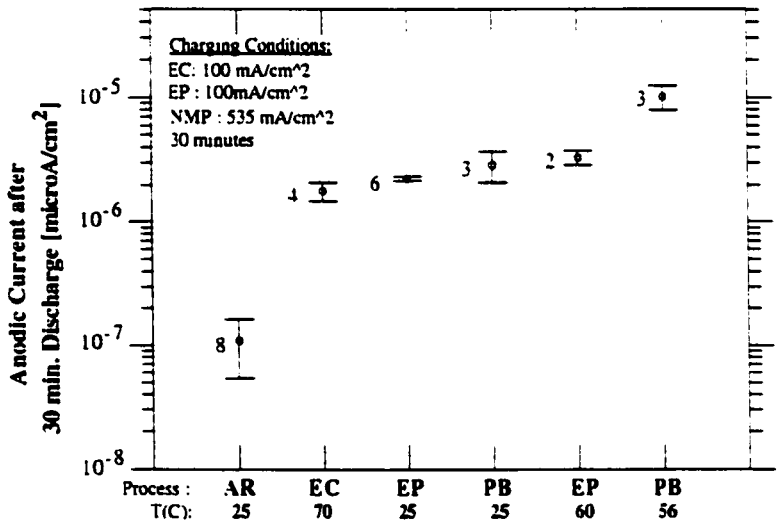

Figure 8.1 Evaluation of the electrocleaning, electropickling and plating buffer solutions, charging currents and temperatures as to their ability to inject hydrogen. The evaluation was performed by the barnacle test technique.

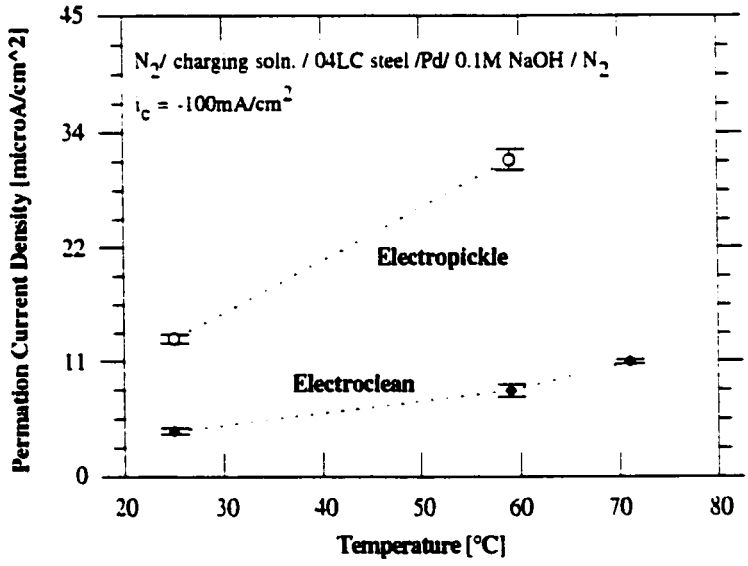

Figure 8.2 The effect of temperature on the steady-state permeation current for the electrocleaning and electropickling solutions. The cathodic current density was held constant at -100 mA/cm^2 for the test.

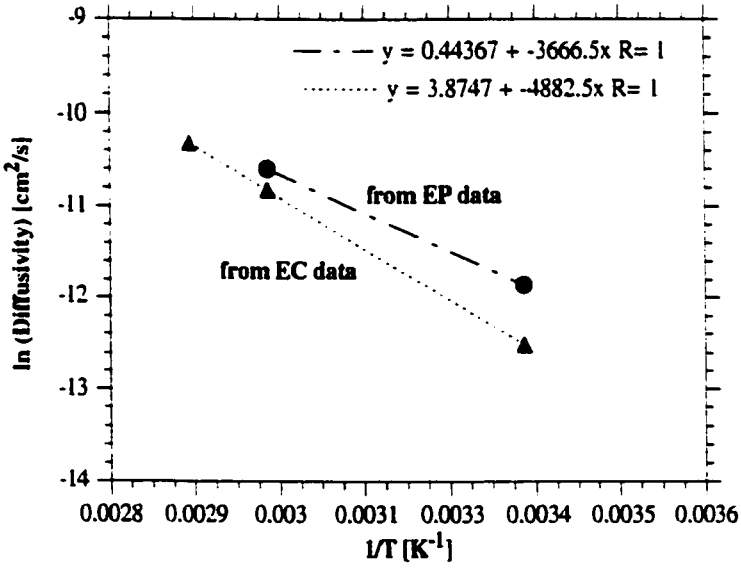

Figure 8.3 The effect of temperature on the hydrogen diffusivity in the low carbon steel used in this study. The tests used both electrocleaning and electropickling processes to obtain the diffusivity.

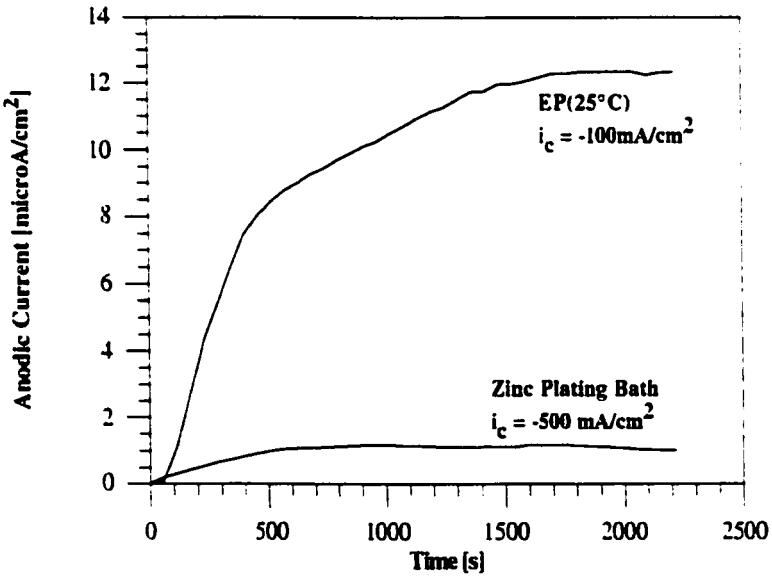

Figure 8.4 The effect of zinc ions in the cathodic solution on permeation behavior is shown. The cathodic cell solution is typical of acidic zinc plating solutions. The current is low because of the constant depostition of the zinc on the steel. The current never decreases to zero because the permeation cell geometry prevents uniform coating. For comparison, the EP charging condition is included. Both tests were performed at 25°C.

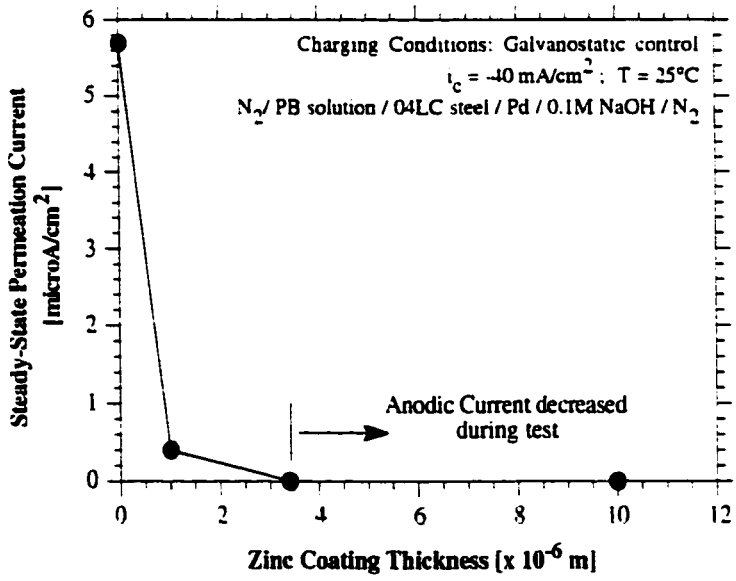

Figure 8.5 The effect of a zinc coating on steel upon the steady-state permeation current. The zinc coating thickness was varied by metallographic techniques.

a)

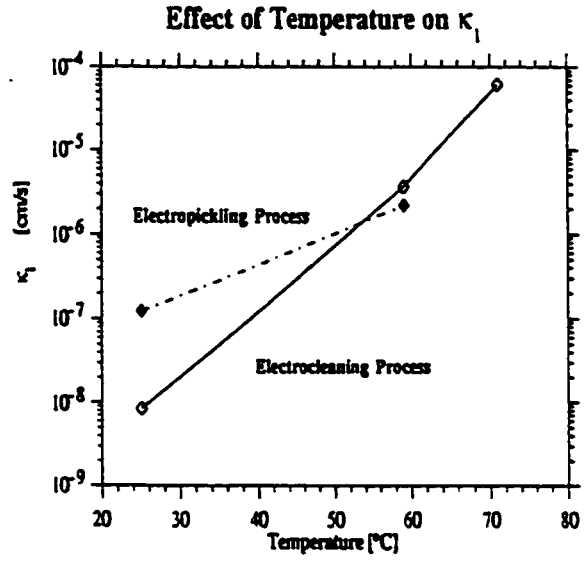

b)

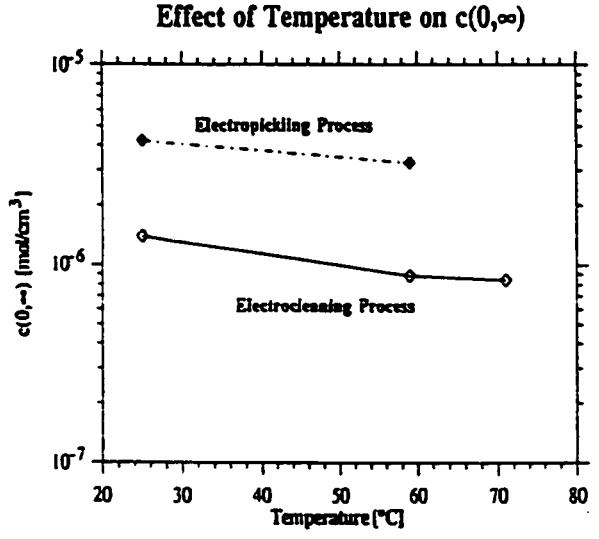

Figure 8.6 The effect of temperature upon $c(0, \infty)$ and κ_1 for the electropickling and electrocleaning environments is shown in figures a) and b). Increasing temperature is shown to increase both parameters.

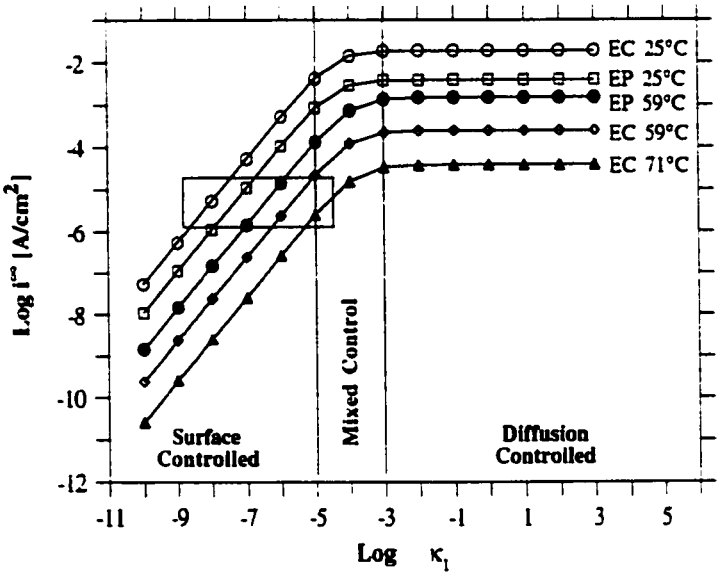

Figure 8.7 The flux control curves for the electroprocess steps at different temperatures is shown. The box represents the range of i^{∞} and κ_l values for the electroprocesses.

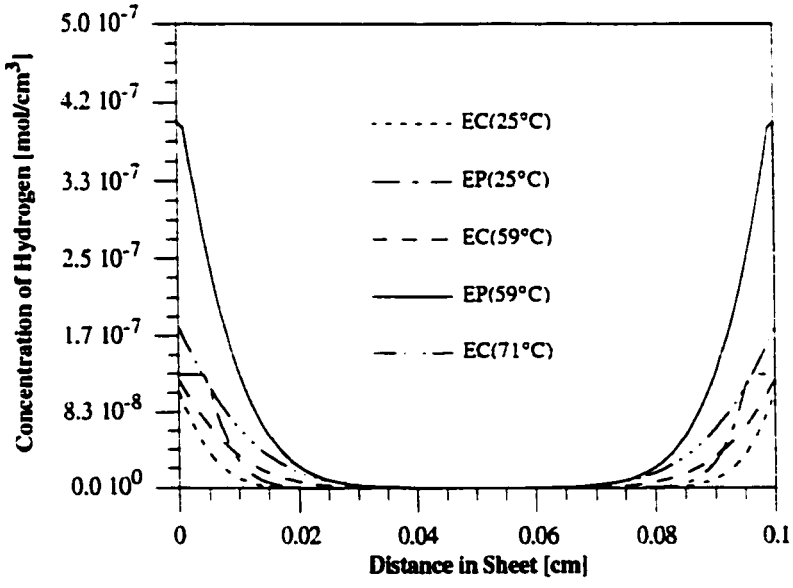

Figure 8.8 The hydrogen concentration profile in a one millimeter sheet that has both surfaces exposed to different electroprocesses for 10 seconds. The solubilities of hydrogen in iron at 25°C (1.24×10^{-7} mol/cm^3), at 59°C (3.95×10^{-7} mol/cm^3) and at 71°C (5.41×10^{-7} mol/cm^3) were taken into account.

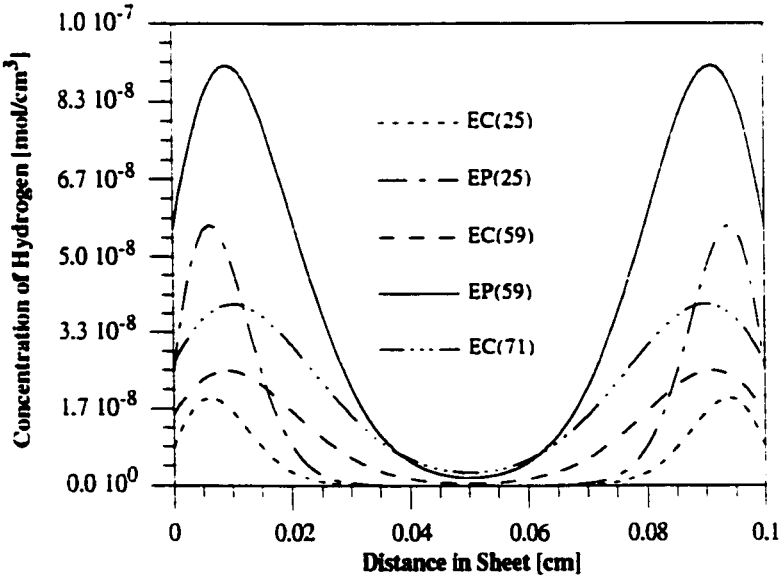

Figure 8.9 The hydrogen concentration profile in a one millimeter sheet that has both surfaces exposed an electroprocess for 10 seconds and then, followed by an anodic cycle. The anodic process assumes low hydrogen coverages (10^{-12} mol/cm^3) and easy exit kinetics ($\kappa_1 = 10^{-3}$ cm/s).

Chapter 9

Application of the Hydrogen Model to Preplating Processes of an Electrogalvanizing Line

9.1 Introduction

There has been recent interest[1,2] in hydrogen that is absorbed from various electrochemical pre-treatment processes on an electrogalvanizing line. Such absorbed hydrogen may diffuse to areas of decohesion along the Zn/Steel interface and form blisters in the coating. Chapter 8 evaluated these processes as to their ability to inject hydrogen. This chapter will address several phenomenological problems associated with the blistering of electrogalvanized low carbon steel. The model presented in Chapter 4 will be applied here as a tool to solve such problems.

9.1.1 The Problems of Interest

Two classes of problems will be discussed in this chapter. It is of interest to have an understanding of how important the entry surface is to the hydrogen permeation behavior. Likewise, it is also important to understand how much time is necessary for the blistering phenomenon to occur.

The following questions will be addressed by this chapter:

- If the surface of a permeation foil changes during the permeation test, how does this affect the permeation current?
- How important is the rate which a surface may change during a given period of time on the permeation current?

- If hydrogen is absorbed by a metal sheet by a charging process and that process changes, how does the hydrogen distribution change over time?
- How does a zinc coating applied to one surface affect the hydrogen profile over time?
- If a charging process injects a quantity of hydrogen and provides a zinc coating how long does it take to fill the blisters from a typical blister density?

9.1.2 How do Surface Changes Affect the Permeation Current?

The standard technique for evaluating the amount of hydrogen absorbed from different environments is the hydrogen permeation test[3]. This test is typically conducted under mild cathodic current densities ($< -1 mA/cm^2$). The reason for this condition is due to a non-steady state anodic current transient that results from using higher cathodic current densities (see figure 3.8). This non-steady state transient may be best described by a decrease in permeation current from a maximum down to a lower plateau over time. Also, if high cathodic currents in acid are used for long times, then the surface morphology can change (Figure 9.1).

Steel that is to be used for automotive applications is typically exposed to several processes (electrocleaning and electropickling) to remove rolling oils, surface oxides and provide a uniform surface prior to an electrogalvanizing treatment. Such processes use high cathodic current densities and have been found to inject hydrogen into the steel that could result in blistering of the zinc coating[4]. Thus, in order to understand the hydrogen absorption reaction during these processes, it is important to understand the non-steady state permeation behavior obtained during testing.

It has been hypothesized[5] that the decrease in permeation current is due to subsurface damage. Such damage is thought to result from a supersaturation of the metal lattice by hydrogen. If the lattice is supersaturated, the lattice could expand to the point where dislocation or void formation occurs. Although this has been the accepted theory for twenty years, there are certain issues that remain unresolved or unclear. First, the minimum amount of hydrogen necessary to cause this effect is very small (less than a ppm). This is an unlikely amount to deform the metal lattice, when the metal lattice can accommodate much larger amounts of larger atoms without significant lattice expansion (e.g., several ppm of C). Secondly, if damage is occurring, why does the damage not continue for long times? In other words, why does the permeation current never decrease to zero? Finally, why does the damage layer not extend through the entire metal sheet for long charge times? These questions are not easily answered by the existing hypothesis. Although this chapter does not attempt to find answers to all of these questions, it will attempt to identify the pertinent variables and issues.

Chapter 4 has shown the permeation current to be very sensitive to the surface condition of the metal sheet to be tested. Since the permeation current decreases over time, it is reasonable to suppose that the entry surface (or subsurface) is changing over time to reflect that condition.

9.1.3 How Much Hydrogen is Required for Blistering to Occur?

Low carbon steel sheet that is electrogalvanized may be susceptible to blistering at the Zn/Steel interface. Recent observations in our laboratory[6] have suggested blister densities of as high as 3000 blisters per square centimeter may occur. Blisters are typically between 5 and 100 microns in diameter with 20 microns being the average size.

To evaluate the electroprocess steps in terms of the blistering behavior requires that some estimate of the amount of hydrogen present to produce blisters be made. Janavicius[7] evaluated several models and estimated 4.1×10^{-11} moles and 2.5×10^{-11} moles of hydrogen would be present in a 20 micron diameter blister at 298 and 500 K, respectively. He assumed a spherical cap model to obtain the volume of the blisters , the flow stress of zinc (150 MN/m^2) to be the minimum pressure to form the blister and the ideal gas law to calculate the moles of hydrogen.

9.2 Results and Discussion

9.2.1 Surface Changes and Permeation Curves

Chapter 4 showed how the steady-state permeation current could be dependent upon the value of κ on the entry surface. Since higher permeation currents were shown to result from higher values of κ and it is assumed that the surface is responsible, it is likely that the decrease in permeation current is due to a decrease in κ_l.

Using the model proposed in Chapter 4, several simulations of permeation experiments were performed where the value of κ_l was decreased at a constant rate over time to a lower value. The results of such simulations is shown in Figure 9.2. Figure 9.2 illustrates four curves which represent different surface conditions. All of the simulations had a value for κ_l of 5×10^{-7} cm/s at time zero. As the test progressed, the values of κ_l for three of the simulations were decreased at the same uniform rate (10^{-9} cm/s per 10s period), but to different final values. The fourth curve illustrates the permeation behavior when the surface does not change (i.e., κ_l remains constant throughout the simulation).

The most notable feature of the simulations in Figure 9.2 is the "hump" in the curve or is the anomalous behavior which resulted for all of the curves which had changing κ_1. Clearly, if there is minimal overall change in κ_1, as seen in the curve representing a change from 5×10^{-7} to 3.5×10^{-7} cm/s, then there is negligible "anomalous" behavior (i.e., only a slight hump in the curve). However, for the other two cases, a significant hump exists which is typical of the anomalous, non-steady state permeation noted by Beck[5].

Figure 9.3 illustrates how the rate at which the surface/subsurface changes affects the permeation current. As above, three of the curves have changing surfaces and one curve representing a non-changing surface is included for reference. The curves labelled A, B, and C have κ_1 values that change from 5×10^{-7} cm/s to the same final value (10^{-7} cm/s). The difference in the curves is in the rate at which the change takes place. The value of κ_1 changes in the order:

Curve:	A	>	B	>	C	
Decrease per 10s:	5×10^{-9}		10^{-9}		5×10^{-10}	in cm/s

Notice that decreasing the rate of surface change broadens the hump in the curve.

These results suggest two ramifications relavent to permeation testing under such conditions. First, changes in the surface or subsurface can significantly affect the permeation current. These changes could give rise to a "hump" in the permeation curve. The size of the hump is dependent upon the initial and final κ_1 values and the rate with which the surface changes from one value to the next. Secondly, estimation of two κ_1 values, one for the permeation maximum and one for the steady-state behavior, will under estimate the initial value of κ_1.

9.2.2 The Change in the Hydrogen Profile with Time

Sometimes the steel sheet is only electrogalvanized on one surface, leaving the other surface bare. Such steel is rarely found to blister[8]. Since the zinc acts as a barrier to hydrogen, the hydrogen can move to the other surface and leave the sheet. The question becomes, "How long does it take to remove the hydrogen from such a sheet?"

To answer such a question, simulations were performed which injected hydrogen into both surfaces of a sheet. Following such hydrogen absorption, one surface was made to be a barrier to hydrogen entry or exit (i.e., $\kappa_1 \sim 0$) and the other surface was assumed to be under a particular charging condition. Although the entry charging conditions have been characterized by this thesis (chapters 5-8), there is little known regarding the exit conditions from steel. Hence, the value for c_2 was maintained at zero and different values for κ_2 were assumed. The simulations produced profiles in the steel for different times following the charging treatment. For these simulations, the temperature chosen was 25°C and the appropriate diffusivity (from Chapter 8) was used.

Figures 9.4-9.6 show the cross sections of steel sheets that were all exposed to the same charging treatment, but assumed different κ_2 for the remainder of the simulation. The influence of κ_2 on hydrogen exit using values of 10^{3}, 10^{-4} and 10^{-7} are illustrated in Figures 9.4, 9.5 and 9.6, respectively. Figure 9.7 illustrates the change in hydrogen concentration over time for the three conditions. Notice that if the exit kinetics are slow (e.g., $\kappa_2 \sim 10^{-7}$), then for short times (e.g., 600s: the extent of the simulations) the surface acts as a barrier to exit. For large values of κ_2 (e.g., 10^{3} cm/s),

the surface is not a hinderance to hydrogen exit, but instead the rate determining step is the diffusion of hydrogen to the surface. This is evident in Figure 9.4.

From these results the time with which hydrogen exits the steel is seen to be significantly a function of the exit kinetics. Assuming the kinetics are very fast ($\kappa \sim 10^3$ cm/s) the concentration of hydrogen in the sheet drops to very low levels (10^{-10} mol/cm^3; this is enough to fill two 20micron blisters at 298K) in 10 minutes at room temperature. If the value of κ_2 is smaller (e.g., $\kappa \sim 10^{-4}$ cm/s), then longer times are necessary. If the value of κ_2 is very small ($\kappa \sim 10^{-7}$ cm/s), then the hydrogen may take time periods which are impractical for industrial purposes.

9.2.3 The Time To Fill Blisters

If a steel sheet absorbs hydrogen through both surfaces by a process or sequence of processes, followed by the application of a zinc coating will effectively hold the hydrogen in the sheet by acting as a barrier to the hydrogen. If there exists perfect adhesion at the Zn/steel interface (i.e., no areas of poor adhesion that could result in blisters), then κ could be assumed to be zero. If areas of poor adhesion developed along the interface, κ for the hydrogen exit would change to values greater than zero to reflect the situation. Despite the difficulty in estimating the exit kinetics, it would be useful to estimate the time it would take for enough hydrogen to exit the sheet to account for that present in the blisters.

To simplify the simulations, several assumptions were made. Only the electrocleaning and electropickling processes were used as the dominant cathodic processes injecting hydrogen for these simulations. The charging parameters and the diffusivities for the appropriate temperature were obtained from Chapter 8. The plating

step was neglected due to the number of assumptions required to estimate the charging conditions and maintain the simplicity of the simulation. It should be noted, however, that the plating process does inject a noticeable amount of hydrogen on a similar order of the electrocleaning process (see Chapter 8).

Each charging process was assumed to act on both sides of the steel sheet for 10 seconds. Immediately after charging, it was assumed that a continuous zinc coating was present on both steel surfaces, thus forcing κ to zero. The hydrogen profiles were allowed to equilibrate at room temperature. These assumptions allow a reasonable amount of hydrogen, relative to that injected from the electrogalvanizing line, to be uniformly distributed in the steel. To obtain our goal, areas of poor adhesion were allowed to exist along the Zn/Steel interface, thus, allowing κ to be non-zero and hydrogen to exit. Using these assumptions, several profiles were calculated for various times. These are shown in Figures 9.8-9.11.

Two different temperatures were used during the charge step. Although equilibration of the profile and future profiles were obtained for 25°C, the different temperatures during charging allowed different amounts of hydrogen to be absorbed. The simulations assumed κ values of either 10^{3} or 10^{-4} cm/s for the surfaces when poorly adhered Zn was present. Thus, four separate simulations were conducted, two for each charging condition.

By integrating the profiles, the amount of hydrogen left in the sheet and the amount that has exited the sheet may be obtained. The amount of hydrogen left in the sheet and that exiting the sheet is illustrated in the b) portion of the figures.

If the amount of hydrogen necessary for one hundred, twenty micron blisters is used as a measure, the simulations performed for charging at 25°C did not inject enough hydrogen to result in blistering. However, if charging is done under the higher temperatures (59°C and 71°C), then there is more than enough hydrogen necessary to produce the blisters. For this latter case, if κ is 10^3 cm/s, then enough hydrogen will exit the sheet to produce the blisters in just over 100 seconds. If κ is 10^{-4} cm/s is present, then the time increases to ~450s.

9.2.4 A Note Regarding the Model

The research presented in Chapters 5-9 illustrate how the model proposed in Chapter 4 can be applied to a few systems. The complexity of the hydrogen entry problem has required the full attention of this thesis work. However, the few examples given in Chapter 9 are presented in the hope that the model may be applied to other systems and utilized to help solve a considerable number of applications.

9.3 Conclusions

The model in Chapter 4 was applied to understand the importance of the entry surface to hydrogen permeation behavior and the importance of exit kinetics upon blistering of electrogalvanized low carbon steel.

High charging conditions (pH=1, Sulfuric Acid, i_c =-100mA/cm^2) were found to alter the steel surface under prolonged charging. Polishing scratches were removed and some cracking was noticed.

If the entry surface kinetics change over time, then the permeation behavior will be significantly affected. Specifically, if the value of κ was decreased over time by a

factor of 2 or larger, the permeation current would rise to a maximum and then would decrease to a steady-state value, producing a "hump" in the curve. This behavior is similar to the non-steady state permeation behavior observed under severe charging conditions.

The breadth of the hump in the permeation curve was noticed to be a function of the rate of change of κ over time. If $d\kappa/dt$ was very large, the hump would appear as a spike in the permeation curve. Alternatively, if $d\kappa/dt$ was very small, the a slow rise to a maximum with a slow decline to a steady state value would be observed in the permeation curve.

These simulations suggest that a new method needs to be developed to analyze permeation data that contains a "hump." Underestimation of the κ term will result if the maximum in the hump is used to obtain an upper bound. The amount of underestimation in the simulations performed here was on the order of 20 to 80%.

The exit kinetics are critical to evaluating the time required for an appropriate amount of hydrogen to leave the steel and participate in the blistering of the electrogalvanized coating. A κ value of 10^{-7} cm/s retains 99.9% of the absorbed hydrogen in the metal sheet over a 10 minute period, while a value of 10^{3} retains only 40%.

It was estimated that a 10 second electrocleaning process, followed by a 10 second electropickling process would not inject enough hydrogen to result in blistering of one hundred, twenty micron diameter blisters in a one centimeter area at 25°C. However, if the electrocleaning process operated at 71°C and the electropickling

process operated at 59°C, there would be more than enough hydrogen present to account for the blistering behavior.

References for Chapter 9

1 J.H. Payer, G.M. Michal, *Proc. of 5th Auto.Prev.of Corr.*, P-250, Dearborn, MI, (1991), 53-63.

2 J.H. Payer, G.M. Michal, C. Rogers: *Corrosion/91*, (1991): paper no. 405.

3 M.A.V. Devanathan and Z. Stachurski: *Proc. Roy. Soc. Lond.* A. 1962, vol. 270, pp. 90-102.

4 J.H. Payer, G.M. Michal and C. Rogers: *Corrosion/91*, paper no. 405, NACE, 1991.

5 W.Beck, J.O'M. Bockris, J. McBreen and L. Nanis: *Proc. of Roy.Soc.Lond.* A, 1965, vol. 290, pp. 220-235.

6 R.J. Zhou, The LTV Steel Corporation, Internal Report, 1989.

7 P. Janavicius, Case Western Reserve University, Internal Report, 1991.

8 Private Communication with George Eierman, The LTV Steel Corporation, Brecksville, Ohio.

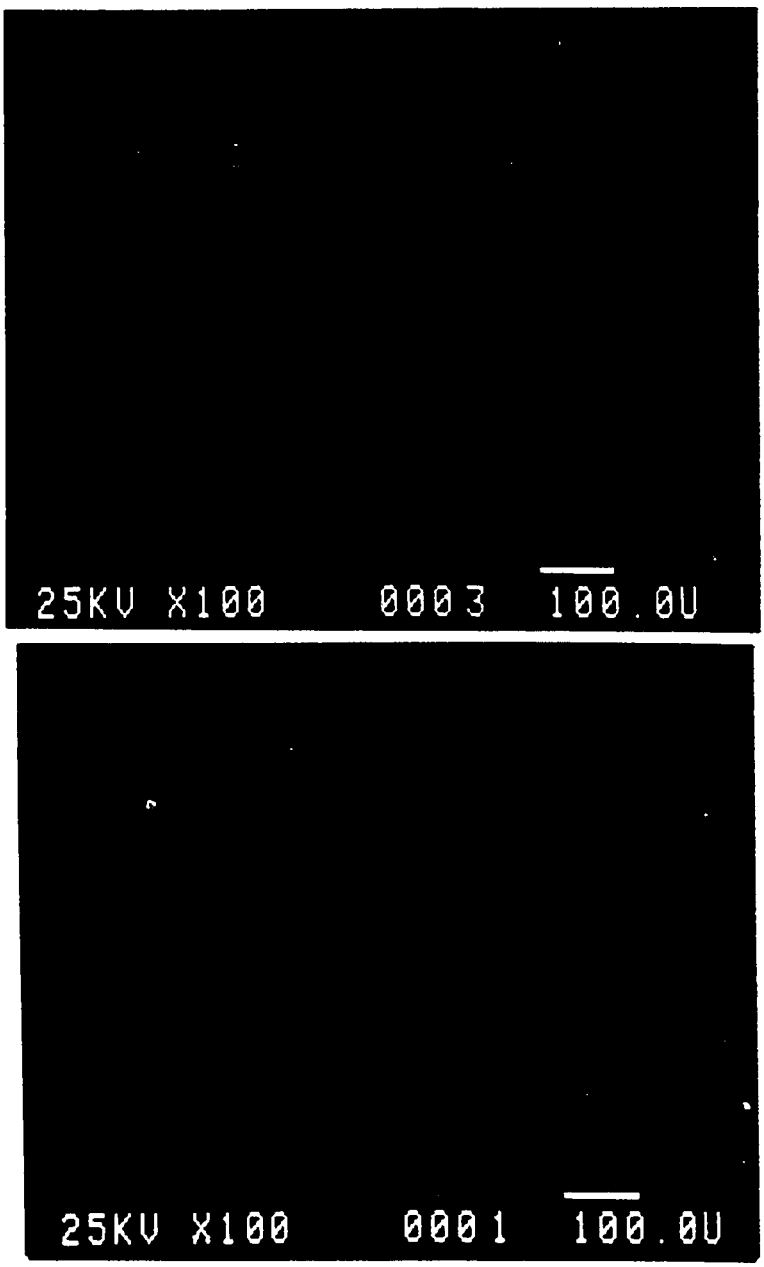

Figure 9.1 An example of a surface (a) prior to and (b) after exposure to a -100mA/cm^2 polarization condition for 1 hour.

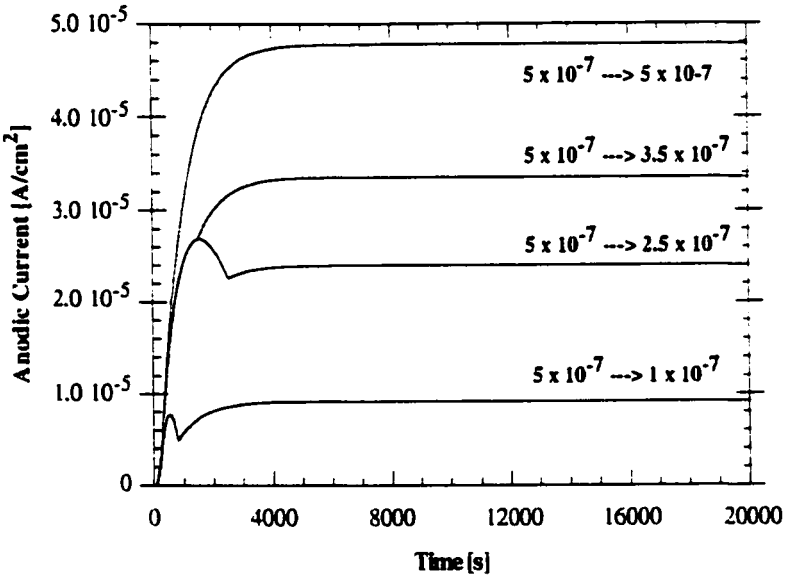

Figure 9.2 The effect of a changing κ_1 over time at a constant rate upon permeation behavior.

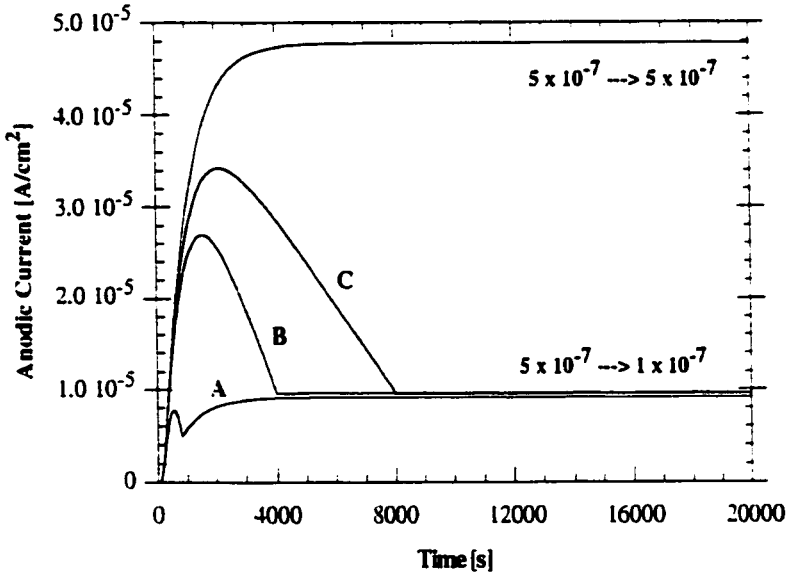

Figure 9.3 The effect of a changing κ_1 over time at a different rates upon permeation behavior.

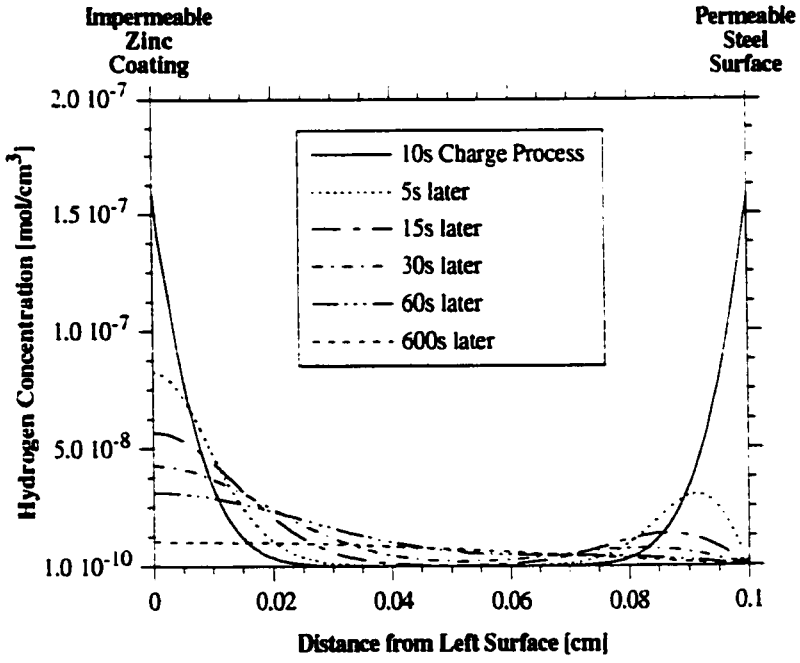

Figure 9.4 The effect of κ upon hydrogen exit -- A hydrogen porfile in a steel sheet that was exposed to a cathodic charging treatment, and then followed with an anodic treatment on the right surface. The left surface is assumed to be an impermeable barrier to hydrogen. κ for the anodic process is assumed to be 10^3 cm/s.

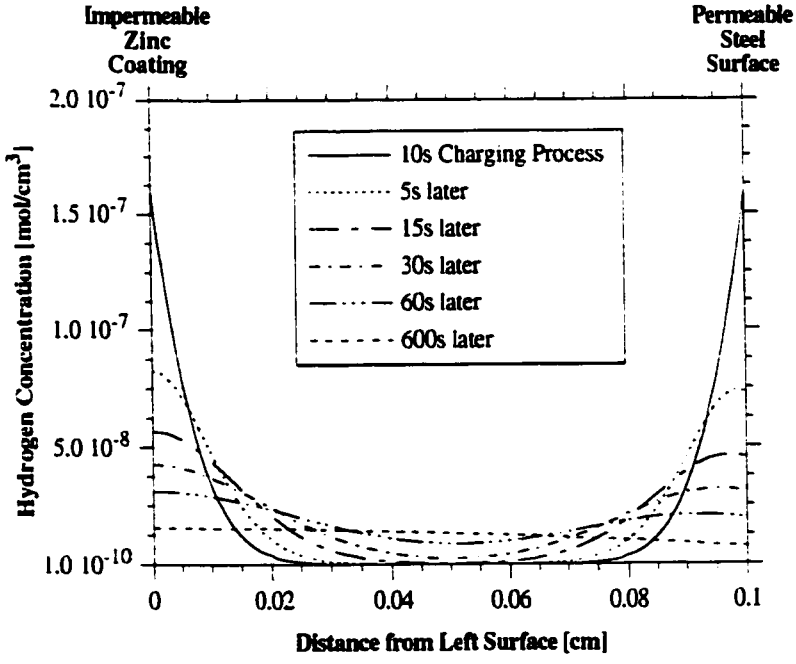

Figure 9.5 The effect of κ upon hydrogen exit -- A hydrogen porfile in a steel sheet that was exposed to a cathodic charging treatment, and then followed with an anodic treatment on the right surface. The left surface is assumed to be an impermeable barrier to hydrogen. κ for the anodic process is assumed to be 10^{-4} cm/s.

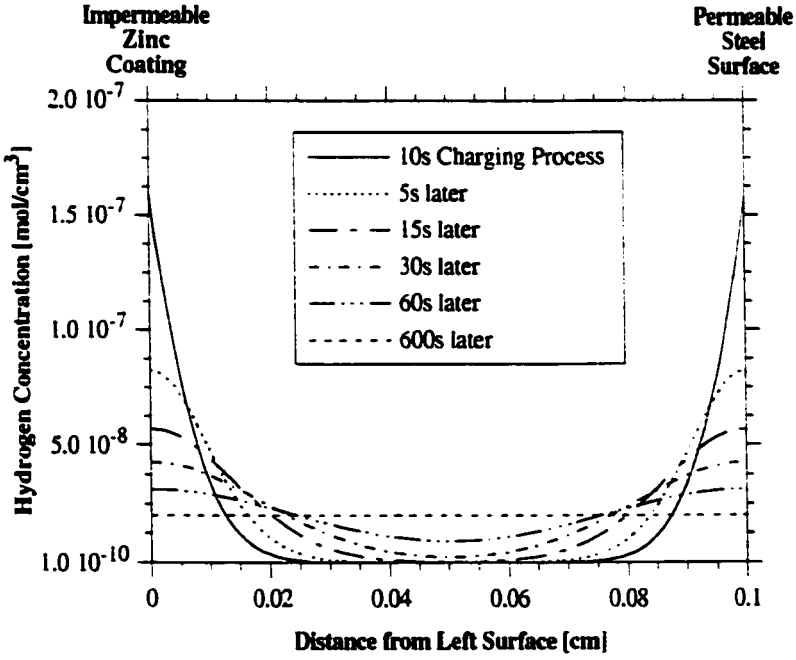

Figure 9.6 The effect of κ upon hydrogen exit -- A hydrogen porfile in a steel sheet that was exposed to a cathodic charging treatment, and then followed with an anodic treatment on the right surface. The left surface is assumed to be an impermeable barrier to hydrogen. κ for the anodic process is assumed to be 10^{-7} cm/s.

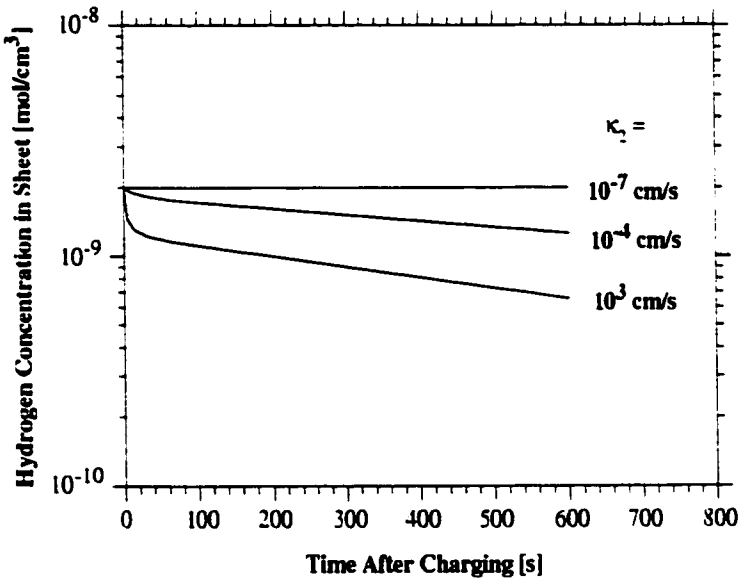

Figure 9.7 The change in hydrogen concentration in the steel sheet over time for the three exit kinetic conditions shown in figures 9.4-9.6.

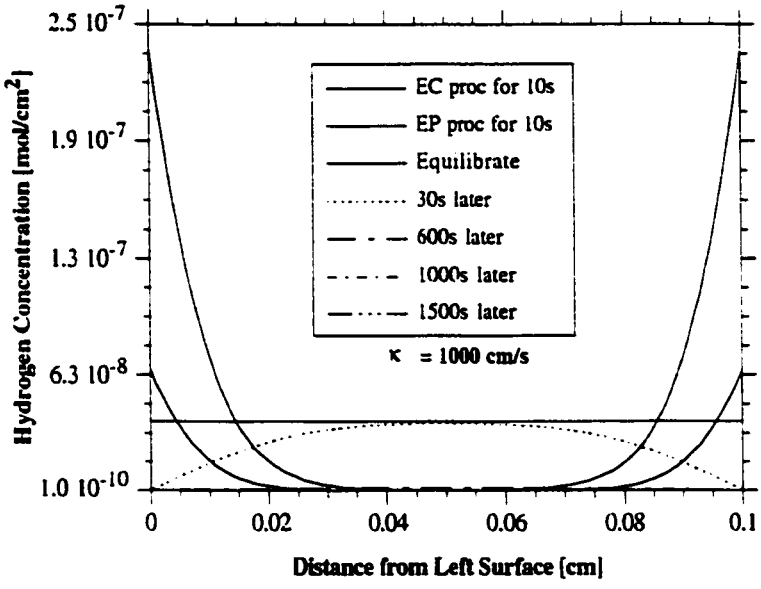

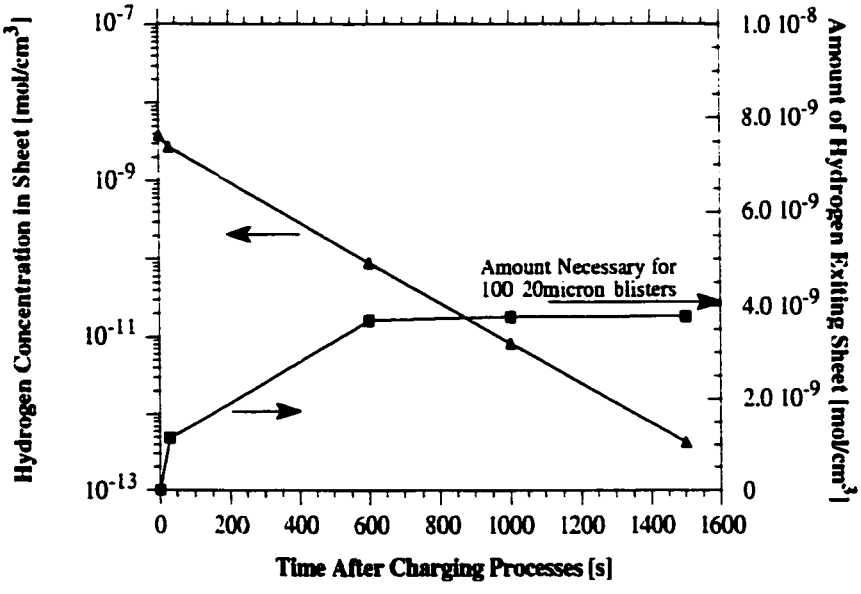

Figure 9.8 The hydrogen concentration profile (a) after two, 25°C cathodic processes, equilibration at 25°C and then effusion. The value for κ for effusion is 10^3cm/s. Part (b) illustrates the change in hydrogen concentration as a function of time.

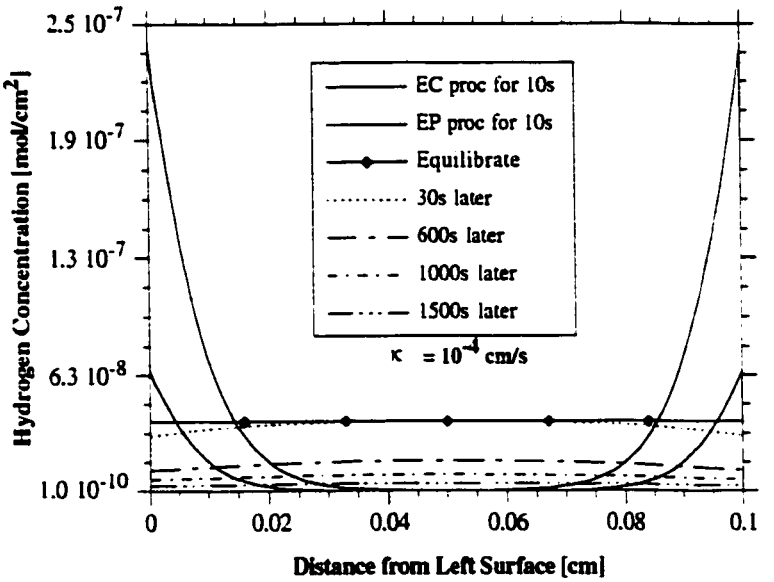

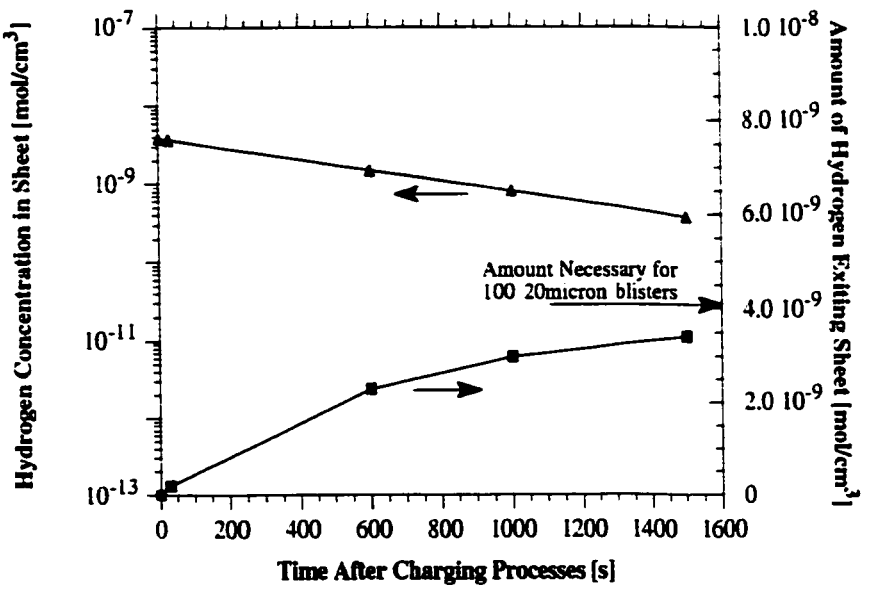

Figure 9.9 The hydrogen concentration profile (a) after two, 25°C cathodic processes, equilibration at 25°C and then effusion. The value for κ for effusion is 10^{-4}cm/s. Part (b) illustrates the change in hydrogen concentration as a function of time.

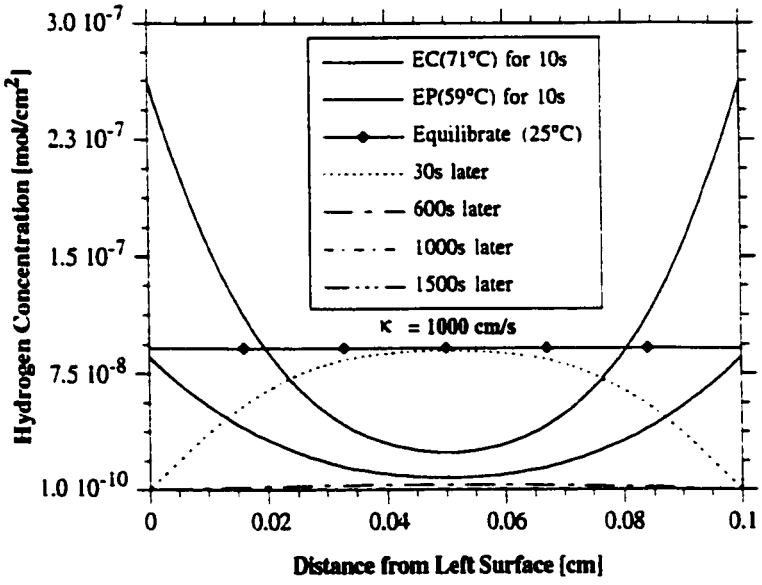

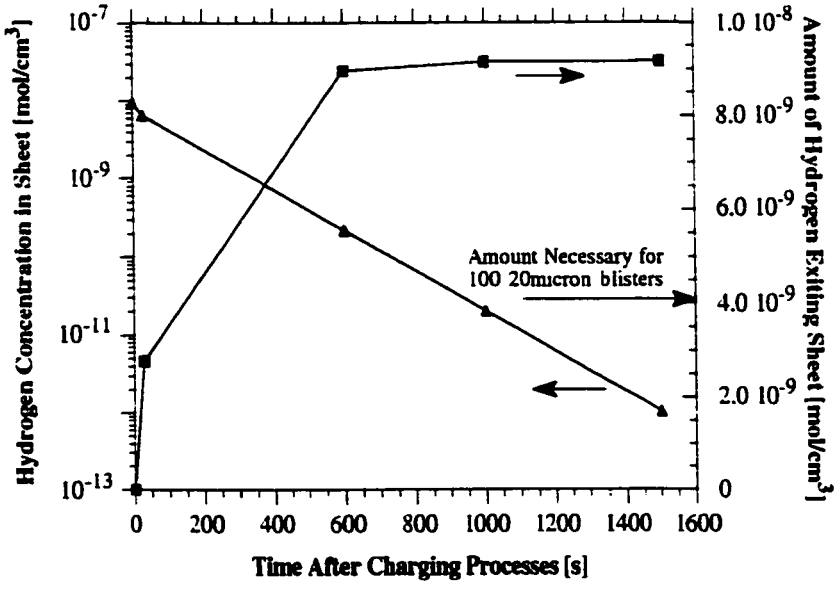

Figure 9.10 The hydrogen concentration profile (a) after a 71°C EC and then a 59°C EP cathodic process, equilibration at 25°C and then effusion. The value for κ for effusion is 10^3cm/s. Part (b) illustrates the change in hydrogen concentration as a function of time.

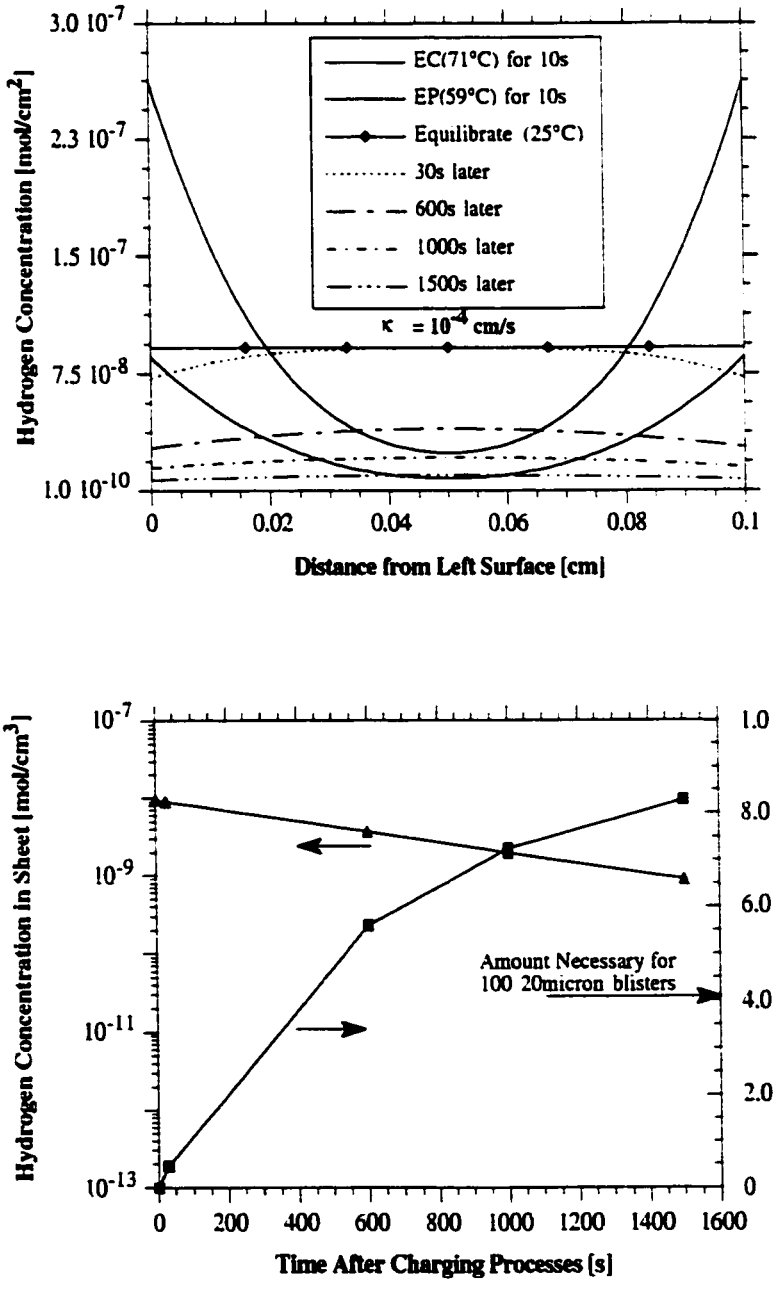

Figure 9.11 The hydrogen concentration profile (a) after a 71°C EC and then a 59°C EP cathodic process, equilibration at 25°C and then effusion. The value for κ for effusion is 10^{-4}cm/s. Part (b) illustrates the change in hydrogen concentration as a function of time.

Chapter 10

Final Statements

10.1 Conclusions from Thesis Study

10.1.1 Conclusions Regarding Model Development

It was the intent of this thesis to examine and understand the hydrogen interactions with steels used for automotive applications as a function of the electrochemical processes present on the electrogalvanizing line. In particular, the knowledge gained was to be used to understand the blistering of an electrogalvanized sheet. The goal was to understand the hydrogen kinetics due to many surface parameters and using this knowledge, recommend practices to minimize hydrogen absorption under industrial conditions.

A model was developed which meets the objectives of this study. The model can be applied to permeation data and can evaluate both surface and metallurgical phenomena. It can handle arbitrary charging conditions on either side of a metal sheet and can keep track of the hydrogen distribution within the sheet with time. Finally, it can be applied to evaluate multiple charging processes.

The treatment is a phenomenological model. All phenomena which result in deviations from Sievertian/Nernstian behavior will be represented by the κ term. Although the model can not inherently identify the mechanism for change in κ, the κ term will allow (a) various surface/subsurface effects to be evaluated, and (b) the appropriate concentration of absorbed hydrogen to be obtained.

Several model parameters were useful in interpreting the results. κ_1 was found to be sensitive to surface phenomena which might influence hydrogen absorption. In addition, for short charge times, the penetration depth of absorbed hydrogen was found to be a function of κ_1, $c(0,\infty)$, and D. At longer charge times, the penetration depth is determined by D and $c(0,\infty)$ alone.

The model was used to demonstrate the effect of D, κ_1, and κ_2 on the permeation of hydrogen through a metal sheet. All three parameters can affect the permeation behavior. The parameter which controls the permeation behavior depends upon the relative magnitudes of L/D versus $1/\kappa_1$ and $1/\kappa_2$.

The model was validated by electrolyte agitation. Curve fitting the model to the experimental data produced a value for the effective diffusivity (6×10^{-6} cm^2/s) which is in the range of reported values for low carbon steel. Agitation of the electrolyte increased both κ_1 and $c(0,\infty)$.

The model was applied to give a plausible explanation for the characteristic "hump" in experimental permeation curves. The hump can be explained by a small decrease in κ_1 over time. The broadness of the hump was shown to be a function of the rate of change in the decrease of κ_1.

The model was applied to establish some boundary limits on the amount of time necessary for blisters to form. Using the amount of hydrogen absorbed from just the electrocleaning and electropickling processes (each applied for 10 seconds), there is enough hydrogen to participate in the blistering of one hundred, twenty micron blisters

per square centimeter. The amount of time necessary for this varied between 100 and 450 seconds at room temperature. The variation in time emphasizes the importance of the value of κ during the exit process.

The model can be applied to a wide variety of applications. Using possible pickling processes, the model was applied to predict behavior on a possible pickling line. Both individual and multiple process steps were evaluated.

10.1.2 Conclusions from the Experimental Evaluations

This study provided a database of parameters which are present in the surface treatment of steel prior to the application of an electrogalvanized coating and their effect upon hydrogen permeation behavior.

With an increase in pH or cathodic current density or a decrease in electrolyte agitation or surface roughness (R_a), the deviation from Nernst/Sievertian behavior was shown to decrease. Furthermore, with increases in either cathodic current density, solution agitation or surface roughness (R_a) or with a decrease in pH, the surface solubility, $c(0,\infty)$, increases.

As the current density was increased, a greater proportion of the current was found to participate in hydrogen evolution. Much less than one percent of the hydrogen discharged permeates through the metal. In addition, by increasing the current density above 10 mA/cm^2 or decreasing the pH to very low levels (<1), anomalous permeation curves were obtained suggesting surface or subsurface damage.

For a given ultra low carbon steel and over several sheet thicknesses, the steady-state permeation currents measured are found to be independent of thickness. An expression was proposed to account for this behavior. It was proposed that the differences in permeation behavior are due to the amount of excess titanium above that added to the steels for stabilization (~0.05 wt.% Ti).

The effect of different amounts of lead, both in solution and on a low carbon steel surface, were shown to affect the hydrogen permeation behavior. The tests run with lead in solution resulted in the lead plating out of the electrolyte over the course of the permeation test. The lead contaminated steel surfaces tested in non-lead solutions resulted in surface morphology changes during hydrogen evolution.

Lead was shown to act as both a promoter (with as much as a 2x enhancement) and a blocker (with a reduction to zero i^{∞}) to hydrogen entry in low carbon steel. The lead acts to reduce the exchange current density of the surface, thus, increasing the amount of hydrogen remaining on the steel surface. In addition, it was proposed that the lead occupies favorable hydrogen absorption/adsorption sites. The dominating mechanism is a function of the amount of lead on the surface of the steel under potentiostatic conditions. Under galvanostatic conditions of both low and high current densities, the increased overpotential of the lead contaminated steel surface was responsible for the increase in permeation current.

The temperature was found to significantly affect the hydrogen permeation behavior by increasing both the diffusivity (up to an order of magnitude from 25° to 71°C) and the efficiency of the hydrogen absorption reaction.

A 10μm Zn coating acts as a barrier to hydrogen entry and exit. A 3.6μm coating shows similar behavior. The high efficiency of the deposition process and the barrier effect of the Zn result in the plating process injecting much less hydrogen than the electropickling process. The plating process probably injects a similar amount to that of the EC process step.

The electropickling process injects 3.7 times the hydrogen as the electrocleaning process when acting at the same temperature. If the electrocleaning step is run at 71°C, the electropickling process injects 2.8 times the amount of hydrogen.

10.2 Recommendations for Minimizing Hydrogen Absorption in Low Carbon Steel During Cathodic Charging Processes

Based upon the above conclusions, the following recommendations are given to reduce the amount of hydrogen absorbed in a low carbon steel sheet that is exposed to the electrogalvanizing line. It should be noted that such recommendations may be in conflict with practical considerations external to this study.

- Decrease the current density applied during cathodic charging processes.
- Increase the pH of the electrolyte.
- Decrease the flow rate of solution.
- Maintain as uniform and smooth a surface as possible.
- Decrease the temperature of the charging processes.
- If ULC steel is used, maintain a low to moderate (i.e., <0.05wt%) titanium level.
- Obtain a continuous zinc coating as early in the plating process as possible.
- Minimize the time in the EP process, it injects by far the most hydrogen.
- Maintain ultra low Pb levels in all charging steps.
- Maintain ultra low levels of all Type IVA-VA elements in charging steps.

10.3 Recommendations for Future Studies

This area of research is still rich with opportunities. Although this study concentrated on modelling development and hydrogen entry behavior, the following is recommended for future work:

- Using very well defined steel metallurgy (i.e., composition, annealed condition, etc.), it is recommended that the effect of thickness upon surface and bulk conditions be evaluated. Under different charging conditions and using Pd coated and bare surfaces, it would be interesting to evaluate the effect of thickness upon κ_1.

- Using the model and a defined charging condition on the entry side of a steel foil, the effect of hydrogen exit should be evaluated. The limiting factor in several calculations in Chapter 9 depend on such information. Very little has been reported in the literature on this subject. The model presented by this thesis may prove useful in this area.

- Using 4 or 5 well characterized ultra-low carbon steels that vary in the amount of excess titanium should be studied by the permeation test. This thesis found an unusual dependence for the amount of excess titanium upon permeation. Unfortunately, only three steels were examined and an additional steel would be necessary to confirm the proposed mechanism.

- The specific mechanism of hydrogen absorption is still lacking. Knowledge of such a mechanism would help to design methods to prevent absorption.

- The context of this thesis ("the severity of the electrogalvanizing line") emphasizes the increased interest in hydrogen reactions under severe conditions. This thesis supports the conclusion that "anomalous permeation" behavior is the result of a change in the steel's entry surface. However, the specifics of that change are still lacking.

- The model developed in Chapter 4 assumes that both κ_1 and D are independent of the hydrogen concentration in the metal sheet. Future studies might wish to consider developing the model further when these two parameters are a function of concentration. This would be particularly useful in the case of the diffusivity. To accomplish such a task would require solving the Laplace equation with an additional term. Although this would substantially increase the complexity of the mathematics, this addition to the model might yield more insight to trapping and damage effects than the current version of the model.

Appendix A

Software Code for the Model

The software written to solve the problems contained in this thesis are to follow. Great effort was exercised to provide code that was reasonably well documented, modular and user friendly. This was done to allow a framework that could be quickly understood if changes need to be made in the future. The software was designed to run on a microVAX, however, the code was written in the C programming language as per the Kernigan and Ritchie standard and should run on most compilers.

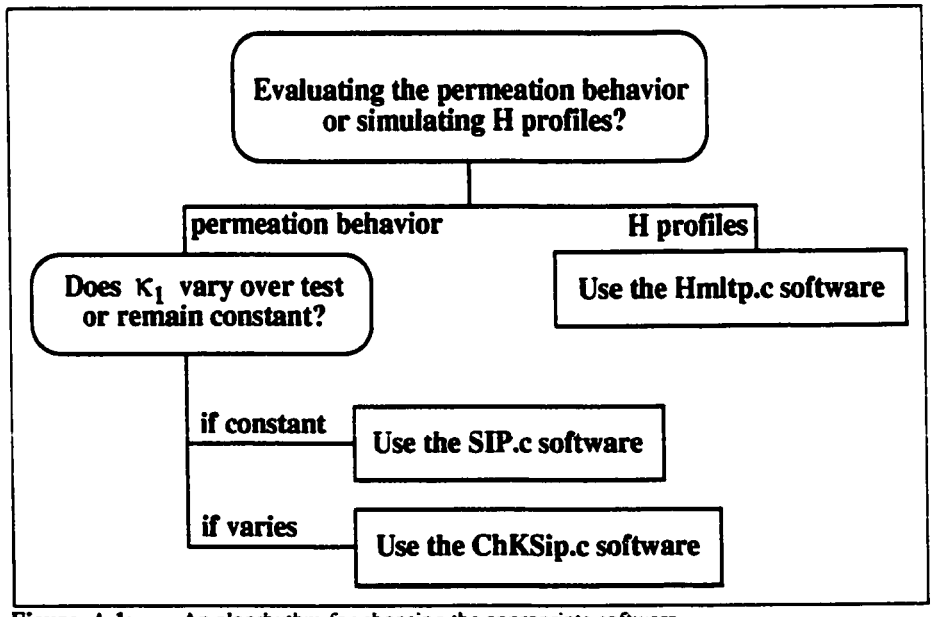

Figure A.1: An algorhythm for choosing the appropriate software.

A.1 Tutorial for Simulations

There are two types of software available for the model: permeation current software and hydrogen profile software. Each type was developed to help evaluate different kinds of hydrogen problems. The output of the permeation current software

(SIP.c or ChKSIP.c) is a set of current (in A/cm^2) values at specific times. Plotting such values will give a current versus time plot similar to that obtained by a permeation test. The output of the profile software (Hmltp.c) is a set of hydrogen concentrations (in mol/cm^3) at specific positions in a metal sheet (in cm). Plotting these values yields a hydrogen distribution in a cross-section of a metal sheet. To help in the use of such software, the following tutorial is given.

A.1.1 Permeation Current Simulations - Tutorial

To use the permeation current software, it is first necessary to decide whether κ_1 changes over the course of the test. If κ_1 does change, then the software "ChKSIP" or "Changing Kappa Simulated current(I) Plot" should be used. If κ_1 remains constant, then the software "SIP" or "Simulated current(I) Plot" should be used. Both sets of software require that the values for c_1, κ_1, D, L, κ_2, and c_2 be provided. If κ_1 varies, then the initial and final value of κ_1 as well as the rate of change, $d\kappa_1/dt$, will need to be provided.

To perform a permeation current simulation with a constant κ_1 the following should be performed:

- From permeation data obtain values for i^{∞}, L, pH (in both permeation cells), the temperature of the test and E_w for both surfaces of the permeation foil. Using the procedure outlined in Chapter 4, obtain the model parameters: c_1, κ_1, D, L, κ_2, and c_2.

- Run the program "SIP" - On a microVax with a VMS operating system, type "Run SIP" at the prompt. The program will then boot up and querry the user for the input of the parameters. After each question, type the number (e.g, 4032 or 4.032e3) and hit a Return. The program will prompt the user with the next query. The final query will be "How long should the simulation be run?"

- After all of the information has been input to the computer, the program will run by itself to completion. To give an indication of the level of completion, as the program calculates the current at a particular time, that time will be shown on the screen.

- When the simulation is complete, an ASCII file will appear in the directory (e.g., IVT.d;1). Such files can be easily manipulated for presentation in any spreadsheet or graphing software. The graphs in this thesis were created on an Apple Macintosh using Kaliedegraph plotting software.

- If κ_1 varies over the course of the test and ChKSIP is used, substitute ChKSIP for SIP above. In addition, querries for two values of κ_1 and a value for $d\kappa_1/dt$ will be given, but the software will run similarly.

- To test a simulation, choose values from any of the tables in Chapters 4-9. When prompted by the software, input the appropriate values and compare to the figure which corresponds to the table. Particularly good plots to simulate are those found in Chapter 4.

A.1.2 Hydrogen Profile Simulations - Tutorial

To use the hydrogen profile software, then the software "Hmltp" or "Hydrogen, MuLTiple charging Profiles" should be used. The software requires that the values for c_1, κ_1, D, L, κ_2, and c_2 be provided for each charging condition. In addition, the number of charging processes and the length of time for those processes will be required. Note that this software is particularly useful for evaluating charging conditions on both sides of a metal sheet (pickling on both sides or single sided plating process steps), in addition to evaluating a sequence of process steps. The current software configuration allows for 7 different process steps to be evaluated with no alteration to the software. If addditional steps are required modification will not be difficult, but will be required.

To perform a hydrogen profile simulation the following should be performed:

- From permeation data for each process step of interest, obtain values for i^{∞}, L, pH (in both permeation cells), the temperature of the test and E_w for both surfaces of the permeation foil. Using the procedure outlined in Chapter 4, obtain the model parameters: c_1, κ_1, D, L, κ_2, and c_2.

- Run the program "Hmltp" - On a microVax with a VMS operating system, type "Run Hmltp" at the prompt. The program will then boot up and querry the user for the input of the parameters. After each question, type the number (e.g, 4032 or 4.032e3) and hit a Return. The program will prompt the user with the next query. The first query will be "How many processes will be simulated?" A process is considered to be a length of time when c_1, κ_1, D, L, κ_2, and c_2 are all constant. The final query for each process will be "How long should the simulation be run?"

- After all of the information has been input to the computer, the program will run by itself to completion. The metal sheet is divided into one hundred sections. To give an indication of the level of completion, as the program calculates the hydrogen concentration for a particular section, that section number will be shown on the screen. For example, if the first 5 sections are complete, the screen should show: 0...1...2...3...4...5

- When the simulation is complete, an ASCII file will appear in the directory (e.g., Hp.d;1). Such files can be easily manipulated for presentation in any spreadsheet or graphing software. The graphs in this thesis were created on an Apple Macintosh using Kaliedegraph plotting software.

- To test a simulation, choose values from any of the tables in Chapters 4-9. When prompted by the software, input the appropriate values and compare to the figure which corresponds to the table. Particularly good plots to simulate are those found in Chapters 4 or 8.

A.2 Troubleshooting Software Crashes

Running this software requires patience. On occasion, a minute or longer may be required before the first value is displayed on the screen indicating the program is running. This time is dependent upon how many other users are on the system and the parameters which were input to the computer. If a value for the first section is calculated, all of the rest will be calculated. If the program has not crashed, it is running correctly. If a value for the first section is not calculated, the program will crash.

If the software crashed, there are several likely reasons:

- The program is trying to divide by zero or multiply by infinity. On most computers, $10^{-30} \sim 0$ and the reciprocal can be considered infinity. Note that such definitions are particularly true if the value is squared or used in an exponential or logarhithm function.

- The program is trying to manipulate κ_1 and κ_2 which have both been defined as zero. This causes mathematical problems with the equations in Chapter 4. κ_1 and κ_2 are always considered to be positive numbers. When trying to evalute impermeable coatings, it is recommended that $\kappa_1 = \kappa_2 = 10^{-8}$ is used.

- The program is trying to manipulate κ_1 and κ_2 which have both been defined as large. In other words, the situation is not surface, but diffusion control. The software tends to break down when the value of L/D approaches the value of either $1/\kappa_1$ or $1/\kappa_2$. In such situations, the best recommendation is to use software which evaluates Choi's equation (see Chapter 2, Equation [2.16]). This assumes no deviation from Severt/Nerstian behavior.

A.3 Software Code

```
/*** ChKSIP.c ******** Stephen L. Amey **** November 7, 1992 *****/
/**                                                              **/
/** Used to Simulate Theoretical Curves setting k1,k2 and D.     **/
/**                                                              **/
/** This software allows parameters to be calculated from perm-  **/
/** eation data.  The permeation test uses the process of        **/
/** interest in the cathodic chamber.  The parameters calcu-     **/
/** lated will allow that process to be studied as to its        **/
/** effect upon hydrogen absorption in a metal.                  **/
/**                                                              **/
/** From Permeation data, the program solves for K[1] and plots  **/
/** an I vs time plot.  Such a plot may be overlayed on real     **/
/** data to determine if the choice of J is correct.             **/
/**                                                              **/
/** The program requires C1,C2,D,k1,k2 and L.                    **/
/** K2a = Co - K2 in analysis.  Here Co = 0.                     **/
/**                                                              **/
/**********************************************************************/
#include    <stdio.h>
#include    <math.h>
#include    "bsolve.h"

#define     F           96500       /** Faraday's Constant **/

extern double           b[2000];

main()
{
            int         n, chkvar;
            int         t, tmax, dt;

            double      k1, k2,
            double      ka, kb, Dk;
            double          L, C1, C2, Dx, h1, h2,
            double      J, co, cl, I, dq, asv, sbh2s;
            double      K1, K2, K2a, as, sum, psum, Lb, denK,
```

```
        double      h2, h1s, h2s, dn, dd, e1, e2, e3.
        double  A, E, trig, S, exms, nsum.
        double  sqrt(), cos(), sin(), abs(), exp().
        double  Thkd, invk1.

        FILE        *fp, *fopen().

/*** Enter Useful Information ***/

        printf("\n\n\n\t**********************************").
        printf("\n\n\t   Welcome to ").
        printf("\n\t       Current-Time Fit!!!").
        printf("\n\n\t     for k1 = function of time ").
        printf("\n\n\n\t**********************************").

        printf("\n\n How thick is your membrane (cm)? ").
        scanf("%lf",&L).
        printf("\n What is C1 (mol/cm^3)? ").
        scanf("%lf",&C1).
        printf("\n What is C2 (mol/cm^3)? ").
        scanf("%lf",&C2).
        printf("\n What is the H diffusivity in the metal (cm^2/s)? ").
        scanf("%lf",&Dx).
        printf("\n What is the initial K1 (cm/s)? ").
        scanf("%lf",&ka).
        printf("\n How long should K1 be active before varying (s)? ").
        scanf("%d",&tk).
        printf("\n What is the final K1 (cm/s)? ").
        scanf("%lf",&kb).
        printf("\n By how much should K1 change in 10s? ").
        scanf("%lf",&Dk).
        printf("\n What is the K2 (cm/s)? ").
        scanf("%lf",&k2).
        printf("\n What is the time duration for the simulation (s)? ").
        scanf("%d",&tmax).

/*** Conversions & Solution of Initial Equations ***/

        k1   = ka.
        I    = (C1 - C2) / ( (1/k1) + (1/k2) + (L/Dx) ).
        h2   = k2 / Dx.
        ci   = (I/k2) + C2.          /** concentration at x=L **/
        co   = ci + ((I*L)/Dx).      /** concentration at x=0 **/
        h1   = k1 / Dx.

/*** Initial Definitions ***/

        denK   = (h1+h2) + (L*h1*h2).
        K1     = ( (C2-C1) * (h1*h2) ) / denK.
        K2     = ((C1*(h1 + (L*h1*h2))) + h2*C2) / denK.
        K2a    = -K2.
        Thkd   = L/Dx.
        invk1  = 1/k1.

        fp = fopen("Ivt.chk","w").
        fprintf(fp, "\n\n h1 = %1.4e  h2 = %1.4e ", h1,h2).
        fprintf(fp, "\n\n k1 = %1.4e  k2 = %1.4e ", k1,k2).
        fprintf(fp, "\n co = %1.4e  ci = %1.4e ", co,ci).
        fprintf(fp, "\n L= %lf  Dx= %1.4e ", L,Dx).
        fprintf(fp, "\n C1= %1.4e  C2= %1.4e ", C1,C2).
        fprintf(fp, "\n\n").

        /*** Check if Surface Effects are Dominant ***/

      printf("\n\n SCANNING INPUT DATA FOR COMPLICATIONS ").
        if (Thkd > invk1){

          printf("\n\n The data that was input is indicative").
          printf("\n of DIFFUSION control or at a minimum. ").
          printf("\n Diffusion dominated control.").
          printf("\n More specifically, k1 is large relative to D/L. ").
          printf("\n\n As a result, mathematical complications may").
          printf("\n arise, causing a stack dump and failure of this ").
          printf("\n program. Have a nice day & kiss my butt. ").

        }
        else {
        printf("\n\n  No obvious problems found--program should run.").
        printf("\n The situation is SURFACE dominated control.").
        }


        for (t=0, t<=tmax; t+=10){

                I     = 0.
                sum   = 0.
                n     = 1.
                chkvar = 1.
                printf("\nT=%d  ",t).

                if (t>tk){          /** should k1 start changing? **/
                  if (k1 > kb){   /** is k1 done changing? **/

                    k1   = k1 - Dk.
                    h1   = k1/Dx.
                    denK = (h1+h2) + (L*h1*h2).
                    K1   = ( (C2-C1) * (h1*h2) ) / denK.
                    K2 = ((C1*(h1 + (L*h1*h2))) + h2*C2) / denK.
                    K2a  = -K2.
                  } /** end if k1 **/
                } /** end if>tk **/

/*** Calculate variables of f(n) ***/

                while(chkvar == 1){

                beolve(n,L,h1,h2);    /** returns b[n] **/
                        b2   = b[n]*b[n].
                        h1s  = h1*h1.
                        h2s  = h2*h2.
                        sbh2s = b2 + h2s.

                  dn = 2 * sbh2s.
                  dd = ((b2 + h1s)*( L*sbh2s) + h2 )) + (h1*sbh2s).
                          dq = dn/dd.
                          A  = sqrt(dq).

                  Lb   = L * b[n].
                  e1   = cos(Lb) * ( (-K1)+(K1*h1*L)+(K2a*h1) ).
                  e2   = sin(Lb) * ( (-K1*L) - (K1*h1/b2) + K2a ).
                  e3   = ( K1 + (K2a*h1) ).
                  E    = (e1/b[n]) + e2 + (e3/b[n]).
                  trig = ( (h1*b[n])*cos(Lb) ) - ( b2*sin(Lb) ).

                          S    = A * A * E * trig.
                          exms = -Dx * b2 * t.
                          nsum = S * exp(exms).

                          sum = sum + nsum.

                          if (n > 1){

                             as   = ( nsum - psum ).

                        ** Do Absolute value of difference **

                                  if (as < 0){
                                      asv = -as.
                                  }
                                  else{
                                       asv = as.
                                  }

                           ** Chk if difference is small **

                                  if (asv < 5e-7){

                                       chkvar = 0.

                                  }   /** end if-asv **/

                          } /** end if-n  **/

                          ++n.
                          psum = nsum.

                }   /** end while **/

        *** Calculate Current as f(n,t) ***

                I = -F * Dx * (K1 + sum).
                fprintf(fp, "\n %d %1.4e ", t, I).

        } /** end for t **/
        fclose(fp).

}  /** end main **/

/*** Betasolve.h ***** Stephen L. Amey ***** February 18, 1992 *****/
/***                                                             ***/
/***  This set of subroutines is called by I.c.  It requires the ***/
/***  values of h1,h2, n, and L.  It calculates b[n] or beta.    ***/
/***  Two convergence criteria are used. 1) (h1+h2)/1e6 and      ***/
/***  2) a difference criteria between consecutive terms         ***/
/***                                                             ***/
/*****************************************************************/
#include    <math.h>
#include    <stdio.h>

#define                 PI          3.1415927

extern      double b[2000].


beolve(n,L,h1,h2)
int         n.
double      L, h1, h2.
{
            double      P1, P2, G.
            double B.

            P1 = ( ( n * PI ) - PI )/L.
            P2 = ( n * PI )/L.
            B  = ( P1 + P2 )/2.
            G  = ( B * B ) - ( h1 * h2 ).

            if (G > 0){     /** the root will be positive **/
                        P2 = B.
                        posroot(n,P1,P2,h1,h2,L,B).
            }
```

```
        else {                          /** the root will be negative **/
                P1 = B.
                negmsmn(n,P1,P2,h1,h2,L,B).
        }
        return;         /** return to hdepth in pconc.h with a beta **/

} /* end bsolve */

posmsmn(n,P1,P2,h1,h2,L,B)
int     n;
double  P1,P2,h1,h2,L,B;
{

        int             chkdone;
        int             Bch;

        double          tan();
        double          R, c, lim;
        double          abval, abv;
        double  pB;
        double          Bdif, Bdv;

        chkdone = 0;
        Bch     = 0;
        pB      = 1e10;
        c       = h1 + h2;

        while(chkdone == 0){

                B = (P1 + P2)/2;
                R = ( ( (B*B)-(h1*h2) ) * tan(B*L) ) / B;

                if (Bch == 1){

                        Bdif = B - pB;

                        if (Bdif < 0){
                                Bdv = -Bdif;
                        }
                        else{
                                Bdv = Bdif;
                        }

                        if (Bdv <= 1e-11){
                                chkdone = 1;
                        }
                }
                else{
                        Bch = 1;
                }
                pB = B;

                if (R > c){     /** cnt fail -- reset P **/
                        P2 = B;
                }
                else {
                        P1 = B;
                }


        } /** end while **/

        b[n]    = B;    /** return to betasolve with beta **/
        return;

} /** end posmsm **/

negmsmn(n,P1,P2,h1,h2,L,B)
int     n;
double  P1,P2,h1,h2,L,B;
{

        int             cdone;
        int             Bchn;

        double          tan();
        double          R, C, lim;
        double  Abval, ABV;
        double  Bdifn, pnB, Bdvn;

        Bchn    = 0;
        cdone   = 0;
        pnB     = 0;
        C       = h1 + h2;

        while(cdone == 0){

                B = (P1 + P2)/2;
                R = ( ((B*B) - (h1*h2)) * tan(B*L) ) / B;

                if (Bchn == 1){

                        Bdifn = B - pnB;

                        if (Bdifn < 0){
                                Bdvn = -Bdifn;
                        }
                        else{
                                Bdvn = Bdifn;
                        }
                        if (Bdvn <= 1e-11){
                                cdone = 1;
                        }
                }
                else{
                        Bchn = 1;
                }
                pnB = B;

                if (R > C){     /** cnt fail--reset P **/
                        P1 = B;
                }
                else{
                        P2 = B;
                }

        } /** end while **/


        b[n]    = B;
        return;         /** return to betasolve with beta **/

} /** end negmsm **/

/*** Hmltp.c **** Stephen L. Amey ** November 7, 1992 **********/
/***                                                           ***/
/***  "Hydrogen Profile" - software designed to calculate conc-***/
/***  tration profiles in a sheet.  Up to 7 different processes***/
/***       may be specified.                                   ***/
/***                                                           ***/
/***  The software is designed to work the model described in the ***/
/***  paper "Modelling H Entry/Exit in metals under multiple charging ***/
/***  conditions." S.L.Amey,G.M.Michal,J.H.Payer              ***/
/***                                                           ***/
/***   The idea is to perform a permeation test with the cathodic cell **/
/***  being the process of interest. Use the software "fplot" to ***/
/***  convert hydrogen permeation data into the model parameters ***/
/***  (i.e., K1,K2).  Use this software (hp.c) to simulate a process ***/
/***  or set of processes for any time and acting upon any thickness ***/
/***  specimen.  The only requirement is that certain parameters are ***/
/***  known for each process.  As stated before, these may be  ***/
/***  obtained by performing permeation tests and using "fplot."  **/
/***                                                           ***/
/***  To drive the model:  K1,K2,D,C1,C2,L,t for each process   ***/
/***                                                           ***/
/***  The output is the concentration of hydrogen as a function of ***/
/***  depth for one or more processes.  The software divides the  ***/
/***  metal into 101 mini-sheets and a concentration is calculated ***/
/***  for each mini-sheet.  The total concentration of hydrogen is ***/
/***  integrated and calculated for the total process simulated.  ***/
/***                                                           ***/
/***  The C(x) and x values are stored in a file, typically "hp.d"  ***/
/***                                                           ***/
/***  "hpdepth()" is the main program.  It gathers the input from the ***/
/***  user and sends it to pconc.h to calculate the distribution.  If ***/
/***  more than one process is used, hpdepth() coordinates the multi-***/
/***  ple processes.  In addition, it calculates the total C(x,t) and ***/
/***  stores the information in a data file.                   ***/
/***                                                           ***/
/***  "hdepth()" is in pconc.h.  It performs the guts of the calcu-***/
/***  lation.                                                  ***/
/***                                                           ***/
/***  "bsolve()" is in betasolve.h called from pconc.h.  This routine ***/
/***  calculates beta values for given Kappa values and sheet thick-***/
/***  nesses.                                                  ***/
/***                                                           ***/
/***  Vardef.h is a file that contains definition information.  The ***/
/***  concentration distribution is stored as a structure-type  ***/
/***  set of values.  This structure is defined here           ***/
/***                                                           ***/
/*************************************************************/
#include        <stdio.h>
#include        <math.h>
#include        "vardef.h"
#include        "pconc.h"

struct conc hpdepth();
struct conc fminupt();
extern struct conc con[101];
extern double b[1000];

main()
{

        int             qv, imr;
        int             s, pn;

        double  t, ta, tb, tc;
        double  td, te, tf, tg;
        double          c1a, c2a, c1b, c2b;
        double          c1c, c2c, c1d, c2d;
        double  c1e, c2e, c1f, c2f;
        double  c1g, c2g;
        double  c1, c2;
        double  L, dx;
        double  K1a, K2a, K1b, K2b, K1c, K2c;
        double  K1d, K2d, K1e, K2e, K1f, K2f;
        double  K1g, K2g;
        double  h1, h2;
        double          D, Da, Db, Dc, Dd, De, Df, Dg;

        /*** Queries ***/

        printf("\n\n ************************************ ");
```

```
printf("\n\n");
printf("\n          Welcome to  ");
printf("\n\n                HYDROGEN PROFILE ");
printf("\n\n");
printf("\n      This program will calculate hydrogen C(x) vs x  ");
printf("\n  profiles in metal sheets for given surface processes ");
printf("\n ");
printf("\n\n ************************************** ");

printf("\n\n How thick is your membrane in cm? ");
scanf("%lf", &L);
printf("\n How many processes will be simulated (1-7)? ");
scanf("%d", &qv);

printf("\n How long will the steel remain in each A cell (seconds)? ");
    scanf("%lf",&ta);
printf("\n What is the hydrogen diffusivity in the A cells (cm^2/s)? ");
    scanf("%lf",&Da);
printf("\n\n What is the fugacity (1) for A charging in mol/cc? ");
    scanf("%lf",&c1a);
    printf("\n What is the fugacity (2) for A charging in mol/cc? ");
    scanf("%lf",&c2a);
    printf("\n What is K1 for process A (cm/s)? ");
    scanf("%lf",&K1a);
    printf("\n What is K2 for process A (cm/s)? ");
    scanf("%lf",&K2a);

    if (qv > 1){
   printf("\n How long will the steel remain in each B cell (secs)? ");
       scanf("%lf",&tb);
   printf("\n What is the H diffusivity in the B cells (cm^2/s)? ");
       scanf("%lf",&Db);
   printf("\n What is the fugacity (1) for B charging in mol/cc? ");
       scanf("%lf", &c1b);
    printf("\n What is the fugacity (2) for B charging in mol/cc? ");
      scanf("%lf", &c2b);
      printf("\n What is K1 for process B (cm/s)? ");
      scanf("%lf",&K1b);
      printf("\n What is K2 for process B (cm/s)? ");
      scanf("%lf",&K2b);
    }
    if (qv > 2){
    printf("\n How long will the steel remain in each C cell in s? ");
      scanf("%lf",&tc);
      printf("\n What is the H diffusivity in the C cell? ");
      scanf("%lf",&Dc);

   printf("\n What is the fugacity (1) for C conditions in mol/cc? ");
      scanf("%lf", &c1c);
   printf("\n What is the fugacity (2) for C conditions in mol/cc? ");
      scanf("%lf",&c2c);
      printf("\n What is K1 for process C (cm/s)? ");
      scanf("%lf",&K1c);
      printf("\n What is K2 for process C (cm/s)? ");
      scanf("%lf",&K2c);
    }

    if (qv > 3){
    printf("\n How long will the steel remain in each D cell in s? ");
      scanf("%lf",&td);
      printf("\n What is the H diffusivity in the D cell? ");
      scanf("%lf",&Dd);

   printf("\n What is the fugacity (1) for D conditions in mol/cc? ");
      scanf("%lf", &c1d);
   printf("\n What is the fugacity (2) for D conditions in mol/cc? ");
      scanf("%lf",&c2d);
      printf("\n What is K1 for process D (cm/s)? ");
      scanf("%lf",&K1d);
      printf("\n What is K2 for process D (cm/s)? ");
      scanf("%lf",&K2d);
    }
    if (qv > 4){
   printf("\n How long will the steel remain in each E cell in s? ");
      scanf("%lf",&te);
      printf("\n What is the H diffusivity in the E cell? ");
      scanf("%lf",&De);

   printf("\n What is the fugacity (1) for E conditions in mol/cc? ");
      scanf("%lf", &c1e);
   printf("\n What is the fugacity (2) for E conditions in mol/cc? ");
      scanf("%lf",&c2e);
      printf("\n What is K1 for process E (cm/s)? ");
      scanf("%lf",&K1e);
      printf("\n What is K2 for process E (cm/s)? ");
      scanf("%lf",&K2e);
    }
    if (qv > 5){
    printf("\n How long will the steel remain in each F cell in s? ");
      scanf("%lf",&tf);
      printf("\n What is the H diffusivity in the F cell? ");
      scanf("%lf",&Df);

    printf("\n What is the fugacity (1) for F conditions in mol/cc? ");
      scanf("%lf", &c1f);
    printf("\n What is the fugacity (2) for F conditions in mol/cc? ");
      scanf("%lf",&c2f);
      printf("\n What is K1 for process F (cm/s)? ");
      scanf("%lf",&K1f);
      printf("\n What is K2 for process F (cm/s)? ");
      scanf("%lf",&K2f);
    }

    if (qv > 6){
    printf("\n How long will the steel remain in each G cell in s? ");
      scanf("%lf",&tg);
      printf("\n What is the H diffusivity in the G cell? ");
      scanf("%lf",&Dg);

    printf("\n What is the fugacity (1) for G conditions in mol/cc? ");
      scanf("%lf", &c1g);
    printf("\n What is the fugacity (2) for G conditions in mol/cc? ");
      scanf("%lf",&c2g);
      printf("\n What is K1 for process G (cm/s)? ");
      scanf("%lf",&K1g);
      printf("\n What is K2 for process G (cm/s)? ");
      scanf("%lf",&K2g);
    }


    dx = L * 0.01;                  /*** integration interval  ***/

    /*** Initialize depths for 0 to L & conc for 0 to start ***/

    for (s=0; s<=100; ++s){

                con[s].x = dx * s;
                con[s].c = 0.

    } /** end for s **/

    imt  = 0;     /** initially there is no f(x) **/

    c1   = c1a;   /** first process assignments  **/
    c2   = c2a;
    t    = ta;
    D    = Da;
    h1   = K1a/Da;
    h2   = K2a/Da;
    pn   = 1.          /** process number **/

    printf("\n\n PROCESS #1 ");
printf("\n\n c1= %1.4e  c2= %1.4e t= %lf  D= %1.4e",c1,c2,t,D);
printf("\n K1= %1.4e  K2= %1.4e  L= %lf  dx= %lf",K1a,K2a,L,dx);
    printf("\n\n");

    bdepth(con, imt, c1, c2, D, L, t, h1, h2);
    fmamp(con, pn, dx);

    if (qv > 1){        /** begin process #2 **/
                imt = 1;
                c1   = c1b;
                c2   = c2b;
                t    = tb;
                D    = Db;
                h1   = K1b/Db;
                h2   = K2b/Db;
                pn   = 2;

          printf("\n\n PROCESS #2 ");
printf("\n\n c1= %1.4e  c2= %1.4e t= %lf  D= %1.4e",c1,c2,t,D);
printf("\n K1= %1.4e  K2= %1.4e  L= %lf  dx= %lf",K1b,K2b,L,dx);
          printf("\n\n");

                bdepth(con, imt, c1, c2, D, L, t, h1, h2);
                fmamp(con, pn, dx);

    }
    if (qv > 2){        /** begin process #3 **/
                imt = 1;
                c1   = c1c;
                c2   = c2c;
                t    = tc;
                D    = Dc;
                h1   = K1c/Dc;
                h2   = K2c/Dc;
                pn   = 3;

          printf("\n\n PROCESS #3 ");
printf("\n\n c1= %1.4e  c2= %1.4e t= %lf  D= %1.4e",c1,c2,t,D);
printf("\n K1= %1.4e  K2= %1.4e  L= %lf  dx= %lf",K1c,K2c,L,dx);
          printf("\n\n");

                bdepth(con, imt, c1, c2, D, L, t, h1, h2);
                fmamp(con, pn, dx);

    }
    if (qv > 3){        /** begin process #4 **/
                imt = 1;
                c1   = c1d;
                c2   = c2d;
                t    = td;
                D    = Dd;
                h1   = K1d/Dd;
                h2   = K2d/Dd;
                pn   = 4;

          printf("\n\n PROCESS #4 ");
printf("\n\n c1= %1.4e  c2= %1.4e t= %lf  D= %1.4e",c1,c2,t,D);
printf("\n K1= %1.4e  K2= %1.4e  L= %lf  dx= %lf",K1d,K2d,L,dx);
          printf("\n\n");

                bdepth(con, imt, c1, c2, D, L, t, h1, h2);
                fmamp(con, pn, dx);
```

```
        }
        if (qv > 4){            /** begin process #5 **/
                        unt = 1.
                        c1   = c1e.
                        c2   = c2e.
                        t    = te.
                        D    = De.
                        h1   = K1e/De.
                        h2   = K2e/De.
                        pn   = 5.

                printf("\n\n PROCESS #5 ").
        printf("\n\n c1 = %1.4e  c2= %1.4e te = %lf  De= %1.4e",c1,c2,t,D).
        printf("\n K1= %1.4e  K2= %1.4e  L= %lf  dx= %lf",K1e,K2e,L,dx).
                printf("\n\n").

                        bdepth(con, unt, c1, c2, D, L, t, h1, h2).
                        fmamp(con, pn, dx).

        }
        if (qv > 5){            /** begin process #6 **/
                        unt = 1.
                        c1   = c1f.
                        c2   = c2f.
                        t    = tf.
                        D    = Df.
                        h1   = K1f/Df.
                        h2   = K2f/Df.
                        pn   = 6.

                printf("\n\n PROCESS #6 ").
        printf("\n\n c1 = %1.4e  c2= %1.4e te = %lf  De= %1.4e",c1,c2,t,D).
        printf("\n K1= %1.4e  K2= %1.4e  L= %lf  dx= %lf",K1f,K2f,L,dx).
                printf("\n\n").

                        bdepth(con, unt, c1, c2, D, L, t, h1, h2).
                        fmamp(con, pn, dx).

        }
        if (qv > 6){            /** begin process #7 **/
                        unt = 1.
                        c1   = c1g.
                        c2   = c2g.
                        t    = tg.
                        D    = Dg.
                        h1   = K1g/Dg.
                        h2   = K2g/Dg.
                        pn   = 7.

                printf("\n\n PROCESS #7 ").
        printf("\n\n c1 = %1.4e  c2= %1.4e te = %lf  De= %1.4e",c1,c2,t,D).
        printf("\n K1= %1.4e  K2= %1.4e  L= %lf  dx= %lf",K1g,K2g,L,dx).
                printf("\n\n").

                        bdepth(con, unt, c1, c2, D, L, t, h1, h2).
                        fmamp(con, pn, dx).

        }

} /** end main **/

struct conc fmamp(con,pn,dx)
struct conc con[101].
int         pn.
double      dx.
{

        FILE        *fp, *fopen().

        int         m.

        double      ctotv, ctot.

        printf("\n\n Calculating total Hydrogen absorbed...").
        printf("\n\n   and storing profile in a file  ").

        if (pn = 1){
                        fp = fopen("hproc1.d","w").
        }
        else if (pn = 2){
                        fp = fopen("hproc2.d","w").
        }
        else if (pn = 3){
                        fp = fopen("hproc3.d","w").
        }
        else if (pn = 4){
                        fp = fopen("hproc4.d","w").
        }
        else if (pn = 5){
                        fp = fopen("hproc5.d","w").
        }
        else if (pn = 6){
                        fp = fopen("hproc6.d","w").
        }
        else {
                        fp = fopen("hproc7.d","w").
        }

        ctot  = 0.                  /** initialize ctot          **/
        ctotv = 0;
        m     = 0;                  /** initialize x for integral  **/

                /** store x, C(x) values **/

        while (m <= 98){

            fprintf(fp, "\n %1.5e %1.5e ", con[m].x, con[m].c).

            fprintf(fp, "\n %1.5e %1.5e ", con[m+1].x, con[m+1].c).

                        if (con[m].c < 0){
                                con[m].c   = 0.
                        }
                        if (con[m+1].c < 0){
                                con[m+1].c = 0.
                        }
                        if (con[m+2].c < 0){
                                con[m+2].c = 0.
                        }

                        /** Integrate by Simpson's Rule **/

                ctotv = (con[m].c) + (4*con[m+1].c) + (con[m+2].c).
                ctot  = ( (dx/3) * ctotv) + ctot.
                m     = m + 2.
        }
        fprintf(fp, "\n %1.5e %1.5e ", con[100].x, con[100].c).
        fprintf(fp, "\n\n %1.5e ", ctot).

        printf("\n\n Total C from charging 1scm is %1.5e mol ",ctot).

        fclose(fp).                 /** close file **/

}               /** end struct fmamp **/
```

```
/*** Betasolve.h ***** Stephen L. Amey ***** February 18, 1992  ****/
/***                                                             ***/
/*** This set of subroutines is called by pconc.h.  It requires  ***/
/*** values of h1,h2, n, and L.  It calculates b[n] or beta.     ***/
/*** Two convergence criteria are used: 1) (h1+h2)/1e6 and       ***/
/***  2) a difference criteria between consecutive terms         ***/
/***                                                             ***/
/*****************************************************************/

#include    math
#include    stdio

#define                 PI          3.1415927

extern      double b[1000].


betasolve(n,L,h1,h2)
int         n.
double      L, h1, h2.
{
            double      P1, P2, G.
            double B.

            P1 = ( ( n * PI ) - PI )/L.
            P2 = ( n * PI )/L.
            B  = ( P1 + P2 )/2.
            G  = ( B * B ) - ( h1 * h2 ).

            if (G > 0){     /** the root will be positive **/
                        P2 = B.
                        posnum(n,P1,P2,h1,h2,L,B).
            }
            else {                  /** the root will be negative **/
                        P1 = B.
                        negnum(n,P1,P2,h1,h2,L,B).
            }
            return;   /** return to bdepth in pconc.h with a beta **/

} /* end beolve */

posnum(n,P1,P2,h1,h2,L,B)
int         n.
double      P1,P2,h1,h2,L,B.
{

            int         chkdone.
            int         Bch.

            double      tan().
            double      R, c, bm.
            double      abval, abv.
            double  pB.
            double      Bdif, Bdv.

            chkdone = 0;
            Bch     = 0.
            pB      = 1e10.
            c       = h1 + h2.
            bm = c/10000000.

            while(chkdone == 0){

                        B = (P1 + P2)/2.
                        R = ( ( (B*B)-(h1*h2) ) * tan(B*L) ) / B.
                        abval = R - c.

                        if (abval < 0){
                                    abv = -abval.
```

```
                }
                else{
                        abv = abval.
                }

                if (abv <= lim){    /** criterion #1 **/
                        chkdone = 1.
                }
                else if (R > c){    /** cnt fail -- reset P **/
                        P2 = B.
                }
                else {
                        P1 = B.
                }

                if (Bch == 1){

                        Bdif = B - pB.

                        if (Bdif < 0){
                                Bdv = -Bdif.
                        }
                        else{
                                Bdv = Bdif.
                        }

                        if (Bdv <= 1e-12){
                                chkdone = 1.
                        }
                }
                else{
                        Bch = 1.
                }
                pB = B.

        } /** end while **/

        b[n]        = B.    /** return to betasolve with beta **/
        return.

} /** end posnum **/

negnum(n,P1,P2,h1,h2,L,B)
int         n.
double      P1,P2,h1,h2,L,B.
{

        int         cdone.
        int         Bchn.

        double      tant().
        double      R, C, lim.
        double  Abval, ABV.
        double  Bdnfn, pnB, Bdvn.

        Bchn        = 0.
        cdone       = 0.
        pnB         = 0.
        C           = h1 + h2.
        lim         = C/10000000.

        while(cdone == 0){

                B = (P1 + P2)/2.
                R = ( ((B*B) - (h1*h2)) * tant(B*L) ) / B.
                Abval = R - C.

                if (Abval < 0){
                        ABV = -Abval.
                }
                else{
                        ABV = Abval.
                }

                if (ABV <= lim){    /** criterion #1 **/

                        cdone = 1.
                }
                else if (R > C){    /** cnt fail--reset P **/
                        P1 = B.
                }
                else{
                        P2 = B.
                }

                if (Bchn == 1){

                        Bdnfn = B - pnB.

                        if (Bdnfn < 0){
                                Bdvn = -Bdnfn.
                        }
                        else{
                                Bdvn = Bdnfn.
                        }
                        if (Bdvn <= 1e-12){
                                cdone = 1.
                        }
                }
                else{
                        Bchn = 1.
                }
                pnB = B.

        } /** end while **/


        b[n]        = B.
        return.     /** return to betasolve with beta **/

} /** end negnum **/

/*** Pconc.h   ** Stephen L. Amey ******** February 16, 1992     ****/
/***                                                             ***/
/***     passes a structure back to bp.c  Figures out C(x) vs x  ***/
/***                                                             ***/
/*****************************************************************/
#include    <math.h>
#include    <stdio.h>
#include    "betasolve.h"

double b[1000].

struct conc hdepth(con, imt, c1, c2, D, L, t, h1, h2)
struct conc con[101].
int         imt.
double      c1, c2,
double  D, L, t,
double      h1, h2.
{

        struct conc dum[101].

        int         chkvar.
        int         n.
        int         q, r, j.

        double      k1, k2.
        double      sum, psum, nsum.
        double      A, Z, Zn, T.
        double      E, e1, e2, e3.
        double      x1, dx.
        double      x2a, bx2a, Tina.
        double      x2b, bx2b, Tinb.
        double      x2c, bx2c, Tinc.

        double      Lb, b2, bs, bx2.
        double      h1s, h2s, sbh2s.
        double      dn, dd, dq, denK.
        double      exnu.
        double      as, asv.
        double      L, Iterm, Iv.

        double  mca, mcb, mcc.

        double  sqrt(), cos(), tan(), exp().


        /** Initial Definitions **/

        dx    = L * 0.01.           /*** integration interval  ***/

        denK  = (h1 + h2) + (L * h1 * h2).
        c1    = ( (c2-c1) * (h1*h2) ) / denK.
        c2    = ( (c1 * ( h1 + (L*h1*h2) ) ) + (h2*c2) ) / denK.


        /** dump initial conc into a dummy **/
        /** array for manipulation        **/

        if (imt==1){        /** for processes 2&3 only  **/
                for (q=0; q<=100; ++q){
                        if (con[q].c < 0){
                                dum[q].c = 0.
                        }
                        else{
                                dum[q].c = con[q].c.
                        }
                }   /** end for q **/
        }  /** end if **/

        for (r=0; r<=100; ++r){  /** Figure out summation for each x **/

                printf("  %d ", r).

                x1          = con[r].x.
                chkvar      = 1.
                n           = 1.
                sum         = 0.
                nsum        = 0.

            while(chkvar == 1){   /** do loop until sum converges **/

                betasolve(n,L,h1,h2);    /** returns b[n] **/

                        b2    = b[n]*b[n].
                        h1s   = h1*h1.
                        h2s   = h2*h2.
                        sbh2s = b2 + h2s.

                    dn = 2 * sbh2s.
                    dd = ((b2 + h1s)*( (L*sbh2s) + h2 )) + (h1*sbh2s).
                    dq = dn/dd.
                     A  = sqrt(dq).
```

```
        tLb   = L * b[n],
        e1    = ( (-k1)+(k1*h1*L)+(k2*h1) ) * cos(Lb);
        e2    = ( (-k1*L) - (k1*h1/h2) - k2 ) * sin(Lb);
                e3    = k1 - (k2*h1),
                E     = (e1/b[n]) + e2 + (e3/b[n]),
                bx    = (x1) * b[n],

                T     = (b[n]*cos(bx)) + (h1*sin(bx)),
                Z     = A * T,
                exnu = -D * h2 * t;

        /** Evaluate imnal dist. integral **/

                Iterm    = 0;

    if (imt==1){     /** if on process 2 or higher **/

                  I              = 0;
                  j              = 0;
                  while (j <= 98){


    /** for x(1) **/
            x2a   = con[j] x,
            bx2a  = (x2a) * b[n],
            Tima  = (b[n]*cos(bx2a)) + (h1*sin(bx2a)),
            mca   = dam[j] c,

    /** for x(2) **/
            x2b = con[j+1] x,
            bx2b = (x2b) * b[n],
            Timb = (b[n]*cos(bx2b)) + (h1*sin(bx2b)),
            mcb     = dam[j+1] c,

      /** for x(3) **/
            x2c     = con[j+2] x,
            bx2c    = (x2c) * b[n],
            Timc = (b[n]*cos(bx2c)) + (h1*sin(bx2c)),
            mcc     = dam[j+2] c,

    /** Integrate by Simpson's Rule **/

    Iv = (Tima*mca)+(4*Timb*mcb)+(Timc*mcc),
                I              = I + ( (dx/3) * Iv),

                j      = j + 2,

                  } /** end while j **/

                            Iterm          = A * I,

                } /** end if imt **/

    /** calculate new term of the summation **/

    nsum = ( Z * exp(exnu) ) * ( (A * E) + Iterm ),

    /** calculate total summation to term n **/

                sum = sum + nsum;


    if (n > 1){  /** has the sum converged? **/

                as    = ( nsum - psum ),

    /** Do Absolute value of difference **/

                            if (as < 0){
                                asv = -as,
                            }
                            else{
                                asv = as;
                            }

                /** Chk if diff is small. **/
                /** Convergence Criterion **/

                            if (asv < 1e-15){

                                chkvar = 0;

                            }   /** end if-asv **/

                } /** end if-n  **/

                ++n;
                psum = nsum;

            } /** end while -chkvar-summation convergence **/


              /** calculate C(x) for x(r) **/

              con[r] c = ( k1 * x1 ) + k2 + sum;

        } /** end for r - end process **/

        return;

    }       /** end hdepth - go back to hp c **/
```

```
/*** Vardef.h ***************** Stephen L. Amery *****/
/**                                                   **/
/** Provides a header file with useful definitions    **/
/** Definitions apply to both hp c, pconc.h, m c      **/
/**                                                   **/
/*******************************************************/

struct conc {
                double      x,   /** keeps track of depth **/
                double  c.   /** keeps track of C(x)  **/
};
```

BIBLIOGRAPHY

Adzic, R.R., D. Gervasio, I. Bae, B. Cahan, and E. Yeager, *NSF/EPRI Workshop on Anomalous Effects in Deuterated Materials*, Washington, D.C., October 16-18, 1989, pp. 1-17.

Amey, S.L., G.M. Michal and J.H. Payer, submitted to *Metallurgical Transactions A*, spring 1992.

Andrew, P.L. and A.A. Haasz, *J. Vac. Sci. Tech. A*, **8**[3] (1990) 1807-1813.

Archer, M.D. and N.C. Grant: *Proc. Roy. Soc. Lon. A*, 1984, vol. 395, pp. 165-183.

ASTM F 1113-87.

BC1200 manual.

Beck, W., J. O'M. Bockris, J. McBreen and L. Nanis, *Proc. Roy. Soc. Lond.*, **290A** (1965) 191-206.

Beck, W., J.O'M. Bockris, J. McBreen and L. Nanis: *Proc. of Roy.Soc.Lond. A*, 1965, vol. 290, pp. 220-235.

Beck, W., J.O'M. Bockris, M.S. Genshaw and P.K. Subramanyan, *Met.allurg. Trans.*, **2A**, (1971): p. 883.

Berman, D.A., W. Beck and J.J. DeLuccia, Hydrogen in Metals, I.M. Bernstein & A.W. Thompson, eds., ASTM, Metals Park, Ohio, (1974): p. 595.

Bockris, J. O'M. and B. E. Conway, *Trans. of the Faraday Soc.*, **45** (1949) 989-999.

Bockris, J. O'M., A. Damjanovic and R.J. Mannan, *Electroanal. Chem. & Interfac. Electrochem.*, **18** (1968) 349-361.

Bockris, J.O'M. and P.K. Subramanyan, *J. Electrochem. Soc.*, **118**[7] (1971) 1114-1119.

Bockris, J.O'M., and A.K.N. Reddy: Modern Electrochemistry, Plenum Press, New York, NY, 1970, pp. 906-908.

Bockris, J.O'M., *Chem. Rev.*, **43** (1948) pp. 525-577.

Bockris, J.O'M., J. McBreen and L. Nanis, *J. Electrochem. Soc.*, **112**[10] (1965) pp. 1025-1031.

Bockris, J.O'M., Proceedings of Stress Corrosion Cracking and Hydrogen Embrittlement of Iron Base Alloys, NACE, 1973: p. 286.

Bolton, K. and L.L. Shreir, *Corrosion Sci.*, **3** (1963): pp. 17-33.

Bryan, W.L. and B.F. Dodge, *A.I.Ch.E.J.*, **9**[2] (1963) pp. 223-228.

Cailletet, L., *Compt. Rend.*, **58**, (1864) 327.

Carslaw, H.S. and J.C. Jaeger, Conduction of Heat in Solids, Clarendon Press, Oxford, U.K., (1959).

Chan, C.Y. and A.T. Kuhn, *Oberflache-Surface*, **20**[1] (1979) pp. 7-14.

Chang, P.L. and W.D.G. Bennett, *J. Iron Steel Inst.*, **170** (1952) pp. 205-213.

Chatterjee, S.S., B. G. Ateya and H.W. Pickering, *Metall. Trans.*, **9A** (1978) 389-395.

Chaudhari, B.S. and T.P. Radhakrishnan, *Corr. Sci.*, **30**[12] (1990) pp. 1219-1234.

Choi, J.Y., *Met. Trans.*, 1 (1970) pp. 911-919.

Conway, B.E. and J.O'M. Bockris, J. Chem. Phys., 26, (1957) pp. 532-541.

Coudreuse, L. and J. Charles: *Corros. Sci.*, 1987, vol. 27, nos. 10/11, pp. 1169-1181.

Crank, J., The Mathematics of Diffusion, Oxford University Press, New York, NY (1956).

Darken, L.S. and R.P. Smith, *Corrosion*, 5, (1949) 1-15.

DeLuccia, J.J. and D.A. Berman, Electrochemical Corrosion Testing, ASTM STP 727, ASTM, (1981): 256-273.

Devanathan, M.A.V. and Z. Stachurski, *Proc. of Roy. Soc. of Lond.* **A270**, (1962) 90-102.

Devanathan, M.A.V. and Z. Stachurski: *J. Electrochem. Soc.*, 1964, vol 111, pp. 619-623.

Devanathan, M.A.V., Z. Stachurski and W. Beck, *J. Electrochem. Soc.*, **110**[8] (1963) 886-890.

Druschitz, A. and P. Gordon, Embrittlement by Liquid and Solid Metals, M.H. Kamdar ed., Metallurgical Soc. of AIME, Warrendale, PA, (1984) pp. 285-315.

Evans, U. R., The Corrosion and Oxidation of Metals: Scientific Principles and Practical Applications, Arnold, London, (1961), p. 397.

Ferber, H., H. Kasten, G.K. Wolf, W.J. Lorenz, H. Schneickert and H. Folger, *Corr. Sci.*, **20** (1980) pp. 117-128.

Fletcher, E.E. and A.R. Elsea, *DMIC Report 219*, (1965) pp. 1-80.

Frank, R.C., D.E. Swets, D.L. Fry, *J. Appl. Phys.*, **29** (1958) pp. 892-898.

Fullenwider, M.A., Hydrogen Entry and Action in Metals, Pergamon Press, Inc., Elmsford, New York, (1983).

Gaskell, D.R., Introduction to Metallurgical Thermodynamics, 2nd edition, Hemisphere Publishing Corporation, New York, 1981, pp. 473.

Handbook of Chemistry and Physics, 63rd edition, R.C. Weast ed., CRC Press, Boca Raton, FL, (1982), pp. F-185-189.

Hill, M.L. and E.W. Johnson, *Trans. Met. Soc. AIME*, **221** (1961) pp. 622-629.

Hirth, J.P., *Metallurg. Trans.*, **11A**, (1980): pp. 861-890.

Hudson, R.M., *Corrosion*, **20** (1969) p.24t.

Ijomah, M.N.C., *J. Electrochem. Soc.*, **134**[12] (1987) pp. 2960-2966.

Ives, D.J.G. and F.R. Smith, *Trans. Far. Soc.*, **63** (1967) 217-233.

Iyer, R.N., H.W. Pickering and M. Zamanzedeh: *J. Electrochem. Soc.*, 1989, vol. 136, no. 9, pp. 2463-2470.

Iyer, R.N., H.W. Pickering, *J. Electrochem. Soc.*, **137**[11] (1990) 3512-3514.

Iyer, R.N.,H.W. Pickering, I. Takeuchi, M. Zamanzadeh, *Scripta Met.*, **22** (1988) 911-916.

Janavicius, P., Case Western Reserve University, Internal Report, 1991.

Johnson, E.W., M.L. Hill. *Trans. Met. Soc. AIME*, **218** (1960) pp. 1104-1112.

Kal'ner, B.D. and V.I. Malkin. *Prot. of Metals*, **15**[2] (1979) 169-170.

Kim, C.D. and B.E. Wilde. *J. Electrochem. Soc.*, **118**[2] (1971) pp. 202-206.

Kortum, G. and J.O'M. Bockris, Textbook of Electrochemistry, vol. II, Elsevier, Amsterdam, 1951. Also, J.O'M. Bocris and A.K.N. Reddy, Modern Electrochemistry, vol. 2, Plenum Press, New York, 1970.

Kudryautsev, V.N., et.al., Metal-Hydrogen Systems, ed. T.N. Veziroglu, Pergamon Press, New York, (1981) pp. 251-258.

Kure/Yeager Thesis, Case Western Reserve University (1956).

Lee, J.-L., J.T. Waber, Y.-K. Park. *Scripta Met.*, **20** (1986) pp. 823-828.

Lewandowski, J.J., Y.S. Kim and N.J.H. Holroyd. *Metall. Trans. A*, **23A** (1992) pp. 1679-1689.

Linderoth,S. and A.V. Shiskin. *Phil. Mag. A*, **55**[3] (1987) 291-300

Lunarska, E., *Hydrogen Degrad. of Ferr. Alloys*, R.A. Oriani, J. Hirth, M. Smialowski, eds., Noyes Publications, Park Ridge, New Jersey, (1985): pp. 712-736.

Makhlouf, M.M and R.D. Sisson, Jr., *Metallurg. Trans. A*, **22A** (1991) 1001-1006.

Marquez, J.A., I. Matsushima, H.H. Uhlig, *Corrosion*, **26** (1970) 215-222.

Matsushima, I. and H.H. Uhlig, *J. Electrochem. Soc.*, **113**[6] (1966) pp. 555-559.

McBreen, J., L. Nanis, and W. Beck: *J. Electrochem. Soc.*, 1966, vol. 113, 1218-1222.

McCright, R.D. and R.W. Staehle. *J. Electrochem. Soc.*, **121**[5] (1974) 609-618.

McCright, R.D., Dissertation, Ohio State University, 1971.

McCright, R.D.,*Proc. of SCC & HE of Iron Base Alloys*, NACE, France (1973).

McNabb, A. and P.K. Foster: *Trans.of TMS-AIME*, vol. 227, (1963): pp. 618-627.

Mostovoy, S. and N.N. Breyer, *Trans. ASM*, **61**, (1968) pp. 219-232

Newman, J. F. and L.L. Shreir, *Corrosion Sci.*, **9** (1969) 631-641.

Nowick, A. S., J.J. Burton, Diffusion in Solids, Academic Press, New York, (1975) pp. 281-284.

Okada, T. ,*Electrochim. Acta*, **27**[9] (1982) 1273-1280.

Pancheshnaya, V.P., V.M. Knyazheva, Zh.V. Klimenko and M.M. Anotova, *Prot. of Metals*, **16**[6] (1980) 550-556.

Parsons,R. and J. O'M. Bockris, *Trans. of Far. Soc.*, **47** (1951) p. 914.

Payer, J.H. and G.M. Michal, *Proc. of 5th Auto.Prev.of Corr.*, P-250, Dearborn, MI, (1991), 53-63.

Payer, J.H. and G.M. Michal: submitted to *SAE Transactions*, Detroit, MI. 1991.

Payer, J.H., G.M. Michal and C. Rogers: *Corrosion/91*, (1991): paper no. 405.

Pedan, K.S., S.P. Bagaev, V.N. Kudryavtsev and Yu. D. Gamburg, *Zashchita Metallov*, **19**[6] (1983) 889-894.

Pound, B.G., *Acta Metallurg.*, **38**[12] (1990) 2373-2381.

Pound, B.G., *Acta Metallurg.*, **39**[9] (1991) 2099-2105.

Pourbaix, M., Atlas of Electrochemical Equilibria in Aqueous Solutions, NACE, Houston, TX, 1974.

Pressouyre, G.M. and I.M. Bernstein, *Metallurg. Trans. A*, **9A** (1978) 1571-1580.

Pumphrey, P.H., Hydrogen in Metals, Bernstein & Thompson, eds., AIME, New York, (1981) 105-111.

Pumphrey,P.H., *Scripta Met.*, **14** (1980) pp. 695-701.

Radhakrishnan, T. P. and L. L. Shreir, *Electrochimica Acta*, **11** (1966) 1007-1021.

Rashkov, S. , C. Bozhkov, V. Kudryavtsev, K. Pedam and S. Bagaev, *J. Electroanal. Chem.*, **248**, (1988): p. 421.

Riecke, E.M., B. Johnen and R. Moeller, *Corrosion Sci.*, ?

Salzberg, H.W., *J. Electrochem. Soc.*, **100**[4] (1953) pp. 146-151. Continued in L.W. Gastnirt and H.W. Salzberg, *J. Electrochem. Soc.*, **104**[12] (1957) pp. 701-703.

Sanchez, H., Y. Meas, I. Gonzalez and M.A. Quiroz, *J. Power Sources*, **32** (1990) pp. 43-53.

Sandoz, G., *Met. Trans.*, **2**, (1971) 1055-1063.

Saraby-Reintjes, A., *Electrochimica Acta*, **31**[2] (1986) pp. 251-254.

Shewman, P., Diffusion in Solids, 2nd edition, Minerals, Metals and Materials Society, Warrandale, PA, 1989, p. 122.

Shirkhanzadeh, M., *Corrosion Sci.*, **2** (1988): 201-206.

Sims, C.E., Gas in Metals,ASM, Cleveland, Ohio, 1953, pp149-150.

Singh, I. and M. Singh, *Corrosion*, **43**[7] (1987) 425-429.

Smialowski, M., Hydrogen in Steel, Pergamon Press, Oxford & Addison-Wesley Publishing, Reading Massachussetts, (1962): pp.88-90.

Smith, D.P., Hydrogen in Metals, University of Chicago Press, Chicago, IL, (1948).

Smithells, C.J. and C.E. Ransley, *Proc. Roy. Soc. Lond.* , **A150**, (1935) pp. 172-197.

Snape, E., *Corrosion*, **24** (1968) 261-282.

Squires, R. R., *J. of Amer. Chem. Soc.*, **107** (1985) pp. 4385-4390.

Stross, T.M. and F.C. Tompkins, *J. Chem. Soc. (Lond)*, (1956) pp. 230-234.

Sykes, C., H.H. Burton, C.C. Gegg, *J. Iron Steel Inst.*, **156** (1947) pp. 155-180.

Tardif, H. P. and H. Marquis, *Can. Metall. Quart.*, **1** (1962) pp. 153-171.

The Making, Shaping and Treating of Steel, 10th ed., eds. W.T. Lankford, Jr., N.L. Samways, R.F. Craven, H.E. McGannon, AISE, Herbick & Held, Pittsburg, PA, (1985), pp. 1283-1287.

Thompson, A. W., I. M. Bernstein, Advances in Corrosion Science and Technology, vol. 7, eds. M.G. Fontana, R.W. Staehle, Plenum Press, New York, 1980, pp. 53-175.

Vagramayan, A.T., Y.S. Petrova, The Mechanical Properties of Electrolytic Deposits, Consultants Bureau, New York, (1962).

Vijayaamohanan, K. and S. Sathyanarayana, *J. Power Sources*, 30[1-4] (1990) pp. 169-175.

Volkl, J. and G. Alefeld: in Diffusion in Solids: Recent Developments, eds. A.S. Nowick, J.J. Burton, Academic Press, New York, 1975, pp. 281-283.

Vollmer, L. W., *Corrosion*, 8 (1952) 326-332.

Wilde, B. E., C.D. Kim, *Corrosion*, 42[4] (1986) pp. 243-245.

Wilde, B. E., T. Shimada, *Scripta Met.*, 22 (1988) p.553.

Wu, E., *J. Electrochem. Soc.*, 134[9] (1987) pp. 2126-2133.

Yang, K., M.Z. Cao, X.J. Wan and C.X. Shi, *Scripta Met.*, 22 (1988) 1373-1378.

Yen,S.K. and H.C. Shih, *J. Electrochem. Soc.*, 135[5] (1988) pp. 1169-1170.

Zakroczynski, T., Hydrogen Degradation of Ferrous Alloys, R. A. Oriani, J. P. Hirth, M. Smialowski, eds., Noyes Pubs., Park Ridge, NJ, 1985, pp. 215-250.

Zamanzadeh, M., A. Allam, H.W. Pickering and G.K. Hubler, *J. Electrochem. Soc.*, 127[8] (1980) 1688-1693.

Zamanzadeh, M., A. Allan, C. Kato, B. Ateya and H.W. Pickering, *J. Electrochem. Soc.*, 129 (1982) 284-289.

Zeilmaker, H., *Electrodepos. & Surf. Treat.*, 1 (1972/73): p. 109.

Zhou, R.J., The LTV Steel Corporation, Internal Report, 1989.